Abstract

Title of Thesis: MIXING CHARACTERISTICS OF SINGLE-PLUME AND MULTI-PLUME HIGH PRESSURE INJECTION TESTS

Philip Leland Knowles, Master of Science, 2007

Thesis directed by: Associate Professor Kenneth T. Kiger
Department of Mechanical Engineering

The purpose of this thesis is to examine effects of multiple plumes in a Pressurized Water Reactor downcomer under scaled Pressurized Thermal Shock conditions, then assess the flow patterns and mixing compared to a single plume. Most computational and experimental studies have been performed using only single plumes; the findings of multiple plume experiments indicate that plume interaction significantly changes the flow pattern in the downcomer. A globally-induced recirculation region was created by the collective interaction of the multiple plumes in the UMD experiments, which does not occur for a single plume under similar conditions. From the evolving concentration field measurements and entrainment theory, it's argued that two merged plumes experience lower entrainment rates than a single plume. This implies the possibility of a higher thermal stress on the downcomer wall than would be inferred from single plume tests. Flow visualization was employed to examine the differences in plume behavior.

MIXING CHARACTERISTICS OF SINGLE-PLUME AND MULTI-PLUME HIGH PRESSURE INJECTION TESTS

by

Philip Leland Knowles

Thesis submitted to the faculty of the Graduate school of the
University of Maryland, College Park in partial fulfillment
of the requirements for the degree of
Master of Science
2007

Advisory Committee:

Associate Professor Kenneth T. Kiger, Chair
Professor James Duncan
Professor Marino di Marzo

Acknowledgements

I would like to thank the Nuclear Regulatory Commission for funding this work under the University of Maryland Co-operative Agreement. I would also like to thank my advisor Dr. Ken Kiger for the opportunity to study this topic under his guidance. Lastly, I would like to thank my wife for giving me the support necessary to finish this work.

Table of Contents

70

Table of Figures

List of abbreviations

HPI	High Pressure Injection
IVO	Imatran Voima Oy
MWe	Mega Watt
PCL	Primary Coolant Loss
PTS	Pressurized Thermal Shock
PWR	Pressurized Water Reactor
RMM	Regional Mixing Model
UMD	University of Maryland
MR	Mixing reagion

Chapter 1:Introduction

Pressurized Thermal shock (PTS) is an accident scenario that can occur under specific conditions inside a Pressurized Water Reactor (PWR). Pressurized Water Reactors are used to increase the thermal energy of an incoming fluid stream, which is subsequently converted into electrical output through a steam turbine and generator arrangement.

Most power generation systems that use a PWR employ a primary and secondary cooling loop system (see figure 1.1). Pressurized coolant (primarily composed of water) leaves the main circulation pump and enters into the PWR. Inside the PWR, heat is transferred from the fuel rods to the circulating coolant fluid. The coolant is then sent to a steam generator where it passes through a heat exchanger and transfers its thermal energy to the secondary loop. The water contained in the secondary loop is maintained at a much lower pressure than the primary loop, and consequently the water in the

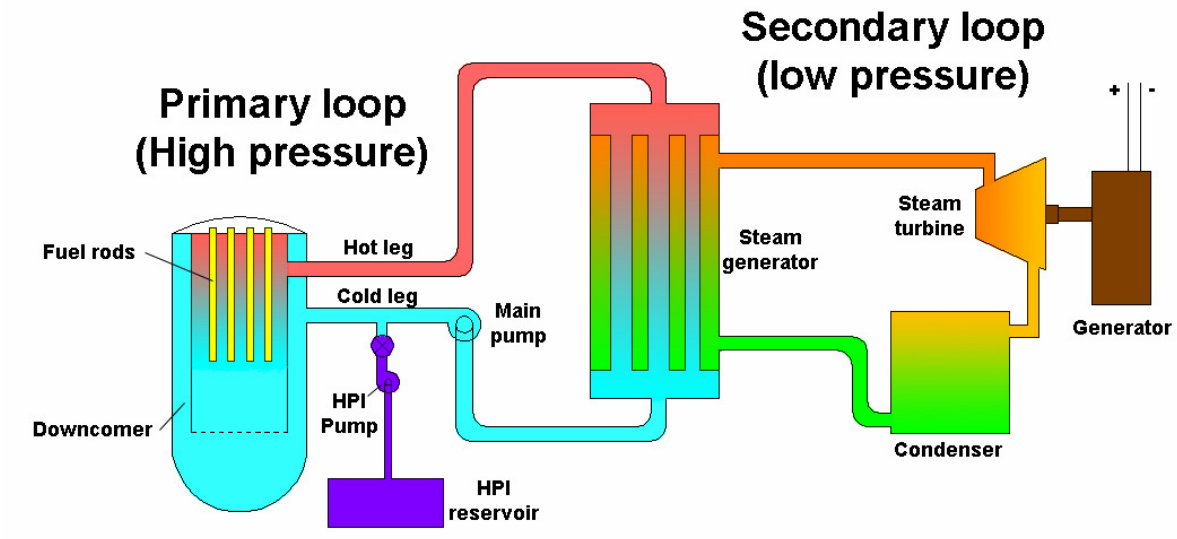

Figure 1.1: PWR coolant loops

secondary loop steam generator is boiled into steam. The superheated water vapor is then sent to a steam turbine, where its thermal and mechanical energy are used to produce electricity via a generator.

In operation, the PWR may encounter an accident condition (such as a coolant pipe breach) where a significant Primary Coolant Loss (PCL) can occur. Under such conditions, a High Pressure Injection (HPI) system injects water into the PWR coolant inlet legs (cold legs) so that the PWR doesn't run out of coolant (possibly leading to unregulated temperature excursions and a catastrophic meltdown of the reactor), as well as to maintain the pressure of the PWR so the coolant remains a liquid. The fluid temperature inside the cold legs under normal conditions is approximately 550 degrees Fahrenheit at a pressure of 1020 psia, while the fluid injected into the cold legs from the HPI system is at room temperature (Reyes, 2004). If the flow rate through the cold legs is low, there will not be sufficient turbulent mixing of the two fluids and stratification will occur inside the cold legs. The stratified flow field will spread down the cold legs and into the vertical downcomer (the annular manifold surrounding the inner core barrel and the fuel rods) of the pressure vessel. Buoyancy driven turbulent plumes are produced from the higher density room-temperature fluid entering into downcomer, which contains lower density hot fluid. These plumes evolve along the vertical wall of the downcomer and may potentially create a thermal stress within the vessel depending on their rate of mixing with the hot fluid in the downcomer.

Hydrogen embrittlement is the process by which steel losses its ductility and strength from the presence of Hydrogen. In nuclear applications, embrittlement can occur from radiation bombardment, which is a concern for high strength steels used in the

construction of the downcomer. The thermal stress applied to the downcomer during PTS combined with an embrittled downcomer can cause failure of the downcomer to contain the coolant in the primary loop.

1.1 Goals

The purpose of this study is to obtain test data characterizing potential single and multiple plume PTS scenarios that could be used to verify the PTS behavior and help develop new reactor safety codes. It is the focus of this study to evaluate differences in plume behavior between single and multiple plume cases in the downcomer under simulated PTS events. The particular reactor geometry being studied is modeled after the Palisades Nuclear Plant located in South Haven, Michigan along Lake Michigan. This 780 MWe facility was designed by Combustion Engineering, and has supplied electricity to the public since 1971. This particular reactor geometry is being studied because of its unique HPI geometry and previous computational models have under predicted the temperatures present in the cold legs with this geometry (Theofanous and Yan, 1991). Reyes, *et al,* (2004) has a scaled experimental facility located at Oregon State University (OSU) which is used to examine downcomer fluid temperatures under various events which activate the HPI safety system in this geometry. The details of this facility will be discussed in the next chapter.

Key features of studying this phenomenon include:

1. Create a "dimensionally similar" model to conduct scaled experiments, to ensure that the flow characteristics in the model accurately represent the relevant conditions of the full-scale case.

2. Resolving the turbulent plumes in the downcomer section of the PWR to observe important flow field differences, which may effect conditions of PTS.
3. Document the differences between the single plume and four plume cases in the downcomer flow field. Determine if the mixing characteristics of the plumes are different in the presence of other plumes.
4. Compare results to recent work obtained in the OSU facility.

Chapter 2: Literature review

PTS has been studied both numerically and experimentally over the last several decades. One of the pioneers in this research is Theofanous, who has published numerous papers relating to PTS. He was a contributor to the development of the first predictive model for cool-down transients under PTS conditions, the regional mixing model (RMM). Experimentally, many facilities of various scales such as CREARE 1/5 (Rothe, Ackerson, 1982), CREARE ½ (Dolan, Valenzuela, 1985), IVO 2/5 (Tuomisto, 1987), Purdue ½ (Iyer and Theofanous,1991), HDR (Theofanous, Angelini, and Yan, 1994), UPTF (Reyes, 2002), and APEX-CE (Reyes, *et al*, 2004) facilities have been used to study PTS.

2.1 Experimental PTS studies

In the early 1980's, the CREARE 1/5 length scale experimental facility was constructed to examine overcooling transients in the complex geometries encountered in PWR's. The facility itself was not geometrically scaled for any particular plant design, but was used to explore the mixing process. The CREARE 1/5 experimental facility was an open loop system, meaning that the fluid removed from the bottom of the downcomer was not re-entered back into the system, with a planar downcomer geometry and a single cold leg entrance. Key features (such as coolant pumps, a weir wall, loop seal, and the lower plenum) were omitted in this test facility. The facility used three different injection nozzles to simulate the HPI event: a large top entrance injector, a small bottom entrance injector, and a large bottom entrance injector. There was no circulation induced by external means, and the facility used thermocouples placed in the downcomer to extract

the temperature in order to infer fluid mixing rates. The facility was run at atmospheric pressure and the buoyancy of the incoming injection was induced both thermally and with a dissolved solute in the water.

The data from the CREARE 1/5 facility was used to correlate the effects of transit time for the incoming injection to reach the downcomer to cooling rates. The experiments were conducted with different injection flow rates and cold leg flow rates to obtain different transit times. For each of the three nozzles, the rate of overcooling in the downcomer decreased as the transit time was decreased. Visual observations of the flow in the cold legs were later used to define an equation to predict stratified or well mixed conditions in the cold legs based on the Froude number, flowrate, and injection flowrate in each cold leg.

A second facility was constructed for follow-on testing called the CREARE 1/2 scale Pressurized Fluid Mixing Facility. This facility incorporated some of the actual PWR features that were not present in the previous CREARE 1/5 scale tests, such as coolant pumps and a loop seal. The downcomer was again a planar section with a single cold leg entering into the downcomer. The facility examined conditions such as the effect of hot leg blockage on PTS events. To accommodate the high pressure required to reproduce the density difference between the HPI and the water in the cold leg thermally, without the need for a solute, the facility was made out of steel. The CREARE 1/2 facility used thermocouples to record temperatures at different points inside the downcomer. It was found that the mixing in the free shear layers in the cold legs are negligible compared to plume entrainment mixing for the top injection case. Also, coefficients of the plume to wall heat transfer were obtained. It was found that the local

heat transfer coefficient was not important to the overall cool-down of the downcomer fluid.

In Finland, the Imatran Voima Oy (IVO) 2/5-Scale Test Facility was constructed to examine thermal mixing of cold high pressure water with hot primary coolant during overcooling accidents. The experiment modeled half of the Loviisa VVER-440 reactor downcomer with three cold legs. The HPI nozzles were seven cold leg diameters upstream of the downcomer, while the nozzles themselves were 1/3rd the size of the cold leg diameter and injected from the top of the cold leg. This facility ran numerous tests with multiple plumes present in the downcomer. While many design and scaling parameters are different from US PWR designs, they noted that the plumes present in the downcomer interacted to produce plume behavior that was different from single plume behavior. It was observed visually that two plumes in the downcomer would merge together to form one larger plume, see figure 2.1. However, they only examined this using two plumes in the downcomer with one stagnant loop flow and the other with a moderate flow rate, which was still small enough for the cold leg to be stratified.

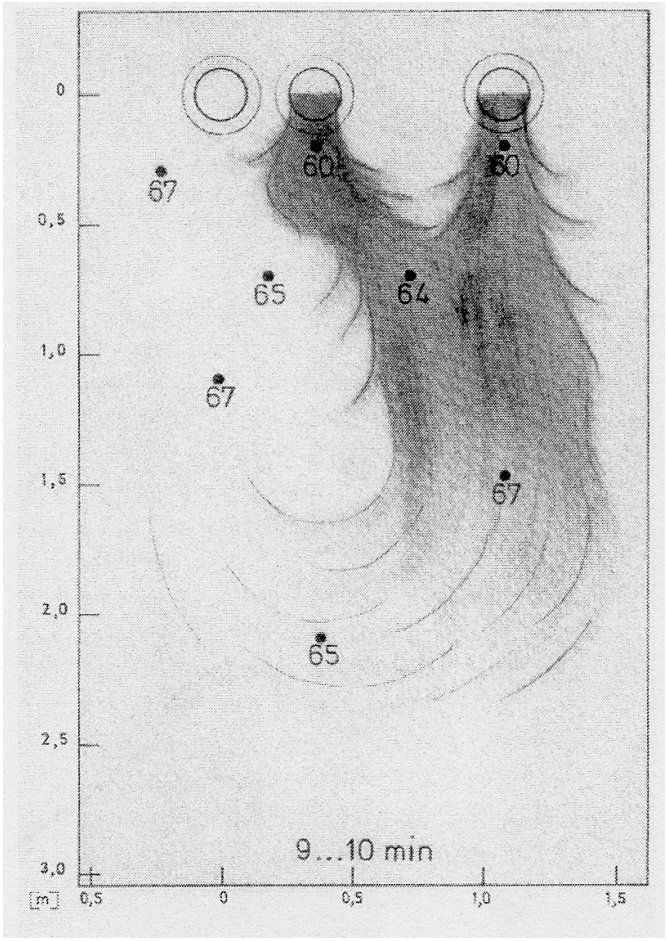

Figure 2.1: IVO multiple plume interaction (Tuomisto, H., P. Mustonen, 1986)

Purdue University built a 1/2-scale transparent facility to obtain visualization of the flow inside the downcomer for a single plume. The facility was constructed out of transparent acrylic to facilitate the optical requirements of flow visualization, which also limited the operational temperature of the facility (Iyer, Gherson, and Theofanous). Because of this, the high temperature fluid in the cold legs was modeled using room temperature water while the higher density of the injected fluid was achieved purely by mixing room temperature water with a solute to obtain the desired density ratio ($\Delta\rho/\rho$ = 0.18 between the two fluids). All the tests were preformed at stagnant loop conditions with the injection line entering from the top of the cold leg.

Purdue's One-Half-Scale HPI Mixing Test Program was developed to provide detailed data, which could test the physics embodied in the Regional Mixing Model (RMM) (Iyer and Theofanous, 1991); the RMM is a computational mixing model that will be discussed later in the chapter. In addition to testing the RMM, the Purdue experiment facility was designed to address scaling questions associated with momentum flux and injection geometry effects such as counter current flow in the injection line expected at low Froude number injections, and to complement the CREARE one-half-scale program (Iyer and Theofanous, 1991). The Purdue facility used transparent acrylic half-scaled by length similar to the Westinghouse four-loop reactor cold legs (see figure 2.2).

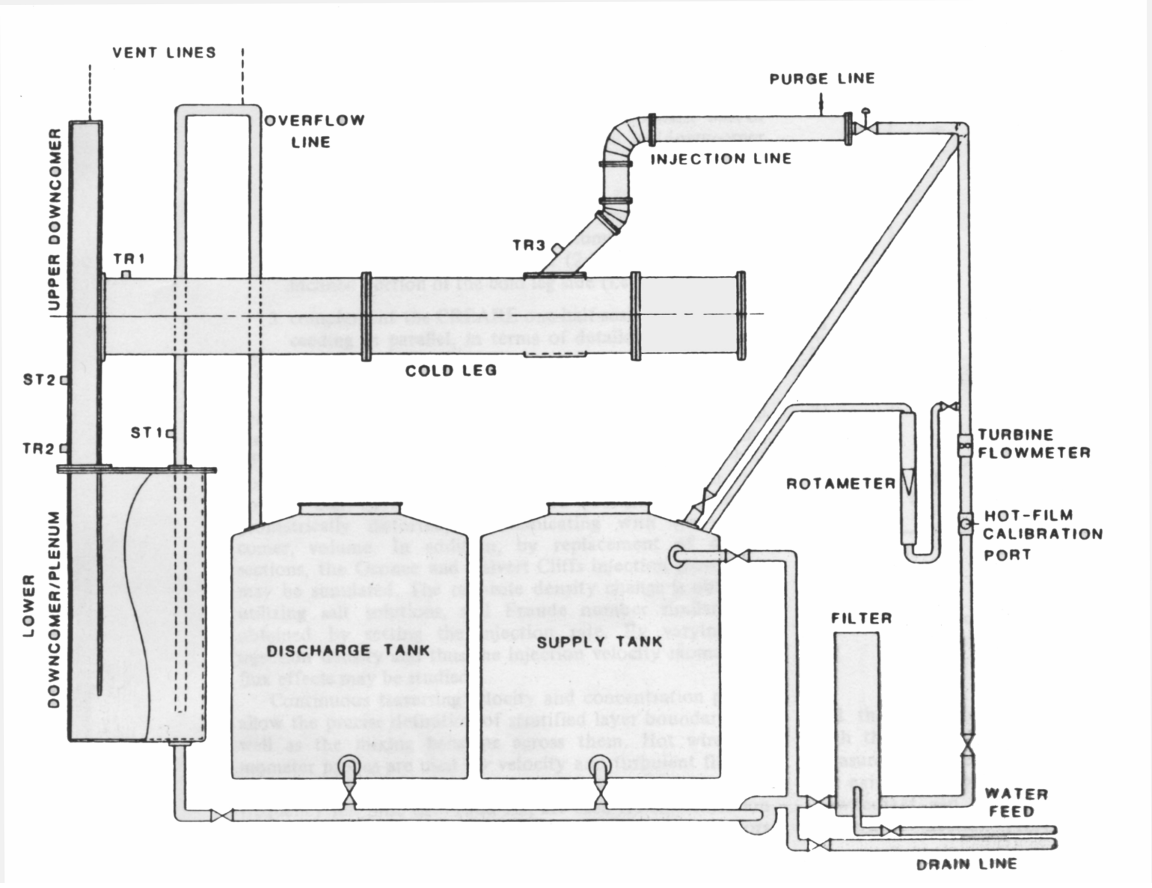

Figure 2.2: Purdue ½-scale facility (Theofanous and Nourbakhsh, 1982)

In the downcomer section of the Purdue facility, the lower plenum was geometrically distorted so that the downcomer volume is scaled appropriately (Iyer and Theofanous, 1991). The downcomer volume has an effect on the proper scaling for the cool down transients inside the downcomer. Traversing velocity and concentration probes were used to define stratified layer boundaries as well as mixing behavior across them. Hot film probes were used to record the velocity and turbulent fluctuations, while homemade conductivity probes were used to measure the concentration; both were measured at the entrance to the downcomer (location TR1 in figure 2.2).

Two full scale facilities were also built for experimental investigation, the Upper Plenum Test Facility and the HDR facility [both located in Germany]; The Upper Plenum Test Facility was primarily built to simulate how cold fluid injected into the core mixes with the hot primary fluid. This facility used thermal effects to simulate the buoyancy differences between the fluids; although the facility was restricted to working temperature differences that were half of what is seen in a typical US PWR. Nonetheless, these conditions were similar to the conditions used in the CREARE 1/2-scale facility. The HDR full scale facility performed experiments at pressures and temperatures that are typical of US PWR's, however geometric details were not similar of US PWR designs. For instance, the HPI nozzle in the HDR test facility was one-forth the size typical to US designs and the gap between the inner and outer barrel of the downcomer was half of typical US PWR's (Theofanous, Angelini, and Yan, 1994).

The HDR and UPTF facility tests uniquely combine full-scale pressure/ temperature conditions in a reactor like geometry. The HDR tests measured the temperature and stress on the vessel wall and provided the thermal response of the

system. The data from the HDR experiments was used to tune and validate various CFD codes, such as REMIX, NEWMIX and ABAQUS. However, in the HDR experiments the multiple plumes in the downcomer had little interaction as compared to the plumes observed in the IVO facility.

The APEX-CE facility was constructed at Oregon State University (OSU) to examine PTS under a variety of possible accident scenarios. The facility was designed to investigate primary loop stagnation, cold leg thermal stratification and downcomer cooling and heat transfer in a 1/4 linear scaled model of the Palisades primary coolant loop (Reyes, 2004). Both solute and temperature effects were used to reproduce the density differences between the water circulating through the cold legs and the injected fluid. The APEX-CE facility at OSU used thermocouples strategically located in the downcomer to capture the effect of mixing in this region. Conductivity probes were located upstream and downstream of the HPI nozzle to measure the concentration of solute in the cold legs. The APEX-CE facility is a closed loop facility: this means water that exits the downcomer is circulated back through the downcomer similar to the Palisades plant.

The APEX-CE facility found that under a PTS injection event with four plumes in the downcomer, two of the plumes merged to form one larger plume similar to what was observed in the IVO experiments. Also the temperature between the plume and the background with four plumes in the downcomer was 150% greater then a single plume in the downcomer. The other two plumes couldn't be detected.

2.2 Analytical and Numerical PTS studies

By examining and comparing the CREARE, Purdue, HDR, and Upper Plenum Test facilities, Theofanous was able to separate some of the different scaling effects in the systems. He separated the different parts of PTS into mixing regions (MR), see figure 2.3.

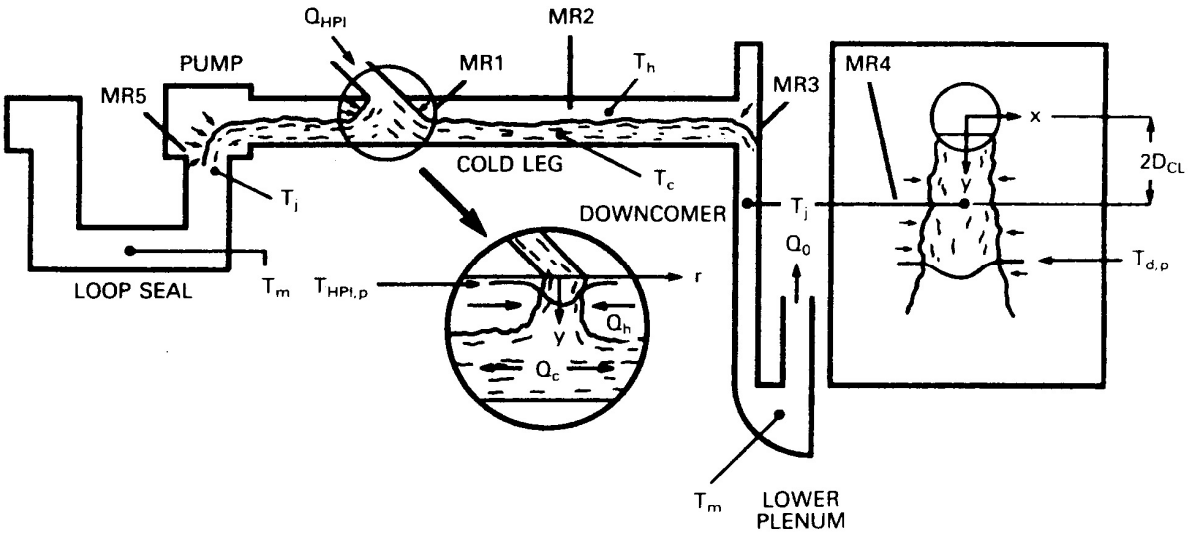

Figure 2.3: Theofanous defined mixing regions for a PTS event (Iyer and Theofanous,1991)

Previous experiments and computations show that under low cold leg flow rates that a significant portion of the fluid mixing takes place in MR1. Mixing Region 1 (MR1) is the region where the injected fluid enters into the cold leg. Mixing Region 2 (MR2) is the region in the cold leg between the injection and the downcomer. MR2 is where a stably stratified shear flow can occur under low cold leg flow conditions. Theofanous found that under stable stratified conditions, the mixing in MR2 has little significance compared to the other Mixing Regions. Mixing Region 3 (MR3) is located at the entrance to the downcomer, this is where the injected fluid turns and spills into the downcomer. Previous to the Purdue ½ scale experiments and numerical work of Theofous, Angelini, and Yan (1994), the mixing in this region was thought to be

negligible and often neglected in CFD calculations. However, they found that when the plume exits the cold leg and strikes the opposite wall, that significant mixing does occur in that region. Mixing Region 4 (MR4) is the region in the downcomer from two cold leg diameters below the cold leg to the bottom of the downcomer. Upstream of the injection is Mixing Region 5 where the injected fluid spills over into the loop seal. The geometry of the Palisades plant and UMD facilities are slightly different than the geometries studied by Theofanous, but the nomenclature and mixing region cataloging will be retained in the discussion of PTS in these facilities. Differences between figure 2.3 and the UMD facility will be discussed in the next chapter.

Theofanous and Nourbakhsh established the flow regime relating to the onset of PTS analytically in 1982. It was documented that a cold stream of fluid originates from the HPI nozzle at the point of injection [MR1] into the cold leg, continues away from the point of injection in both the upstream and downstream directions [MR2 and MR5 respectfully], and decays away as the plumes fall into the downcomer section [MR3 and MR4] (Theofanous and Nourbakhsh, 1982). Because of the stagnant loop condition, a hot stream of fluid must flow counter current to the cold stream injected by the HPI system in MR2. The cold stream in this case has a special role, since its presence induces this counter current flow pattern in the cold leg. The counter current flow is necessary for significant mixing under stagnant loop conditions (Theofanous and Nourbakhsh, 1982).

The Regional Mixing Model (RMM), with the computer codes REMIX and NEWMIX, is a model used for computation experiments examining PTS as well as other phenomena. The model is run on two different levels. First the model calculates global

results from the initial conditions forward in time assuming that the injection of the cold stream becomes well mixed as it enters the cold leg. Then it calculates the global effects under these assumptions, which can be used to obtain global cool down quantities as they change in time. The other part of the model is local and matches the mass and energy transferred between the hot and cold streams based on mixing rates from experimental data and counter current flow requirements (Theofanous and Yan, 1991). The local computation uses a zonal approach to the calculations by computing quantities of interest in the different Mixing Regions and passing the results to the next Mixing Region (Theofanous and Yan, 1991). The local part captures the detail of what is happening in the cold legs and downcomer without running the calculation over the entire global domain. The local part of the calculation uses data obtained from the global calculation to account for the changing cold leg parameters over long times.

The RMM model's integration of local plume mixing behavior into an overall system response agrees well with the CREARE one-fifth-scale tests and Purdue's One-half-scale tests (Iyer and Theofanous, 1991). The RMM model can be used to predict cool down transients and the degree of stratification with confidence under stagnated loop conditions with single plumes in the downcomer (Iyer and Theofanous, 1991). Theofanous correlated the thermal stratification data in the cold leg from the CREARE 1/5 scale experiments. A mixture Froude number of unity implies that the density in the high pressure injection line is uniform:

$$Fr_{HPI/CL} = \left[1 + \frac{Q_{CL}}{Q_{HPI}}\right]^{-\frac{7}{5}} \qquad \textbf{Equation 2.1}$$

Where $Fr_{HPI/CL}$ is the mixture Froude number, Q_{CL} is the volumetric flow rate in the cold leg, and Q_{HPI} is the volumetric flow rate of the injected fluid. Later an equation for non-uniform density in the injection line was developed:

$$Fr_{HPI/CL} = \left[\frac{\beta_{CL}}{\beta_{HPI}}\right]^{-\frac{1}{2}}\left[1+\frac{Q_{CL}}{Q_{HPI}}\right]^{-\frac{3}{2}} \qquad \textbf{Equation 2.2}$$

Where β_{CL} is the fraction of cold leg fluid that mixes with the injected fluid and β_{HPI} is the fraction of injected fluid that mixes with the fluid in the cold leg. Figure 2.4 shows the comparison of the RMM to data obtained in the cold leg for a .44 Froude number

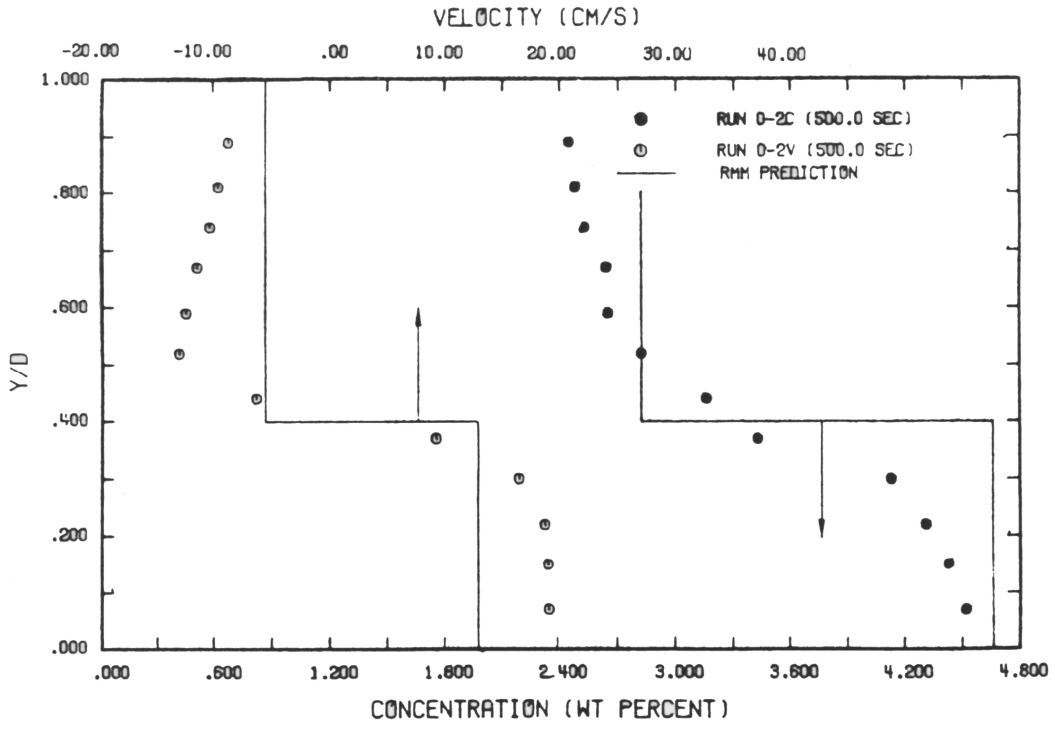

Figure 2.4: Comparison of RMM and Purdue ½-scale data [3].

injection at a density difference of 9.7% after 500 seconds (Iyer and Theofanous, 1991). Interesting to note is how the RMM assumes uniform concentration and velocity profiles

for the different temperature fluids, while the experimental data indicates a smoother velocity profile. One critical part of this local analysis is the correct prediction of the counter current flow in the cold leg. The counter current flow dramatically affects the temperature transients in the system (Iyer and Theofanous, 1991).

The work preformed up to this point was key in establishing the criteria to predict the loop flow and HPI flow conditions that yield thermal stratification in the cold legs. The CREARE 1/5-scale test produced some measurements of plume to wall heat transfer rates in the downcomer. In addition, the range of scaled facilities, from 1/5 to full scale, established a database of experimental information to compare to computer codes which attempt to predict key parameters such as cool down rates in the downcomer under PTS events.

The APEX-CE facility took the correlation from Theofanous, in equation 2.2, a step farther by matching the stratified and mixing data of the CREARE 1/5th scale facility developing:

$$Fr_{HPI/CL} = \left[1 + \frac{\rho_L * Q_H}{\rho_H * Q_{CL}}\right]^{-\frac{1}{2}} \left[1 + \frac{Q_{CL}}{Q_{HPI}}\right]^{-\frac{3}{2}} \qquad \textbf{Equation 2.3}$$

Where ρ_L is the density of the hot fluid in the cold legs, ρ_H is the density of the injected fluid, and Q_H is the flow rate of the hot fluid counter current over the injected fluid. Equation 2.3 has the same form as equation 2.2, where the constants β_{CL} and β_{HPI} in equation 2 are substituted. Figure 2.5 shows the CREARE 1/5 data against both Equation 2.1 and equation 2.3.

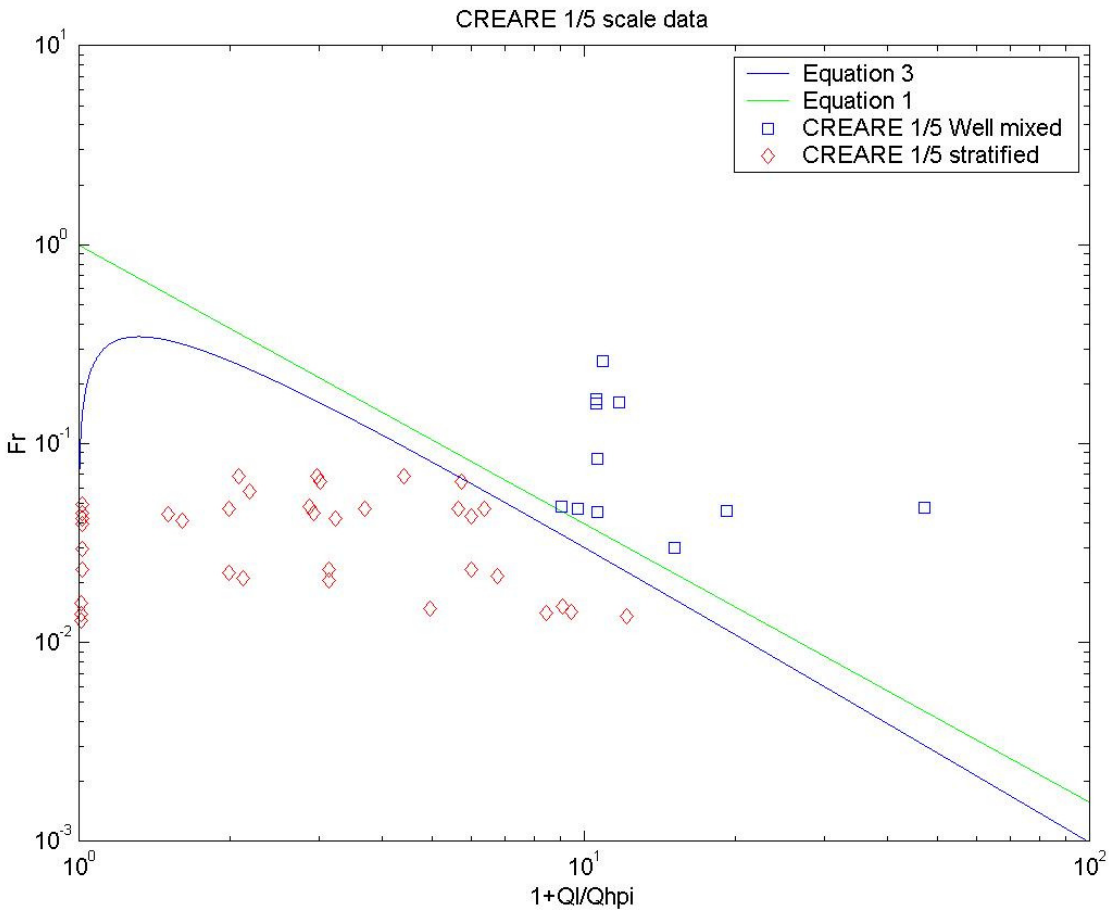

Figure 2.5: Comparison of stratified and well-mixed conditions observed in the CREARE 1/5 scale tests.

It can be seen in figure 2.5 how equations 2.1 and 2.3 divide the stratified cold leg data and the well mixed data indicating that equations 2.1 and 2.3 can be used prior to an injection event to determine if the flow inside the cold legs will be stratified or not. The significance of this discovery is that if the cold leg flow is well mixed, then the thermal stress on the downcomer is minimal.

2.3 Flow decomposition

The study of PTS involves many different physical phenomena interacting under specific conditions to produce thermal stresses along the walls of the pressure vessel. The general flow patterns involved in PTS can be decomposed into three prototypical flows: confined jets, stratified shear layers, and buoyancy driven turbulent plumes. At the HPI nozzle, a confined jet emanates out of the nozzle and into the cold leg in MR1. Under conditions applicable to PTS, the flow in the cold leg is low, so that a stratification of the cold leg fluid and the injected fluid forms. When the injected fluid falls into the downcomer, a buoyancy driven turbulent plume develops. Each of these prototypical flows plays a role in the mixing process and will be examined in detail in the next section.

2.3.1 Stratified flow/shear layers

Stratified flows arise from a non-uniform density field under condition of a moderate Reynolds number that is low enough to prevent turbulent mixing from effectively homogenizing the species present. The stratification is hydrostatically stable when the higher density fluid is beneath the fluid of lower density. Due to buoyancy forces in the flow, a stably stratified pipe flow will transition to turbulence at a higher Reynolds number than a uniform density fluid flow. This results from the fact that the buoyancy force of the fluid resists the formation of small disturbances, which could grow and cause the flow to become turbulent (Turner, 1973). For instance, turbulent energy is required to mix a stably stratified fluid as it does work lifting the higher density fluid while being dispersed through the field of interest. The turbulent energy required to disperse the higher density fluid is greater for larger density differences, therefore the

larger the density difference, the larger the Reynolds number required for the flow to become turbulent.

The most classic work concerning stratified layers is the Miles-Howard theorem, which states that an inviscid stratified flow will be stable when the local Richardson number is greater than 0.25 throughout the flow (Turner, 1973). The local Richardson number at a single point is defined by:

$$Ri = \frac{g * h * (\frac{\Delta\rho}{\rho})}{\Delta U^2} = \frac{1}{\sqrt{Fr}} \qquad \textbf{Equation 2.4}$$

where g is the acceleration of gravity, h is a length scale, $\Delta\rho$ is the difference in density between the fluids, ρ is density, ΔU is the velocity difference of the stratified layers and Fr is the Froude number.

Benjamin (1963) did extensive work in classifying different types of instabilities that can occur in unbounded stratified shear layers. First, what Benjamin called Class A instabilities are the same kind as Tollmien-Schlichting waves found in traditional uniform-density boundary layers (Turner, 1973). In classical uniform density flows, these waves use the presence of viscosity and Reynolds stress to grow from a region close to a solid boundary outward into the flow field. Viscosity plays an important role in this instability, as larger viscosities can cause the waves to be damped. The second category of instability, called Class B disturbances, occurs primarily in external flows and is caused by instability at the interface when the wavelength is much longer than the height of the layer (Turner, 1973). Class B type surface waves can exist in the flexible medium when there is no flow over it (Turner, 1973). The last category of instability is referred to as Class C, Kelvin-Helmholtz instabilities. The Class C instability occurs

when the velocity of the fluid on ether side of the interface travel at different velocities (Defina, Lanzoni, and Susin, 1999). This mechanism has been found to be relatively independent of viscosity and leads to rapid mixing between the layers. The key to Benjamin's work was to determine when the three classes of instabilities would occur. It was found that for small density differences, Class A instabilities were the first to occur, but the growth rate of this instability is so small that Class C instabilities usually overwhelm the flow while the shear continues to increase (Turner, 1973). Therefore we will focus our attention on the formation of Class C instabilities as the primary mixing agent in the cold legs.

In relation to PTS, if the flow in the cold leg is well mixed, then the buoyancy forces between the fluid in the downcomer and the cold leg are small. However, stratification tends to delay the transition to turbulence, which requires a higher Reynolds number to achieve a well mixed condition in the cold legs (Huq and Britter, 1995). If the incoming fluid is well mixed in the cold leg, then there is a smaller density difference between the fluid in the downcomer to the fluid in the cold leg, and the resulting turbulent plumes in the downcomer that cause PTS are much weaker. However, the area of interest for this study lies in the stratification conditions where the turbulent plumes develop and produce large thermal stress's on the downcomer.

2.3.2 Turbulent plumes and entrainment

Plumes, sometimes referred to as buoyant jets, arise from the point injection of a fluid with a different density then the surrounding fluid. Plumes are generally considered to be non-forced jets where the buoyancy of the fluid drives the motion and mixing in the flow. Most of the mixing in the turbulent plumes happens by a mechanism called

entrainment, provided that the Reynolds number is large enough (Townsend, 1970). Townsend examined entrainment for two typical flows: entrainment in a boundary layer and entrainment in a wake. Townsend's observations and theories for wakes have been used to describe entrainment in other shear flows such as turbulent plumes and jets (Turner, 1973).

Entrainment is the mechanism by which fluid outside of a turbulent flow is brought inside and mixed with the fluid inside of the turbulent flow. The buoyant force between the two fluids causes motion of one fluid relative to the other in the direction of the buoyancy force; this motion causes a shear at the interface between the two fluids. From the shear at the interface, vortices are formed between the buoyant fluid inside the plume and the fluid outside of the plume. In an unbounded buoyant plume, the vortical structure on the interface was observed to be in the form of rings around the plume (Shusser and Gharib, 2000). This vortical motion acts as a pump, forcing external fluid into the plume, which diminishes the net buoyancy force of the fluid. Townsend as well as Morton, Tayol, and Turner (1956) found that the rate of entrainment of external fluid into the buoyant plume is proportional to the velocity gradient at the interface, the buoyancy force, the distance from the source, and a constant he labeled the entrainment constant.

Classical observations of plumes from area sources show that the plume will spread at a linear rate with distance downstream (Turner, 1973). By assuming a sharp interface between the plume and the surrounding fluid in a non-compressible, unbounded, Newtonian fluid, it can be found analytically that the spread of a single vertical plume in a uniform, infinite environment is linear (Turner, 1973). Another assumption is that the

Boussinesq approximation can be made, so that the density difference between the fluids only appears in the buoyancy term. It also assumes that the Reynolds number is large such that the molecular properties such as thermal and momentum diffusivities don't play a large role in the overall properties of the turbulent plume. Lastly, it assumes that the buoyancy flux is constant as the plume travels vertically. The angle of linear spreading is also dependant on the concentration difference between the plume and its environment (Wicks, 1992). Specifically the density difference between the plume and the external fluid must be small enough that the Boussinesq approximation can be made. By assuming fluid with a constant buoyancy is released from a point source (producing a plume), and the properties of the fluid have one constant value inside the plume and one outside the plume, a similarity solution can be constructed. An important feature of the analytical solution is that when the above assumptions are valid, conservation of mass states that the rate of entrainment is proportional to the angle of spread of the plume:

$$b = \frac{6}{5}\alpha z \qquad \textbf{Equation 2.5}$$

where b is the radius of the plume at the distance z from the source and α is the entrainment constant (Turner, 1973). So it can be seen from equation 2.5, that the half angle of spread ($\frac{6}{5}\alpha$) of a plume in a uniform environment is proportional to the entrainment constant.

Most literature and modeling of plumes doesn't completely explore the extreme density gradients seen in a PTS event. As such, most assumptions like the Boussinesq approximation have not been proven to apply to density differences as large as what is seen in the PTS events (typically 17-18% density differences in US designs). The only

valid criteria are primarily found in Meteorological applications where the Reynolds numbers are often very large. These limitations focus the attention of the plume data to be compared directly to other PTS studies. While quantitative studies may not be applicable to these PTS events, the physical trends are expected to remain similar.

The interaction of turbulent plumes in close proximity can produce a low frequency oscillation between the plumes, which in turn can alter the flow characteristics of the plumes. Villermaux and Hopfinger (1994), investigated how the merging length and oscillation frequency of multiple, closely-spaced, co-flowing jets changed as a function of Reynolds number. They placed a plate with a predetermined pattern into an air stream to produce multiple co-flowing jets and measured the velocity using hot wire probes. At moderate Reynolds numbers (300 to 5000), the plumes interacted to produce a low-frequency oscillation in the plume merging distance and a high frequency oscillation that corresponds to the vortex shedding frequency (as predicted by the Strouhal number). Villermaux and Hopfinger (1994) found that as the Reynolds number of the jets increased, the frequency of jet merging increased linearly while the mean plume merging distance decreased linearly. It was also observed that after plume merging occurred, the merged jet showed a strong decrease in velocity as compared to the individual jet prior to merging.

2.4 What's missing

In the presence of multiple plumes, the dynamics of the flow in the downcomer can be altered from the single plume case. For instance, a single plume has been found to spread linearly in the direction of the buoyancy force, while flow fields involving multiple plumes in certain geometries have been found to be significantly different.

Wicks has found numerically that two plumes in proximity to each other will effect the rate of spreading and the horizontal motion of each plume in an open channel flow (Wicks, 1992). This has a direct effect on the amount of fluid entrained into the plumes and therefore the mixing characteristics in downcomer.

The RMM is a useful tool for guidance into the systems response to well mixed conditions. On the other hand, the model was initially compared to the Purdue ½ Scale HPI mixing test, which uses a single plume to characterize the mixing in the downcomer section. This raises the question of whether the plume dynamics with respect to mixing are similar for one plume and in the presence of multiple plumes. The IVO fluid mixing tests show that two plumes in the downcomer behave differently than a single plume. This is of great importance, considering that typical PWR designs employ multiple loops that generate multiple plumes in the downcomer. Also, from turbulent plume experiments and mathematical investigations completed by Wicks, it is understood that the presence of multiple turbulent plumes will change the rate of spreading and the mixing characteristics of the plumes and is highly dependent upon the initial conditions of the plume (Wicks, 1992).

Due to the possible differences in plume behavior between single and multiple plumes in some reactor geometries, the UMD experimental facility will conduct an investigation into single and multiple plume behavior in the Combustion Engineering reactor geometry. The results will identify if multiple plumes interact similar to the IVO facility or have marginal effect like the HDR facility and provide quantitative data as to the differences between single and multiple plumes in the downcomer. This investigation is critical to identify possible scenarios in which PTS maybe different then previously

explored experimentally and compared to the numerical simulations under these conditions.

Chapter 3:Experimental Setup and Scaling

The APEX-CE test facility at Oregon State University produced an extensive scaling analysis for the Palisades Nuclear Plant which details the critical parameters that must be matched in order to reproduce the important characteristics of the full-scale flow field in a scaled model. This analysis, along with previous multi-scale experiments, is a guide into what non-dimensional parameters are most important for sustaining key features to the problem. The UMD experimental test facility is focused upon creating similarity for the stratification in the cold legs and the mixing phenomenon in the downcomer of the Palisades plant.

In examining MR1, Theofanous separated the cases into high and low Froude number injections and was able to note that the Froude number of the HPI played an important role in the mixing in that region. For low Froude number injections, a counter current flow formed at the HPI nozzle, while for high Froude number injections there was no counter current flow. The Froude number of the injection is important because it affects the characteristics of the confined jet, which in turn affects the mixing in MR1 (see figure 3.1).

Also, the flow rate through the entire system is going to have an effect on the inlet conditions to the downcomer, specifically in the regions MR1 and MR2. In some of the closed loop tests examining hot leg blockage, careful attention was made to matching the loop flow resistance of the system so that the facility would exhibit similar natural circulation over the duration of the tests; typically on the order of half an hour. The UMD facility is an open loop system, meaning that the fluid exiting the downcomer doesn't enter the system and instead is sent to a head tank. Because of the holding

capacity of the UMD facility and data storage limitations from high resolution experiments, a test can be run for approximately 5 minutes. Instead of using loop resistance to regulate the flow rate through the system caused by natural circulation, the UMD facility is driving the equivalent natural circulation flow rate in the cold legs through the use of circulation pumps. This allows for control over the equivalent natural circulation flow rate in the loop without the careful calibration of loop resistance necessary for setting the flow rate.

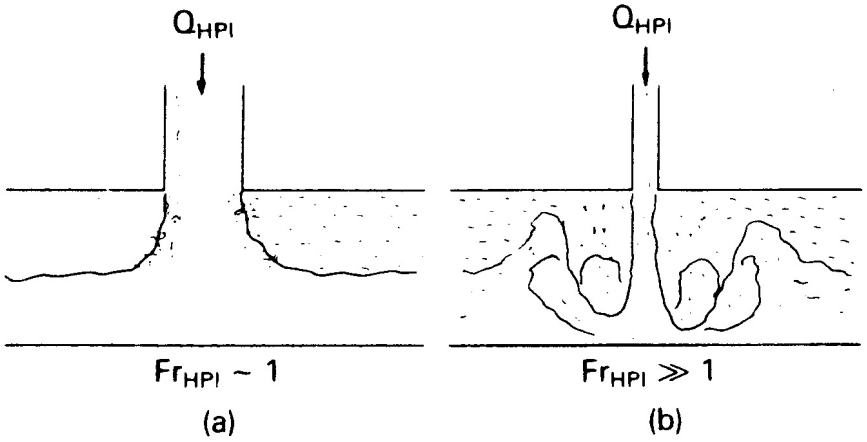

Figure 3.1: Observations of injection Froude number on mixing and jet characteristics (Iyer and Theofanous, 1991)

Theofanous, et al, successfully correlated stagnant cold leg thermal stratification data using equation 3.1, which is a Froude number for the HPI (Theofanous, Angelini, and Yan, 1994):

$$Fr_{HPI/CL} = \frac{Q_{HPI}}{A_{CL}} \left(g * D_{CL} * \frac{\Delta\rho}{\rho_{HPI}} \right)^{-\frac{1}{2}} \qquad \textbf{Equation 3.1}$$

It was derived from equation 2.4, which is the traditional representation of the Froude number, replacing the velocity with a representative bulk velocity and using the diameter

of the cold leg as a length scale. The injection Froude number in the Palisades plant is typically less than one (Reyes, 2002).

While maintaining Froude number similarity between the model and the prototype, the Reynolds number similarity can't be maintained. However, in both the model and prototype the injection jet falls and produces a stratified countercurrent flow in the injection line. Maintaining Froude number similarity more accurately recreates the effect of mixing at the point of injection for this type of behavior. The Reynolds number is calculated for a jet from:

$$\mathrm{Re}_{JET} = \frac{V * D}{\upsilon} \qquad \textbf{Equation 3.2}$$

Where V is the bulk velocity of the jet, D is the diameter of the nozzle, and υ is the kinematic viscosity of water. The Reynolds number for the model is approximately 4500, while the maximum Reynolds number for the prototype can be as large as 360,000 depending upon operating conditions. The UMD experimental data can not be compared for all working ranges of the prototype injection parameters, but as long as the Reynolds number in the prototype is such that the buoyancy and Froude number effects cause the mixing to be dominated by the large scale motion the Reynolds number similarity is not as important as the Froude number similarity.

There are several design differences between the geometry that Theofanous studied, the UMD facility, and the Palisades plant. The circulation pumps in the Palisades plant force coolant over a weir wall in the cold leg, see figure 3.2. Theofanous's geometry excluded a weir wall on the outlet of the pump, while the UMD facility incorporated this feature into the experiment. The weir wall affects the use of Theofanous's findings from MR5, because the UMD facility has a different flow in that

region. The presence of the weir wall aids in stratifying the flow in the cold legs, however Theofanous's findings prove to be a guide into the rest of the flow field.

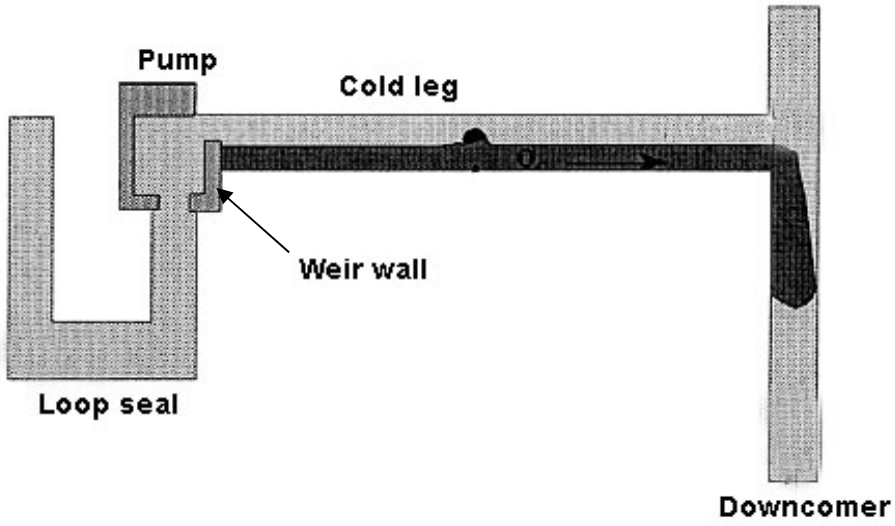

Figure 3.2: Schematic showing location of the weir wall (Reyes, 2002)

The UMD facility was constructed to be an approximate geometrically scaled replica (in length) the Palisades plant. See table 3.1 for facility dimensions; detailed part dimensions are located in appendix A. Since the injection Froude number was critical to match between the model and prototype, the closest nominal pipe size HPI nozzle was selected. Geometrically, the cold leg diameter is approximately three times the diameter of the HPI nozzle; this similarity was maintained along with the injection angle. In the Palisades plant, the four nozzles are orientated so that two are injected on the inside of the cold leg bends and the other two are injected from the outside bend, see figure 3.3. However, due to space requirements in the laboratory, the injection nozzles where oriented between the cold legs (on the inside of the pipe bend) similar to the APEX facility, see figure 3.4.

Component	Units	Palisades	APEX-CE	UMD
Reactor vessel ID	in	172	25	23
Core Barrel OD	in	152.75	20	18
Downcomer gap	in	9.625	2.5	2.5
Downcomer length (below cold leg)	in	207.7	60.5	47.5
Downcomer volume (below cold leg)	ft^3	590.1	6.19	6
Downcomer aspect ratio (Gap/length)		1/21.6	1/24.2	1/19.0
Cold leg ID	in	30	3.54	3.1
Cold leg length	ft	19.1	5.81	3.67
Cold leg Volume	ft^3	93.8	0.40	0.19
Safety injection nozzle ID	in	11.375	1.13	1.05
Maximum HPSI Flow rate	gpm	1459.2	5.29	5

Table 3.1: Table of dimensionally important features

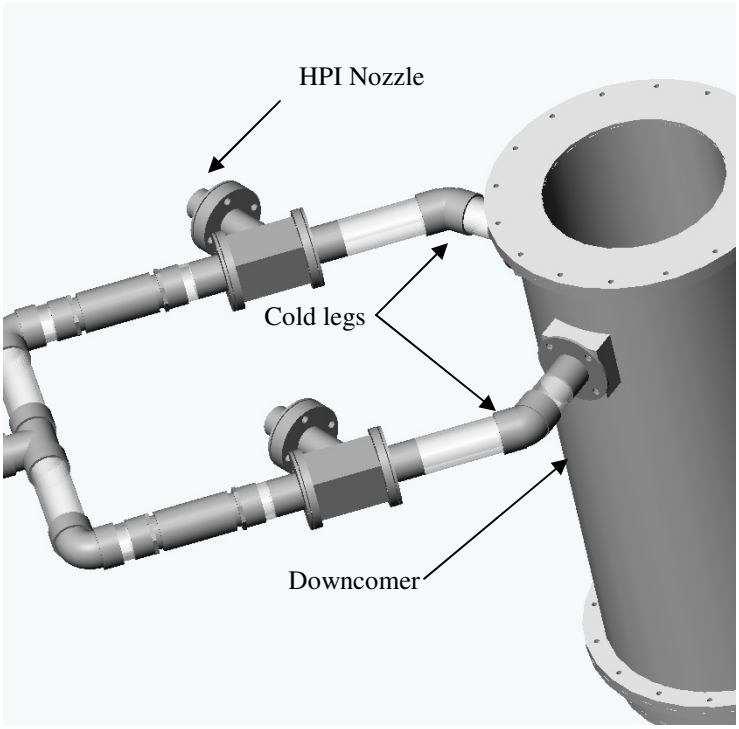

Figure 3.3: Palisades plant HPI configuration with top nozzle in figure on the outside of the cold leg bend and the lower nozzle on the inside of the clod leg bend

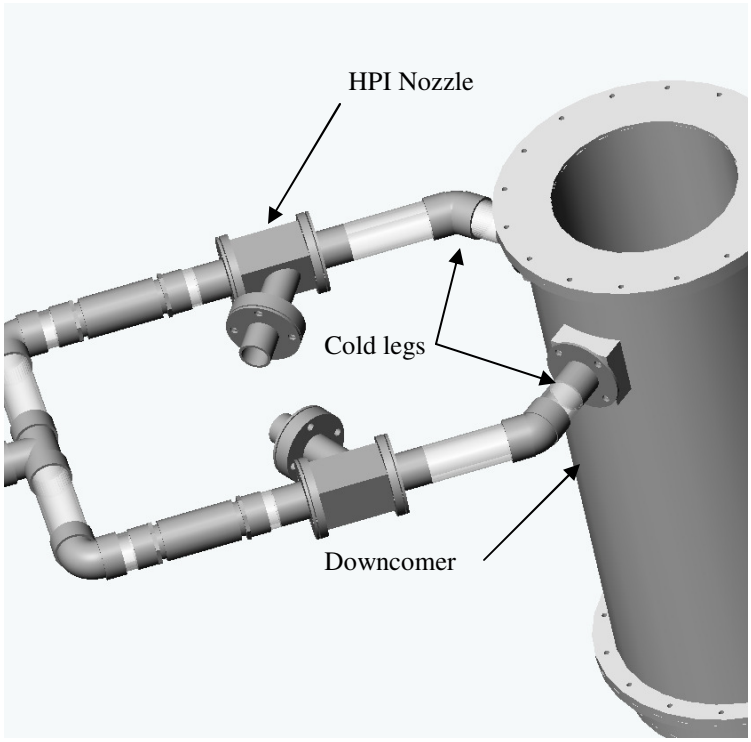

Figure 3.4: UMD facility and APEX HPI configuration with both nozzles on the inside of the cold leg bends

3.1 Different density fluids

In the APEX testing facility, the temperature of the water in the cold legs was typically measured at 400 degrees Fahrenheit, while the injected water from the HPI system was 70 Fahrenheit (Reyes); this produced a relative density difference of 17.6%. In order to simulate this large density difference in the low-temperature transparent UMD facility, Magnesium Sulfate ($MgSO_4$) was mixed into water to simulate the effects of the cold, denser fluid, while pure water at ambient temperature was used to simulate the low-density, high temperature fluid of the prototype. By using concentration differences instead of temperature along with a transparent vessel, optical measurement and flow visualization techniques can be employed. The advantage of using quantitative optical

visualizations is that the entire flow field can be recorded with high spatial and temporal resolution, capturing the mixing process in detail. The transparent acrylic vessel constrains the ranges of temperature in the experiment to less then 50^{o} Celsius and the pressure to be approximately atmospheric; the Magnesium Sulfate allows the densities in the prototype to be reproduced in the model with the temperature and pressure at standard conditions. Salt solutions have been used previously to simulate stratification and plume dynamics in similar experiments, under the assumption that a similarity between mass and heat transfer processes can be justified in the presence of turbulence. The drawback of this method is that the flow field inside the model is not exactly similar to the prototype because differences in the molecular, thermal, and mass diffusivities are orders of magnitude apart. The Schmidt number is the ratio of momentum diffusivity to mass diffusivity and is around 700 for $MgSO_4$ in water, while the Prandtl number is the ratio of momentum diffusivity to thermal diffusivity and is around 6 for water at standard conditions. Because these numbers are orders of magnitude apart, simply changing from a thermally diffusing scalar to a mass diffusing scalar will not necessarily produce the same results because the tracers diffuse at different rates. For laminar flow, the time for diffusion to significantly mix fluids on the length scales of interest is orders of magnitude longer then the transient time of the fluid in the system (less then 1 minute). Therefore, the effects of molecular diffusion over these time scales in laminar flow are insignificant. However, for turbulent flows, this will have an impact on the smallest scales of motion, but very little impact on the inertial scales resolved by the optical measurements. Also since the plumes are turbulent, the transfer of mass purely from molecular diffusion is very small compared to the enhanced mixing from turbulence.

Another concern about using salt concentration to characterize the thermal system is that in the thermal case heat is transferred from the center of the downcomer and lost to the outer wall of the downcomer. By using a mass scalar, the scalar is not lost or gained through the walls like it is in the thermal case. By using a simple heat transfer correlation for a boundary layer over an isothermal flat plate, the effect of the heat transfer through the wall can be estimated. The Reynolds number for this was evaluated using:

$$\mathrm{Re}_{BL} = \frac{V * L_D}{\upsilon} \qquad \textbf{Equation 3.3}$$

Where Re is the Reynolds number, V is the velocity of the plume, L_D is the length from the cold leg to the bottom of the downcomer, and ν is the kinematic viscosity of the plume. The length of the prototype downcomer from the cold leg downward is 5.28 m and the kinematic viscosity of water at 25° C is 1.37×10^{-5} m^2/s. The velocity of the plume in the UMD experiments was observed to be 10 cm/s. Reyes (2003) using the same downcomer geometry estimated the velocity of the plume in the prototype to be 4 times greater then the velocity in the ¼-scale model. Using 40 cm/s as the velocity for the prototype, results in a Reynolds number of 1.54×10^7 for the prototype. The following correlation is for the average Nusselt number over a flat plate for Reynolds numbers between 5×10^5 and 1×10^8:

$$\overline{Nu_L} = 0.037 * \mathrm{Re}^{.8}\,\mathrm{Pr}^{.33} \qquad \textbf{Equation 3.4}$$

Where $\overline{Nu_L}$ is the average Nusselt number, Re is the Reynolds number, and Pr is the Prandtl number (Incropera and DeWitt, 1996). Using .87 for the Prandtl number of water at Palisades operation conditions yielded an average Nusselt number of the entire length of the downcomer of 19,900. Then using the definition of the Nusselt number:

$$\overline{Nu_L} \equiv \frac{\bar{h} * L}{k}$$ **Equation 3.5**

Where $\bar{h}$ is the average heat transfer coefficient over the length of the downcomer, and k is the thermal conductivity of water. Using .580 W/(m*K) for k, gave a value of 2184 W/(m^2*K) for h. Assuming that the temperature of the wall is constant allows the use of the following equation for the temperature change of the plume:

$$\frac{T_s - T_m(x)}{T_s - T_{m,i}} = \exp(\frac{-P * x * \bar{h}}{\dot{m} * C_P})$$ **Equation 3.6**

Where T_s is the temperature of the wall, $T_m(x)$ is the temperature of the plume with distance along the downcomer, $T_{m,I}$ is the starting temperature of the plume, P is the surface parameter, x is the distance at which the temperature of the plume is desired, $\dot{m}$ is the mass per second of water flow over the wall, and C_p is the specific heat at constant pressure of water. Using 400^o C for T_s, 25^o C for $T_{m,I}$, 1.52 m for P, 67.7 Kg/s for $\dot{m}$, and 5202 J/(Kg*K) for C_P yields a value of 31.2^o C for $T_m(x)$ at the bottom of the downcomer. P was calculated from the observation that in the UMD facility the plume spread to an average width of twice the diameter of the cold leg. Assuming similar behavior in the Palisades plant, the parameter of contact between the wall and the plume is 1.52 m, which is twice the diameter of the cold leg in the Palisades plant. The maximum change in plume temperature over the entire downcomer due only to heat transfer from the wall was estimated to change by 18^o C, which is insignificant to the temperature changes from turbulent mixing in the downcomer. Therefore the heat transfer through the wall is small and a mass tracer is sufficient to model the mixing in the downcomer. This is consistant with the results from the HDR test facility where they

found the heat transfer through the downcomer wall to have insignificant effect on cooling the downcomer fluid (Theofanous, Angelini, and Yan, 1994).

Because of the optical measuring techniques used in this study, the salted fluid needed to be optically clear with an index of refraction close to that of pure water. At the full density difference required for the experiment, the Magnesium Sulfate solution was still optically transparent with a slight shift in index of refraction (see figure 3.5). Figure 3.5 shows the index of refraction of water with Magnesium Sulfate verses the specific gravity of the solution; the index of refraction was measured using a refractometer with the sample in a 72^{o}F bath. Magnesium Sulfate is one of the few salts that has a solubility

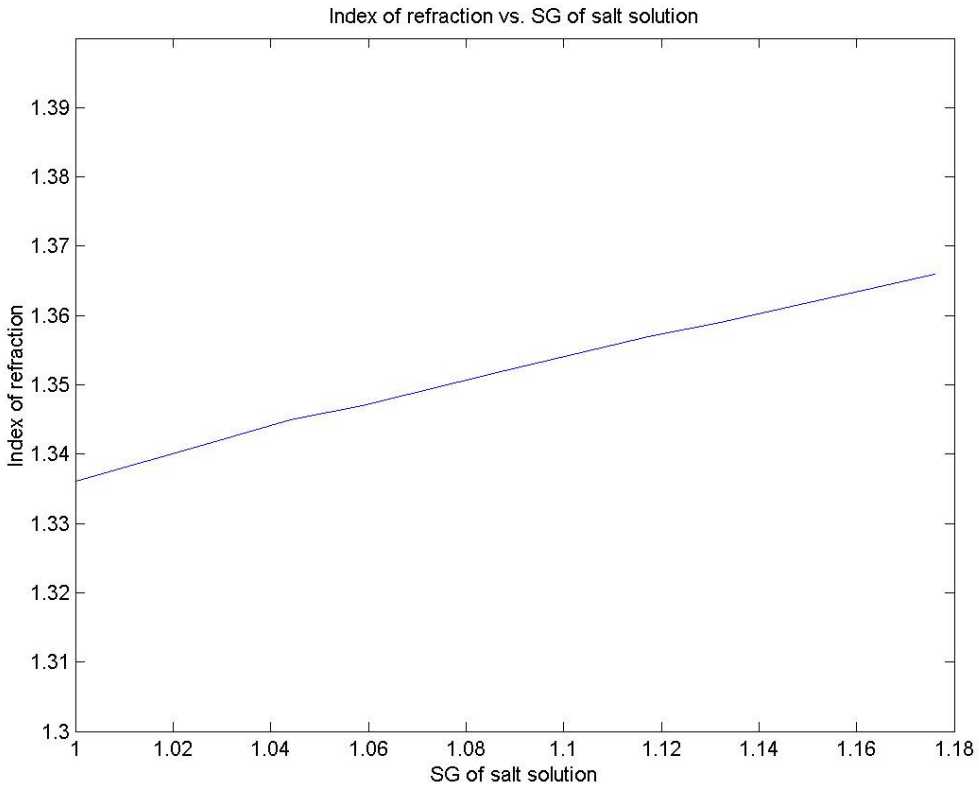

Figure 3.5: Index of refraction verses SG of salt solution

limit high enough to achieve the required solution specific gravity of 1.176. Another factor in selecting a salt was the time required for the salt to homogenize into a solution. The time required for Magnesium Sulfate to fully dissolve in water was relatively short, even at the relatively high densities required by the experiments (typical solution could be fully mixed in approximately 15 minutes).

3.2 Description of Set-up

In order to achieve the goals set forth, a quarter scale model of the reactor was constructed to study the buoyant turbulent plumes developed under primary coolant loss conditions. The entire experimental set-up consisted of several systems: the downcomer and piping, optics, line-scan camera, and data loggers. The downcomer and piping system was responsible for flowing and containing the fluid streams while allowing for optical mixing visualization in select regions of the system. The purpose of the interior optics was to visualize the concentration of dye inside the downcomer, while the line-scan camera captured the dye concentration just before the fluid enters the downcomer. The data logging system was responsible for recording and storing of the pertinent data.

3.2.1 Laser Induced Fluoresce (LIF)

The concentration measurements used in this study were obtained by use of a technique called Laser Induced Fluoresce (LIF). LIF has been used extensively to measure the concentration of tracers dissolved in a liquid, primarily used to study transport and mixing phenomena. When excited by radiation of a proper wavelength, some molecules respond by transitioning into a higher electronic energy state and then returning to their ground state via emission of a photon of light (Walker, 1985). This process can happen very rapidly; typically on the order of 10^{-9} seconds. When the

molecule is in an excited state, electron collisions cause the molecule to lose a small amount of its excited energy. This is significant because the amount of energy emitted by the molecule in the form of light is less than the energy initially absorbed. Because of this small energy loss, the wavelength of light emitted is longer than the wavelength of light absorbed. The emission of this longer wavelength light is known as fluorescence. By choosing dyes that exhibit a large separation between the wavelength of light used to excite the molecule and the wavelength of light emitted, quantitative concentration measurements can be preformed with the appropriate optical filters.

LIF has the advantage of providing a high degree of spatial and time resolved concentration measurements as compared to more traditional measurements using thermocouples and conductivity probes, with the added advantage of being a non-intrusive measurement technique. Using the molecular properties described above, LIF can be used to obtain a quantitative measure of the averaged concentration. As a laser beam passes through a region of dye, the intensity of the laser light diminishes because of absorption. The intensity of laser light at a distance x into the dyed region is:

$$I(x) = I_O \exp-[\int_O^x \varepsilon_l C(\gamma) d\gamma] \qquad \textbf{Equation 3.7}$$

Where I_O is the incoming intensity of the laser light, ε_1 is the molar absorption coefficient of the dyed solution at the wavelength of the incident laser light, $C(\gamma)$ is the concentration of dye at length γ. At the low dye concentration used in these experiments (.1 ppm), the molar absorption coefficient can be assumed reasonably uniform over the laser beam path (Igarashi et al., 1995). The average dye concentration over the region of dyed fluid can be defined as:

$$\overline{C_X} = \frac{1}{x}\int_0^x C(\gamma)d\gamma$$ **Equation 3.8**

Substituting definition 3.8 into equation 3.7 yields:

$$I(x) = I_O \exp[-\varepsilon_l \overline{C_x} x] \approx I_O(1 - \varepsilon_l \overline{C_x} x)$$ **Equation 3.9**

where the exponential term is approximated by a first order series expansion in x, which requires that $\varepsilon_l \overline{C_x} << 1$.

The amount of fluorescent light emitted by an incident laser beam per unit volume is given by:

$$F(x) = \varphi \varepsilon_l C(x) I(x) \approx \varphi \varepsilon_l C(x) I_O(1 - \varepsilon_l \overline{C}_x x)$$ **Equation 3.10**

where φ is the quantum yield of the fluorescence. Some of the light emitted by the dye can potentially be reabsorbed by the dye. However, for the dye used in the current work the absorption coefficient in the region of emission is much smaller then ε_l, so it can be neglected. Therefore by utilizing these properties of LIF, the average concentration of fluorescent dye over the length of the laser beam can be obtained.

A 10W Argon Ion laser (Spectra Physics model Stabilite 1700) and Rhodamine 6G fluorescent dye were chosen because the peak of the dyes absorption band is located around 500 nm which is suitable for using an ion-Argon laser which primarily emits wavelengths of 488 and 514 nm. Rhodamine 6G emits light from around 535 nm up to 620 nm with the peak emission around 555 nm. Through the use of filters, the light emitted from the dye can be separated from the incoming laser light.

3.2.2 LIF optical assemblies

The purpose of each LIF optical assembly is to scan the flow field to obtain scalar concentration measurements using the LIF technique in regions of interest. The UMD

experiment employed two separate LIF optical assemblies. One assembly was used for obtaining the concentration measurements in the downcomer and the other to obtain concentration measurements in the cold leg at the entrance to the downcomer.

3.2.2.1 LIF optical assembly for the downcomer

The optical assembly for scanning the downcomer was constructed to direct the laser beam through the downcomer gap from inside the downcomer. The laser beam excites the fluorescent dye in the gap, and a portion of the light emitted from dye would be collected, filtered, and focused onto a receiving fiber for conversion into a comparable voltage by a Photo Multiplier Tube (PMT). By comparing the PMT output voltage to a calibrated voltage, the average concentration over the fluid volume illuminated by the laser can be measured. In order to obtain the concentration over the entire downcomer, the laser beam is swept vertically in the z direction and azimuthally in the θ direction as indicated by the coordinate system in figure 3.6. The origin of the z-axis is located in the center of the cold legs, while the origin for the azimuthal direction (θ) is located on a hot leg. Vertical sweeping of the laser beam is accomplished by reflecting the laser beam off an octagonal rotating mirror, while the azimuthal scanning is achieved by mounting the entire optically assembly on a motor-driven bearing. The entire optical assembly rotates at approximately 60 rpm and the octagonal mirror rotates at 4000 rpm. This results in the entire downcomer being scanned at a frequency of 1 Hz, with approximately 533 vertical sweeps per revolution. Figure 3.7 shows a detailed schematic of the optical assembly inside the downcomer. A collimated laser beam is aligned along the center axis of the downcomer, from the top, and enters an optical assembly referred to as the fluorscope. The fluorscope utilizes a series of optical filters, lenses, and mirrors in order to allow the

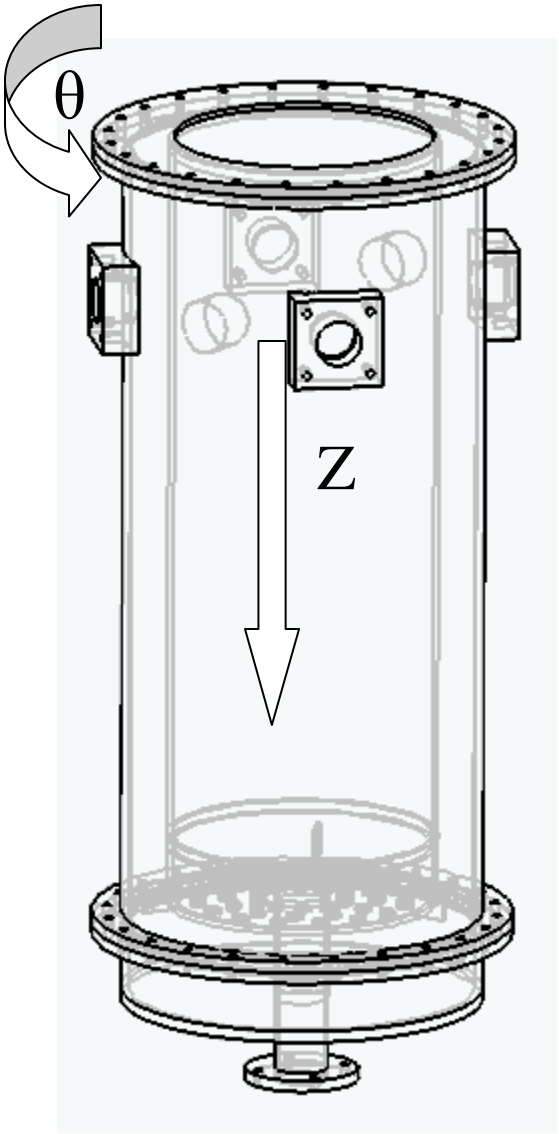

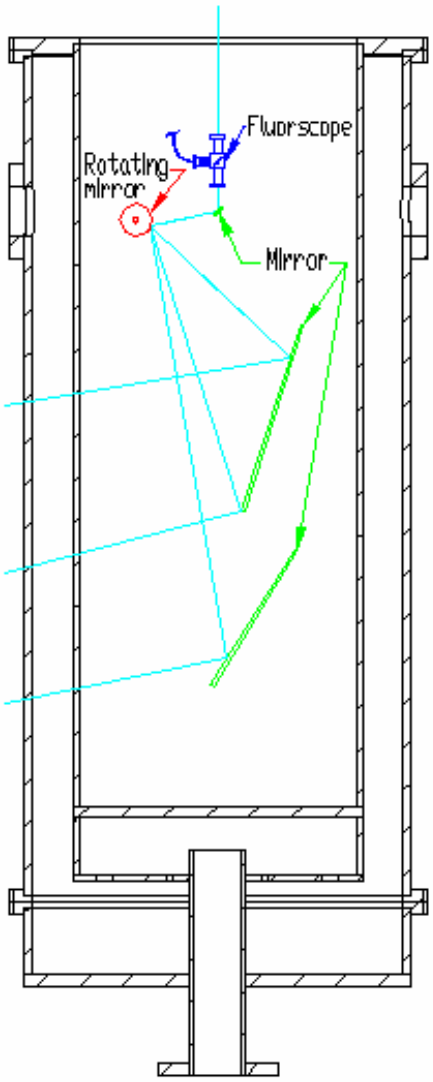

Figure 3.6: Coordinate system **Figure 3.7: Interior optics for Downcomer visualization**

laser beam to pass through the scope while collecting, filtering, and focusing light emitted by the dye, see figure 3.8. Once the laser light has passed through the fluoroscope, it is reflected by a one-inch flat mirror onto a rotating mirror. The rotating mirror is a thin, 8-sided, reflector attached to an electric motor spinning at 4000 rpm. As the rotating mirror spins, the reflected laser beam sweeps out a path, which is then reflected into the downcomer by two long thin flat mirrors. The two mirrors are aligned so that the beam from the rotating mirror sweeps out a vertical slice of the downcomer

with some overlap in the middle where the beam switches mirrors. The amount of overlap was determined by placing a 20 striped fluorescent target on the outside of the downcomer. By knowing the number of stripes on the target and comparing to the number of stripes in the images, the region that was overlapped could be determined and removed from of the downcomer images. The data from the lower mirror was used in the overlap region because it provided higher resolution imaging in that region.

When the laser beam strikes the dye in the downcomer gap, some of the laser is absorbed, and the dye emits light proportional to the average concentration contained in the volume illuminated by the laser. The fluorscope has several focusing optics designed to efficiently collect the light emitted by the fluorescent dye that is directed back along the path of the laser beam. The fluoroscope passes light collected from the downcomer through a 540 nm high pass optical filter to allow the emission of light by the Rhodamine 6G to pass while blocking background and laser light. The light is then focused onto a fiber optic and sent to the Photo Multiplier Tube (PMT) where the intensity of the light is

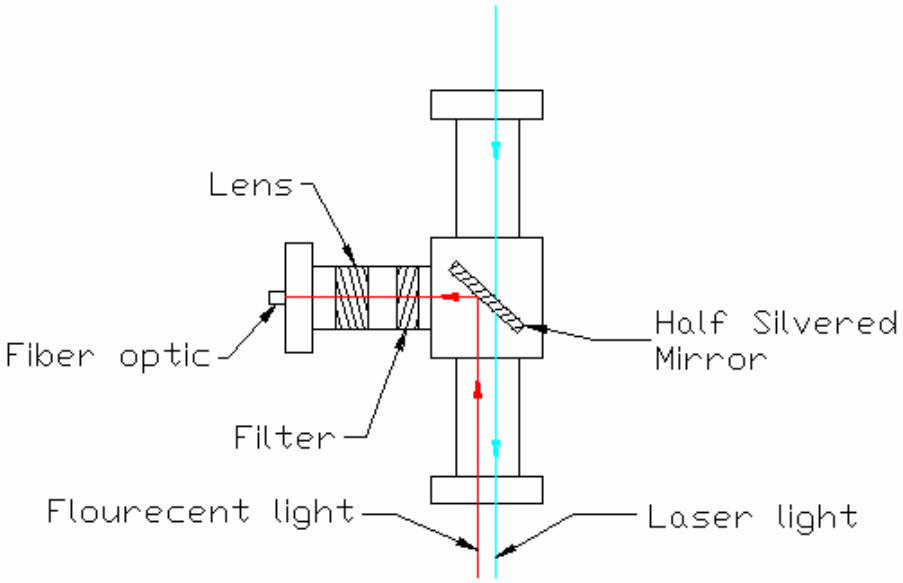

Figure 3.8: Details of 1-pixel fluorscope

converted into an output voltage; the output voltage is directly proportional to the amount of light received. A Hamamatsu 1477-06 PMT was selected for its low noise, high sensitivity, and quick response time.

For the entire flow field to be visualized, the complete optical assembly contained inside the vessel must rotate azimuthally during the experiment. To handle this challenge, the entire optical assembly was mounted on a Rollex bearing held in place by an extruded aluminum structure. All optics were rigidly mounted to a second extruded aluminum frame which rested inside the vessel supported by the bearing. A 4-wire slip ring was installed to facilitate the power requirements of the electronics rotating with the assembly. A Winsmith Maximizer 913 gear reducer and a Dayton variable speed electronic motor was used to spin the optical assembly through a belt drive system. While in operation, the rotating mirror would sweep the laser beam through the downcomer section in the Z direction while the whole optical assembly rotated azimuthally in the θ direction. This produces concentration measurements that are two-dimensional and averaged over the radial direction of the downcomer.

3.2.3 Downcomer and piping

The downcomer section was built using optically transparent Plexiglas. This allowed for non-intrusive flow visualization and measurement techniques such as Laser Induced Fluorescence to be utilized. A schematic of the system is shown in figure 3.9, and a detailed drawing of each component is given in appendix A. As seen in figure 3.9, clean water from the supply tanks is drawn down into the cold legs by the circulation pumps on each side and then split into two cold legs. The higher density salted water is injected into the cold legs through the HPI nozzles. The two fluid streams interact in the

cold legs and are swept into the downcomer section, then out the bottom of the downcomer to the return tanks. As mentioned in the beginning of chapter 3, the UMD facility was scaled to match the geometry of the Oregon State APEX-CE reactor with some minor experimental design changes to accommodate the optical instrumentation and testing procedures. Figure 3.10 shows a coolant flow diagram through the UMD downcomer and what the flow path would look like through an unmodified downcomer. In the prototype, coolant enters the downcomer from the cold legs, travels through the downcomer, flows up through the center of the vessel over the fuel rods, and then exits

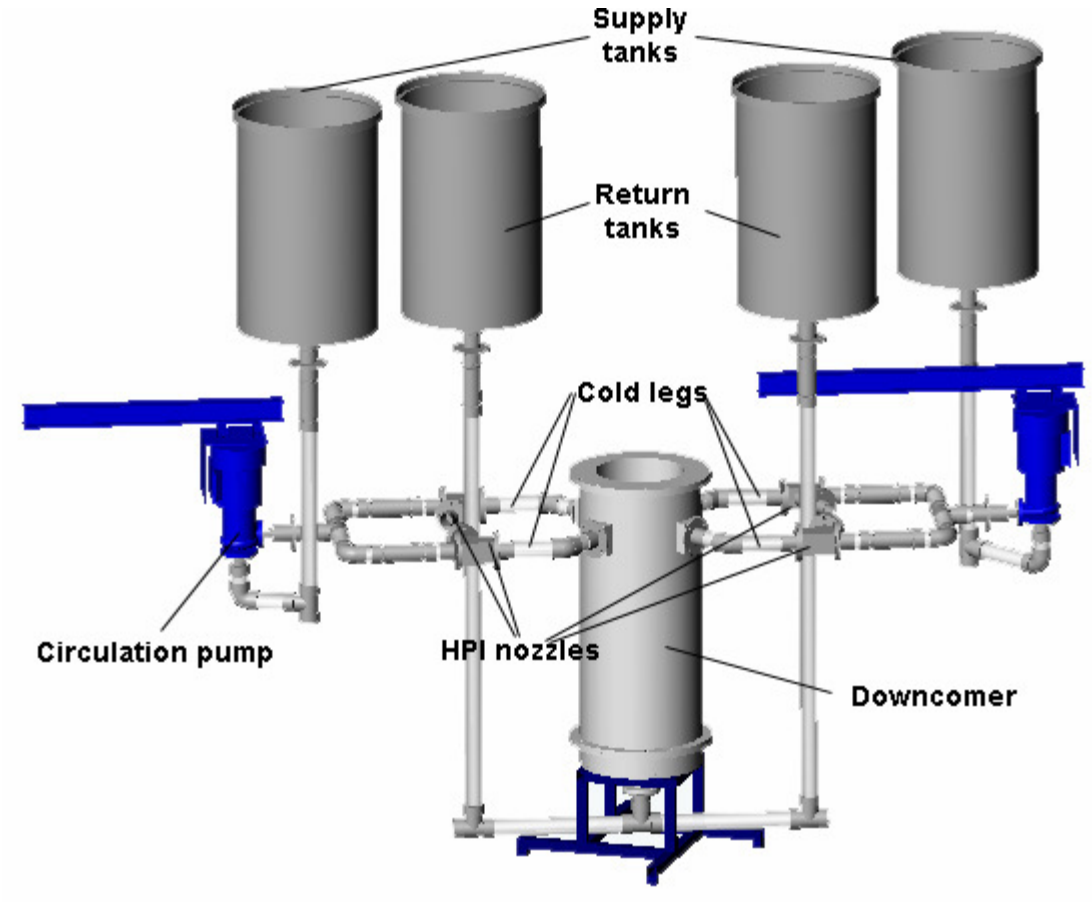

Figure 3.9: Scale drawing of UMD optical test facility, showing the supply/receiving tanks, cold leg circulation pumps, cold legs, HPI nozzles and acrylic test vessel Downcomer.

through the hot legs that protrude out of the vessel at approximately the same height as the cold legs. Since the buoyant plumes are of interest in the downcomer, the path of coolant flow was redirected to accommodate the placement of the optical assembly in the center of the vessel. In the UMD facility, the flow path exits the bottom of the vessel instead of through the center and out the hot legs. To minimize any adverse effects this might have in the downcomer region, the fluid at the bottom of the downcomer was directed upward through a perforated plate similar to the prototype and then directed out the bottom of the vessel. To keep the flow within the downcomer similar to the prototype, two artificial hot leg obstructions were constructed to simulate the pipes that travel from the core through the downcomer and out to the steam generators. To simulate the natural circulation in the full-scale loop, two (one on each side) Dayton variable speed 3hp centrifugal pumps were used. These pumps operated at various speeds to provide a specified flow rate in the cold legs. In the actual facility each cold leg is supplied by its own pump, where as in the UMD experiment the outlet of the circulation pump was sent to a tee junction, which supplied fluid to two cold legs. This allowed the use of only two circulation pumps to drive the flow in the UMD facility.

To simulate the High Pressure Injection (HPI) system, two Cole-Parmer Masterflex constant displacement pumps were used. The Masterflex pumps provide a constant flow rate, which is independent of the pressure on each side of the pumps when used within the specified operational characteristics of the pump. Two pump heads were mounted on each Masterflex pump so that four injection nozzles could be simulated using two pumps. The HPI injection nozzles were constructed in one of two different methods: one nozzle was made from transparent acrylic to allow for visualization and monitoring

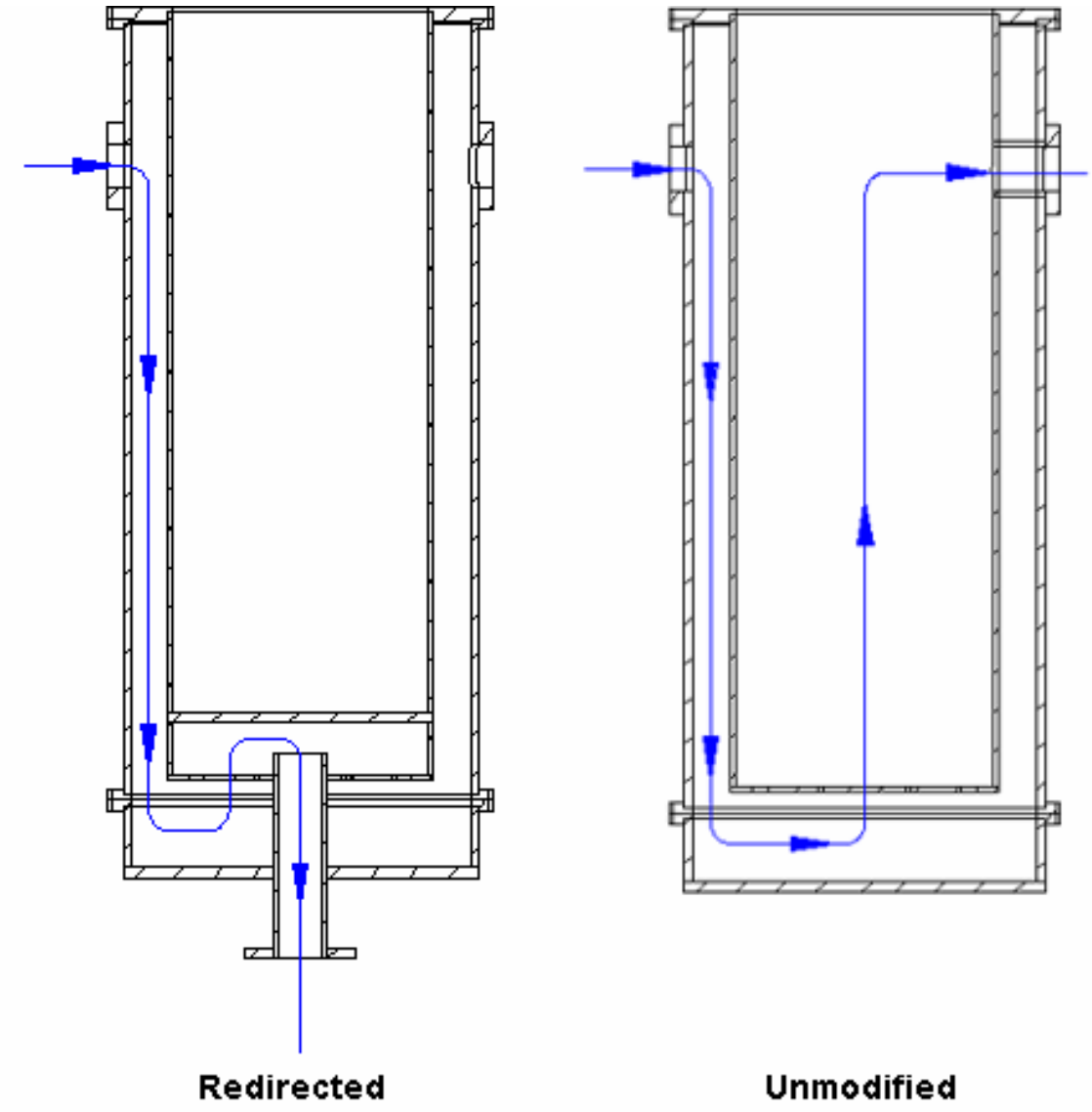

Figure 3.10: Coolant flow through the redirected UMD downcomer and flow through an unmodified downcomer

of the injection conditions (as shown in figure 3.11), while the other three nozzles were constructed from opaque Poly-Vinyl Chloride (PVC). For the transparent HPI nozzle, the flange and pipe inside the injection nozzle was constructed to accept different injection diameters to allow different Reynolds numbers of the incoming injected fluid. The injection leg was encased in a box of transparent acrylic that would be filled with water.

This allowed the mixing inside the pipe to be seen while minimizing the image distortion caused by the curvature of the transparent pipe and differences in the index of refraction between the surrounding air and the acrylic. The other three injection legs were constructed out of three inch PVC pipe to give the same injection characteristics as the acrylic leg without to need for transparency.

To contain sufficient water for the system, four (2 inlet and 2 exit) 100-gallon water tanks were used. Three-inch bulkhead fittings were used in the bottom of the tanks to allow entry and exit of the fluids. Three-inch ball valves were placed throughout the piping network to control the flow of water through the system, allowing for alternate flow paths if the test required it.

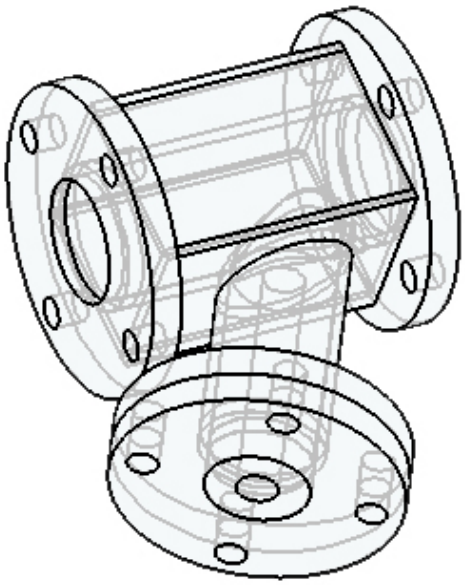

Figure 3.11: Transparent acrylic HPI nozzle

3.2.4 Line scan camera

To obtain the inlet concentration profile into the downcomer, a Dalsa 2048 pixel digital line scan camera measured the florescent dye concentration using the LIF technique in the cold leg just upstream of the downcomer. The camera was mounted onto a stationary tripod pointed at the cold leg, with a portion of the Ion-Argon laser beam traveling through the measurement volume to excite the dye molecules, see figure 3.12. A high pass filter was used to block out the light intensity from the laser beam and to capture the fluorescent light emitted from the dye. An acrylic viewing window was placed at the end of the cold leg (at the entrance to the downcomer) to allow optical measurements from the line scan camera in this region. The pipe entering the downcomer was cut from a solid acrylic square with a circular hole drilled through the center, this configuration minimizes optical distortion caused by changes in index of refraction along curved surfaces.

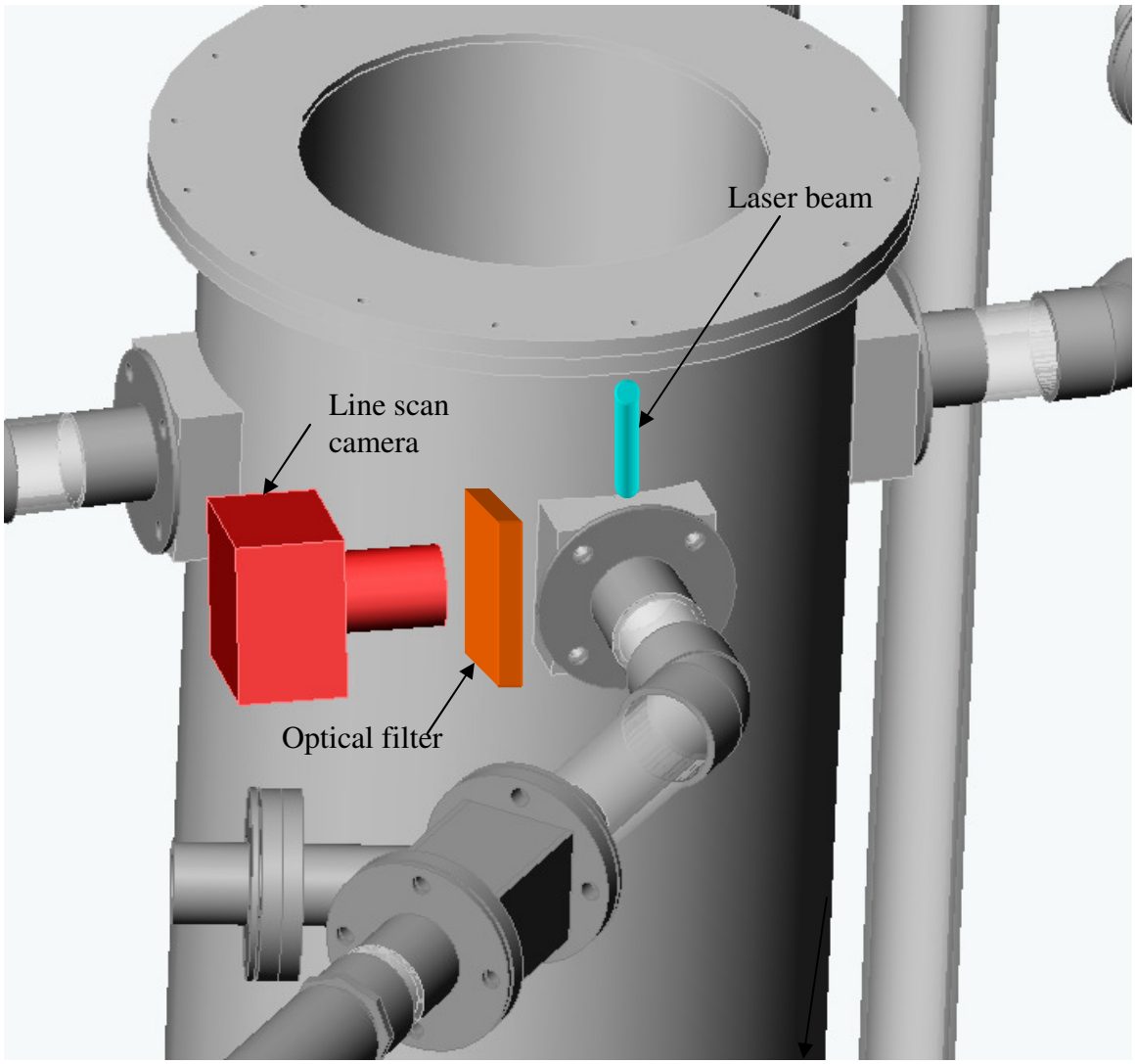

Figure 3.12: Line scan camera set-up

3.2.5 Data loggers

To simultaneously record the data from the multiple instruments used in the data acquisition system, two synchronized analog-to-digital (A/D) converter boards were used. This was done to accommodate the bandwidth requirements of the high-speed PMT data acquisition and the low speed acquisition from the other instruments. The signal from the Photo-Multiplier Tube must be sampled at a high frequency to obtain the data necessary to recreate high resolution two-dimensional images of the flow field as it

evolves in time. The higher the scan rate, the more points that are captured to describe the concentration in the downcomer. The PMT is also sampled by both the high speed and low speed A/D boards. It was found that there was a significant non-constant delay between the start of the data acquisition for each board. To synchronize the two data streams, the PMT was sampled by both data logging boards and cross-correlated during post processing. In order to minimize the delay between the start of the acquisition computers, the computer used for low-speed data acquisition was configured to output a trigger signal when it received a manual input from the experimentalist to start acquisition. The computer used for high-speed data acquisition would start recording data when the trigger signal was received.

One computer was dedicated to sampling the PMT signal at a high sampling rate while the other was sampling the slower changing output from the pressure transducers and pumps. The first analog to digital converter was a Computerboads model CIO-DAS16/M1 board, which was used exclusively for sampling the PMT at 250,000 Hz; the second analog to digital converter was model PCI-MIO-16E-1 built by National Instruments, which sampled the slower quantities on multiple channels. Labview software was used to control the converters and output the data to a binary file. Since the plumes in the downcomer are highly dependent on the inlet pipe conditions, pressure transducers were placed on each of the supply tanks to measure the hydrostatic pressure as it varied during the experiment; the hydrostatic pressure measurements can be used to monitor the amount of fluid in the tank and hence provide the flow rate of supply water out of the supply tank. The flow rate of the salted high-density HPI injection water was controlled and recorded directly by the Labview program. The constant displacement

pumps used for injecting the salted water simultaneously provide a voltage signal that is comparable to the flow rate; this signal was recorded by the slow A/D board to monitor the flow rate and assure that it matched the specified flow rate.

3.2.6 Data processing

The goals of the data processing were to evaluate different parameters in the experiment and reconstruct quantitative spatial concentration maps produced by the turbulent plumes. The data recorded by the data loggers was manipulated by Matlab programs under the 7.2 SUSE Linux environment in the Computational Processing Lab to formulate the quantities of interest. To process the massive about of data recorded from a single test (approximately 1 gigabyte for a single 300 second test), the data files had to be processed in smaller pieces which could be handled by the available amount of computer memory.

First, the processing computer had to synchronize the two data files; the slow-sampled circulation pump speed, the HPI pump flow rate, and the hydrostatic pressures from the inlet tanks along with the high-speed sampling of the PMT. Since the computers have some delay between the time that they initiated data acquisition, each file was searched and cross correlated by comparing three consecutive points in the slower data file with the same three points in time in the faster data file. The data files were correlated by looking for the largest cross-correlation coefficient between the points in the files. When the largest correlation was found, it was taken to be the beginning of each data file. To smooth the signal and remove some of the high frequency noise from the PMT, a 9 point median filter technique was employed. After filtering, the computer searched the data to find specific geometric markers placed inside the downcomer to

indicate when the optical assembly had completed a full revolution. On the interior of the downcomer vessel a small 1" x 1" patch of dyed cloth was taped to the inside on one of the fake hot legs. By placing the patch over one of the fake hot legs, the patch acted as a marker indicating when the assembly rotated through one complete revolution. The revolution detection was done offline after the complete set of data was collected. By placing the patch over an area where there is no dye was present, it created a unique marker which could be found in each rotation.

The code then split the data into discrete revolutions, numbering them from one to the last revolution recorded by that test. Prior to each test, the optical assembly was aligned, and a calibration revolution was performed using a 0.1 ppm dye concentration. The concentration level corresponds to the 100% concentration level in the tests and was used during post processing to properly normalize the test data. The LIF measurements are affected by geometry, measurement length across the downcomer gap, incident angle of light on the acrylic, and length from fluorescent emission to the fluorscope. Because these effects are a function of position in the downcomer, each data point in the downcomer requires it's own calibration as a function of position; a calibration sweep containing all the measurement points of the entire downcomer was necessary. By comparing the concentration test data to a calibrated concentration at the same geometric location in the downcomer, the geometric effects that change the LIF measurements could be cancelled out of the measurements. Equation 3.7 was used to extract a normalized concentration value for each point:

$$\frac{C}{C_0} = \frac{v - v_b}{v_0 - v_b} \qquad \textbf{Equation 3.7}$$

Where C/C_0 is the normalized concentration, v is the voltage recorded during a test, v_b is the background voltage taken from the first revolution in the test before the dyed fluid entered the downcomer, and v_0 is the voltage recorded from the downcomer filled with dye during the calibration. Equation 3.7 was applied to each point in the downcomer individually and not as a global average. Before the test data was normalized, it was linearly interpolated to a size equal to the first revolution, so that it could be normalized using the same number of points at the same location for every revolution. In the Z direction, the number of points describing each vertical slice was not consistent owing to slight variations in the speed of the rotating mirror. The largest observed variation in the number of points in the Z direction was 0.4%. To normalize the raw data, the vertical slices were interpolated onto the same grid. The number of points in the azimuthal direction varied by a maximum of 2% between the initial calibration revolution and the subsequent test data revolutions. The 2% variation is an indication that the revolution speed of the entire assembly was not constant, however it was assumed that this variation was caused by the control feedback loop of the motor trying to keep the assembly rotating at a near constant speed. The variations in speed happened over a longer time than the time to measure one revolution of the downcomer. So the speed for each revolution was assumed constant for that revolution and the test data was interpolated to match the size of the calibration revolution.

The measurement points along the vertical direction of the downcomer are not evenly spaced due to the geometry of the optical assembly, so a relationship between the pixel and its spatial location was developed to obtain the spatial position of each measurement. This was obtained separately by placing 2.54 cm wide markers spaced

2.54 cm apart on the outside of the far wall of the downcomer spanning the entire Z direction. This functional relationship is necessary to correlate the position of each pixel to a spatial location. Minor realignment of the optics seemed to have no effect on the vertical spacing of the points. Key features within the geometry (such as the fake hot legs and cold legs) always appeared at the same location in the data files within .25 cm.

3.3 Experimental test conditions

The experimental test matrix shown in table 3.2 was constructed to produce stratification in the cold legs at varying Froude numbers spanning the range of interest concerning PTS under natural circulation conditions. The HPI flow rate of 1.5 GPM with one and four plumes were chosen in order to provide conditions that could be compared with the work accomplished at OSU. The cold leg flow rate in the cold legs was changed in order to vary the cold-leg Froude number, while the initial density difference between the fluid streams was constant. The upper bound of interest for the Froude number is when there is no stratified flow in the cold legs (fully mixed condition), which would produce significantly less thermal stress along the walls of the downcomer than the stratified cold leg conditions.

Case	HPI Flow Rate (GPM)	# Plumes	Cold leg circulation flow Rate (GPM per leg)	Salt Sg	Fr:=ΔU(gD(Δp/p))^-.5 (equation 2.4)
SP1	1.5	1	0	1.176	0.161
SP2	1.5	1	2.42	1.176	0.080
SP3	1.5	1	3.75	1.176	0.077
SP4	1.5	1	6.77	1.176	0.038
SP5	1.5	1	10.78	1.176	0.186
SP6	1.5	1	14.7	1.176	0.245
MP1	1.5	4	0	1.176	0.161
MP2	1.5	4	2.1	1.176	0.099
MP3	1.5	4	3.1	1.176	0.022
MP4	1.5	4	6	1.176	0.054
MP5	1.5	4	10.2	1.176	0.177

Table 3.2: Test matrix with operational conditions for each test.

3.4 Experimental uncertainty

There are several possible sources of uncertainty encountered in the experiments. First, the technique employed for flow visualization gives a 2 dimensional representation of a 3 dimensional phenomenon. The concentration in the downcomer was inherently averaged over the (approximate) radial direction by the experimental technique, so some of the detailed structure of the plumes and the entire flow field are lost. In examining the visualization of the plumes, careful attention must be given in extracting flow characteristics from these 2 dimensional images. For instance, fluid motions out of the viewing plane can not be seen, only their results in changing the average radial concentration can be detected.

By using a non-intrusive optical measurement method, the optical quality and optical properties of the observation mediums has an effect on the measurement, resulting in a non-uniform voltage output for a given uniform concentration. Fortunately, by filling the vessel with 100% dye concentration (.1ppm) before the actual test and using that as a calibration reference, optical properties such as optical quality and geometry remain the same between the calibration and the test. This is an advantage as the effects of these phenomena on the measurements cancel out through the normalization. However, errors can occur in the measurements because of vibrations in the optical assembly which alter the path of the beam and speed variance in the motors responsible for sweeping the laser beam through the downcomer. To estimate this error, each of the calibration sweeps with the downcomer full of 100% concentration fluid were compared. A total of 102 revolutions were compared by taking the RMS of the PMT voltage at each location in space. The results showed that the RMS had a no noticeable dependence on

the θ direction, but showed significant dependence on the location in the Z direction. Since the RMS was only dependant on the Z direction, each of the 102 revolutions was averaged over the azimuthal scan direction to gain an ensemble of more than 50,000 vertical sweeps for estimation of the error. Figure 3.13 shows the RMS of the ensemble of vertical sweeps, since the concentration of dye was constant, this is a representation of the absolute error due to the optical and motive assemblies. For some of the cases which have a low concentration in the downcomer (about 10%), this error is significant and reduces the measurement a more qualitative representation of the concentration.

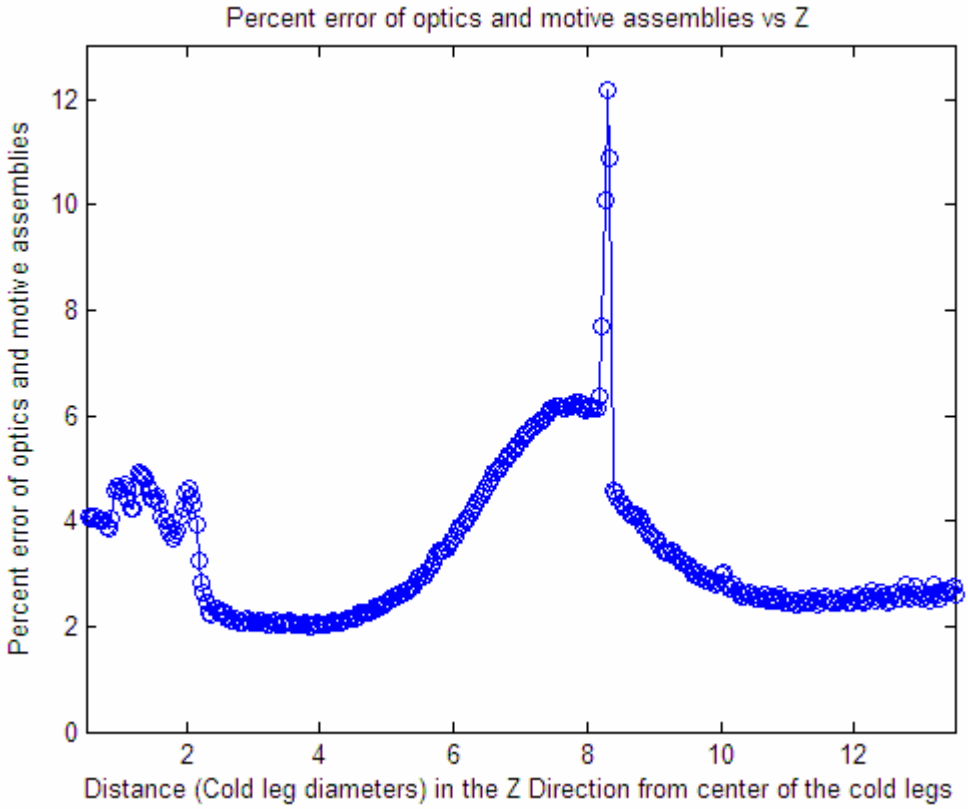

Figure 3.13: Absolute percent error for optics and motor control assemblies

During the tests, the plumes are present in the downcomer whereas in the calibration they are not. As seen previously in figure 3.5, the plume has a slightly different index of refraction than the water used in the calibration (approximately 2%).

By having a difference in index of refraction, the path that the laser beam travels is slightly different then the path in the calibration. This alteration in path changes the path length in equation 3.6, thus inducing an error in the measurement of concentration. Figure 3.14 shows a situation where the incoming laser beam hits an interface between the salted water and the unsalted water in the downcomer and the trajectory of the laser beam is altered resulting in a longer path length. Θ_3 is the angle of the incoming laser beam from the interior optics with respect to the radius of the downcomer, Θ_1 is the angle between the incoming laser beam and the surface normal of the interface, and Θ_2 is the angle between the refracted laser beam and the normal of the interface. Using this geometry, Figure 3.15 is a plot of the percent difference in path length vs Θ_1 with the different color curves representing different incoming laser beam angles Θ_3. A change in path length is directly proportional to the difference in laser intensity received from the measurement, so a 3% increase in path length equates to a 3% larger value for the concentration in the downcomer according to equation 3.6. The curves in figure 3.15 were constructed by taking the percent difference in path length between a laser beam which passed through pure water versus a laser beam which passed through the salted fluid at 100% salt concentration used in the experiments. The error estimate used an interface placed at the interior wall of the downcomer, which should yield the largest possible deviation from the calibration. The maximum incoming angle for the laser is 15 degrees, which corresponds to the largest error of 7.5% from this phenomenon. The plots in figure 3.15 also assume that there is only one interface between the two fluids, if a second interface is allowed in the calculation (so that the laser beam goes from water to salted water back to water), the error can reach a maximum possible value of 23%. These

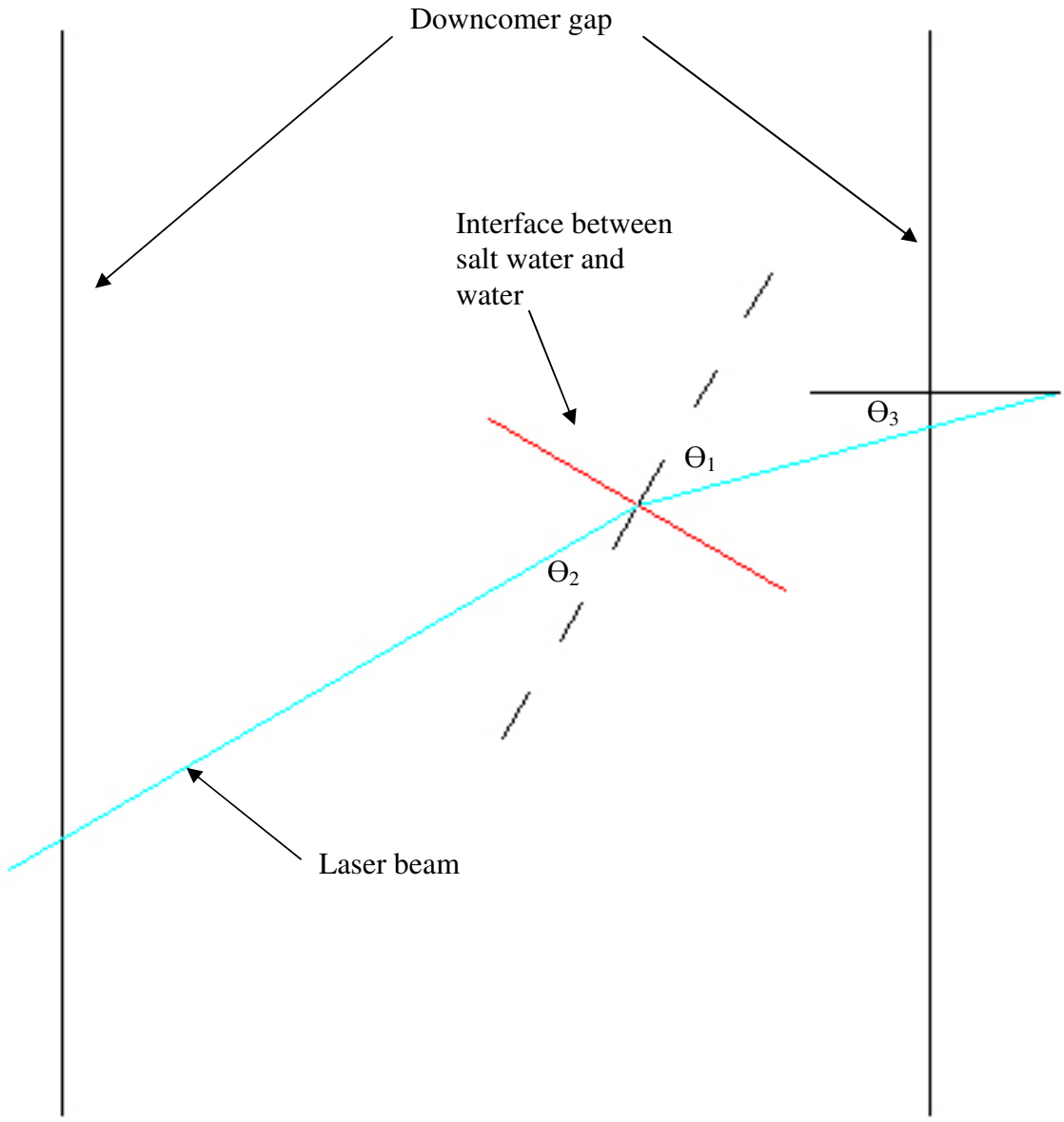

Figure 3.14 : Laser beam path change from index of refraction effects

errors are only possible when the incoming angle of the laser beam (Θ_3) is large, which occurs in the bottom portion of the downcomer. To minimize this error, the fluorescent dye was placed into the injected salted fluid instead of the background water to minimize the path length. Since the background water makes up most of the fluid in the

downcomer, if the path length of the beam is altered from changes in index of refraction then the increase in intensity is minimal since the majority of the fluid has no dye present.

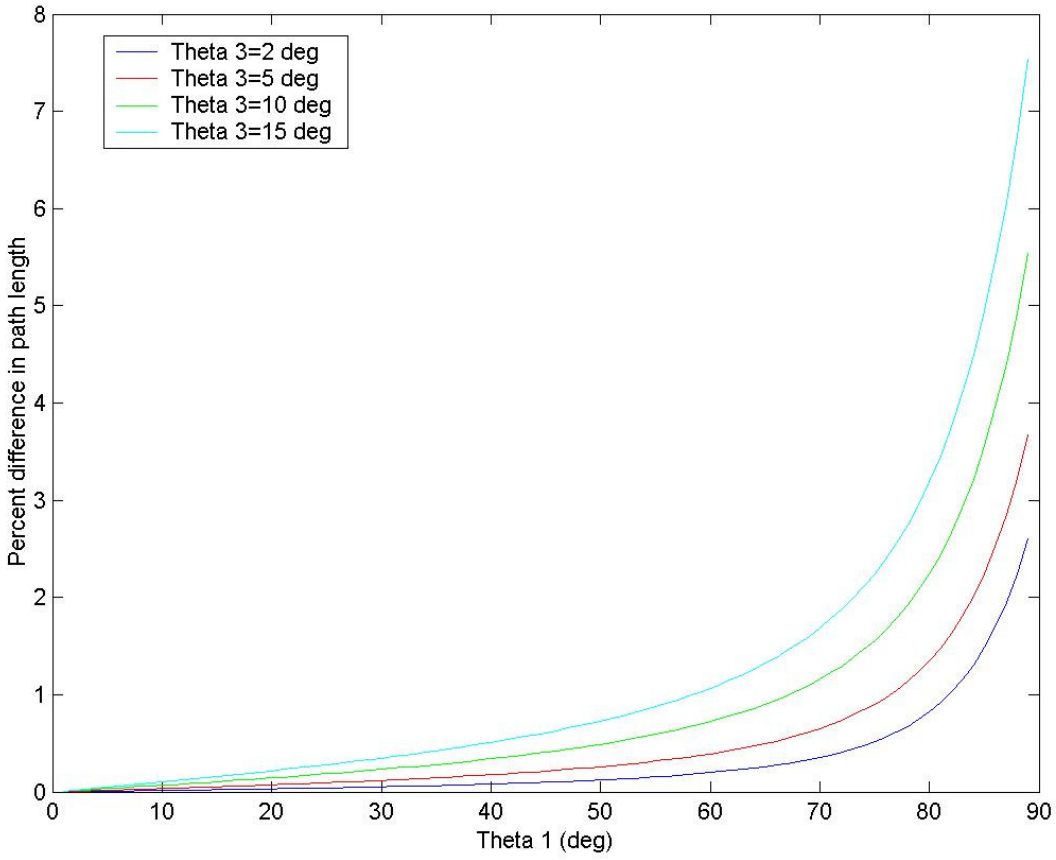

Figure 3.15: Percent difference in path length vs Θ_1

There are a few possible systematic errors in the experiments. For every calibration sweep and test case, the total volume of fluid in the entire system and the injection tanks must be known so that the appropriate about of dye could be added. For the calibration sweep, dye was added to the inlet tanks filled with pure water to reach a concentration of .1 ppm, while for the test cases dye was added to the injection tanks with salted water to reach a concentration of .13 ppm. In the salted water solution, .13ppm dye concentration gave the same voltage on the PMT as pure water with .1 ppm of dye.

This was determined using a small calibration chamber, which illuminated a laser beam through a small volume of dyed liquid. First, pure water with .1 ppm dye concentration was placed in the calibration chamber, the output voltage on the PMT was recorded. The water was replaced with salted water with a specific gravity of 1.176 (the value used in the experiments). Dye was slowly added and mixed into the chamber until the voltage of the pure water with .1 ppm dye was achieved. The accuracy of measuring the amount of dye required for the experiment was estimated to be 2%, with 2% corresponding to the distance between graduations for the volume of dye used in the experiments. A 2% bias in dye added to the inlet tanks would correspond to a 2% change in the measured concentration in the downcomer. This error applies to mixing the dye for the calibration sweep and mixing a separate batch of dye for the actual test.

By examining all of these sources of error, the optical and motive assemblies seem to be the largest contributor to the overall system error. To calculate the overall system error, the square root of the sum of the squares of each error source was taken to yield the error curve in figure 3.16. The shape of the error curve is similar to the shape of the curve for the optical and motive assemblies in figure 3.13. This is no surprise since those assemblies seem to produce the largest source of error. A systematic error of 2% for mixing the exact quantity of dye, a 1.5% error for index of refraction changes in path length, and the curve in figure 3.13 where used to produce the curve in figure 3.16. 1.5% was used as a conservative estimation for the maximum deviations in path length as seen in the downcomer, from figure 3.15. Since this was the smallest error reported, it had the smallest effect on the overall system error. It can be seen from figure 3.16 that the middle of the downcomer yielded the largest percent error. The sharp spike around 8.3

cold leg diameters is where the laser beam transitions between mirrors. Note that this error is an absolute error, which is in reference to 100% concentration.

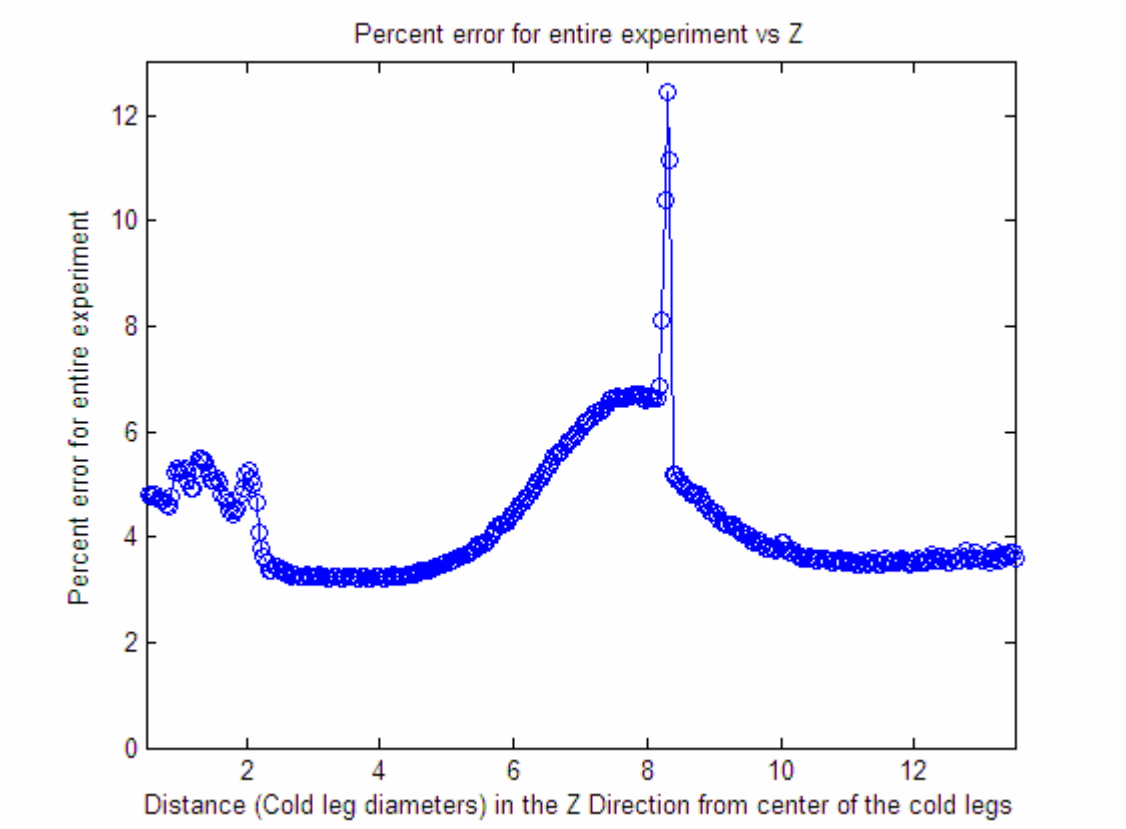

Figure 3.16: Total absolute experimental error verses Z

Chapter 4: Results and Discussion

4.1 Inlet conditions (HPI and cold legs)

The line-scan camera data was used to extract the inlet concentration profile history in one of the cold legs, just upstream of the downcomer section. From the camera data, it was determined which Froude number cases were still stratified and which ones exhibited significant mixing in the cold legs. The Froude number for the stratified cases were calculated using equation 2.4, where D*U was estimated by extracting the height occupied by each stream. A cut-off threshold of 50% in intensity between the maximum and minimum concentrations in the pipe was considered the boundary between the two layers. Using the height of each layer from the linescan camera, the diameter of the circular pipe, and the known flow rates, a bulk velocity of each layer was computed and used in equation 2.4. This approach doesn't work for the well-mixed conditions inside the cold leg because there are no longer two different fluid streams. For those cases, a traditional Froude number was used for the well-mixed cases, as given by equation 4.1:

$$Fr = \frac{U}{\sqrt{g * D}} \qquad \textbf{Equation 4.1}$$

Where U is the Bulk velocity of the well-mixed fluid, g is the acceleration of gravity, and D is the diameter of the cold leg. Figures 4.1 through 4.6 show the percent concentration at the entrance to the downcomer versus distance from the center of the pipe obtained from the line scan camera. The plots are in order of increasing Fr for the single and multiple plume cases. Due to step-up and calibration errors, accurate cold leg concentration data was not acquired for all cases.

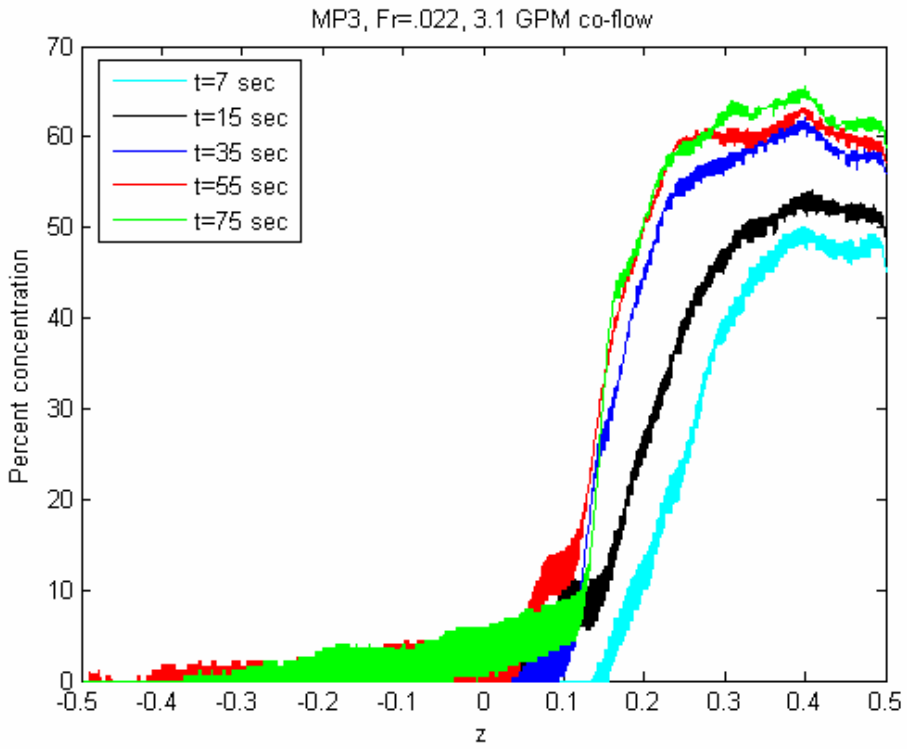

Figure 4.1: % Concentration verses distance from inlet center for MP3, Fr=.022 at times t=7, 15, 35, 55, and 75 seconds

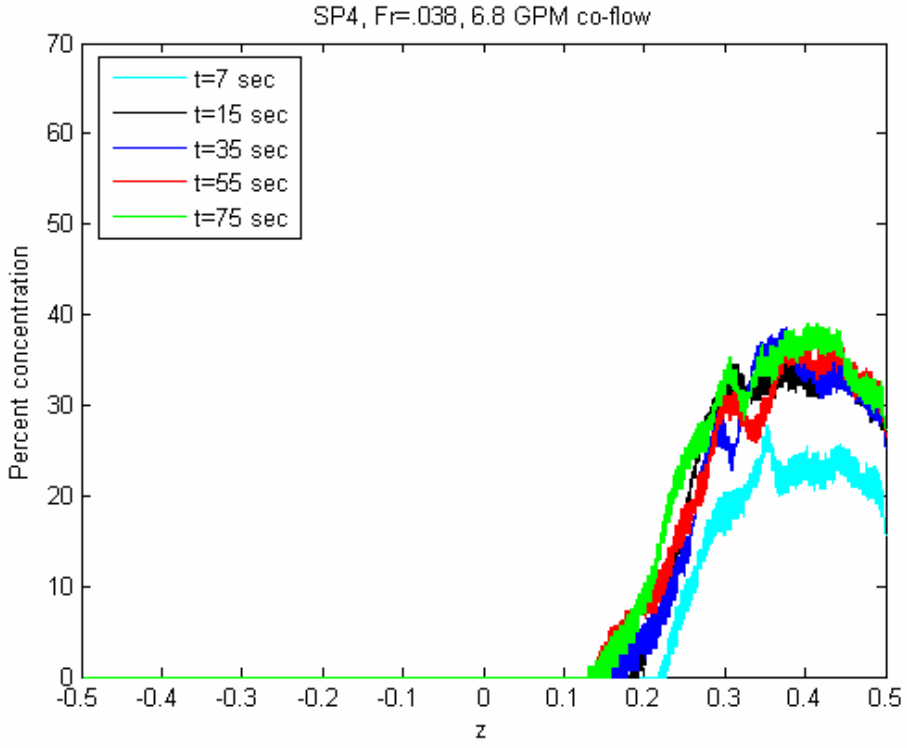

Figure 4.2: % Concentration verses distance from inlet center for SP4, Fr=.038 at times t=7, 15, 35, 55, and 75 seconds

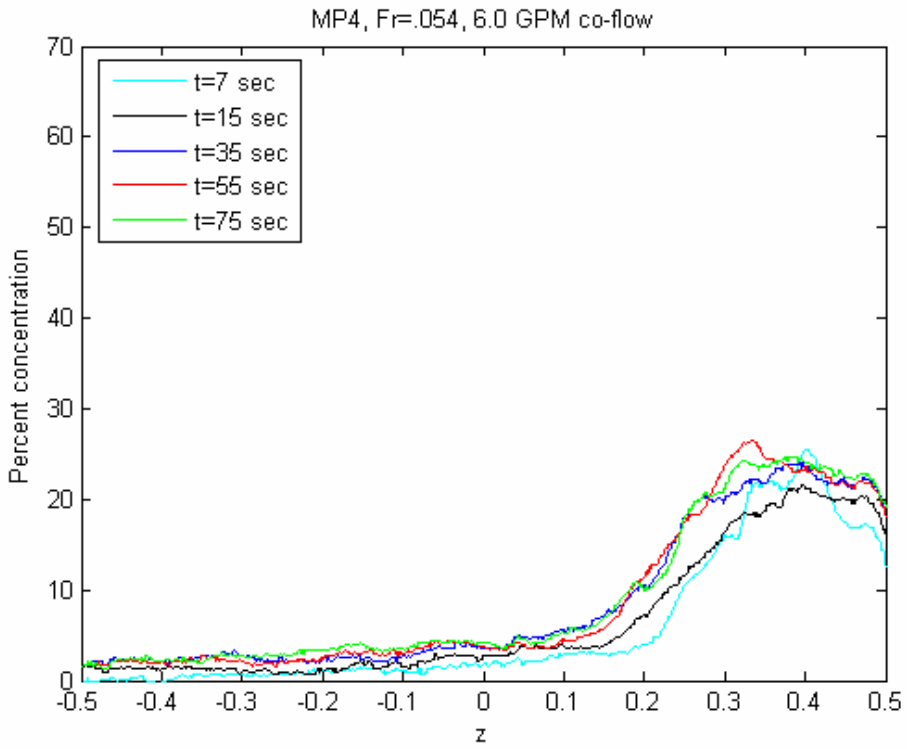

Figure 4.3: % Concentration verses distance from inlet center for MP4, Fr=.054 at times t=7, 15, 35, 55, and 75 seconds

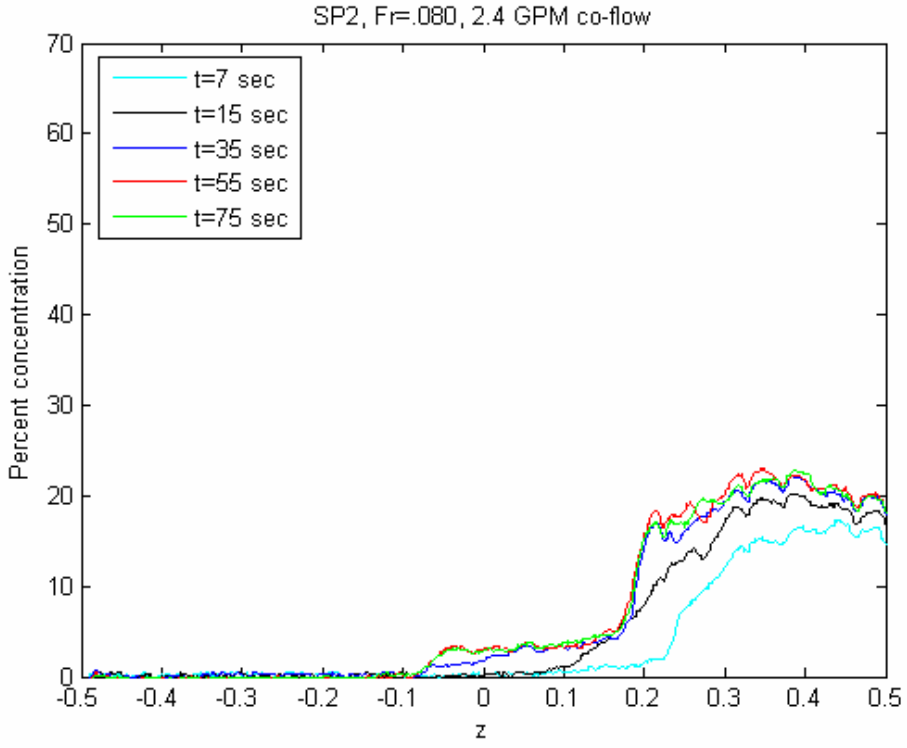

Figure 4.4: % Concentration verses distance from inlet center for SP2, Fr=.080 at times t=7, 15, 35, 55, and 75 seconds

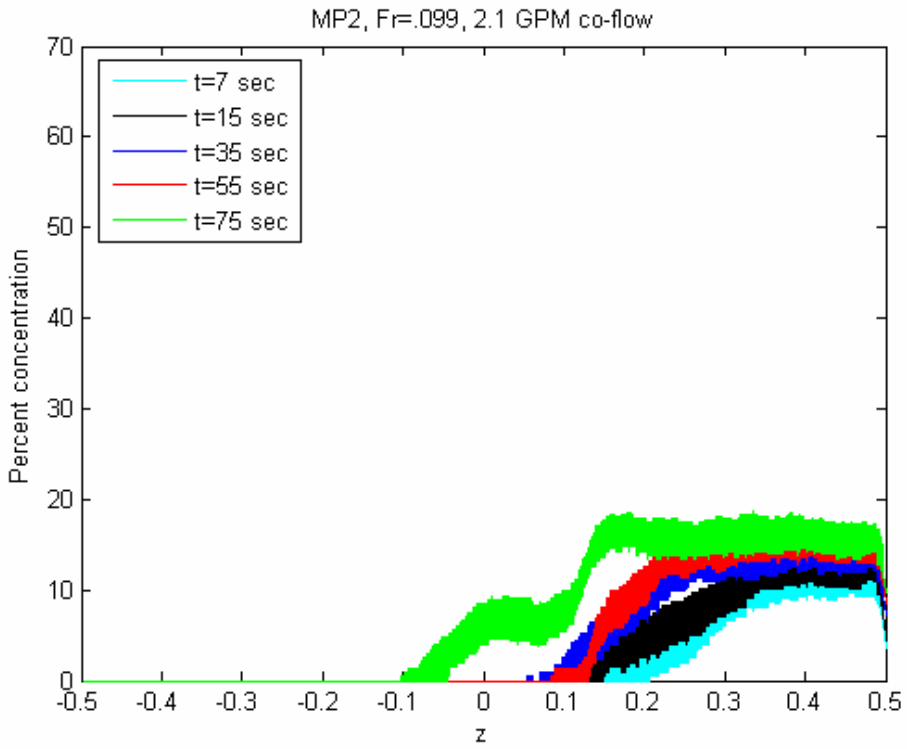

Figure 4.5: % Concentration verses distance from inlet center for MP2, Fr=.099 at times t=7, 15, 35, 55, and 75 seconds

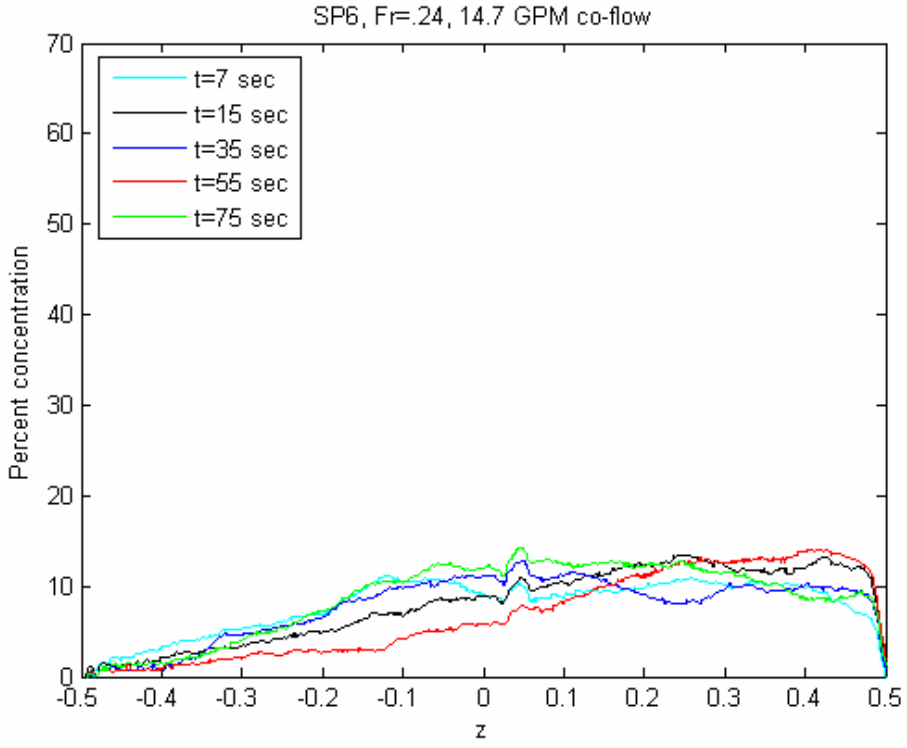

Figure 4.6: % Concentration verses distance from inlet center for SP6, Fr=.24 at times t=7, 15, 35, 55, and 75 seconds

Interesting to note is the shape and position of the stratification. In all the cases with Fr < 0.18, the cold legs remained significantly stratified, while the other cases were observed visually (and through the camera data) to be experiencing turbulent mixing. This can be seen from the relatively uniform concentration across most of the cold leg in figures 4.6, while figures 4.1 through 4.5 show a clear and rapid decrease in concentration at a specific height in the cold leg. Also note the fluorescent intensity as the Froude number is increased. For the lower Froude numbers, the fluorescent intensity is large, and as the Froude number is increased, the maximum concentration of dye seen at the inlet to the downcomer is decreased. This is an indication of increased mixing across the interface of the two fluids as the Froude number is increased, which is most likely occurring from increased shearing at the point of injection. It is important to understand from this data that the value of the Froude number in the cold legs directly affects the concentration of fluid before it enters the downcomer, which changes the buoyancy of the plumes.

For all cases, the fluorescence intensity appears to be increasing with time. This increase is due to the filling of the cold legs with the injected fluid and the gradually changing conditions in the downcomer. As seen in the figures above, the concentration profiles are generally increasing in intensity as time increases. This increase in concentration primarily occurs from the cold legs filling and reaching a quasi steady state condition. When the injection is started, some of the injected fluid mixes with the surrounding fluid in the cold leg, and the rest of the fluid settles on the bottom of the cold leg. As more fluid is injected, the cold leg begins to fill with injected fluid and the injected fluid flows in both directions (upstream and downstream) of the injection orifice.

The injected fluid travels upstream until it contacts the weir wall in the cold leg. The injected fluid in the cold leg then continues to fill the leg and reaches a steady state height. This cold leg filling transient time seems to be on the order of 30 seconds, as can be seen from the fact that the concentration profiles in the cold legs remain similar for most cases from 35 to 75 seconds (see figures 4.1 to 4.4).

4.2 Downcomer

As the injected fluid enters the downcomer section, it forms a plume and mixes with the surrounding fluid, causing the average density in the downcomer to slowly rise in time. Figure 4.7 shows the increase in concentration with time for a low Froude number case (all other cases showed similar treads). The plot in figure 4.7 is generated from the average concentration values taken from a vertical averaging region for each revolution. The averaging region was located on approximately the opposite side of the downcomer from where the plume enters the downcomer. Note that the increase in concentration is approximately 5% increase over 80 seconds, but is a concern when comparing data spanning over long times where this trend may play a role. Note that in figure 4.4, that the concentration in the cold leg for SP2 is 20%. At 120 seconds the background concentration is half of the incoming concentration. This means the net buoyancy force between the plume and the surrounding fluid at 120 seconds has been reduced to half of its initial value.

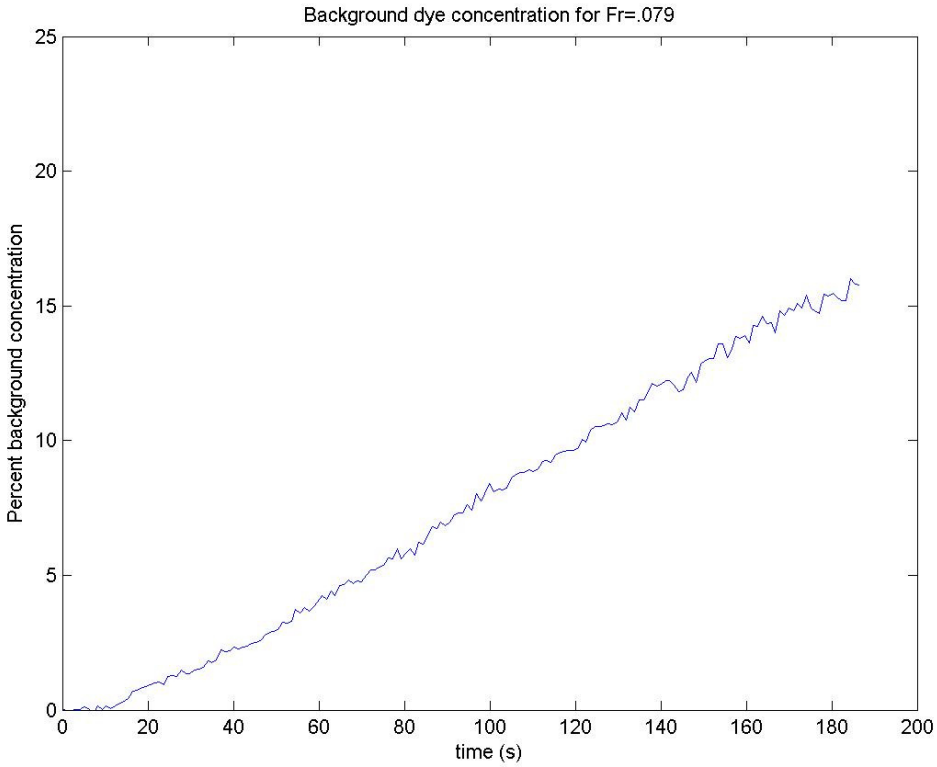

Figure 4.7: Downcomer background concentration over duration of test. Test conditions correspond to case SP2.

4.2.1 Turbulent plumes from a single leg

There are many interesting phenomena encountered in the visualization of the single leg turbulent plumes (see figure 4.8). The figure is a filled contour plot of the percent concentration of scalar dye in the downcomer at each azimuthal and axial position. It can be seen that the single plume enters the downcomer from the cold leg with diminishing concentration as the plume progresses downward and spreads.

The effect of large scale structures on each side of the plume can be seen by the wavy interface between the plume and the surrounding fluid. The following sequence of images in figures 4.9 through 4.17 show that the single plume falls into the downcomer with the centerline of the plume predominantly along the vertical direction. The plume

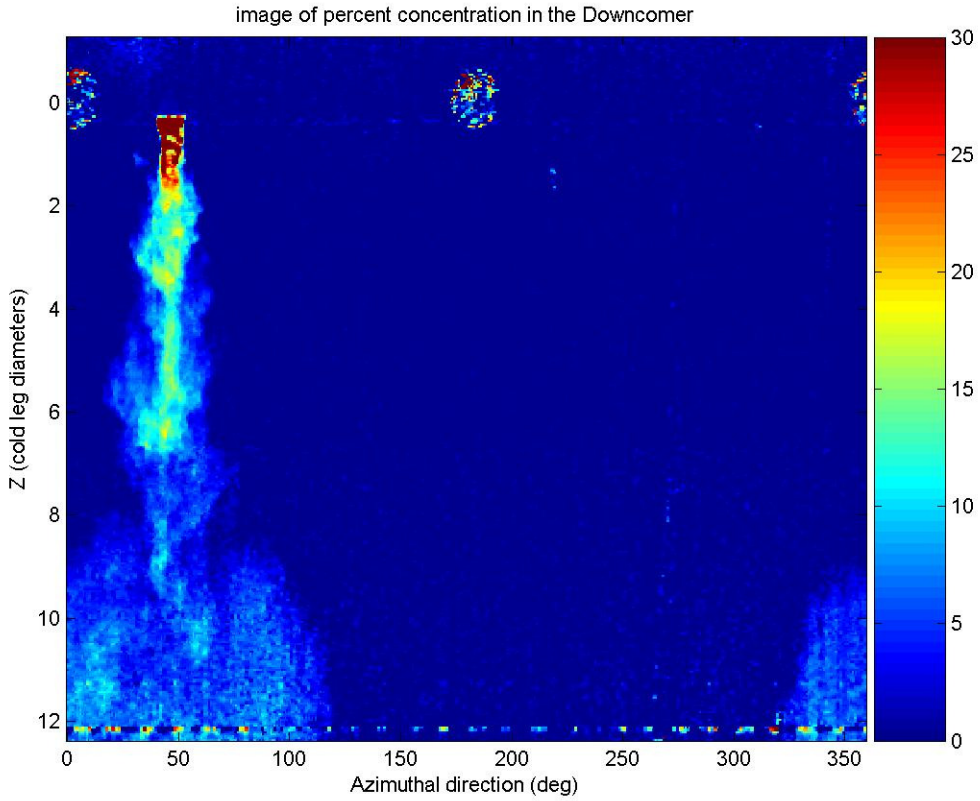

Figure 4.8: Filled contour plot of the normalized concentration of SP1 at t=10 sec

remains approximately vertical with some very small movement back and forth, likely due to the vortical structures on the sides of the plume. All of the single plume cases exhibit the same characteristic of falling predominantly along the vertical direction. The only significant difference between the cases is the higher cold leg flow rates caused the intensity of the incoming plume to decrease because of the increased mixing in MR1. The different intensities of the plumes had effects on the mixing behavior in the downcomer.

Figures 4.15 through 4.17 document the process by which the background intensity in the downcomer started to rise. At t=10 seconds, the downcomer is almost entirely filled with un-salted water, with a concentration around 0. But as time

progressed, the heavy salted fluid begins to settle around the bottom of the downcomer. Around 35 seconds after plume entry, a pocket of lightly salted fluid is seen growing and filling the downcomer from the bottom upward as more highly concentrated salted fluid continues to spill into the downcomer from the cold leg, indicating incomplete mixing with the pre-existing fluid.

Another important observation in the single plume cases is the presence of a small recirculation within the downcomer. A t=25 and t=35 (figures 4.15 and 4.16), there is a small mushroom-shaped cloud of salted fluid that slowly rises from the lower plenum, with the peak of the cloud approximately 180 degrees from the cold leg (local fluid motion is qualitatively indicated by the red arrows). The concave downward mushroom shaped cloud indicates an upward velocity around the peak of the cloud.

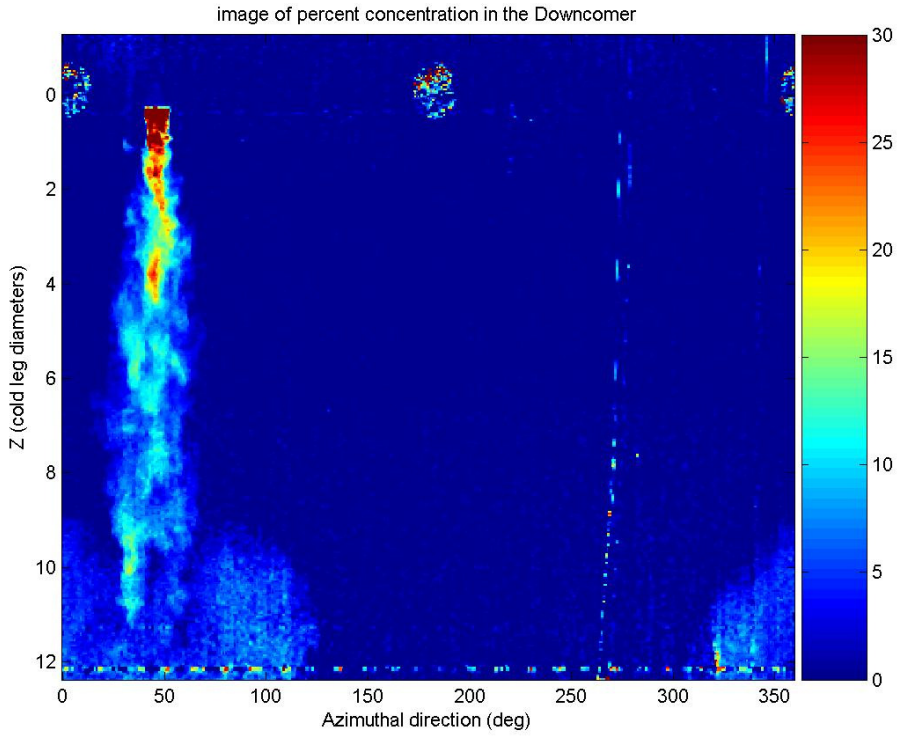

Figure 4.8: Filled contour plot of concentration in the downcomer for SP1 at 11 seconds

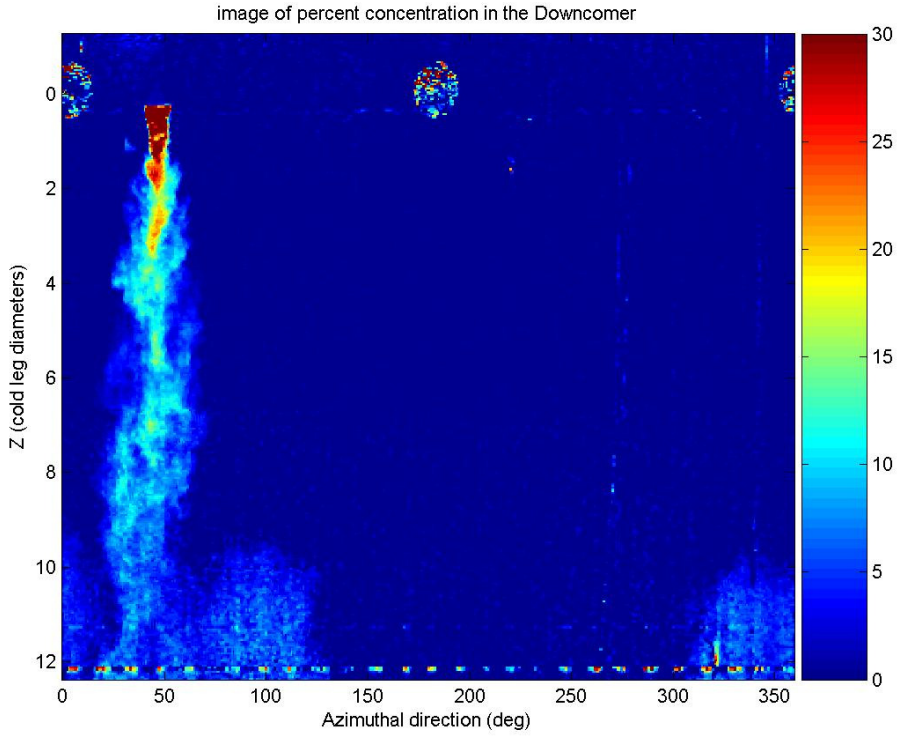

Figure 4.9: Filled contour plot of concentration in the downcomer for SP1 at 12 seconds

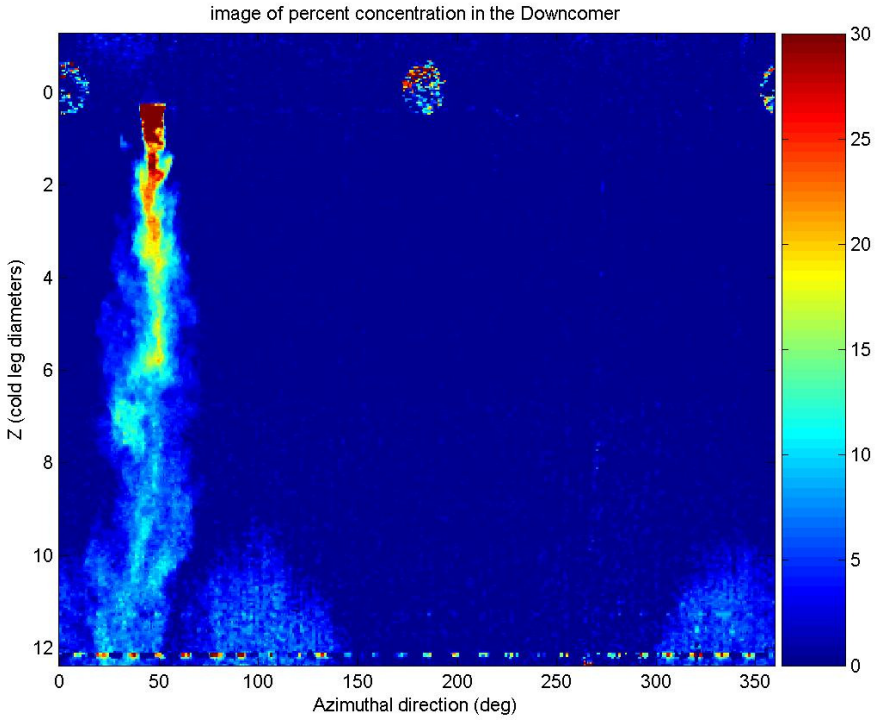

Figure 4.10: Filled contour plot of concentration in the downcomer for SP1 at 13 seconds

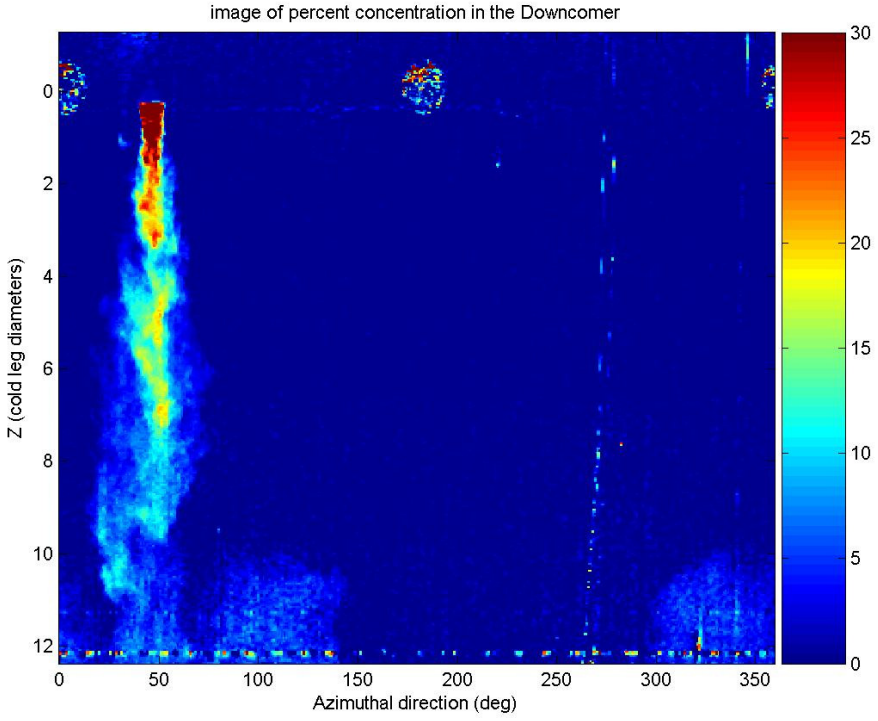

Figure 4.11: Filled contour plot of concentration in the downcomer for SP1 at 14 seconds

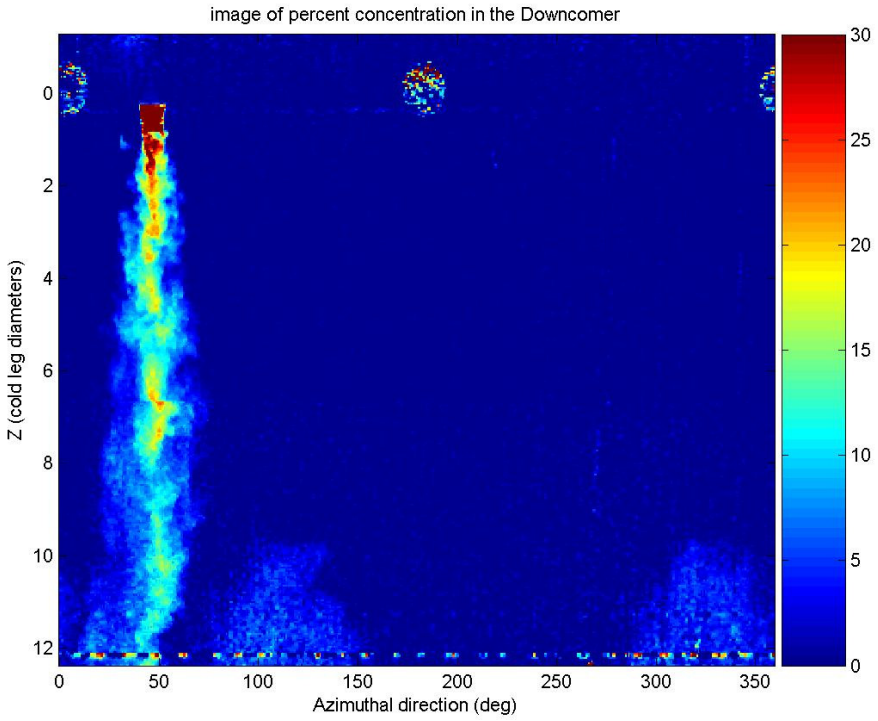

Figure 4.12: Filled contour plot of concentration in the downcomer for SP1 at 15 seconds

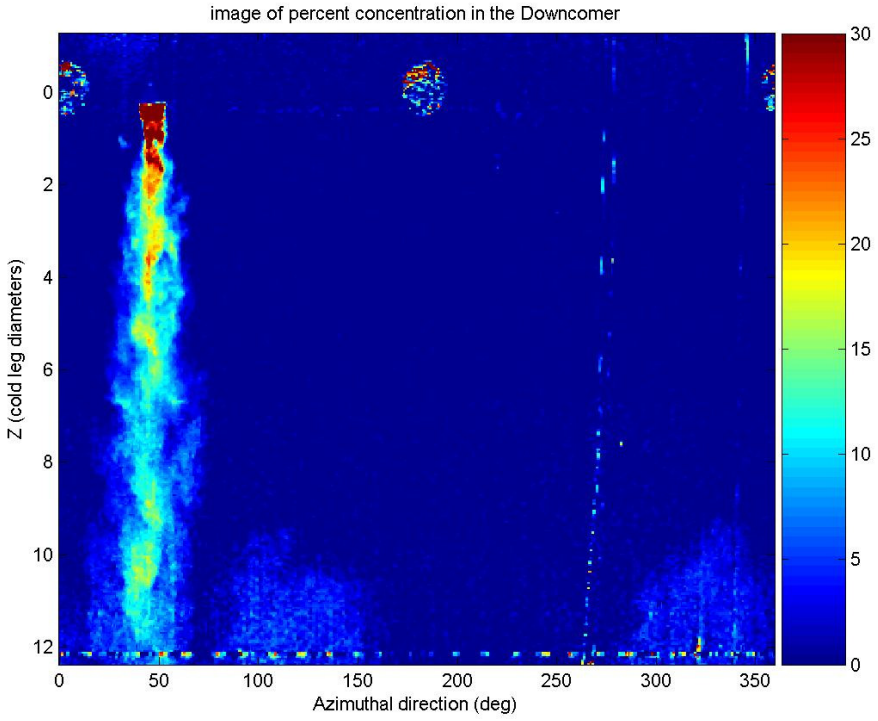

Figure 4.13: Filled contour plot of concentration in the downcomer for SP1 at 16 seconds

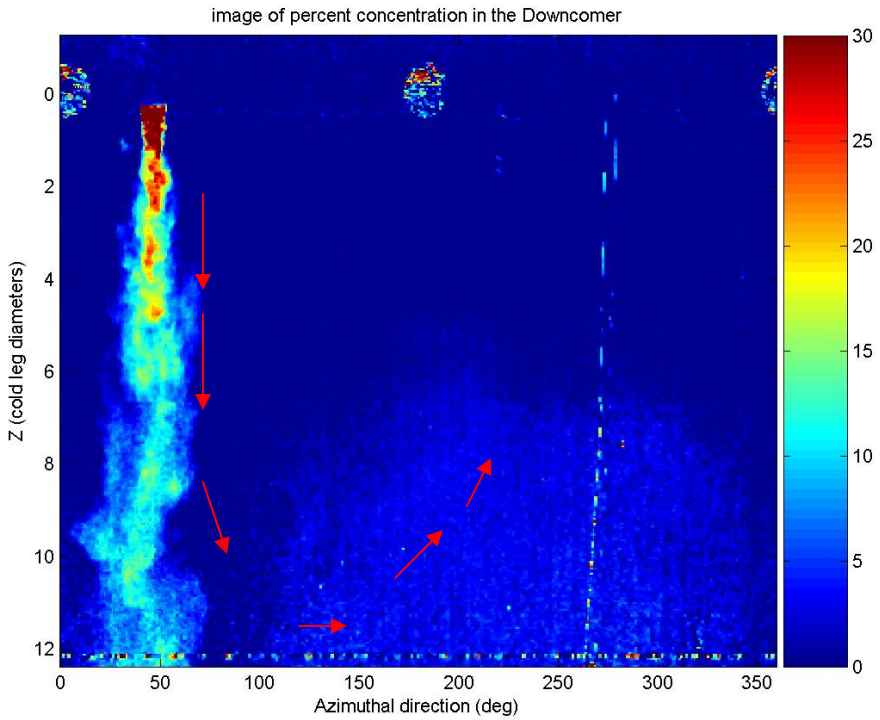

Figure 4.14: Filled contour plot of concentration in the downcomer for SP1 at 25 seconds

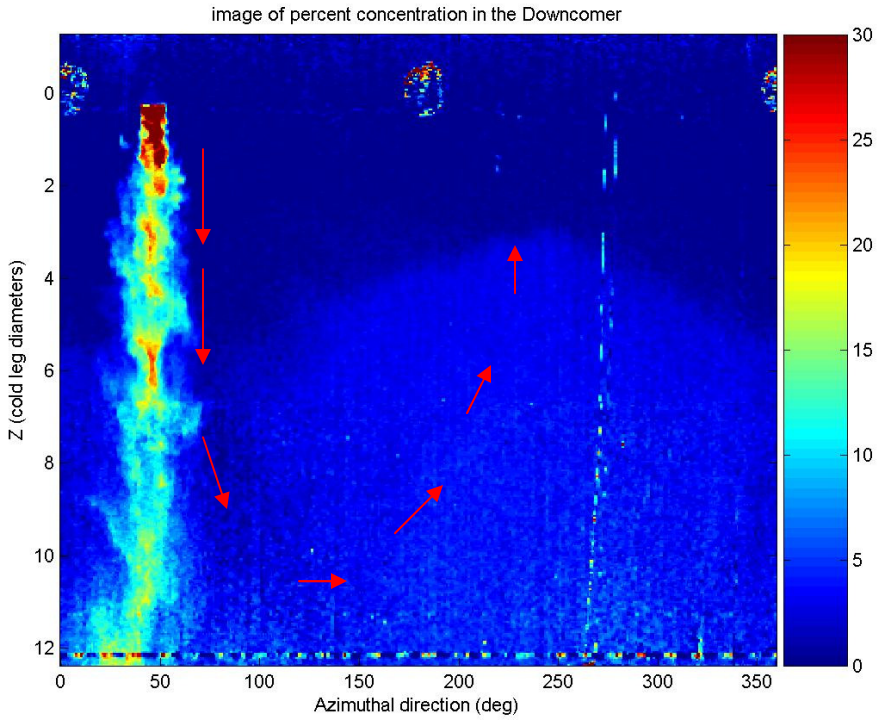

Figure 4.15: Filled contour plot of concentration in the downcomer for SP1 at 35 seconds

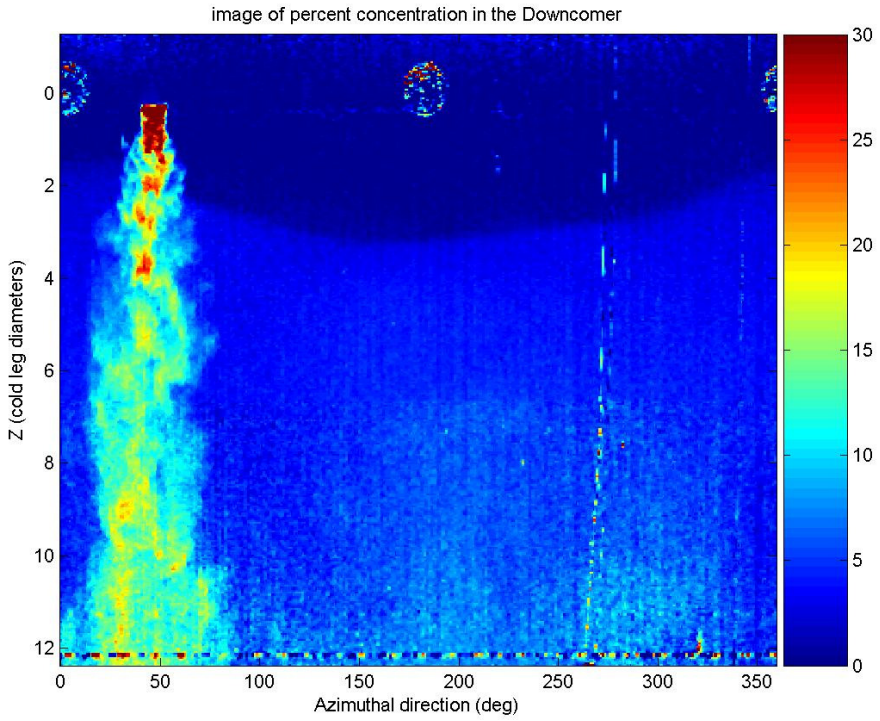

Figure 4.16: Filled contour plot of concentration in the downcomer for SP1 at 50 seconds

4.2.2 Plume Width

For the single plume cases, the width of the plumes could be extracted by comparing the maximum intensity of the dye inside the plume to the maximum intensity outside of the plume at each z location. The plume interface itself was arbitrarily determined to be the location where the concentration falls to 30% of the maximum inside the plume relative to the maximum outside the plume. Figure 4.18 shows a plot of the plume width vs. the length below the cold leg (z). Each of the times was averaged over 10 seconds for an ensemble average and the mean time is represented in the legend.

It can clearly be seen that the plumes are increasing in width as time progresses. In the beginning, the cold leg is still filling with injected fluid; notice how the width of the plume at 15 seconds is smaller near the cold leg than at later times. After the cold leg

has filled, around 30 seconds, the plumes from 35 seconds onward remain similar for small values of z and continue to widen as time progress's for larger values of z. This widening in time is due to the increase in density of the background fluid as the injected fluid continues to fall into the downcomer. This change in density linearly affects the buoyancy of the plumes, causing them to become less buoyant as time progresses. The lower buoyancy force of the incoming fluid from the cold leg causes the salted fluid to fall downward with a decreased velocity. Since the injection flow rate is constant during the test, the plume must increase in width as its velocity decreases for the flow rate to remain the same.

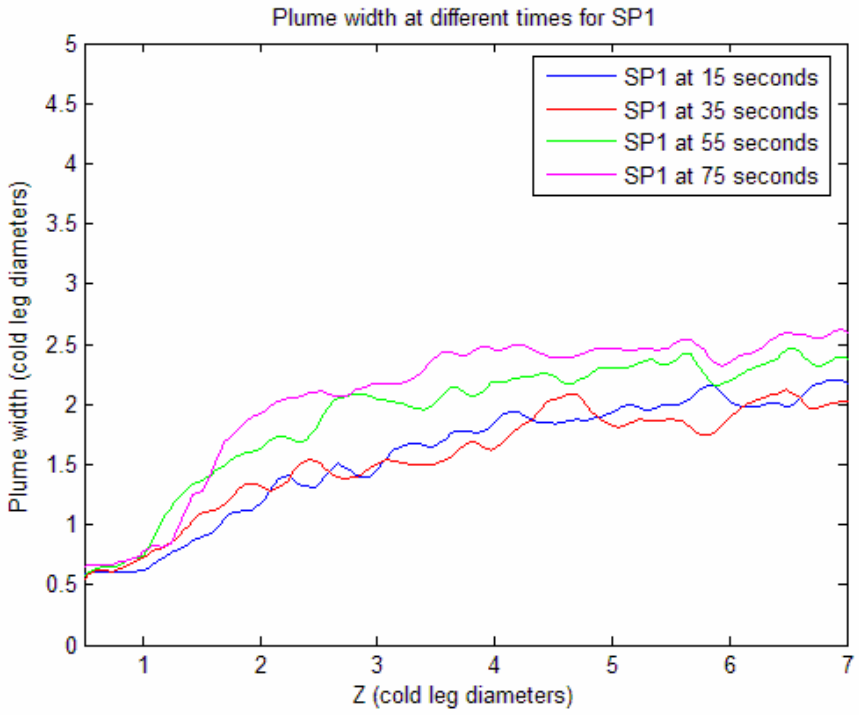

Figure 4.17: Plume width variation over duration of test case SP1.

4.2.3 Turbulent plumes from four legs

Interest in how the presence of surrounding plumes affect the mixing characteristics prompted a series of four-plume tests in the downcomer section. The numbering nomenclature for the multiple plumes in the downcomer is shown in Figure 4.19. Figure 4.20 shows one instance where the plumes are interacting and changing what would be seen in the single plume cases. The single plume fell primarily in the vertical direction, while the collective behavior of the multiple plumes drastically alters the flow path of the individual plumes. It can be seen visually from the images that the multiple plumes in the downcomer produce a recirculation similar to the single plumes, but the recirculation in the multiple plume cases has a much stronger effect on the dynamics of the plumes themselves. Figures 4.21 through 4.29 depict a time sequence of the MP1 case. Figures 4.21 and 4.22 show how in the beginning of the experiment, the

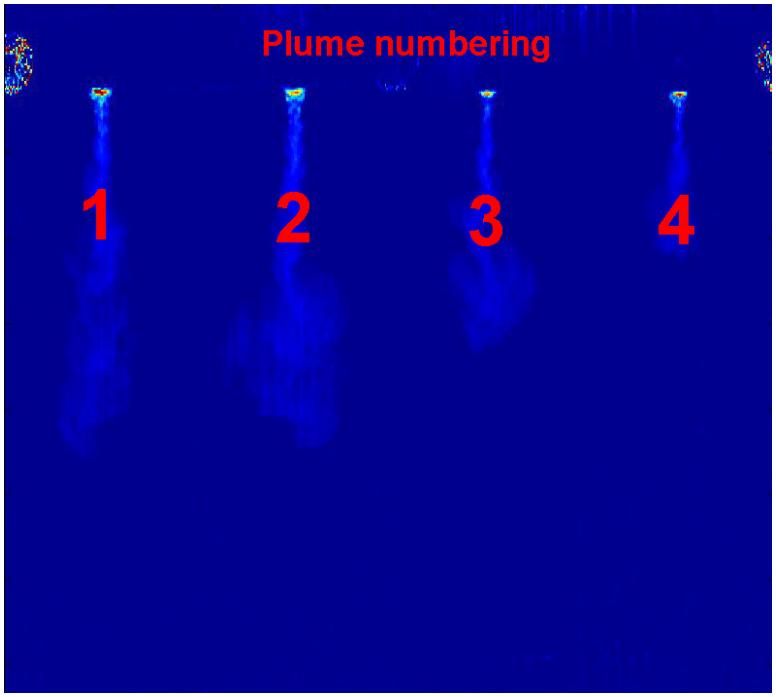

Figure 4.19: Numbering of plumes

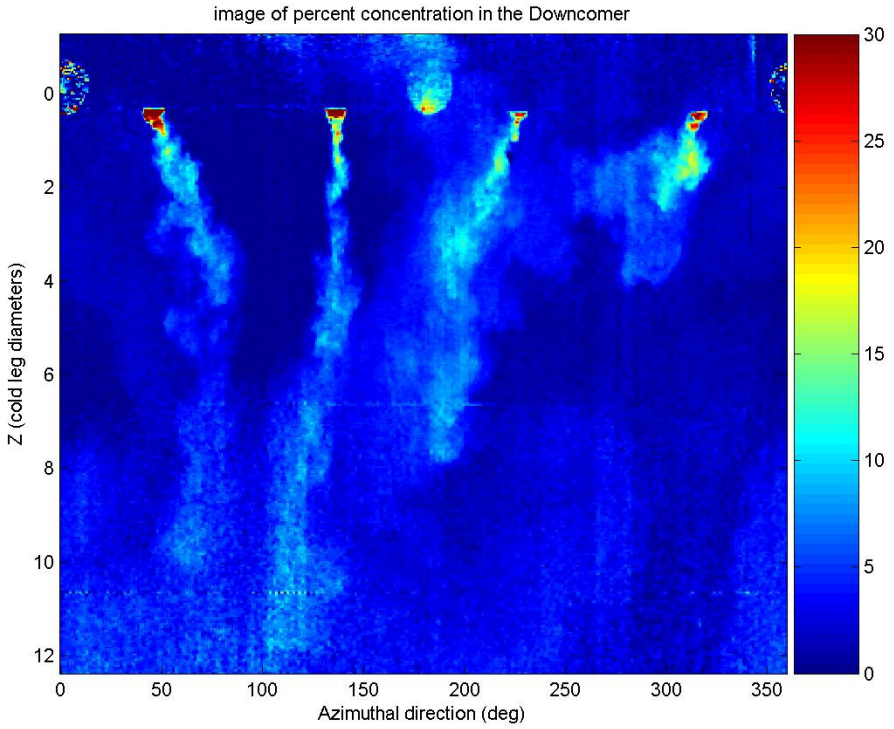

Figure 4.20: Filled contour image of downcomer concentration for MP1 at 31 seconds

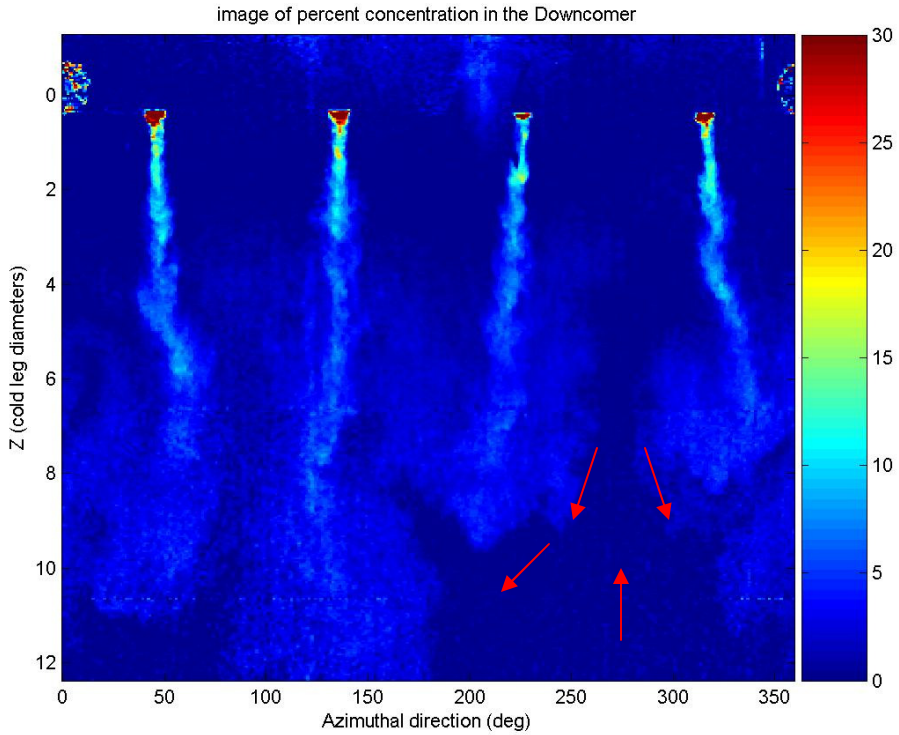

Figure 4.21: Filled contour image of downcomer concentration for MP1 at 13 seconds

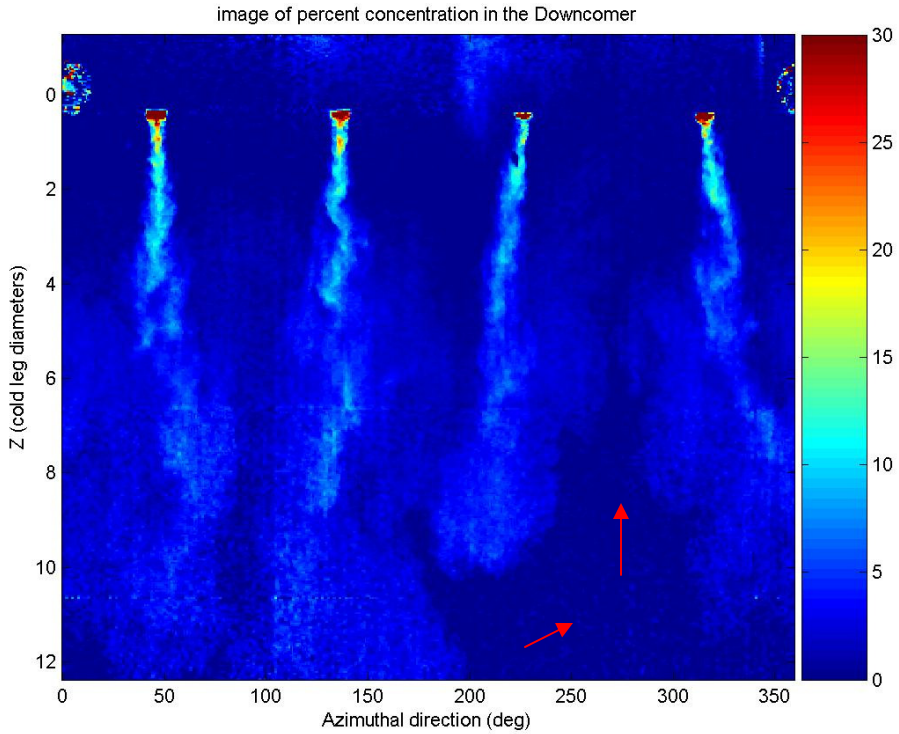

Figure 4.22: Filled contour image of downcomer concentration for MP1 at 15 seconds

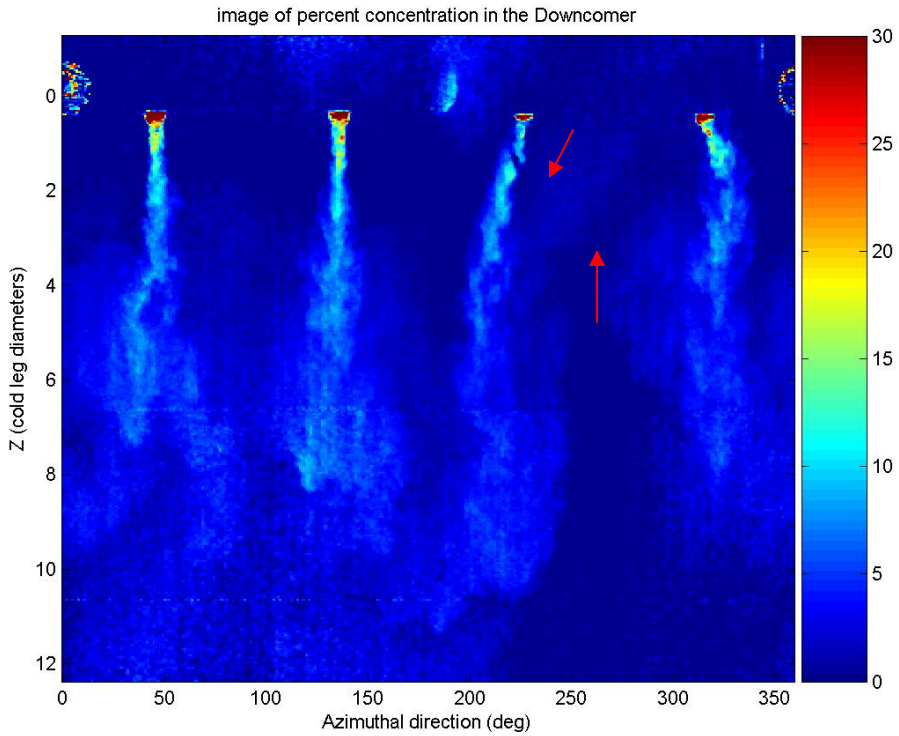

Figure 4.23: Filled contour image of downcomer concentration for MP1 at 18 seconds

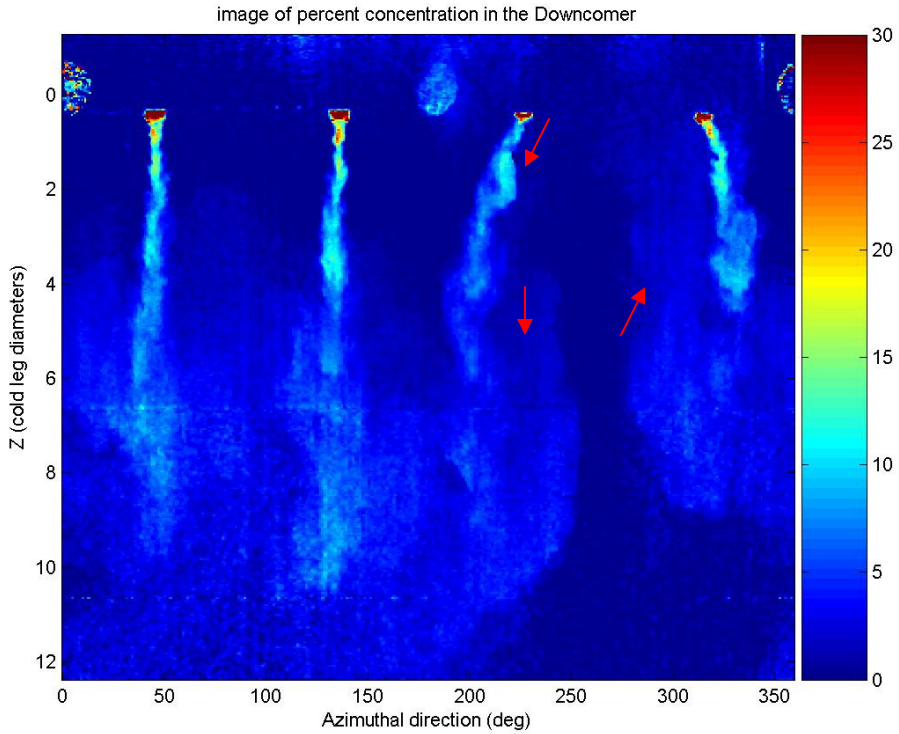

Figure 4.24: Filled contour image of downcomer concentration for MP1 at 20 seconds

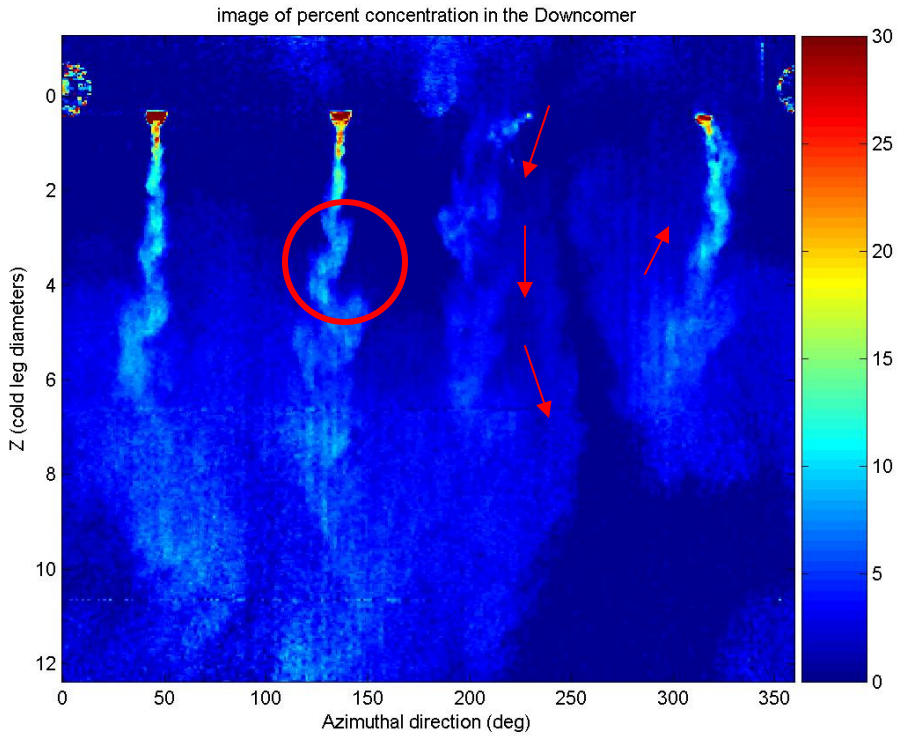

Figure 4.25: Filled contour image of downcomer concentration for MP1 at 22 seconds

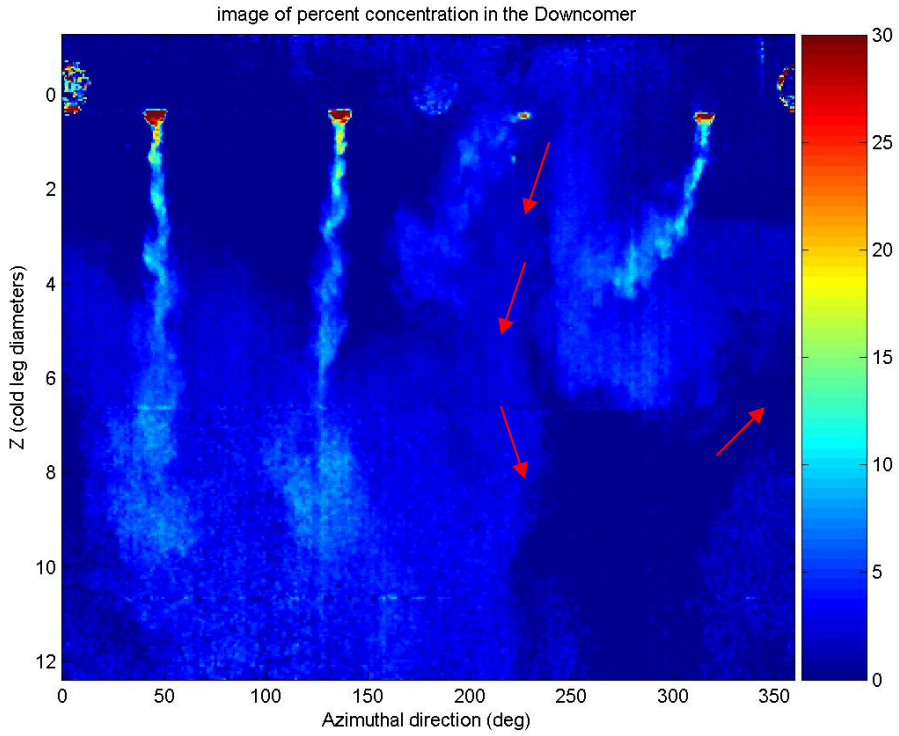

Figure 4.26: Filled contour image of downcomer concentration for MP1 at 25 seconds

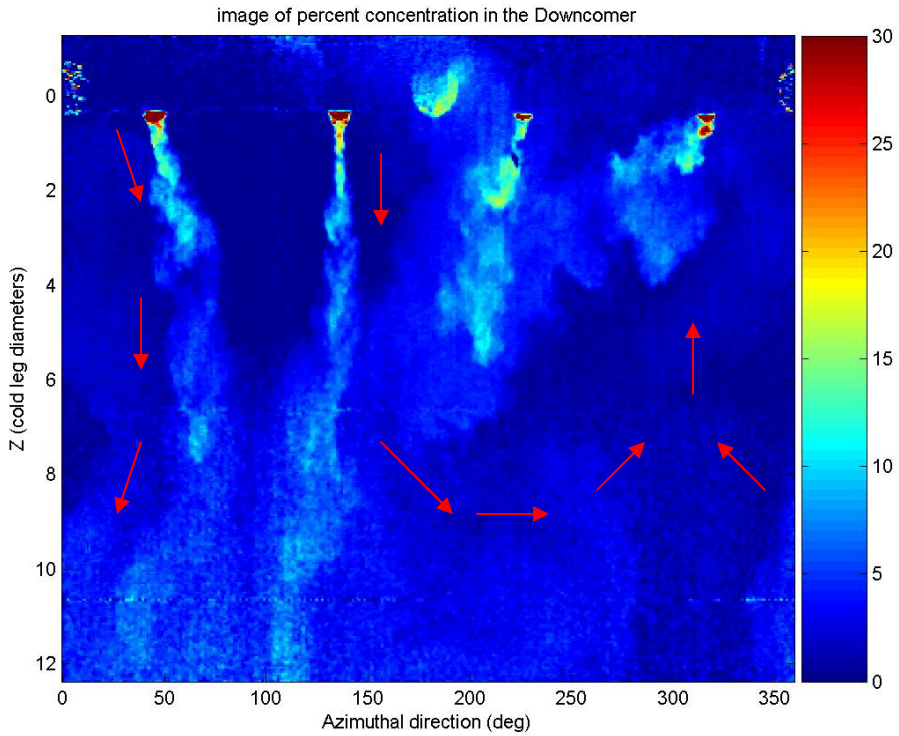

Figure 4.27: Filled contour image of downcomer concentration for MP1 at 30 seconds

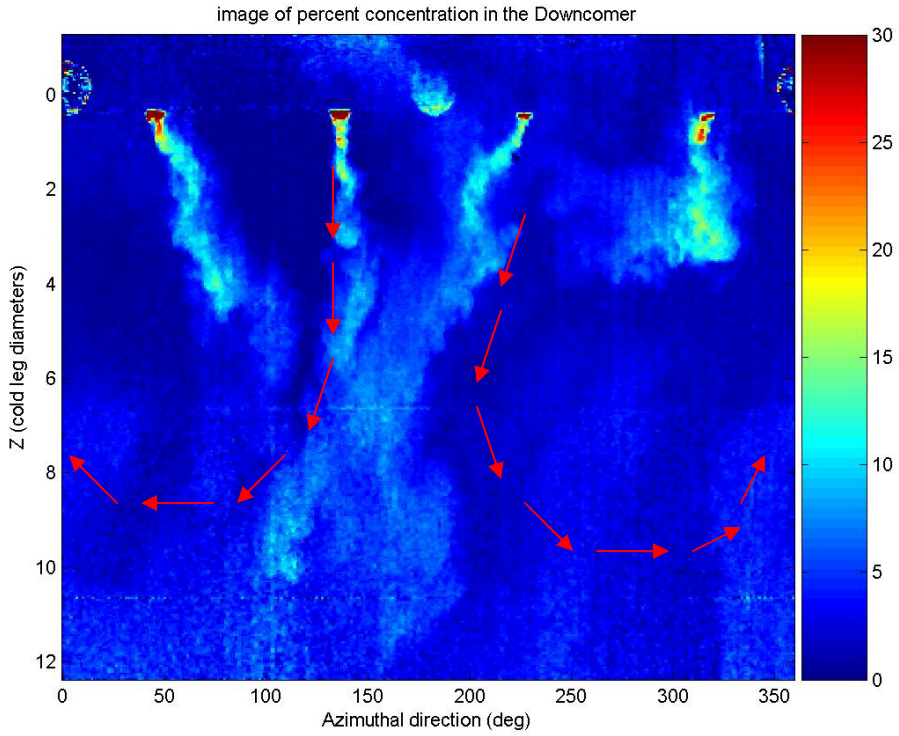

Figure 4.28: Filled contour image of downcomer concentration for MP1 at 33 seconds

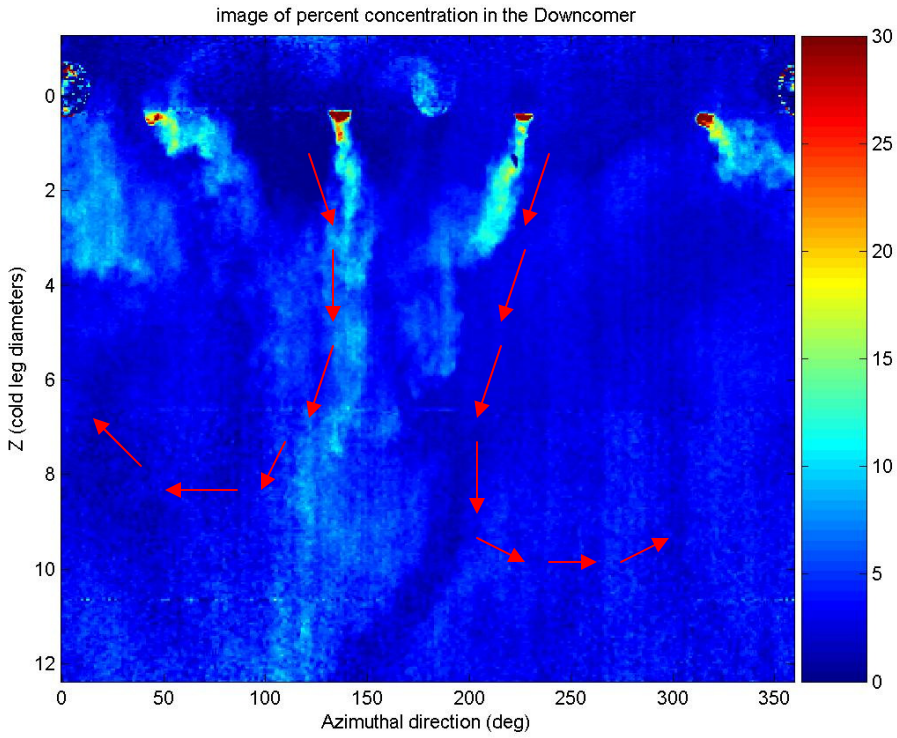

Figure 4.29: Filled contour image of downcomer concentration for MP1 at 37 seconds

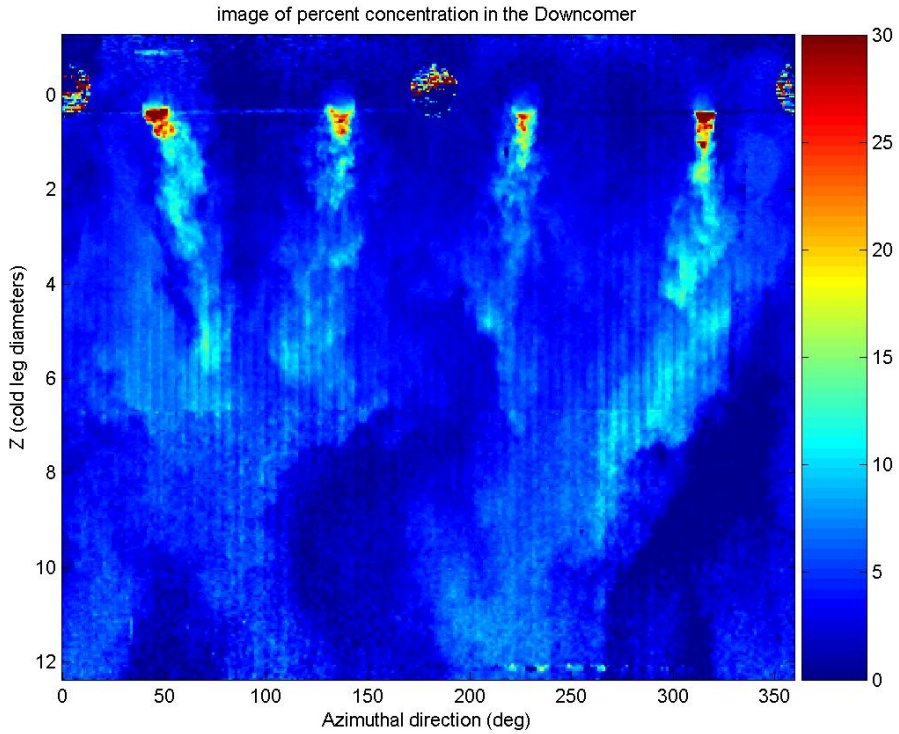

Figure 4.30: MP4 at 14 seconds showing interaction, but no strong recirculation

multiple plumes behave similarly to the single plume cases, falling mostly in the vertical direction. In figure 4.23, at approximately 18 seconds after the plume entered the downcomer, plume 3 begins to move closer to plume 2. This is an indication that there is a local motion of the fluid in the downcomer as indicated by the red arrows; the red arrows in figures 4.23 through 4.29 are all in the direction of presumed fluid motion. The global circulation in the downcomer indicated qualitatively by the red arrows was determined from observing the animations of the full time sequence, where it is more immediately evident. At 18 seconds, plumes three and four are observed to be moving away from each other, indicating a possible upwelling of fluid between them. At 20 seconds into the test, plumes three and four have transitioned from moving primarily in the vertical to the horizontal direction. At 22 seconds into the test, plume number three is no longer discernable due to the surrounding background fluid now moving across the

entrance of the plume. Also notice the wavy plume structure located in the red circle of figure 4.25, this disturbance is an indication of the vortices formed on the interface between the plumes and the surrounding fluid. At 25 seconds (figure 4.26) a counter-clockwise circulation of background fluid can be seen as indicated again by the red arrows. At 30 seconds into the test, a second circulation, rotating in the opposite direction of the first, can be seen. Both of the circulations are having a significant impact not only on the direction of the falling plumes, but also on their width, intensity, and how they are mixing with the surrounding fluid. Notice how at 30 seconds (figure 4.27) that plumes three and four are much wider than plumes one and two; this is a result of the recirculation forming in the downcomer which causes the background fluid in the downcomer to have an average upward velocity for plumes three and four, while having an average downward velocity for plumes one and two at this instant in time. This changes the relative plume velocity and shear rate, consequently altering the local mixing around each plume. In figures 4.28 and 4.29, recirculation patterns have been established. The plumes continue to switch which plumes pair together for the remainder of the test. Overall, plumes two and three stay within the region of strong downward motion, while plumes one and four experience a more general upwelling of fluid. Figure 4.30 shows for comparison case MP4, where there is significant plume interaction, but no strong circulation establishes. Notice how the plumes in figure 4.30 fall primarily in the vertical direction, but still interact to slightly alter the path of the plumes.

Figure 4.31 shows a schematic map of which plumes merge for all multiple plume cases. In the figure, when the colored lines are next to each other then the plumes have qualitatively been observed to merge into a single larger plume. When the lines are at the

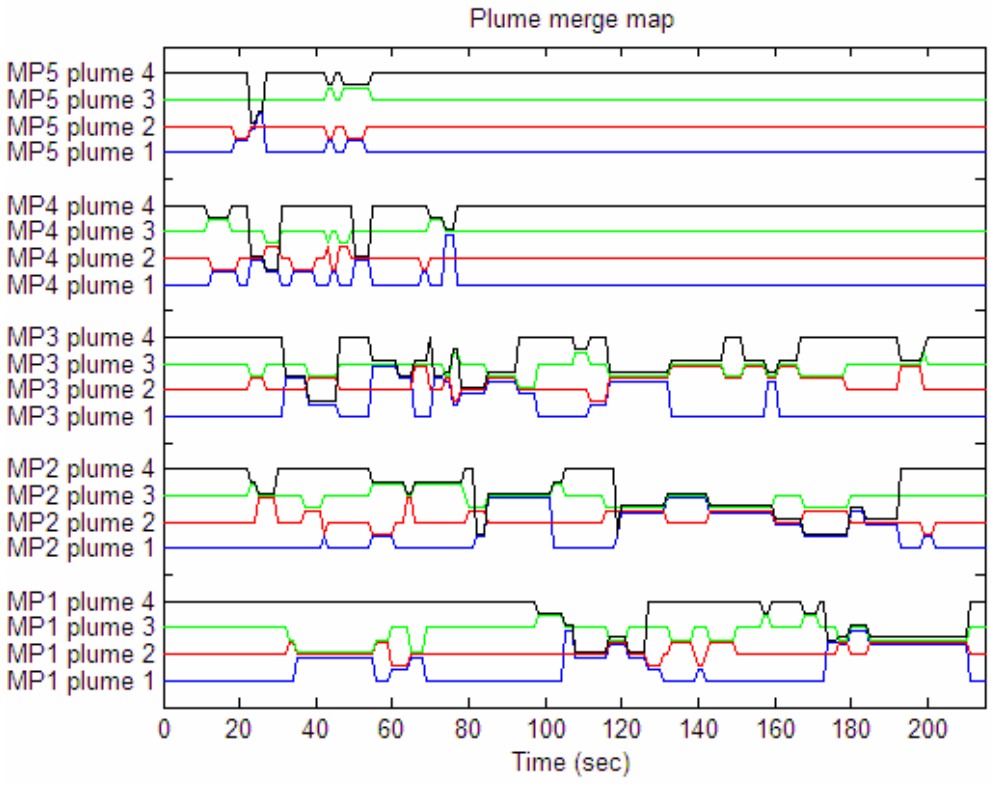

Figure 4.31: Schematic of which plumes merge verses time for all multiple plume cases

same vertical position as when they started, then the plume has not merged with another plume. First, notice how as the co-flow is increased from case MP1 to MP5, the frequency of switching between different merging plumes increases. For MP1 the plumes are slow to change states, keeping merged with the same plumes longer than the higher co-flow cases. As the co-flow in the cold legs increases, the frequency of switching becomes higher (the plumes switch back and forth between different merged states). Second, notice that the plumes cease to interact for MP4 after 77 seconds and MP5 after 55 seconds. The plumes continue to mix with the surrounding fluid, but they fall straight down in the downcomer similar to the single plume cases. Figure 4.32 shows the plume merge map verses the downcomer flow through time, which is the total flow rate through the cold leg divided by the downcomer volume. The plumes in cases MP4 and MP5 ceased interaction after a downcomer flow through time of approximately 1.5,

while the plumes in the lower co-flow cases continued to interact throughout the duration of the test, which corresponds from 0.75 to 2.3 flow through time scales.. The concentration in the cold legs for cases MP5 and MP4 were well mixed prior to entering the downcomer while the other cases were significantly stratified.

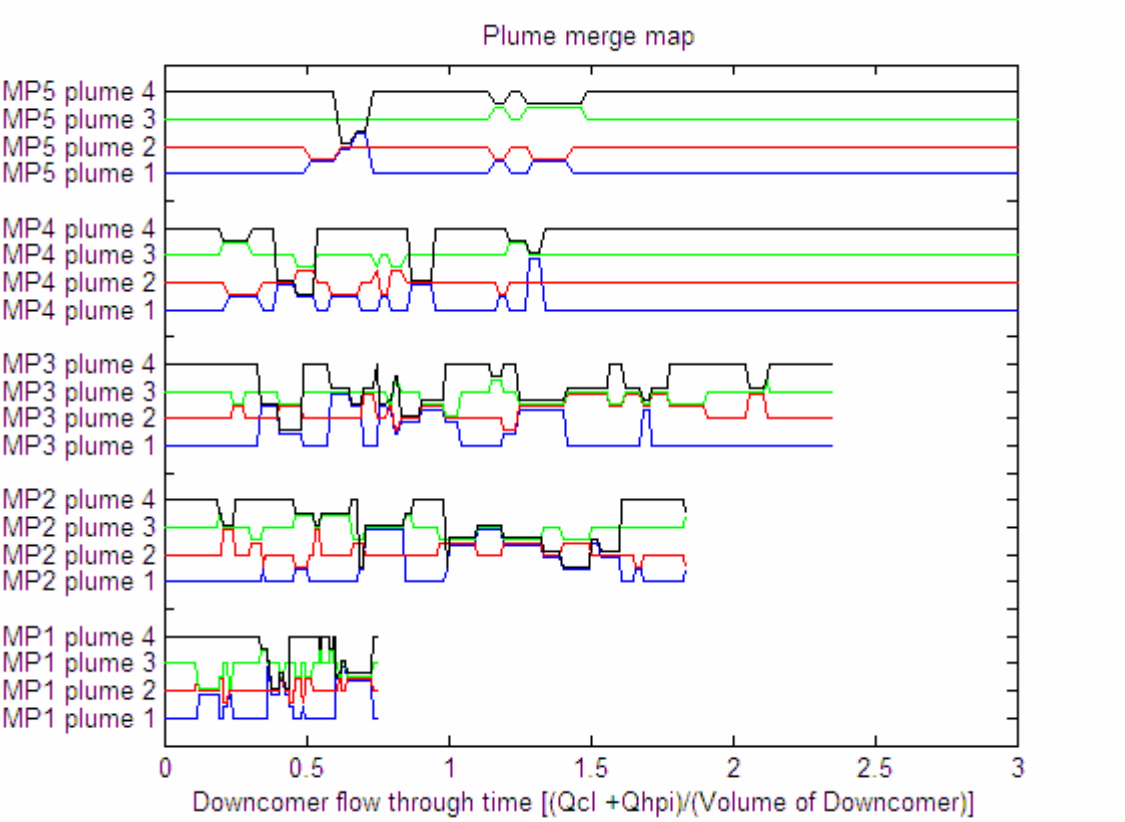

Figure 4.32: Schematic of which plumes merge verses downcomer flow through time for all multiple plume cases

Figure 4.33 shows the percent occurrence of all the possible plume merging configurations for each of the multiple plume cases. For the figure notation, the "+" between the plumes indicates that they have merged, while the "," indicates that separate simultaneous plume merging has taken place. For example the notation "1+2" means plumes 1 and 2 have merged while plumes 3 and 4 haven't, while "1+2,3+4" indicates that plumes 1 and 2 have merged while plumes 3 and 4 have also merged resulting in two

large plumes at the bottom of the downcomer. For pairing of two plumes, figure 4.33 shows no significant preference of one merging configuration over another. However, for merging of 3 or 4 plumes the percent occurrence was much higher for case MP1 through MP3 than for MP4 and MP5.

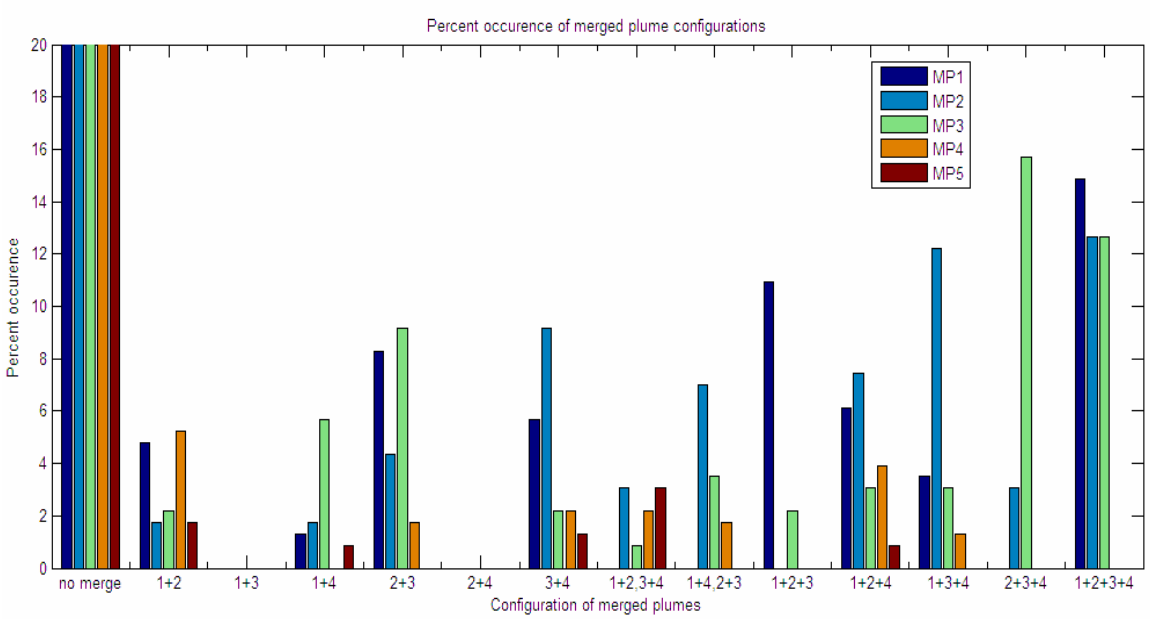

Figure 4.33: Percent occurrence of plume merging verses configuration of merged plumes for all multiple plume cases. For axis labels, "+" indicates merged plumes, while a "," indicates separate, simultaneous plumes.

As the plumes mix in the downcomer, the concentration of the entire downcomer increases with time. This causes the density difference or buoyancy force between the plume and the surrounding fluid to decrease in time. Figures 4.34 through 4.38 show the background concentration of the downcomer with Z as it changes with time along with the maximum concentration measured in the cold legs. Thin vertical slices about 20 pixels wide between each of the plumes was taken as a representation of the background fluid. Because the hot legs are present between the plumes at -.5 to .5 cold leg diameters, the concentration at those heights was only sampled for the two vertical slices that didn't

pass through the hot legs. Each curve in figures 4.34 through 4.38 is an average of the concentration data from 2 seconds before and after the indicated time.

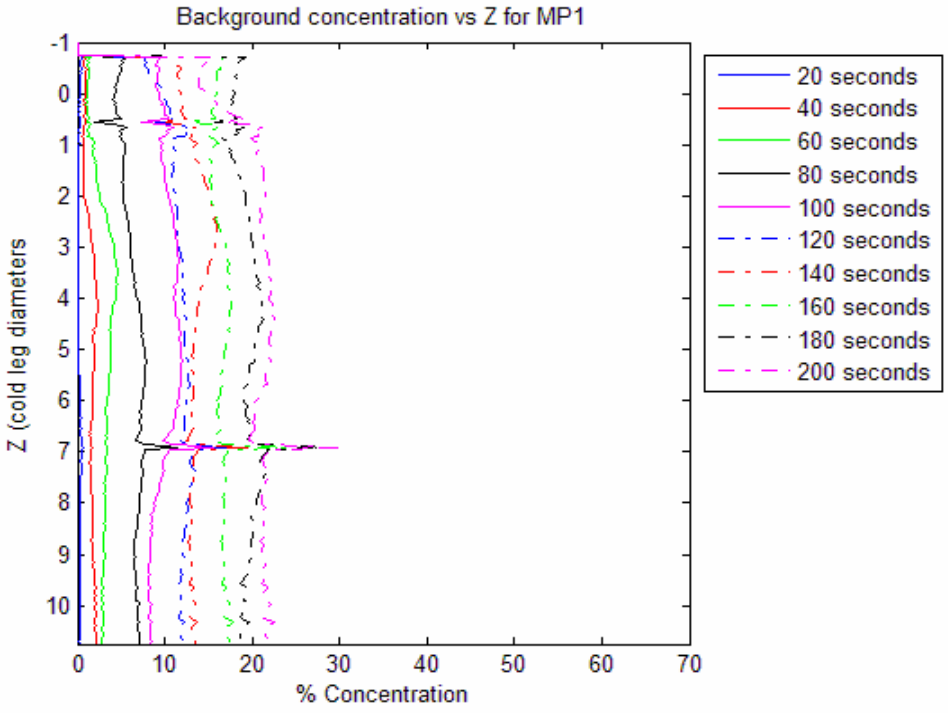

Figure 4.34: MP1 Background concentration verses Z at various times

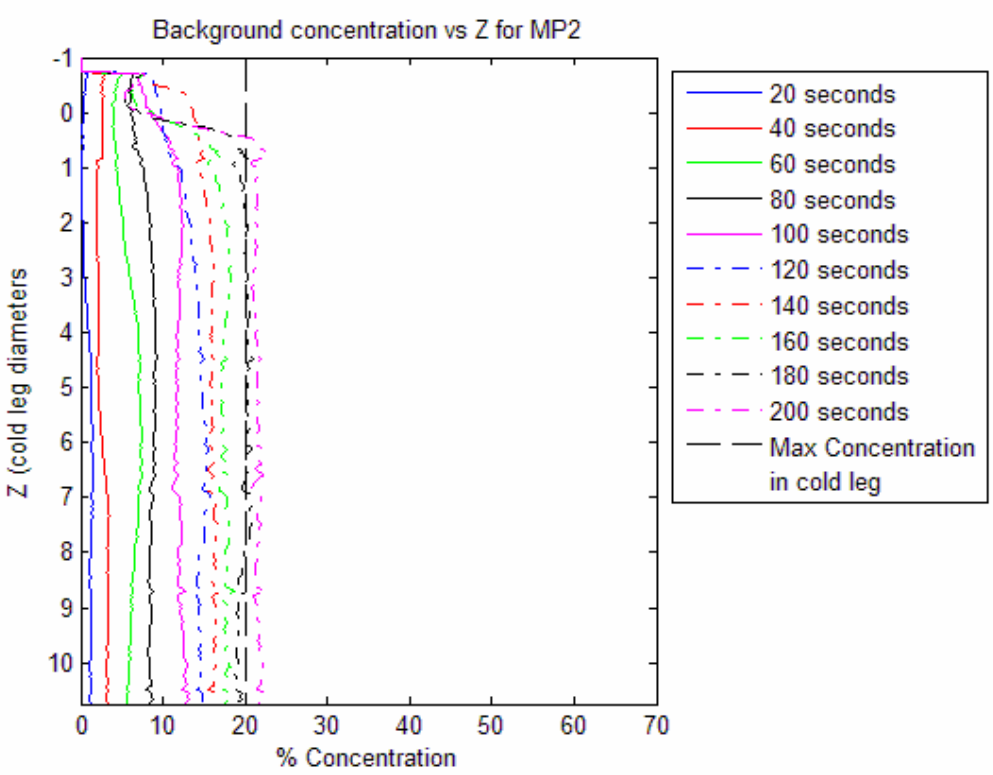

Figure 4.35: MP2 background concentration verses Z at various times

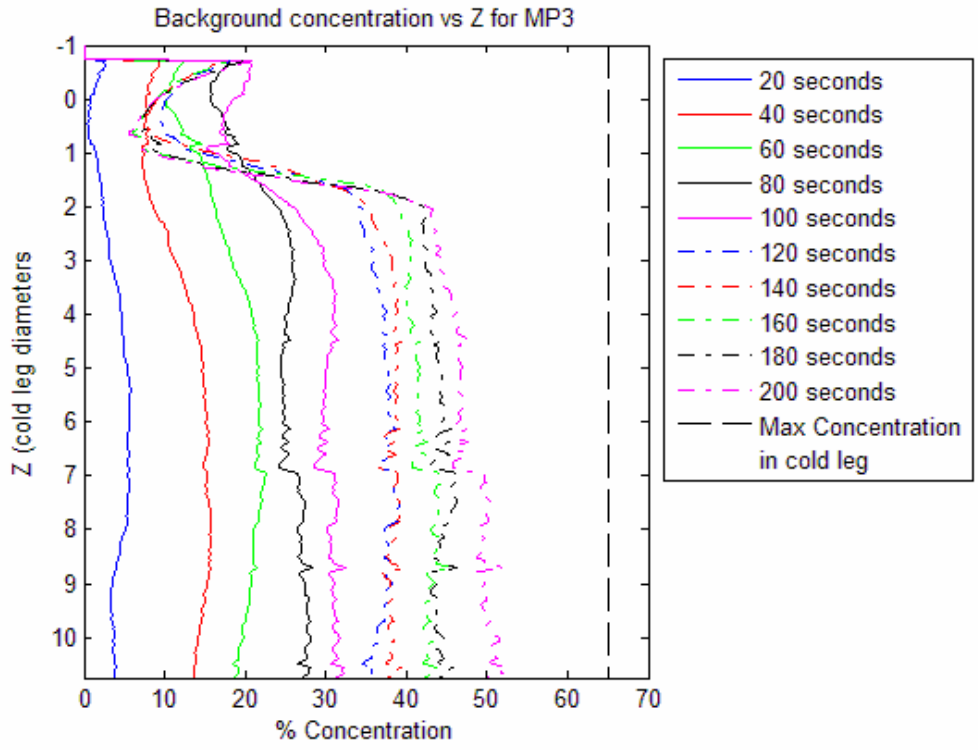

Figure 4.36: MP3 background concentration verses Z at various times

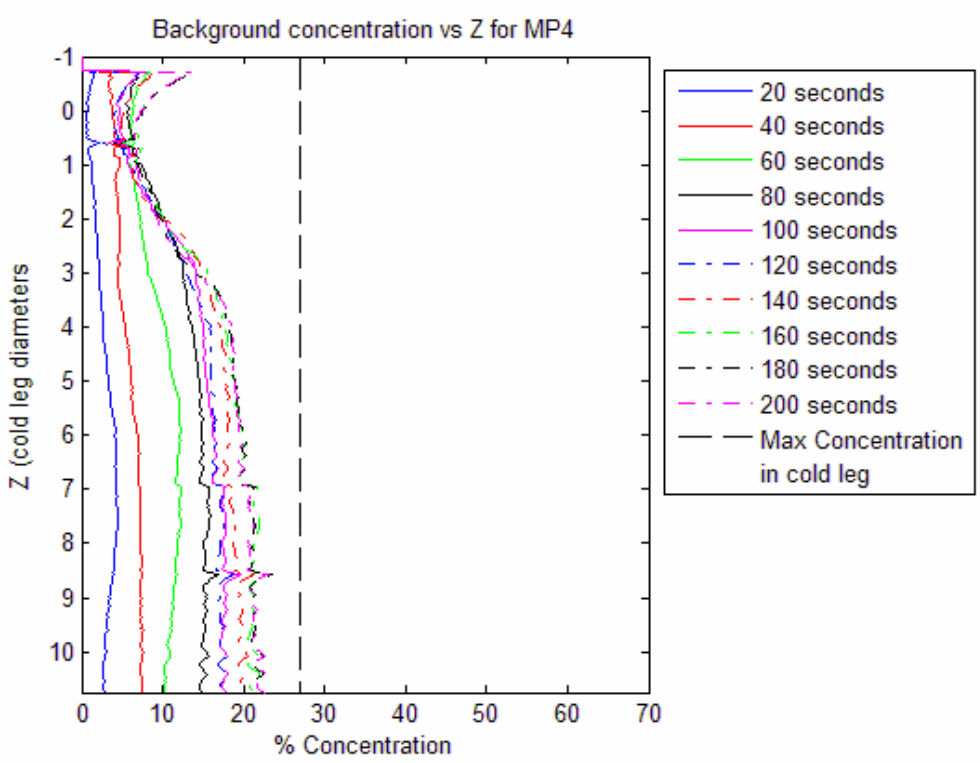

Figure 4.37: MP4 Background concentration verses Z at various times

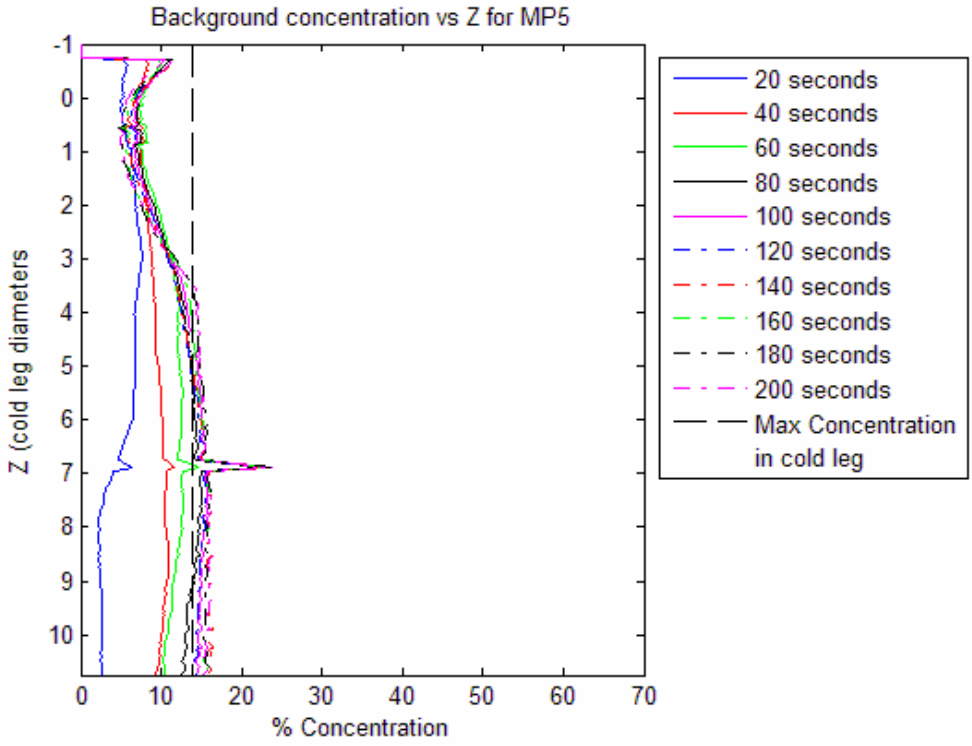

Figure 4.38: MP5 Background concentration verses Z at various times

Cases MP4 and MP5 both showed that both the HPI and co-flow streams inside the cold leg were well mixed. Because they were well mixed, the maximum concentration that can be achieved for those two cases is:

$$\textbf{Well Mixed concentration in cold leg} = \frac{Q_{HPI}}{Q_{HPI} + Q_{CL}} \qquad \textbf{Equation 4.2}$$

where Q_{HPI} is the flow rate from the HPI nozzle and Q_{CL} is the flow rate from the simulated natural circulation in a cold leg. Using the flow rates from table 3.2, the Maximum concentration for MP4 is 20% and for MP5 is 13%. In figures 4.36 and 4.37 notice how the downcomer concentration for cases MP4 and MP5 asymptotes toward the values from equation 4.2. By comparing figures 4.31, 4.37, and 4.38, the plumes stop interacting and merging when the background concentration is with in 2% (MP5) and 9% (MP4) of the incoming plume concentration in the cold legs.

A quasi-steady recirculation pattern was clearly observed in the two lowest co-flow, multi-plume cases (MP1 and MP2). For the largest two co-flow cases (MP4 and MP5), plume interaction was present for a short time into the test, but a quasi-steady recirculation was not present and the plumes fell primarily vertically similar to the single plumes, see figure 4.28. The MP3 case showed similar plume dynamics to cases MP1 and MP2, but the recirculation was not stationary in the downcomer.

Examining the data from the line-scan camera for cases MP2 and MP4, the density of the fluids in the cold legs at the inlet to the downcomer were similar, see figures 4.3 and 4.5. However, for MP2 a recirculation established in the downcomer and for MP4 no recirculation was observed. The key difference between these two situations was the mixing at the entrance to the downcomer (Mixing Region 3). Figure 4.41 shows plume number 3 for tests MP4 and MP2 at 4 seconds. The plume in MP4 is much wider

then the MP2 plume. Knowing that the spreading angle of the plumes is directly related to the entrainment of fluid into the plume (Wicks, 1992), it can be noted that the MP4 plume is experiencing greater mixing at the entrance to the downcomer then the MP2 plume. This caused the plumes in the downcomer to be weaker for MP4 and MP5 compared to the lower co-flow cases, MP1 through MP3. The result is the downcomer plumes in the higher co-flow cases could not establish a recirculation pattern in the downcomer.

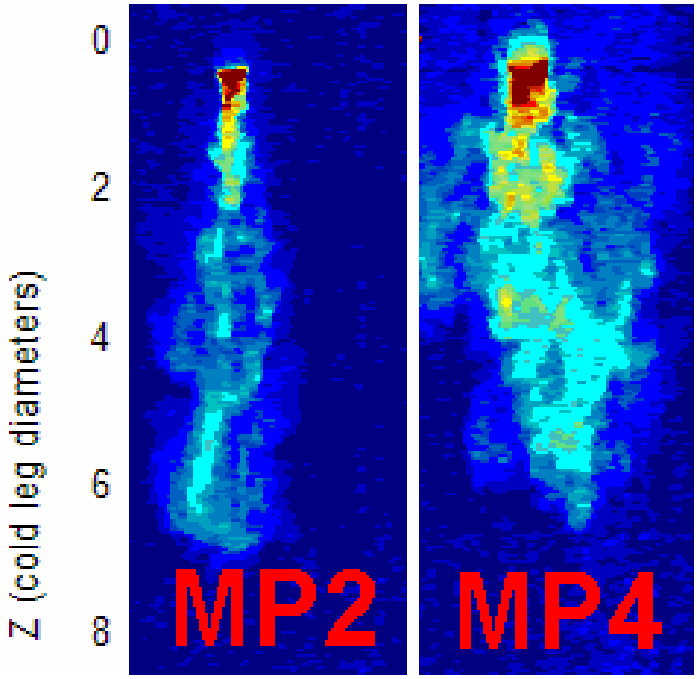

Figure 4.39: Plume visualizations for MP2 and MP4

4.3 Comparison to other results

In figure 4.40, the cold leg observations from the CREARE 1/5 scale experiments are plotted with the UMD data obtained from the current experiments. The UMD experiments agree well with the previously published data. The data points that are above a Froude number of .19 were clearly in a well mixed condition; this was observed in the camera data as well as visually. For instance, in the Froude number 0.25 case

(SP6), the dye was distributed across the whole diameter of the pipe and therefore was very weak in intensity across the whole cold leg. The camera data at Froude numbers of .177 (MP5) and .186 (SP5), appeared well-mixed with slight increase in concentration at the bottom of the cold leg similar to a stratified condition. The Froude number .186 case showed that the dye was relatively weak, but after the co-flow was stopped, a clear stratification appeared. This indicates that the low concentration was from significant mixing across the pipe. Figure 4.41, shows the concentration profiles for this case. Notice how before the cessation of co-flow the concentration profile is much more uniform than the profile after the co-flow is stopped.

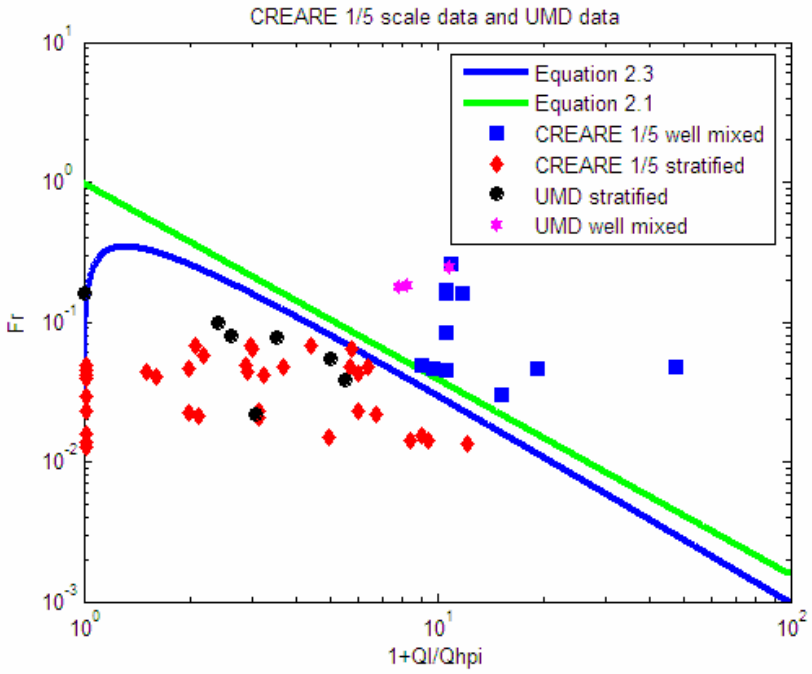

Figure 4.40: Comparison of UMD data to theoretical predictions of stratified vs. well-mixed in the cold legs and CREARE 1/5 observations.

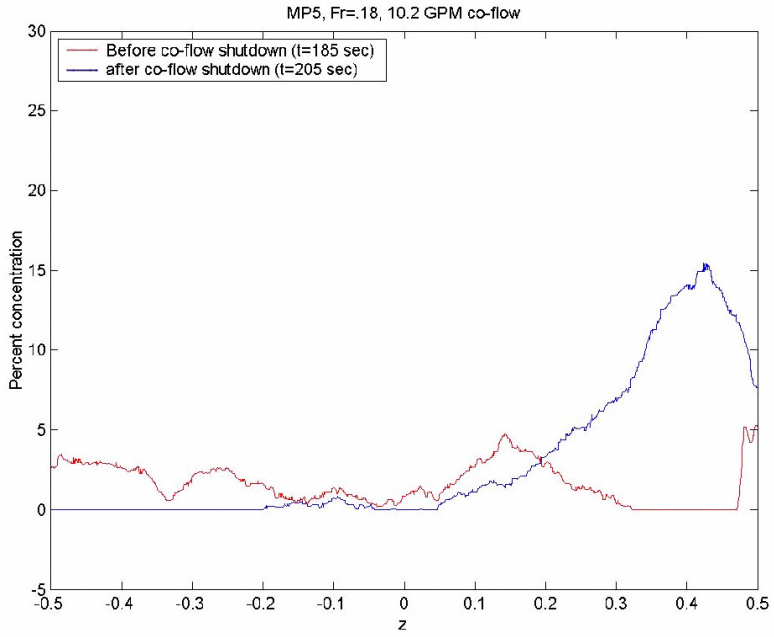

Figure 4.41: Cold leg concentration profile at downcomer inlet immediately after recirculation pump shut-down. Note that the flow is clearly stratified, whereas prior to shut-down, the flow was well-mixed.

4.3.1 Plume characteristics and mixing

Many interesting characteristics can be observed in the visualization of the plumes in the downcomer. As a negatively buoyant plume falls into the downcomer, it causes a shear between the negatively buoyant plume in motion and the initially nearly stagnant fluid surrounding the plume. This shear layer produces vortical motion along the interface between the plume and its surrounding fluid, and is responsible for entraining surrounding fluid into the negatively buoyant plume (Morton, Taylor, and Turner, 1956). The wavy interface along the outer edge of the plumes is an indication of vortices which are responsible for entrainment on both sides of the plumes. The vortices in the single plume cases interfere and interact similar to how they would act in a mixing layer, rolling up and forming into larger vortical structures farther down the path of the

plume. Similar behavior for thermal plumes was reported by Turner, 1957, also by Shusser and Gharib, 2000. At some instances, this can be observed as a swirling motion along the edges of the plume, which tends to cause a momentary disruption in the quasi-steady and predictable motion of a single plume in the downcomer.

To understand how the plumes mix with the surrounding fluid, entrainment rates for the plumes are extracted from the visualization of growth rates observed in the downcomer. From open channel plume theory, the entrainment rate of a plume is directly proportional to the plume's angle of spread (Tuner, 1973), see section 2.3.2 for more details. To extract the plume angle of spread, a sequence of plume images from a nominally similar time were averaged together resulting in a single image that represents the plumes. From this single averaged image, a threshold of 30% between the highest concentration inside the plume and the highest concentration of the background fluid was taken to define the interface between the plume and the surrounding fluid. Since the plume decays with distance into the downcomer, the threshold was calculated for each azmuthal slice of the downcomer, making it a function of Z. Figures 4.42 and 4.43 show the width of the plumes for the various single plume cases along with the linear curve fit to extract the entrainment rate. Figure 4.44 shows the sensitivity of the calculated entrainment rate to the selection of the arbitrary threshold, and table 4.1 shows the entrainment rates. Because of large unsteady plume motions in the bottom of the downcomer, the plumes for SP5 and SP6 were only plotted up to 6 cold leg diameters. The flow in the downcomer from .5 to 2 cold leg diameters is a complicated 3 dimensional flow (Theofanous, 1991), since the entrainment theory is not applicable in this region, the plume width curves were fitted from 2.5 to 10 cold leg diameters. The

width of the plumes showed a change in slope around 6 cold legs diameters, so the widths were linearly fitted from 2.5 to 6 cold leg diameters and another fit from 6 to 10 cold leg was preformed.

From figures 4.42, 4.43, and table 4.1, it can be seen that the plumes get wider as the cold leg flow rate is increased from cases SP1 to SP6. Although the plume in SP1 is the narrowest, it has the largest entrainment rate from 2.5 to 6 cold leg diameters in the downcomer. The plumes in SP5 and SP6 start out wide and as they traverse in the Z direction, they thin to give a negative entrainment rate. Without external manipulation, the entrainment of miscible fluids cannot be negative. The observed thinning of the plumes is possible if the plume is accelerating while traversing the downcomer. Because the injected fluid in the cold legs is well-mixed, the entire cold leg is filled with higher density fluid then the downcomer. When the well-mixed fluid enters the downcomer, the initial plume is much wider then the initial plums in case SP1 through SP4. Because the plume is much wider the initial velocity is also much lower and not in equilibrium with the buoyancy dynamics. Because of this the plumes for SP5 and SP6 accelerate and contract as they fall in the downcomer.

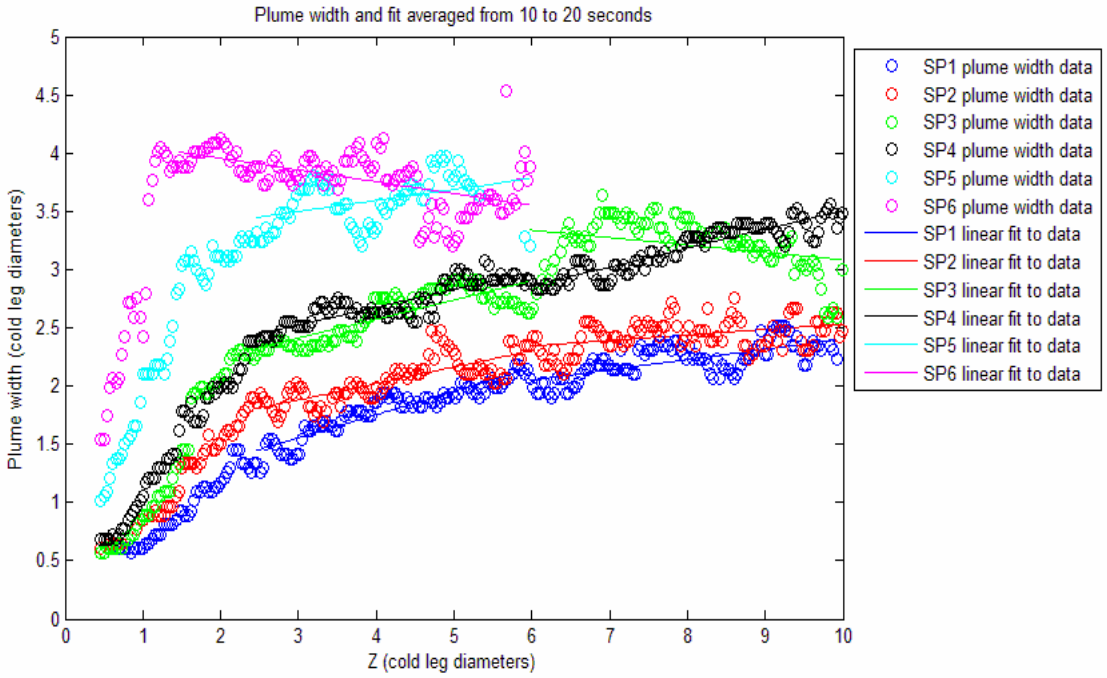

Figure 4.42: Plume width verses Z for single plume cases averaged from 10 to 20 seconds

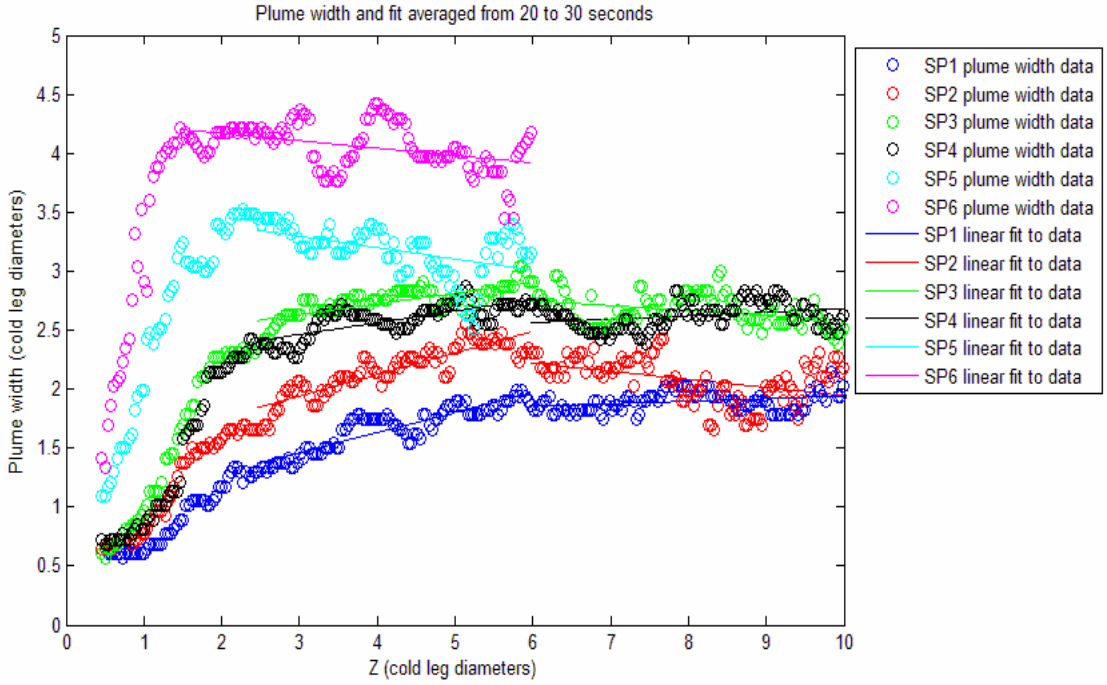

Figure 4.43: Plume width verses Z for single plume cases averaged from 20 to 30 seconds

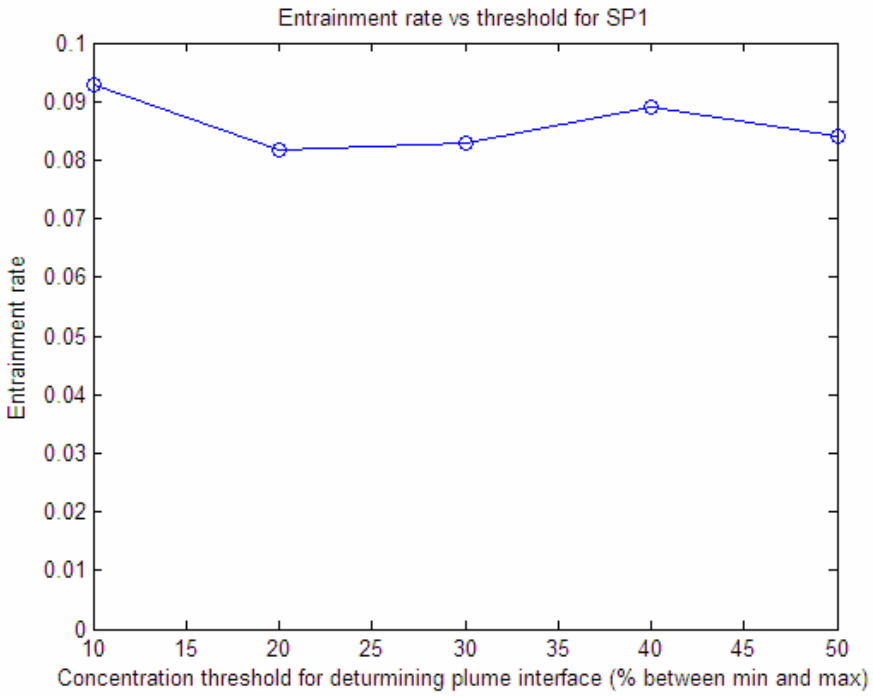

Figure 4.44: Entrainment rate verses Concentration thresh hold for SP1

The entrainment rate for an open area plume has been found experimentally to be between .10 and .12, (Turner, 1973). Many numerical simulations are using the entrainment rates gathered experimentally from open area plumes to simulate the PTS plumes in the downcomer (Theofanous, 1991). However, for the confined plumes in the UMD downcomer, all of the entrainment rates were found to be less then those reported experimentally for open area plumes. This can have a significant impact on the concentration of plume at the bottom of the downcomer, as a reduced entrainment rate, results in a higher plume concentration. Also, all the plumes showed a change in slope around 6 cold leg diameters. For most cases, the entrainment rate was decreased in the bottom portion of the downcomer in comparison to the upper part of the downcomer.

Plume interactions in the downcomer made extracting entrainment rates for the multiple plume tests unfeasible. However, it is evident from the visualization inside the

downcomer that the plumes are interfering to cause net circulation within the downcomer. This circulation usually establishes two plumes that pair together and become dominate plumes that drive a net circulation within the downcomer. The dominant plumes tend to be in the region where the velocity of the fluid inside the downcomer is downward while the remaining two plumes are in the area of upward velocity, as indicated by the paths of the plumes (see figure 4.27). The figure shows the middle two plumes in the downward part of the recirculation and the outside plumes are in the upward path of the recirculation inside the downcomer.

To help quantify the mixing in the downcomer section for the multiple plume conditions, Probability Density Functions (PDF's) of the plume concentration were constructed. For analysis, the downcomer section was split into four regions, Q1 through Q4, which spanned from the bottom of the cold legs to 6 cold leg diameters below the center of the cold legs in the downcomer section (see figure 4.45). Each region's horizontal center was located at the cold leg inlet within the region, and were numbered consecutively starting left to right. For the single plume cases, Q1 was the only region examined, since the other regions contained no plumes. For the PDF plots, the data is averaged for a time period extending two seconds before the time reported through two seconds after to obtain an ensemble average.

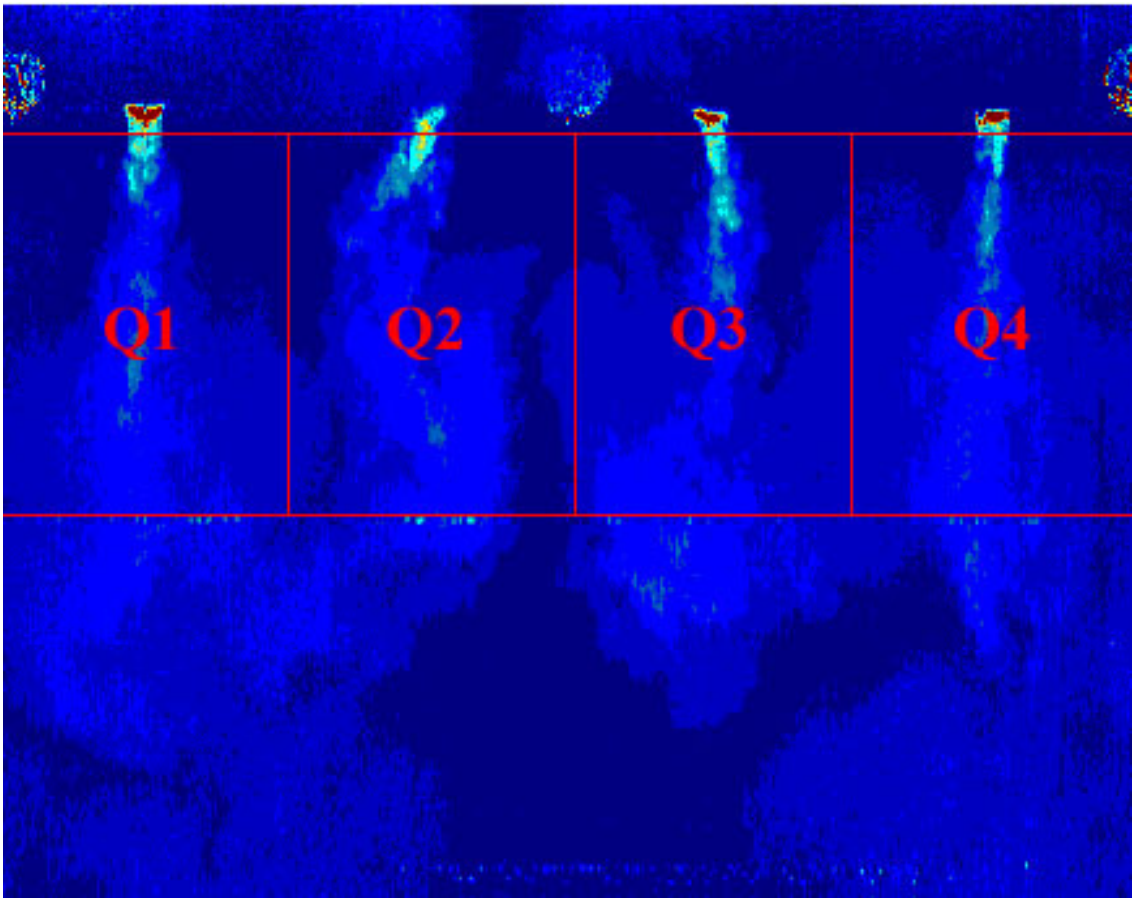

Figure 4.45: Division of downcomer into sampling regions for the construction of concentration PDFs.

Figure 4.46 depicts three possible plume mixing scenarios and how the appropriate PDF's would appear. If a plume enters the downcomer and has little or no mixing with the surrounding fluid, the PDF would have two peaks, one peak indicating the concentration of the background fluid while the other peak will be located around the concentration of the plume. However if the incoming plume mixes rapidly with the surrounding fluid, the PDF should be uni-model with the peak located between the initial concentration of the incoming fluid and the initial concentration of the background fluid. If the plume only partially mixes with the surrounding fluid, the PDF should appear bi-model with many different concentrations present.

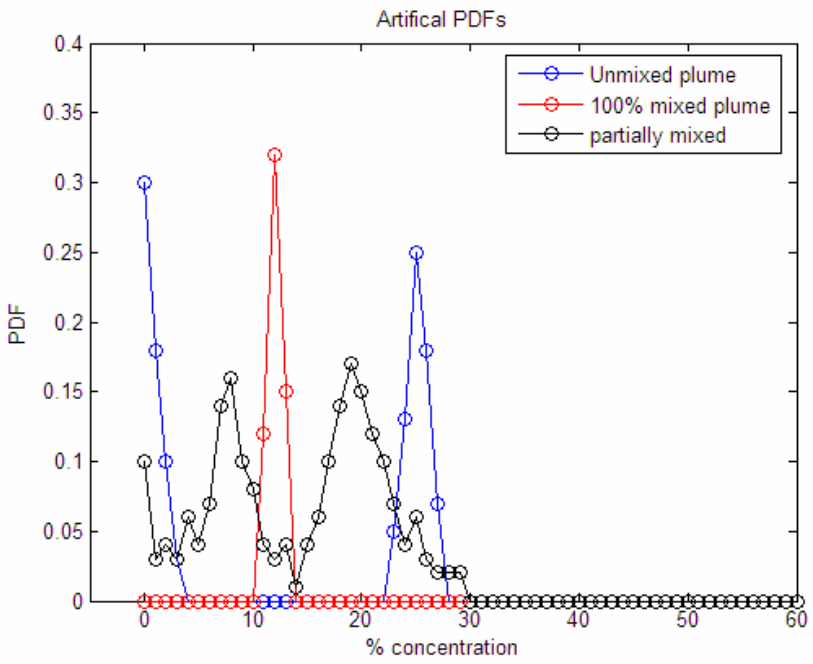

Figure 4.46: Artificial PDF's depicting possible mixing scenario's in the downcomer

First, the single plume cases will be considered; figures 4.47 through 4.52 show all single plume cases at 15 seconds. Notice how for the low and moderate co-flow rates, (figures 4.47 through 4.49) the plots appear to have a small mode shape around 8% concentration, which is easier to see for the moderate co-flow conditions. This is an indication that there is some increased mixing in the cold leg and the downcomer for the moderate co-flow cases vs. the no co-flow condition. At higher co-flow rates, the mixing inside the pipe was increased significantly before the plume enters the downcomer. This is evident from the more uni-model shape of the PDF's and the uniform concentration of dye across the pipe from the line scan camera data. For each single plume case, the PDF's at later times showed similar characteristics to the corresponding cases shown at 15 seconds. The only difference observed was the plume's concentration increased as the cold legs completely filled and then the concentration increased much slower in time as the background fluid concentration in the downcomer gradually increased.

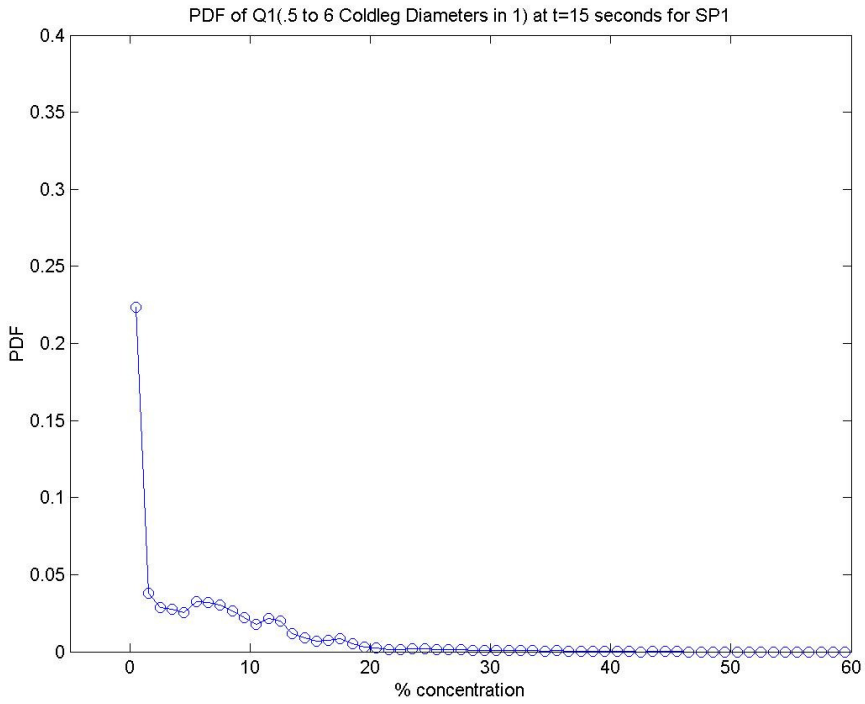

Figure 4.47: PDF of SP1 from .5 to 6 cold leg diameters below the center of the cold leg in Q1 at 15 seconds

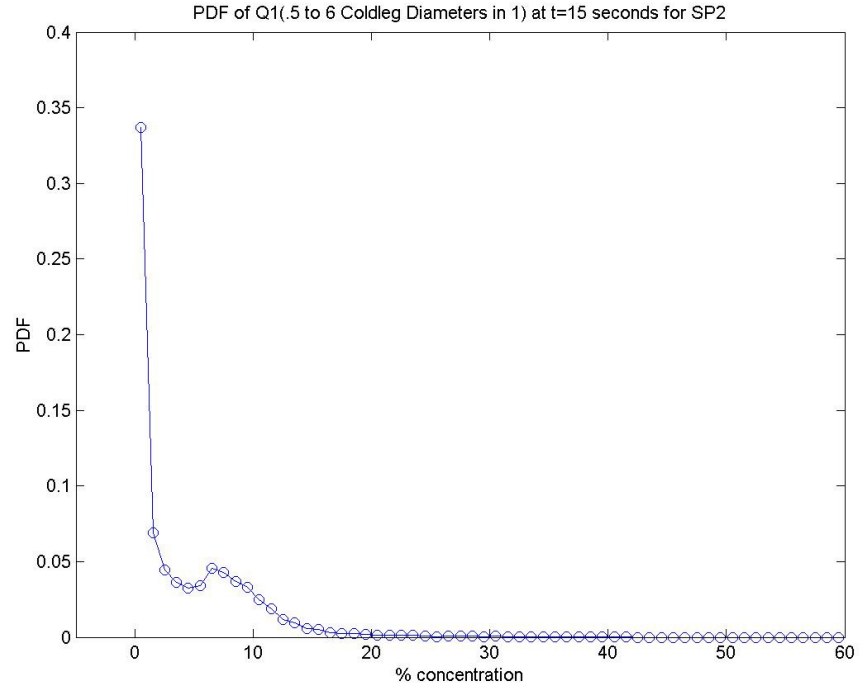

Figure 4.48: PDF of SP2 from .5 to 6 cold leg diameters below the center of the cold leg in Q1 at 15 seconds

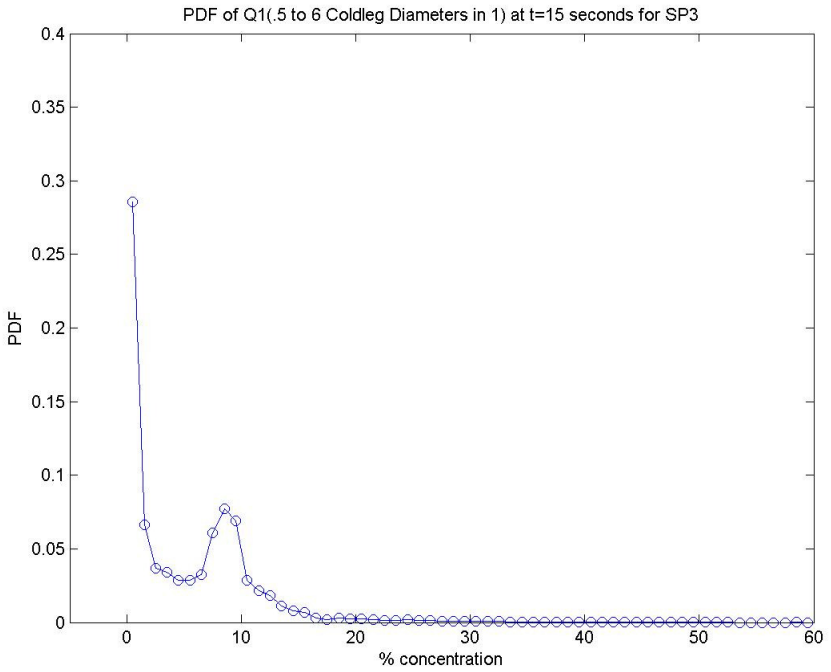

Figure 4.49: PDF of SP3 from .5 to 6 cold leg diameters below the center of the cold leg in Q1 at 15 seconds

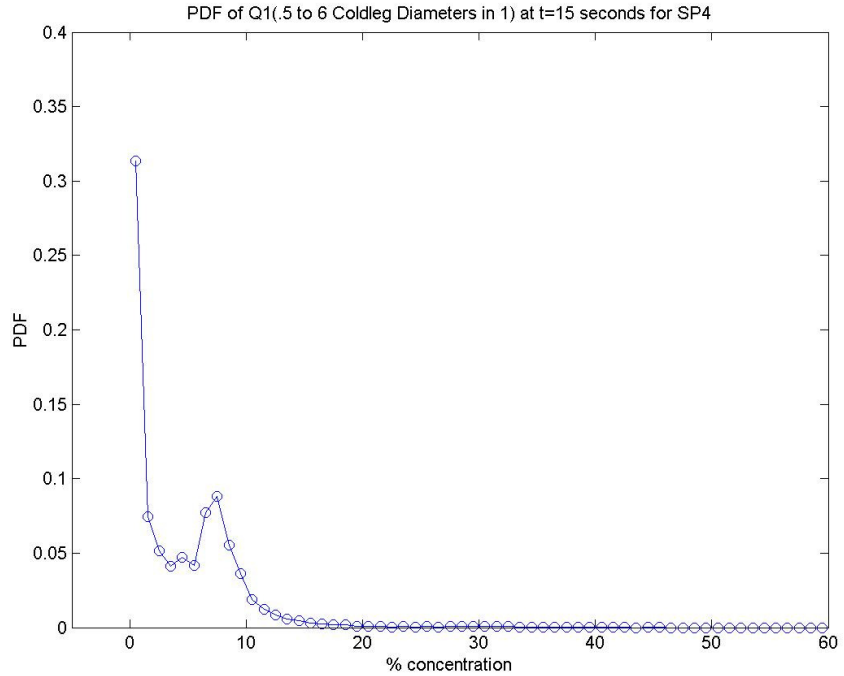

Figure 4.50: PDF of SP4 from .5 to 6 cold leg diameters below the center of the cold leg in Q1 at 15 seconds

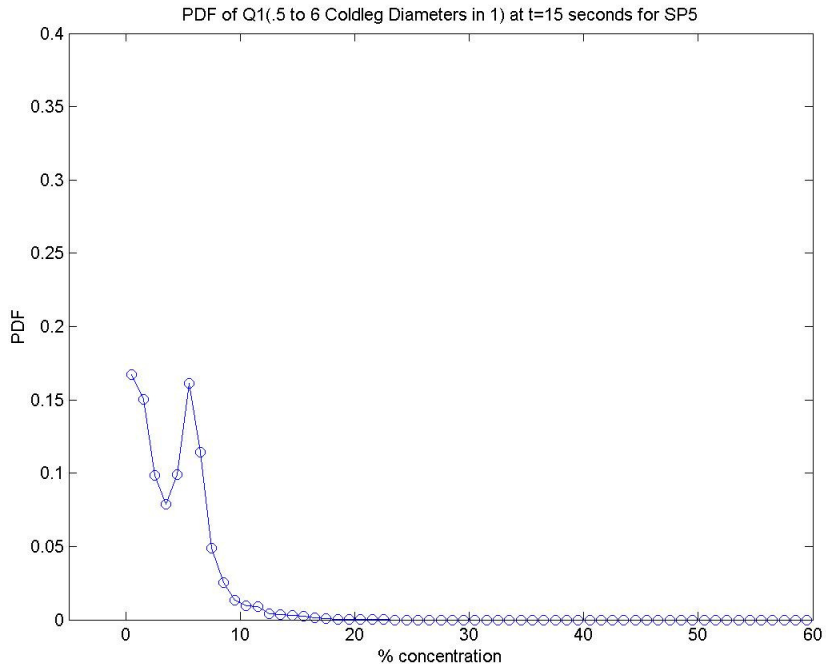

Figure 4.51: PDF of SP5 from .5 to 6 cold leg diameters below the center of the cold leg in Q1 at 15 seconds

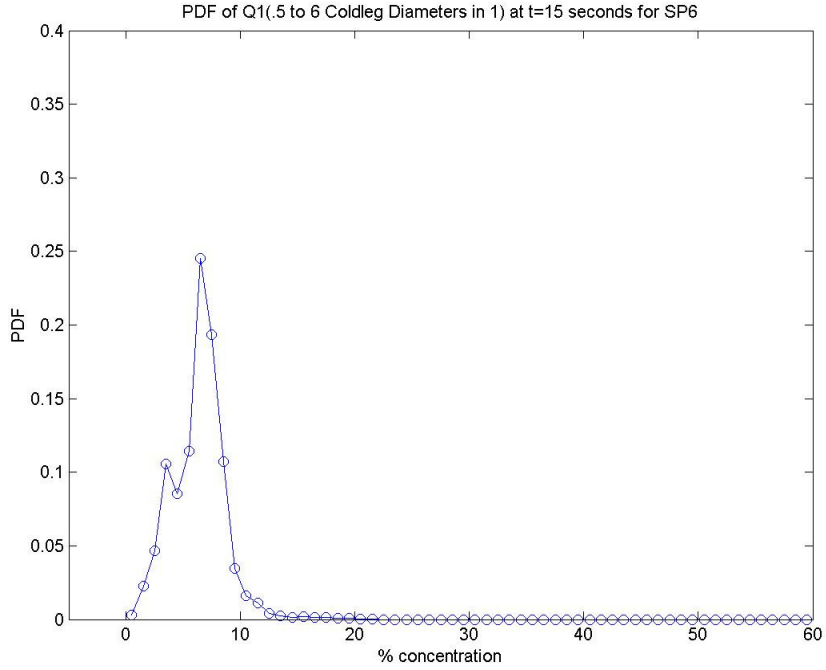

Figure 4.52: PDF of SP6 from .5 to 6 cold leg diameters below the center of the cold leg in Q1 at 15 seconds

Figures 4.53 through 4.57 show PDF's of the multiple plume case MP1 at different instances in time. Initially, at t=10 seconds (4.53), all of the plumes look similar and have very similar concentrations. As time progresses, the concentration of the plumes grows stronger and some plumes have higher concentrations than others indicating that as the flow in the cold legs reaches equilibrium, the concentration entering the downcomer is increasing. For instance at 25 seconds (figure 4.55), the PDF's show that plume 3 has an larger concentration and concentration distribution than plumes 1, 2, and 4, suggesting that plumes 1, 2, and 4 are mixing more rapidly with the surrounding fluid then plume 3. At 50 seconds (figure 4.57) and beyond, the plots showed plumes 2 and 3 having a larger concentration than plumes 1 and 4.

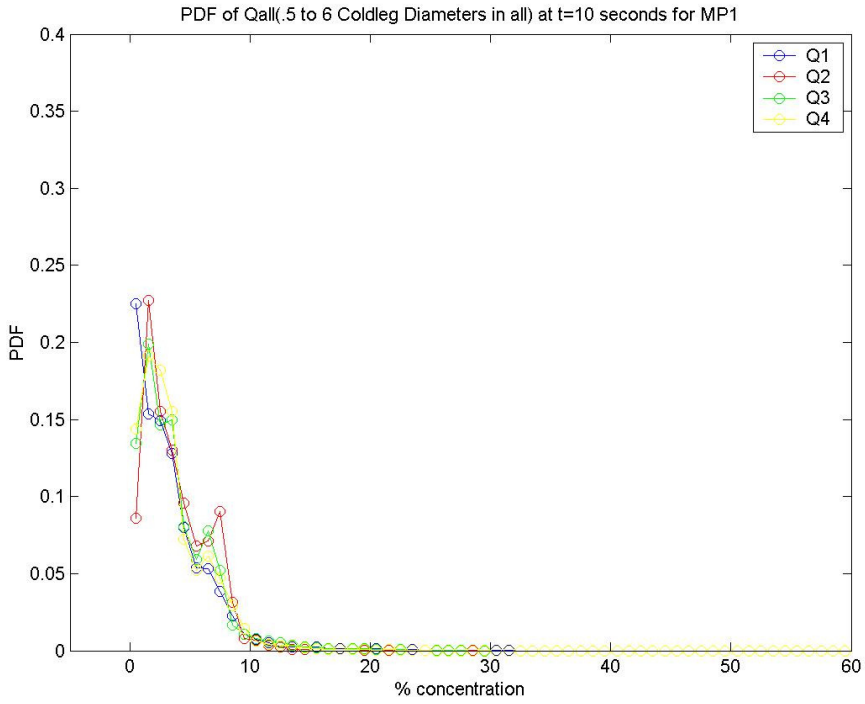

Figure 4.53: PDF of MP1 from .5 to 6 cold leg diameters below the center of the cold leg at 10 seconds

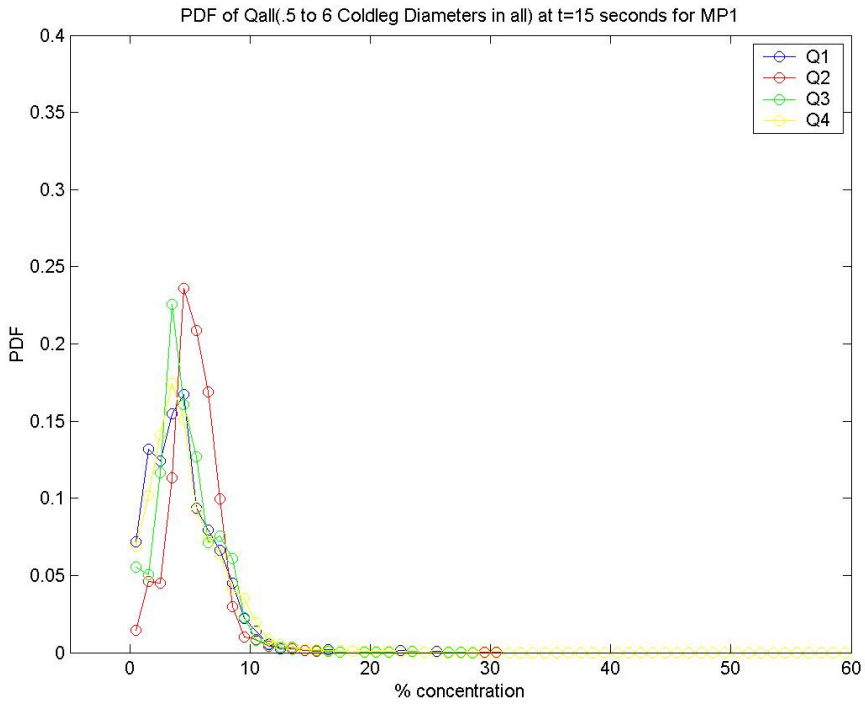

Figure 4.54: PDF of MP1 from .5 to 6 cold leg diameters below the center of the cold leg at 15 seconds

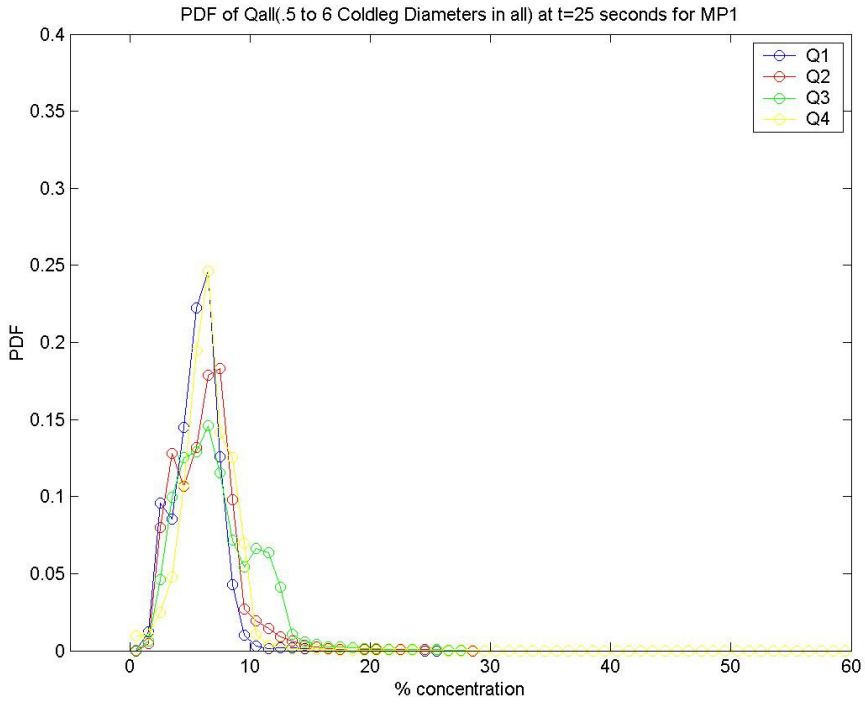

Figure 4.55: PDF of MP1 from .5 to 6 cold leg diameters below the center of the cold leg at 25 seconds

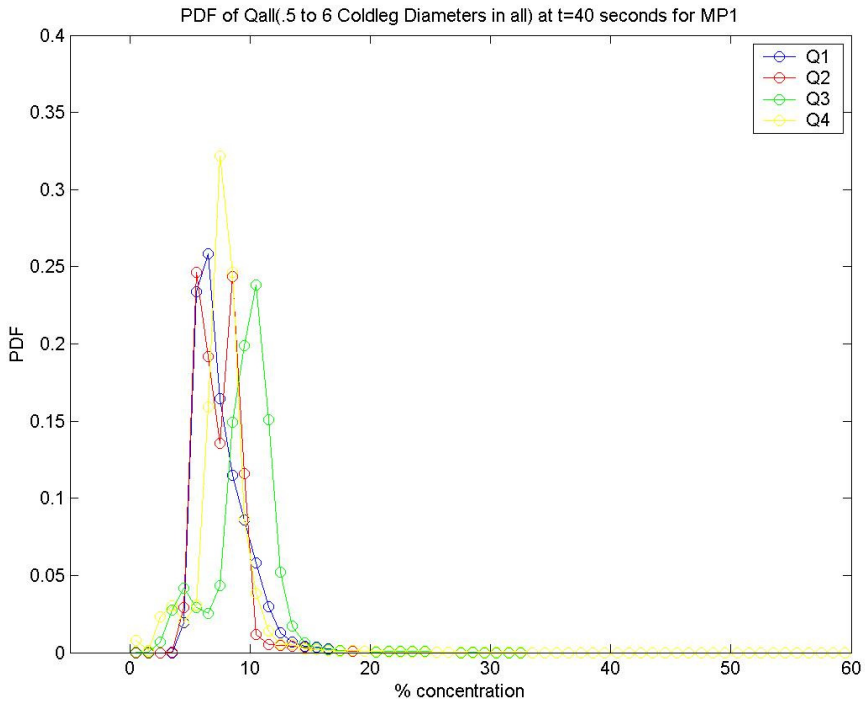

Figure 4.56: PDF of MP1 from .5 to 6 cold leg diameters below the center of the cold leg at 40 seconds

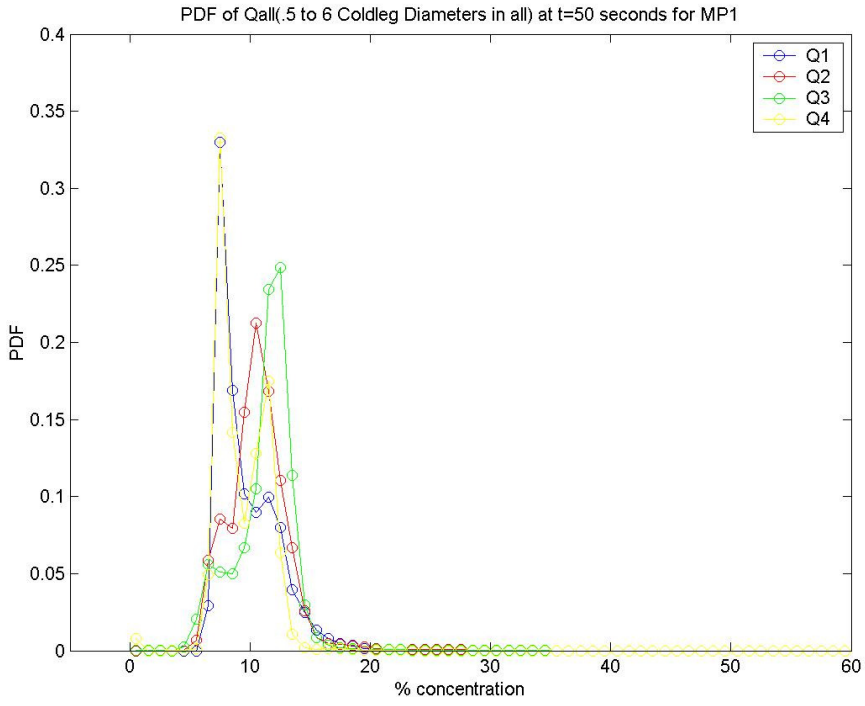

Figure 4.57: PDF of MP1 from .5 to 6 cold leg diameters below the center of the cold leg at 50 seconds

By examining the PDF's, it can be seen that for the single plume case SP1 (figure 4.47) the distribution of the concentrations present is relatively uniform from roughly 1% through 12% then diminishing in probability between 12% and 20%; there is a high probability of near zero concentration, which represents the area outside of the plume. In contrast, the four plume PDF at 15 seconds (figure 4.54) shows that the probability of seeing concentrations above 10% for the same Froude number is quite small, which indicates that the presence of the other plumes tends to change the mixing characteristics in the downcomer. Since the two tests were run at the same conditions with no co-flow, the mixing in the cold legs should be identical for the single plume vs. four plume conditions. Therefore, the changes seen in the PDF's are due entirely to the presences of the multiple plumes. This is further noticed at very early times in the test. Figure 4.58 shows PDF's for SP1 and MP1 at seven seconds into the test, while figure 4.59 shows the same cases at 15 seconds. Notice how the PDF's at 7 seconds look almost identical. Also note how rapidly the plume interaction in the down comer has an effect on the concentration of the plumes. At 7 seconds, the PDF's for SP1 and MP1 showed similar effects while the plumes look very different at 15 seconds into the test. Notice the pronounced mode shape to the PDF in figure 4.58 for MP1, which is not seen at 7 seconds into MP1 and is not near as pronounced in the SP1 test as it is in MP1.

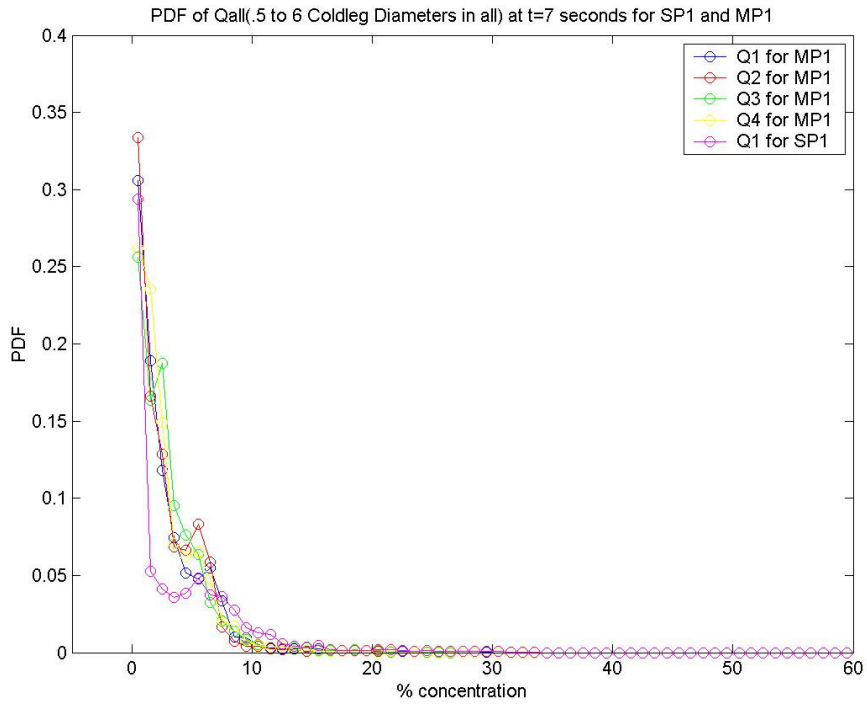

Figure 4.58: PDF of MP1 and SP1 from .5 to 6 cold leg diameters below the center of the cold leg at 7 seconds

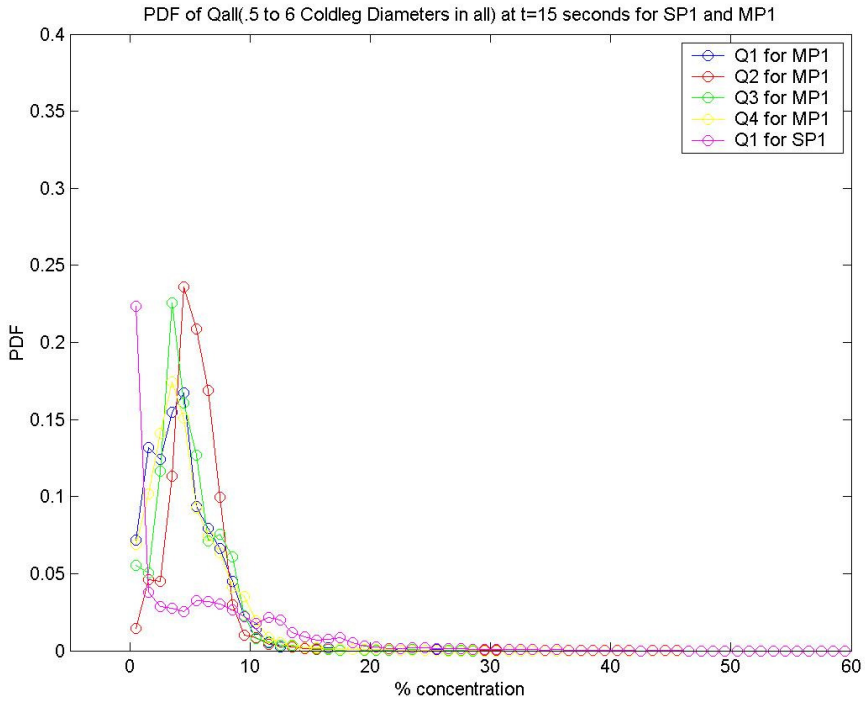

Figure 4.59: PDF of MP1 and SP1 from .5 to 6 cold leg diameters below the center of the cold leg at 15 seconds

The shape of the PDF's for the four plume case look more uni-modal as compared to the single plume case, indicating that the presence of the other plumes enhances mixing in the downcomer as compared to the single plume cases. It is expected that as the rate of mixing is increased inside the downcomer, the PDF's would become narrower in the range of concentrations present and show a pronounced peak around the average concentration in the downcomer (see figure 4.46). For a completely mixed downcomer only one concentration would be present. While for no mixing the PDF's would show a peak around the concentration of the background fluid and a peak around the concentration of the incoming injected fluid, similar to a bi-modal distribution. The PDF's for the no co-flow, single plume case show evidence from their shape that there is some significant amounts of mixing taking place, while the multiple plume cases show a much more mixed condition as compared to the shape of their single plume counterparts.

As the circulation in the downcomer develops for the multiple plume cases, the plumes seem to pair together to form two dominate plumes. The effect of this pairing can be seen in the PDF's for the multiple plumes. Figure 4.60 is a PDF for case MP1 and SP1 at 45 seconds. Notice how in the MP1 case, that plumes 2 and 3 have a higher overall concentration then plumes 1 and 4. At 45 seconds the circulation is well established with plumes 2 and 3 in the downward moving part of the circulation and plumes 1 and 4 in the upward moving part. Figure 4.61 shows a filled contour plot with the red arrows indicating the direction of flow. From figure 4.61 it can be seen that the circulation is affecting the plumes differently depending on where they are in the circulation. Plumes 2 and 3 have a higher overall concentration which suggests that they are not mixing as rapidly with the surrounding fluid as compared to plumes 1 and 4.

Since the entrainment of fluid into the plumes is a function of the velocity difference between the plume and the surrounding fluid, a higher overall concentration indicates that the velocity gradient is less. This indicates that the direction of the circulation present is downward for plumes 2 and 3 while the velocity is upward for plumes 1 and 4 resulting in a lower velocity gradient for plumes 2 and 3, while plumes 1 and 4 have a larger velocity gradient.

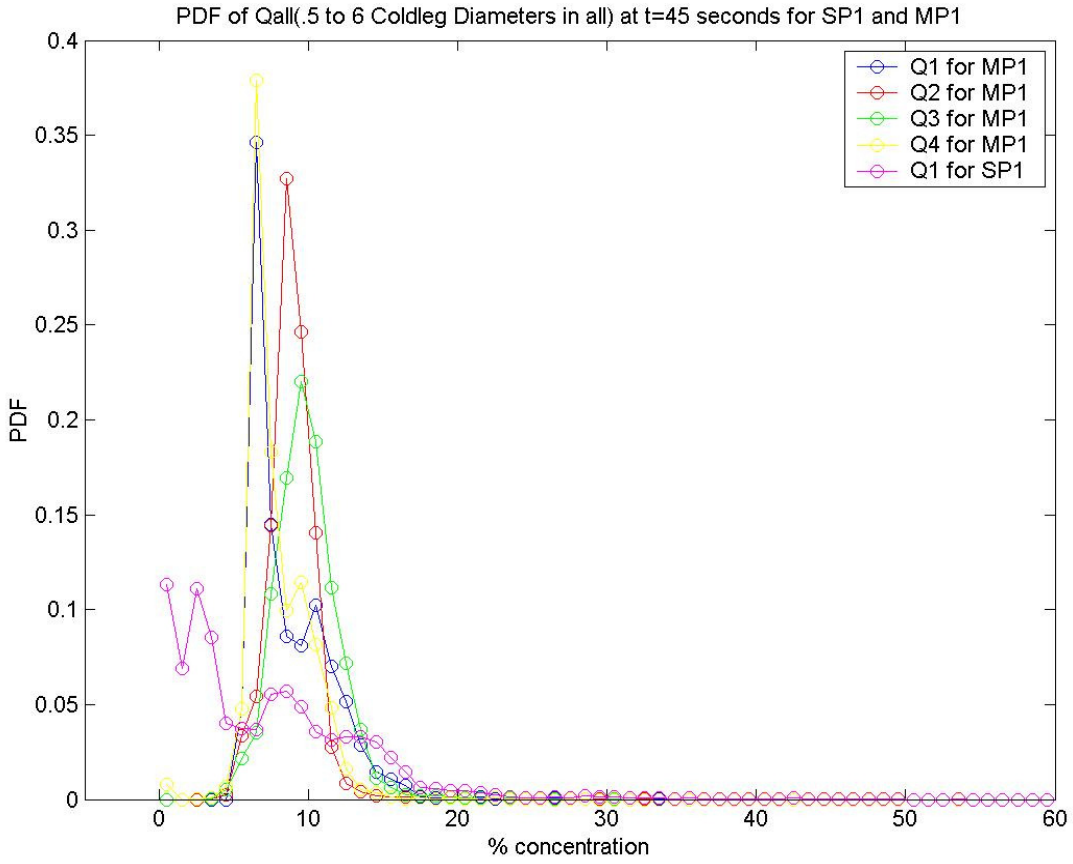

Figure 4.60: PDF of concentration for MP1 and SP1 at 45 seconds.

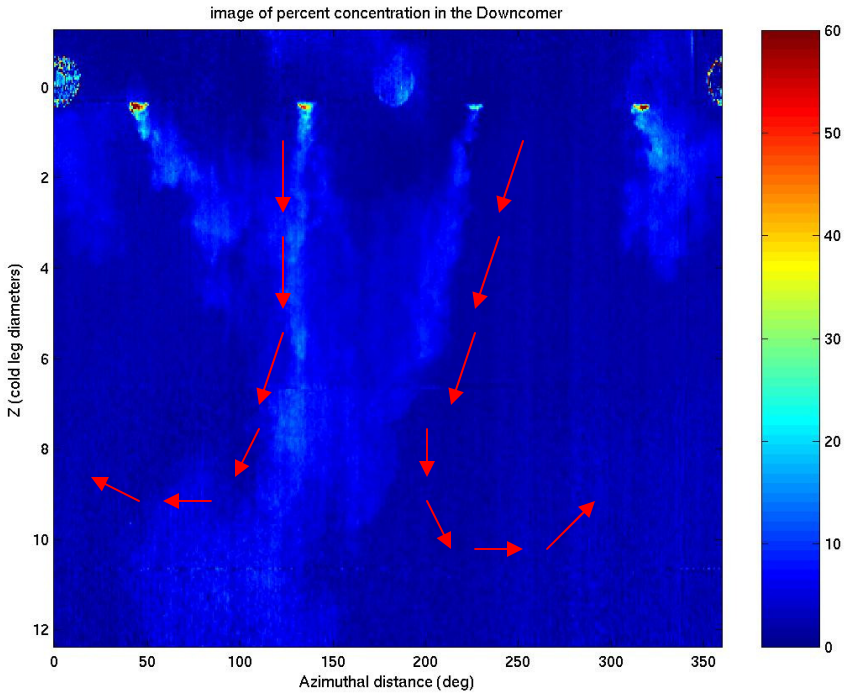

Figure 4.61: Filled contour plot of concentration for MP1 at 45 seconds.

The decay in concentration of the plumes is directly coupled to the entrainment of outside fluid into the plume. How the presence of the multiple plumes in the downcomer affects the entrainment rate is important to understanding if this situation is a possible safety concern. Examination of how the plume concentration changes as it falls in the downcomer gives insight into the magnitude of the entrainment rate. As seen in the previous PDF plots for multiple plume cases, plumes that are next to each other in the downcomer pair together and the flow visualization indicates that the concentration of the plumes are changed from the single plume case by a circulation in the downcomer. The plots in figures 4.62 through 4.67 show the maximum concentration of the plume vs. Z for MP3 and SP3 at different times. The plots in figures 4.62 through 4.66 were constructed by averaging the five largest concentration values inside the plume at each height z, and then averaging them over a time span of 5 seconds to form an ensemble of

images. This process yields a measure of the maximum intensity of the plume as a function of height.

In figure 4.62 it can be seen that at early times before the multiple plume circulation is established that the maximum concentration of the plumes looks very similar to each other. At 10 seconds, figure 4.63 shows the plumes as plumes 2 and 3 are becoming the dominate plume pair. At 15 seconds (figure 4.64) the single plume case has a slightly higher concentration then any of the multiple plumes. This is because the circulation in the downcomer from the multiple plumes tends to enhance mixing as the plumes enter the downcomer. Figure 4.65 shows how plumes 2 and 3 are at a higher concentration in the downcomer than plumes 1 and 4, moreover notice how the single plume case (SP3) is at a lower concentration at the bottom of the downcomer then plumes 2 and 3 from case MP3. Even though the single plume starts out at an higher concentration then the multiple plumes, the concentration of the single plume decays faster than the multiple plumes. This is an indication that the multiple plumes have a lower entrainment rate then the single plume case. Figure 4.66 shows the plumes at 30 seconds. Again notice how the single plume concentration is decaying faster then the multiple plumes and how the single plume concentration in the bottom of the downcomer is significantly smaller than for all the plumes in case MP3. At 30 seconds there is a transition from plumes 2 and 3 being the dominate plumes to plumes 1 and 4 being the dominate pair. Figure 4.67 shows the plumes at 40 seconds in the test and plumes 1 and 4 are higher in concentration in the bottom of the downcomer then plumes 2 and 3. The concentration of the multiple plumes continues to be higher then the concentration of the single plume in the bottom of the downcomer where PTS is a concern.

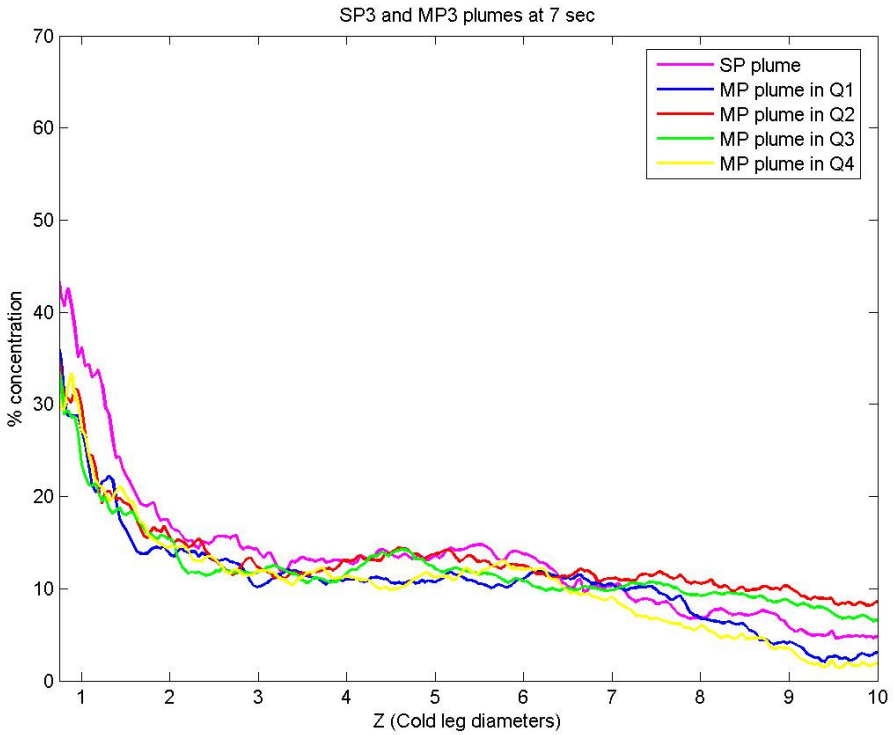

Figure 4.62: Plot of maximum concentration vs Z for SP3 and MP3 at 7 seconds

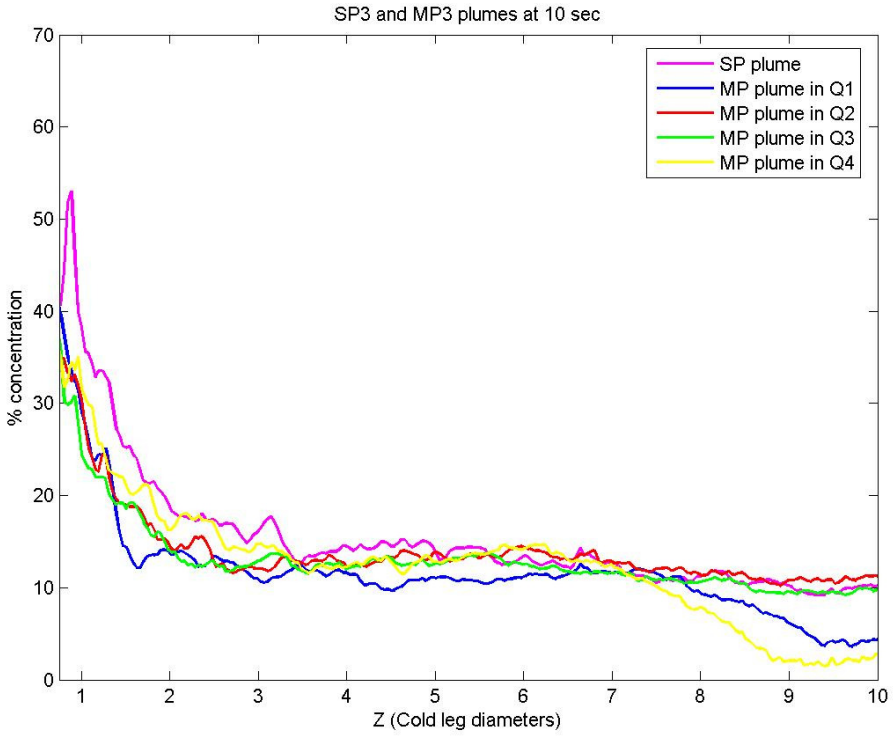

Figure 4.63: Plot of maximum concentration vs Z for SP3 and MP3 at 10 seconds

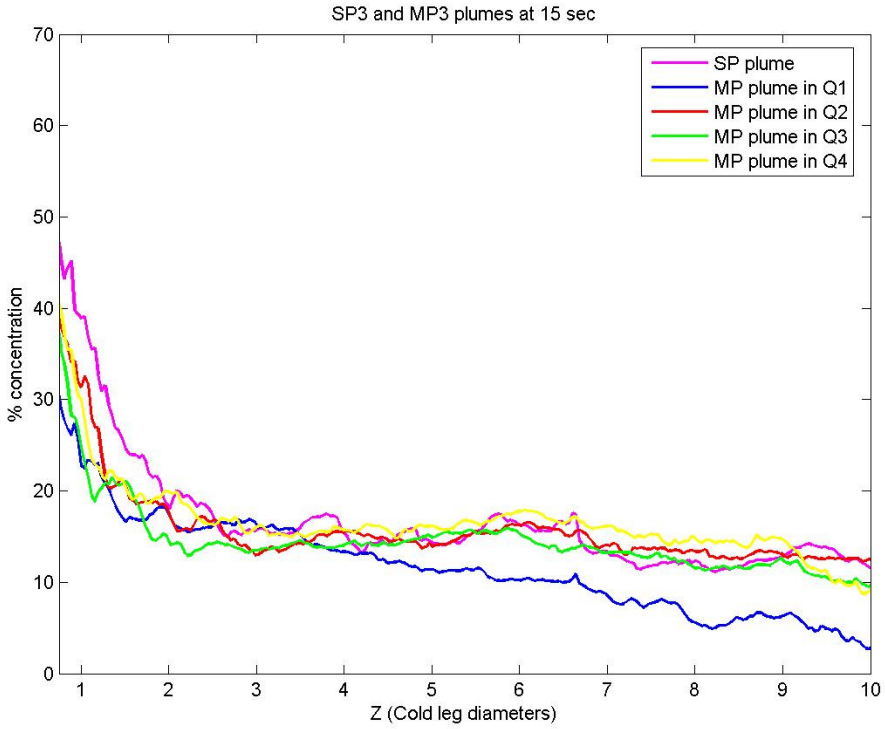

Figure 4.64: Plot of maximum concentration vs Z for SP3 and MP3 at 15 seconds

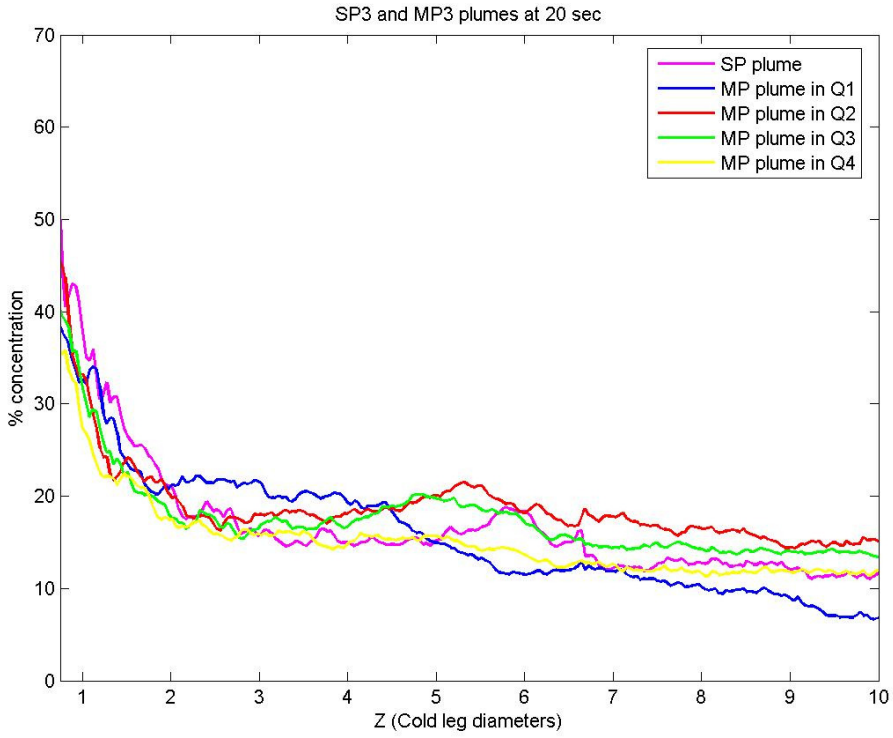

Figure 4.65: Plot of maximum concentration vs Z for SP3 and MP3 at 20 seconds

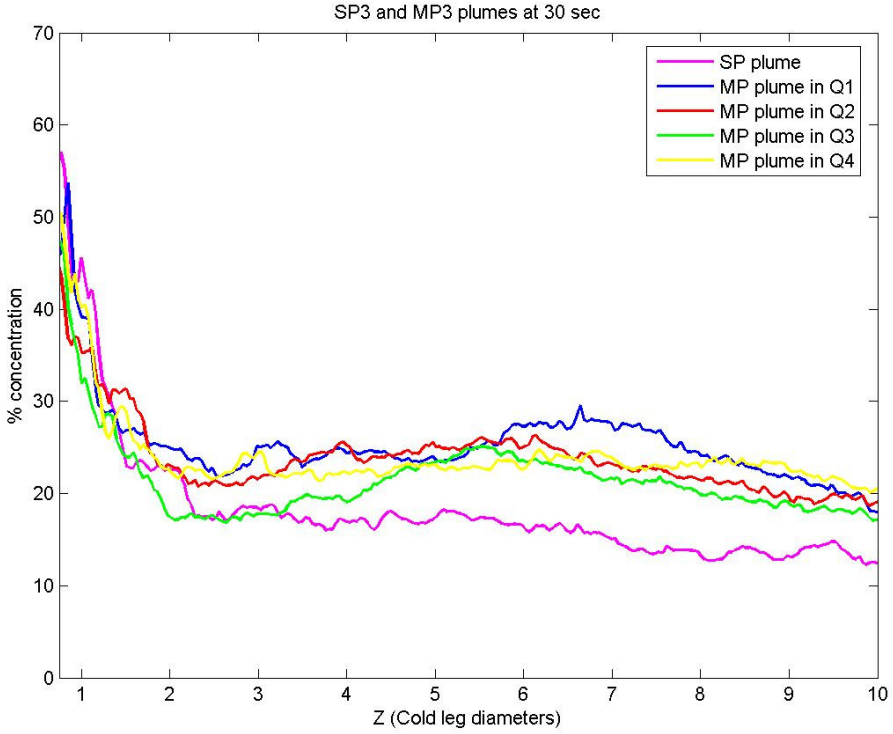

Figure 4.66: Plot of maximum concentration vs Z for SP3 and MP3 at 30 seconds

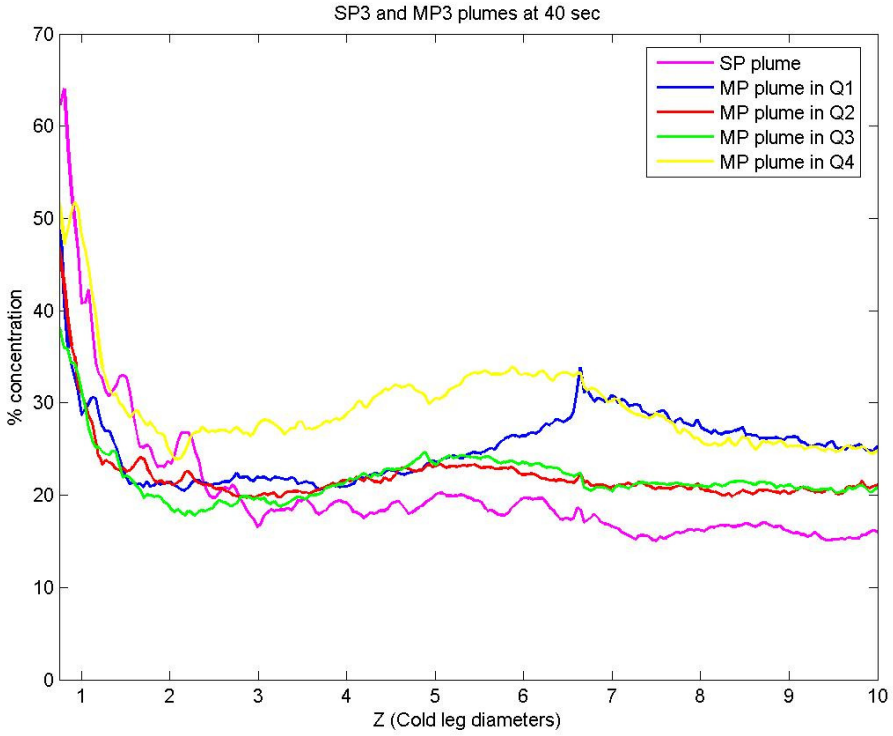

Figure 4.67: Plot of maximum concentration vs Z for SP3 and MP3 at 40 seconds

This agrees well with Townsend's entrainment theory (details on theory located in literature section), which suggests that entrainment rate of outside fluid into a plume is proportional to the velocity gradient between the plume and the surrounding fluid. It can be seen in figure 4.65 at 20 seconds where plumes 2 and 3 are paired together and the decay in concentration of the plumes is less than that of plumes 1 and 4. Plumes 1 and 4 are experiencing a larger velocity gradient between the plume and the surrounding fluid, which implies a larger entrainment rate and faster decay in concentration.

In the single plume cases, the velocity of the background fluid is small, while because of buoyancy forces the plume has a downward velocity. For the multiple plume cases, the velocity of the background fluid is no longer small. After the circulation has established itself in the downcomer, the background fluid has a downward velocity in the vicinity of plumes 2 and 3 and an upward velocity around plumes 1 and 4. For plumes 2 and 3, the velocity gradient between the plume and the background is less than for the single plume case. According to Townsend's entrainment theory, if the velocity gradient is reduced, the entrainment and mixing of the two fluids will be less. However, the recirculation in the downcomer significantly increases the mixing in Mixing Region 3 (the first 2 cold leg diameters in the downcomer), resulting in weaker initial plumes for the multiple plume case then for the single plume cases. Therefore, the higher concentration of plumes 2 and 3 due to the circulation is a concern because of the decreased mixing for those plumes. With decreased mixing there will be a larger temperature gradient between the plumes and the wall of the downcomer then in the single plume case. The thermal stress on the downcomer wall is directly proportional to the temperature gradient between the fluid and the downcomer wall.

Chapter 5: Conclusion

The occurrence of Pressurized Thermal Shock in the downcomer section of a Pressurized Water Reactor is a safety concern to operators and designers of these facilities. The UMD facility was a ¼ linear scale model of the Palisades nuclear facility, with some slight changes to accomplish experimental investigation. The tests preformed in the UMD facility show that there are significant differences in the plume behavior between single plume and multiple plume cases, which were not completely considered in previous studies. Multiple plumes in the downcomer produce a large recirculation region in the downcomer, which alters the entrainment of fluid into the plumes and changes the mixing characteristics inside the downcomer. As the recirculation begins to form, some plumes experience higher entrainment rates than others in the downcomer. This can be seen by plumes with lower entrainment rates having a higher concentration in the downcomer. As time progresses, the recirculation grows and establishes itself. Because of the geometry of the downcomer, plumes 2 and 3 are paired together, while plumes 1 and 4 are paired. The presence of the hot legs constrains the circulation to be symmetric around plumes 2 and 3 or 1 and 4 after the circulation is established. It's observed that the pairs of plumes randomly switch back and forth between dominate and recessive pairing. However in the UMD experiments, plumes 2 and 3 tended to spend more time being dominate then plumes 1 and 4.

It is postulated that the higher and lower entrainment rates of the multiple plumes as compared to the single plume are from the motion of the background fluid in relation to the velocity of the plumes. By using Townsend's entrainment theory, it can be seen that as the difference in velocity between the background fluid and the plume increases,

the entrainment rate will also increase, which increases the mixing of the plume with its surroundings. The converse is also true, that as the velocity of the background fluid approaches the velocity of the plume, the entrainment rate goes down, resulting in a plume that remains relatively un-mixed as compared to the single plume cases. The circulation in the downcomer affects the velocity of the background fluid. When plumes 2 and 3 are the dominate pairing, the velocity gradient between plumes 2 or 3 and the background fluid is less then the velocity gradient between plumes 1 or 4 and the background fluid. This causes plumes 2 and 3 to remain relatively unmixed causing a high concentration of unmixed fluid in the bottom of the downcomer below cold legs 2 and 3. The higher concentration could potentially give rise to a larger thermal stress along the bottom of the downcomer, as compared to cases where only a single plume is present; this area of the downcomer is where hydrogen enbrittlement of the vessel wall is a concern. The circulation is not as strong with only one plume in the downcomer, and most quantitative experiments have only examined PTS with a single incoming plume. Because of the motion of the background fluid with four plumes, the multiple plume case may produce a higher stress on the walls of the downcomer then previously studied in single plume experiments. The plots of concentration vs. distance below the cold legs for the four plume cases shows that plumes 2 and 3 decay very slowly as they fall farther into the downcomer, while plumes 1 and 4 decay faster. Townsend's entrainment theory suggests that the lower entrainment rate for plumes 2 and 3 will cause their concentration to be larger then the single plume case.

The uncertainty of the measurements in this location of the downcomer makes the experiment more qualitative rather then quantitative. In the bottom of the downcomer the

angle of the incoming laser beam was 10 to 15 degrees which made the measurement more sensitive to changes in index of refraction between the two fluids. As calculated previously in the experimental error section, this can give rise to errors around 6% in this region of the downcomer making direct measurements difficult. However, the flow field visualization and detailed concentration measurements in other regions of the downcomer suggest that the four plume circulation in the downcomer can produce larger thermal stress's then the single plume cases previously studied.

5.1 Future work

The plume visualizations indicate that mixing is reduced for plumes 2 and 3 because of the circulation inside the downcomer. To gain farther insight into this phenomenon, obtaining detailed measurements of the velocity field could prove valuable and may give more insight into the entrainment rates of the plumes.

Second, because of the possibility of large errors in the bottom of the downcomer, the measurements in that region are more qualitative rather then quantitative. This presents difficulties in comparing the single plume cases to their four plume counter parts. The optical measurements made by the UMD facility were focused on capturing the entire downcomer and compromises were made in the accuracy in the bottom of the downcomer to facilitate the measurement of the entire flow field. With the knowledge of the recirculation in the downcomer, future optical facilities could shift there focus on accurately capturing 3-D concentration fields in the bottom of the downcomer to see how the concentration of the multiple plume cases compares with the single plume cases.

Appendix A: Part Drawings for UMD Facility

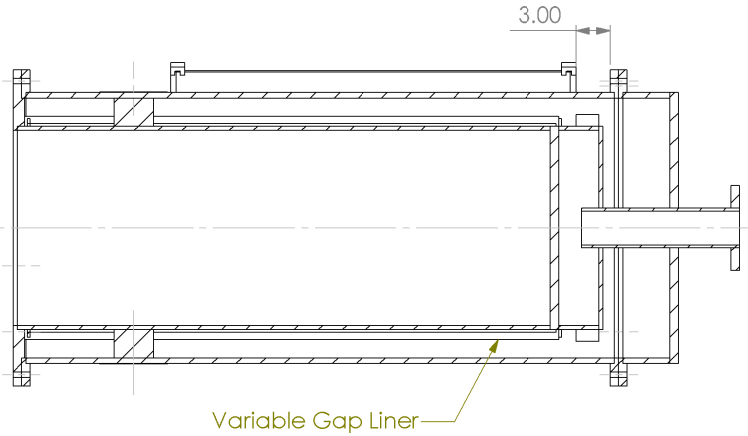

Section A-A (1 : 12)

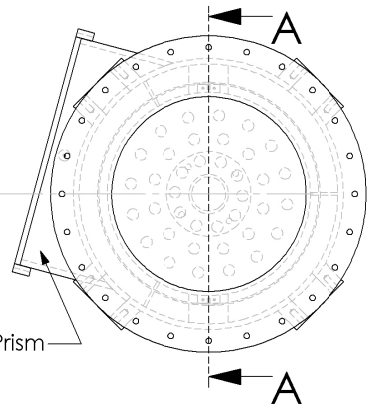

Note:
1. Viewing Prism assembly will not be glued to outer barrel.

ITEM NO.	PART OR IDENTIFYING NO.	NOMENCLATURE OR DESCRIPTION	MATERIAL SPECIFICATION	QTY REQD

PARTS LIST

UNLESS OTHERWISE SPECIFIED DIMENSIONS ARE IN INCHES
TOLERANCES ARE:
FRACTIONS DECIMALS ANGLES
.XX ± 0.05 .XX ± 0.5°
.XXX ± 0.01 .XXX ± 1/8

MATERIAL Perspex
FINISH --

NEXT ASSY | USED ON
APPLICATION
DO NOT SCALE DRAWING

CAD GENERATED DRAWING, DO NOT MANUALLY UPDATE

APPROVALS	DATE
DRAWN	
CHECKED	
RESP ENG	
MFG ENG	
QUAL ENG	

UNIVERSITY OF MARYLAND

Whole Assembly

SIZE A | DWG. NO. | REV.
SCALE | CAD FILE: | SHEET OF

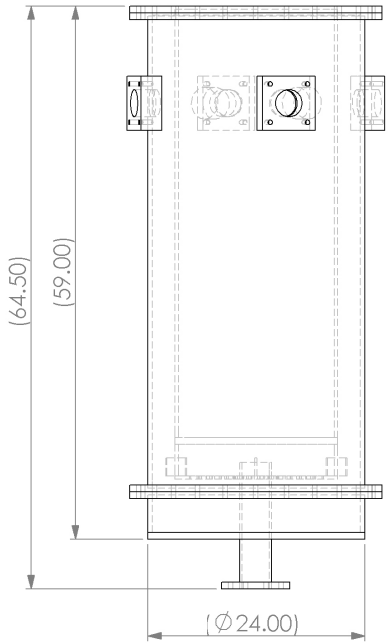

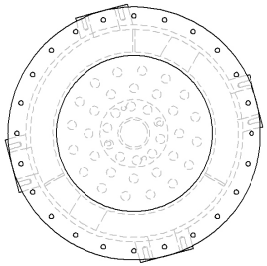

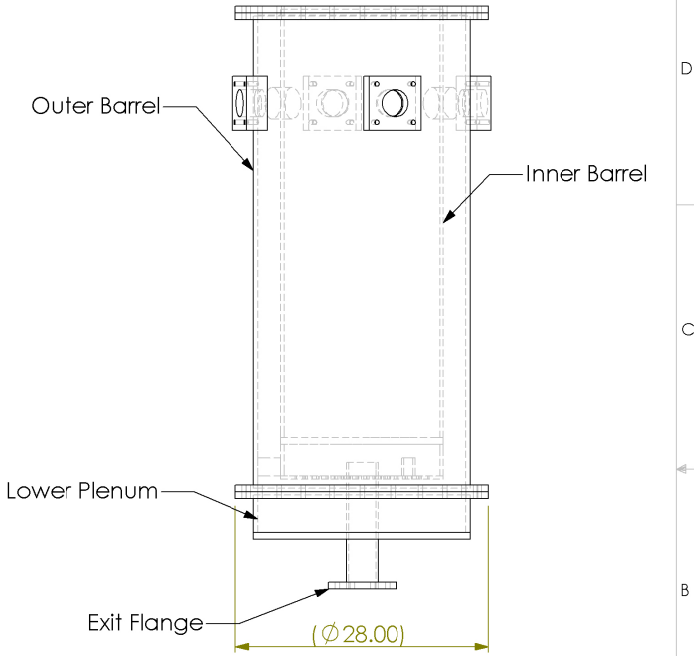

ITEM NO.	PART OR IDENTIFYING NO.	NOMENCLATURE OR DESCRIPTION	MATERIAL SPECIFICATION	QTY REQD

PARTS LIST

UNLESS OTHERWISE SPECIFIED DIMENSIONS ARE IN INCHES
TOLERANCES ARE:
FRACTIONS DECIMALS ANGLES
.XX ± 0.05 .XX ± 0.5°
.XXX ± 0.01 .XXX ± 1/8

MATERIAL Perspex
FINISH --

NEXT ASSY | USED ON
APPLICATION
DO NOT SCALE DRAWING

CAD GENERATED DRAWING.
DO NOT MANUALLY UPDATE

APPROVALS	DATE
DRAWN	
CHECKED	
RESP ENG	
MFG ENG	
QUAL ENG	

UNIVERSITY OF MARYLAND

Assembly

SIZE A | DWG. NO. | REV.
SCALE: 1:15 | CAD FILE: | SHEET OF

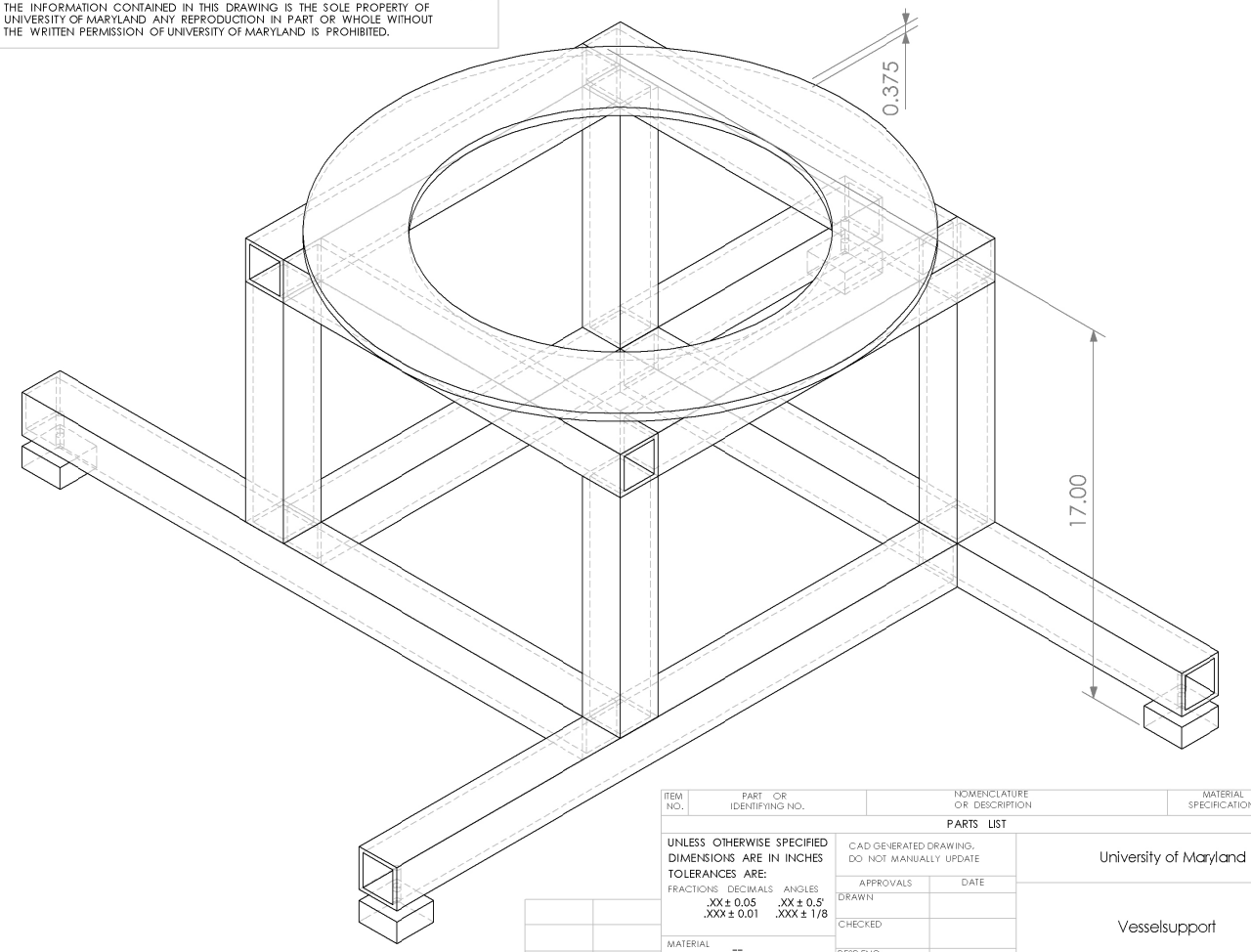

ITEM NO.	PART OR IDENTIFYING NO.	NOMENCLATURE OR DESCRIPTION	MATERIAL SPECIFICATION	QTY REQD

PARTS LIST

UNLESS OTHERWISE SPECIFIED DIMENSIONS ARE IN INCHES
TOLERANCES ARE:
FRACTIONS DECIMALS ANGLES
.XX ± 0.05 .XX ± 0.5°
.XXX ± 0.01 .XXX ± 1/8

MATERIAL --

FINISH --

DO NOT SCALE DRAWING

CAD GENERATED DRAWING.
DO NOT MANUALLY UPDATE

APPROVALS	DATE
DRAWN	
CHECKED	
RESP ENG	
MFG ENG	
QUAL ENG	

NEXT ASSY | USED ON

APPLICATION

University of Maryland

Vesselsupport

SIZE A | DWG. NO. | REV.

SCALE: 1:1 | CAD FILE: | SHEET 1 OF 1

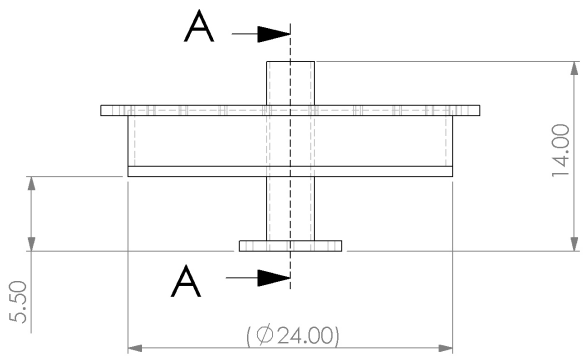

Section A-A

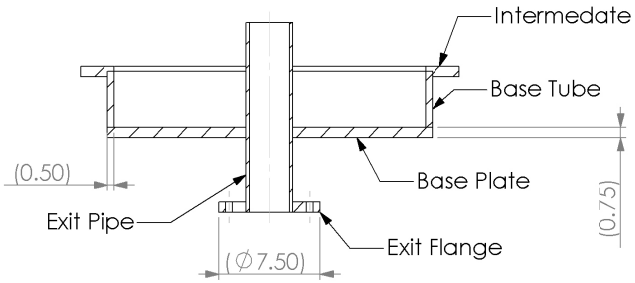

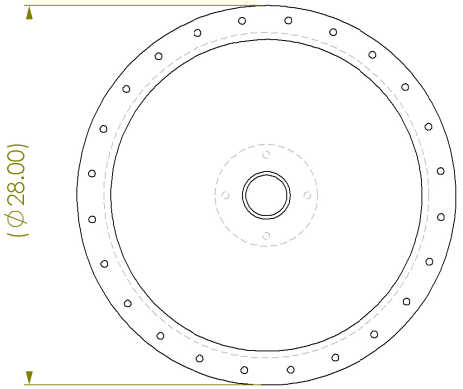

ITEM NO.	PART OR IDENTIFYING NO.	NOMENCLATURE OR DESCRIPTION	MATERIAL SPECIFICATION	QTY REQD
		PARTS LIST		

UNLESS OTHERWISE SPECIFIED DIMENSIONS ARE IN INCHES
TOLERANCES ARE:
FRACTIONS DECIMALS ANGLES
.XX ± 0.05 .XX ± 0.5'
.XXX ± 0.01 .XXX ± 1/8

MATERIAL Perspex
FINISH --

NEXT ASSY | USED ON
APPLICATION
DO NOT SCALE DRAWING

CAD GENERATED DRAWING, DO NOT MANUALLY UPDATE

APPROVALS	DATE
DRAWN	
CHECKED	
RESP ENG	
MFG ENG	
QUAL ENG	

UNIVERSITY OF MARYLAND

A - Lower Plenum

SIZE A | DWG. NO. | REV.
SCALE: 1 : 10 | CAD FILE: | SHEET OF

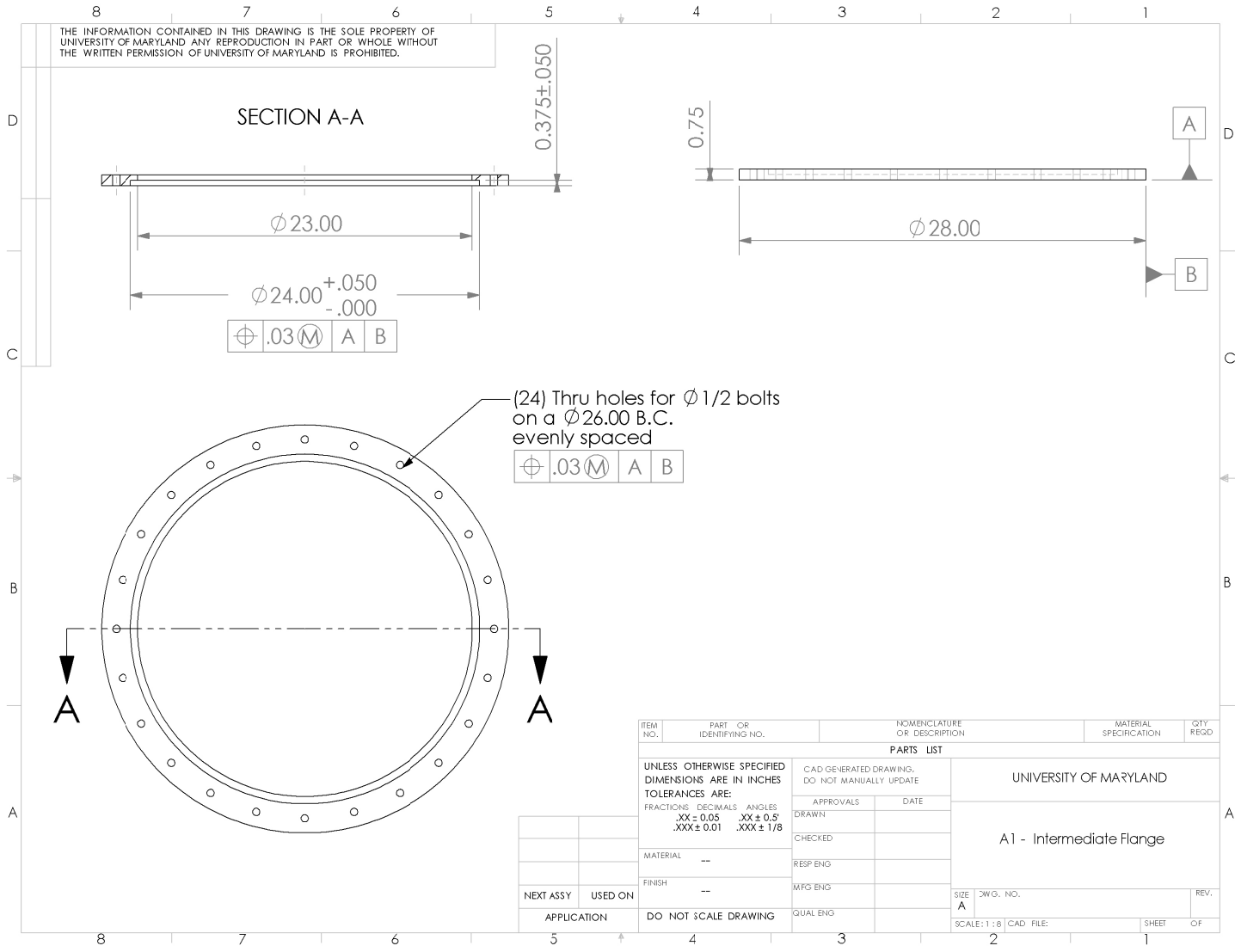

ITEM NO.	PART OR IDENTIFYING NO.	NOMENCLATURE OR DESCRIPTION	MATERIAL SPECIFICATION	QTY REQD

PARTS LIST

UNLESS OTHERWISE SPECIFIED DIMENSIONS ARE IN INCHES
TOLERANCES ARE:
FRACTIONS DECIMALS ANGLES
.XX ± 0.05 .XX ± 0.5°
.XXX ± 0.01 .XXX ± 1/8

MATERIAL --
FINISH --

NEXT ASSY | USED ON
APPLICATION | DO NOT SCALE DRAWING

CAD GENERATED DRAWING, DO NOT MANUALLY UPDATE

APPROVALS	DATE
DRAWN	
CHECKED	
RESP ENG	
MFG ENG	
QUAL ENG	

UNIVERSITY OF MARYLAND

A1 - Intermediate Flange

SIZE A | DWG. NO. | REV.
SCALE: 1 : 8 | CAD FILE: | SHEET OF

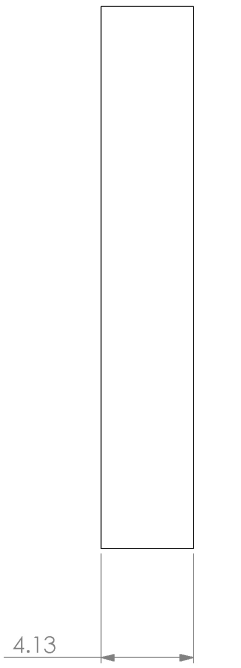

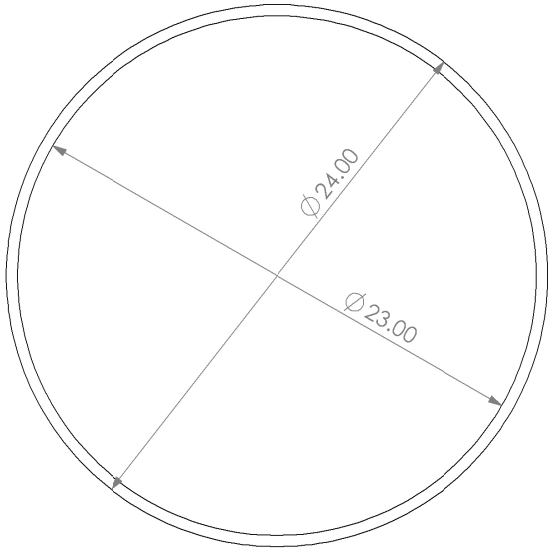

Note:
1. To be cut from standard sized pipe

ITEM NO.	PART OR IDENTIFYING NO.	NOMENCLATURE OR DESCRIPTION	MATERIAL SPECIFICATION	QTY REQD

PARTS LIST

UNLESS OTHERWISE SPECIFIED DIMENSIONS ARE IN INCHES
TOLERANCES ARE:
FRACTIONS DECIMALS ANGLES
.XX ± 0.05 .XX ± 0.5°
.XXX ± 0.01 .XXX ± 1/8

MATERIAL Perspex
FINISH --

NEXT ASSY | USED ON
APPLICATION
DO NOT SCALE DRAWING

CAD GENERATED DRAWING.
DO NOT MANUALLY UPDATE

APPROVALS	DATE
DRAWN	
CHECKED	
RESP ENG	
MFG ENG	
QUAL ENG	

UNIVERSITY OF MARYLAND

A2 - Base Tube

SIZE A | DWG. NO. | REV.
SCALE : 1 : 3 | CAD FILE: | SHEET OF

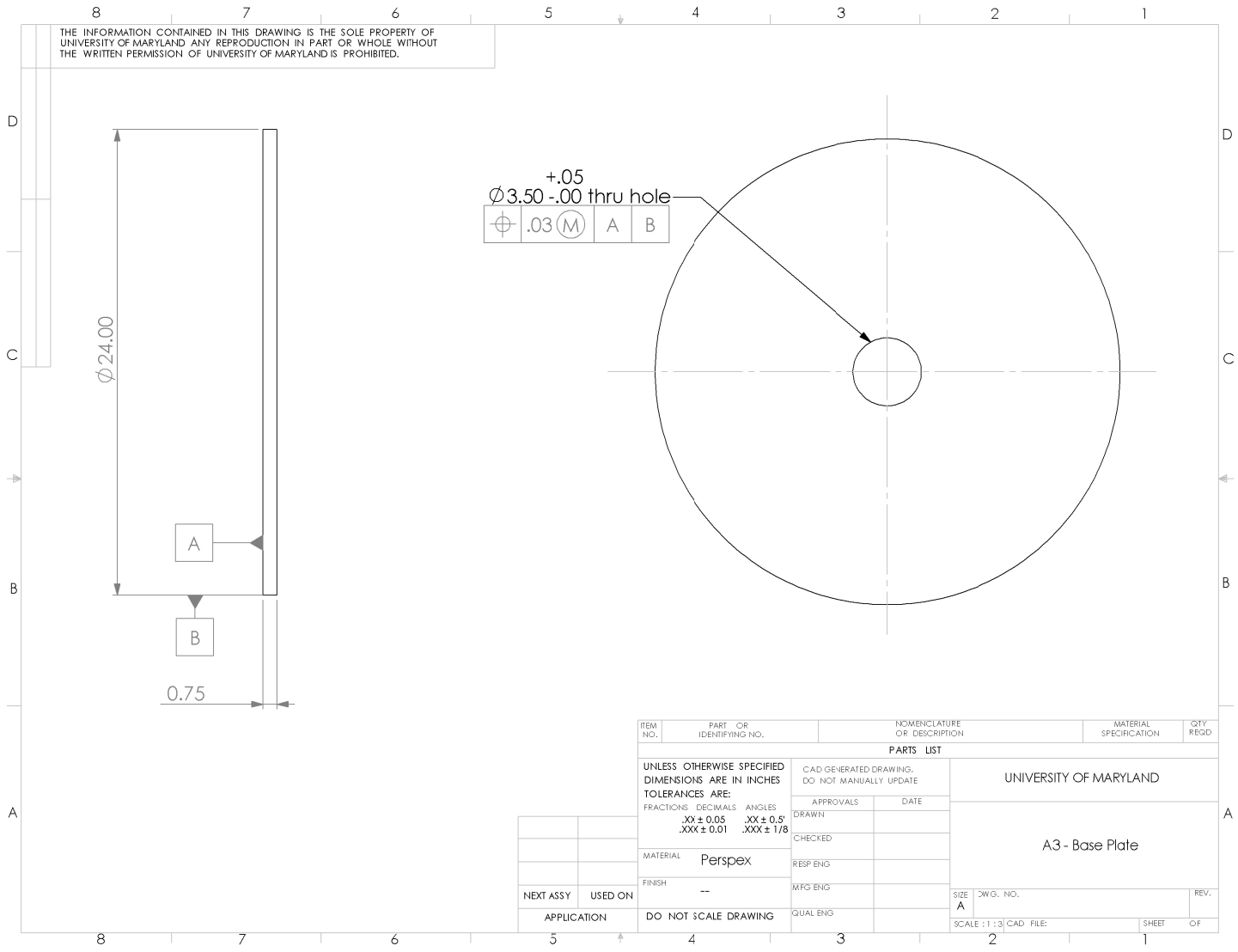
THE INFORMATION CONTAINED IN THIS DRAWING IS THE SOLE PROPERTY OF UNIVERSITY OF MARYLAND ANY REPRODUCTION IN PART OR WHOLE WITHOUT THE WRITTEN PERMISSION OF UNIVERSITY OF MARYLAND IS PROHIBITED.
+.05
∅3.50 -.00 thru hole
.03 M A B
∅24.00
A
B
0.75
ITEM NO.
PART OR IDENTIFYING NO.
NOMENCLATURE OR DESCRIPTION
MATERIAL SPECIFICATION
QTY REQD
PARTS LIST
UNLESS OTHERWISE SPECIFIED DIMENSIONS ARE IN INCHES
TOLERANCES ARE:
FRACTIONS DECIMALS ANGLES
.XX ± 0.05 .XX ± 0.5°
.XXX ± 0.01 .XXX ± 1/8
CAD GENERATED DRAWING. DO NOT MANUALLY UPDATE
APPROVALS DATE
DRAWN
CHECKED
RESP ENG
MFG ENG
QUAL ENG
MATERIAL Perspex
FINISH --
NEXT ASSY USED ON
APPLICATION
DO NOT SCALE DRAWING
UNIVERSITY OF MARYLAND
A3 - Base Plate
SIZE A
DWG. NO.
REV.
SCALE : 1 : 3
CAD FILE:
SHEET OF

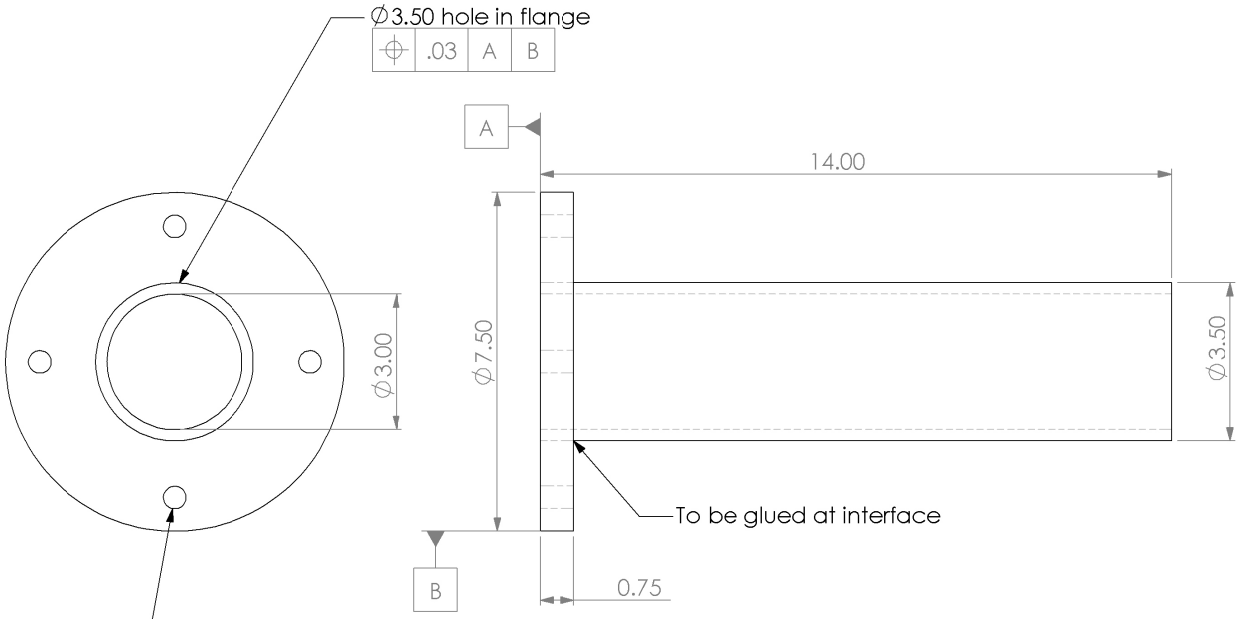

Notes:
1. Two pieces, glued at interface

ITEM NO.	PART OR IDENTIFYING NO.	NOMENCLATURE OR DESCRIPTION	MATERIAL SPECIFICATION	QTY REQD

PARTS LIST

UNLESS OTHERWISE SPECIFIED
DIMENSIONS ARE IN INCHES
TOLERANCES ARE:
FRACTIONS DECIMALS ANGLES
.XX ± 0.05 .XX ± 0.5°
.XXX ± 0.01 .XXX ± 1/8

MATERIAL Perspex

FINISH --

DO NOT SCALE DRAWING

CAD GENERATED DRAWING,
DO NOT MANUALLY UPDATE

APPROVALS	DATE
DRAWN	
CHECKED	
RESP ENG	
MFG ENG	
QUAL ENG	

UNIVERSITY OF MARYLAND

A4 - Exit Pipe and Exit Flange

SIZE A | DWG. NO. | REV.

SCALE : 1 : 3 | CAD FILE: | SHEET OF

NEXT ASSY | USED ON

APPLICATION

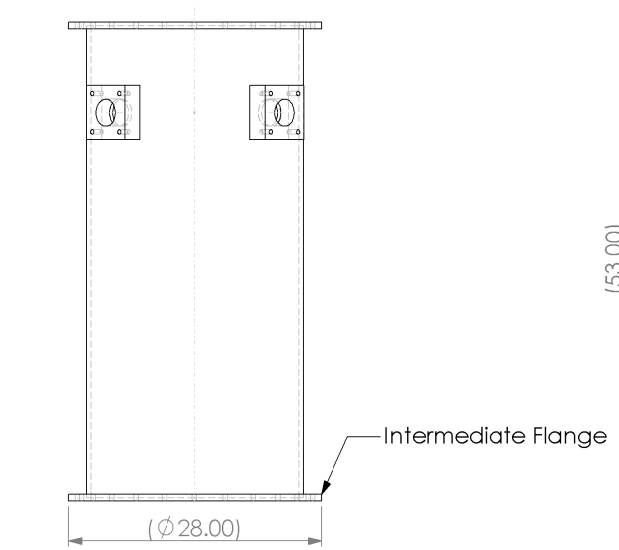

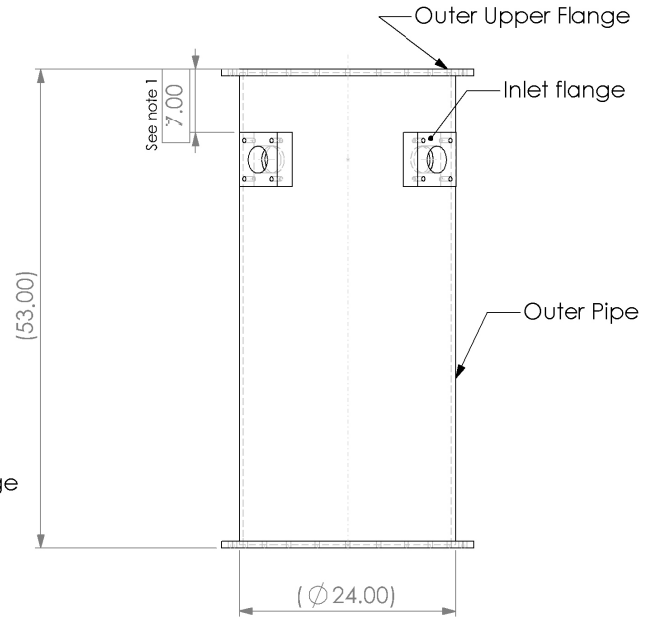

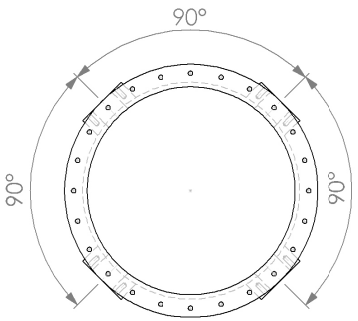

Note:
1. Dimension used for a guide, the Inlet Flange should mate concentricly with the hole.

ITEM NO.	PART OR IDENTIFYING NO.	NOMENCLATURE OR DESCRIPTION	MATERIAL SPECIFICATION	QTY REQD

PARTS LIST

UNLESS OTHERWISE SPECIFIED DIMENSIONS ARE IN INCHES
TOLERANCES ARE:
FRACTIONS DECIMALS ANGLES
.XX ± 0.05 .XX ± 0.5°
.XXX ± 0.01 .XXX ± 1/8

MATERIAL: Perspex
FINISH: --

NEXT ASSY | USED ON
APPLICATION
DO NOT SCALE DRAWING

CAD GENERATED DRAWING, DO NOT MANUALLY UPDATE

APPROVALS	DATE
DRAWN	
CHECKED	
RESP ENG	
MFG ENG	
QUAL ENG	

UNIVERSITY OF MARYLAND

B - Outer Barrel and Flange

SIZE A | DWG. NO. | REV.
SCALE: 1 : 15 | CAD FILE: | SHEET OF

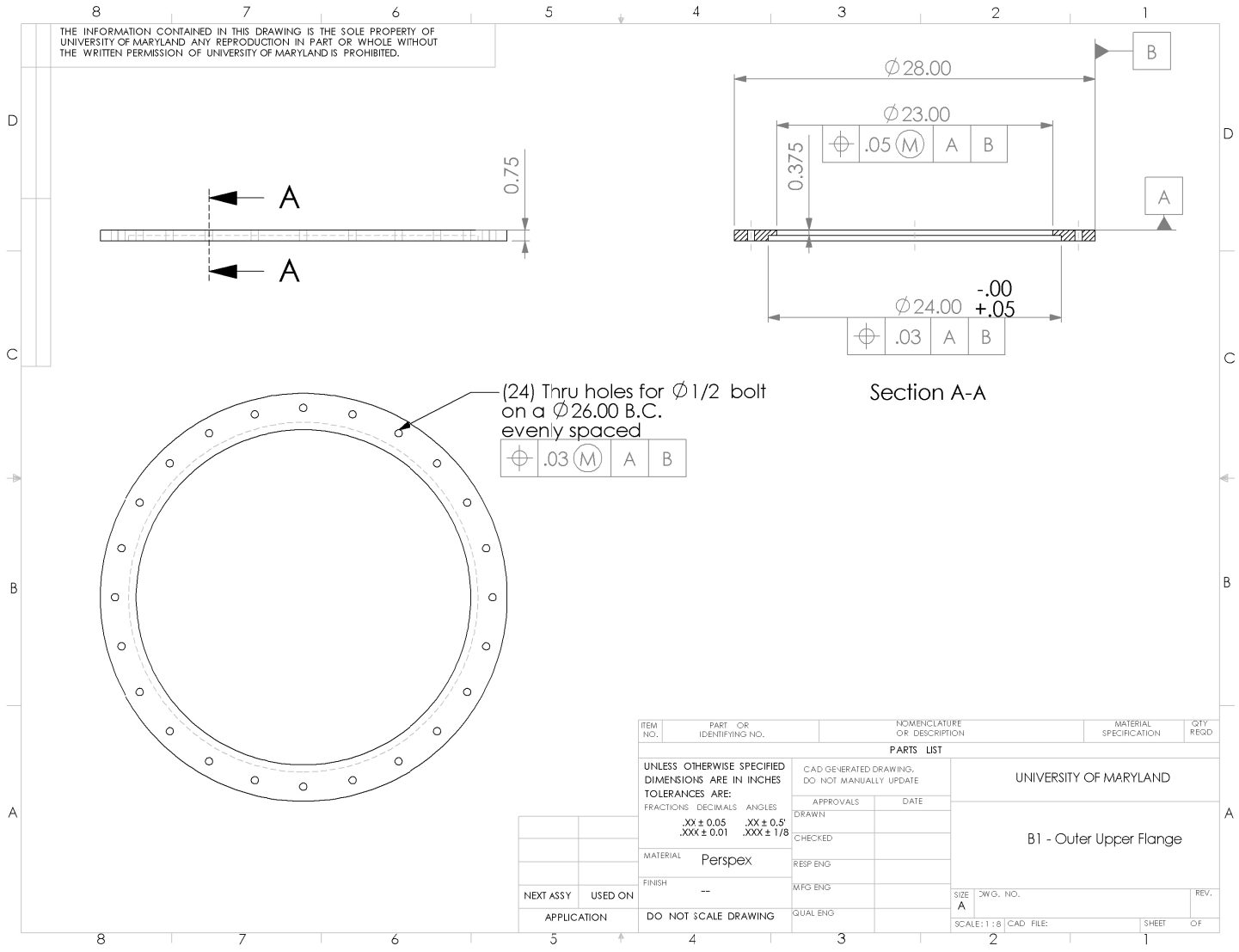
THE INFORMATION CONTAINED IN THIS DRAWING IS THE SOLE PROPERTY OF UNIVERSITY OF MARYLAND ANY REPRODUCTION IN PART OR WHOLE WITHOUT THE WRITTEN PERMISSION OF UNIVERSITY OF MARYLAND IS PROHIBITED.
A
A
0.75
∅28.00
∅23.00
.05 M A B
0.375
B
A
-.00
∅24.00 +.05
.03 A B
Section A-A
(24) Thru holes for ∅1/2 bolt on a ∅26.00 B.C. evenly spaced
.03 M A B
PARTS LIST
ITEM NO.
PART OR IDENTIFYING NO.
NOMENCLATURE OR DESCRIPTION
MATERIAL SPECIFICATION
QTY REQD
UNLESS OTHERWISE SPECIFIED DIMENSIONS ARE IN INCHES
TOLERANCES ARE:
FRACTIONS DECIMALS ANGLES
.XX ± 0.05 .XX ± 0.5°
.XXX ± 0.01 .XXX ± 1/8
MATERIAL Perspex
FINISH --
CAD GENERATED DRAWING, DO NOT MANUALLY UPDATE
APPROVALS DATE
DRAWN
CHECKED
RESP ENG
MFG ENG
QUAL ENG
UNIVERSITY OF MARYLAND
B1 - Outer Upper Flange
SIZE A
DWG. NO.
REV.
SCALE: 1 : 8
CAD FILE:
SHEET OF
NEXT ASSY
USED ON
APPLICATION
DO NOT SCALE DRAWING

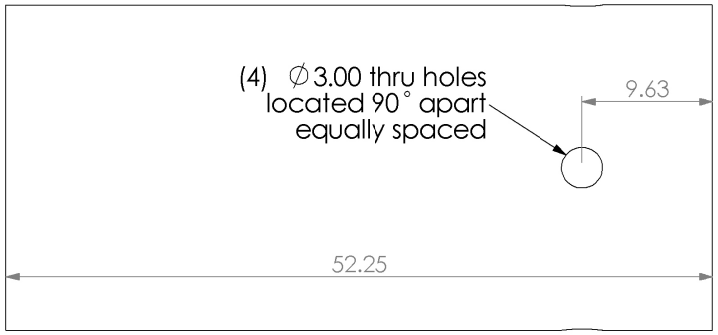

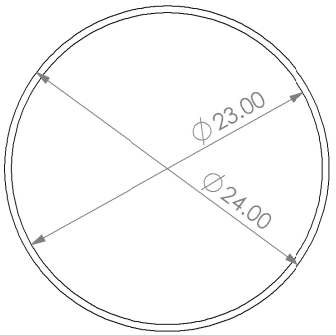

ITEM NO.	PART OR IDENTIFYING NO.	NOMENCLATURE OR DESCRIPTION	MATERIAL SPECIFICATION	QTY REQD

PARTS LIST

UNLESS OTHERWISE SPECIFIED DIMENSIONS ARE IN INCHES
TOLERANCES ARE:
FRACTIONS DECIMALS ANGLES
+ .XX+ .XX + 1
.XXX+.XXX

MATERIAL Perspex

FINISH --

NEXT ASSY | USED ON

APPLICATION

DO NOT SCALE DRAWING

CAD GENERATED DRAWING.
DO NOT MANUALLY UPDATE

APPROVALS	DATE
DRAWN	
CHECKED	
RESP ENG	
MFG ENG	
QUAL ENG	

UNIVERSITY OF MARYLAND

B2 - Outer Pipe

SIZE A | DWG. NO. | REV.

SCALE: 1:5 | CAD FILE: | SHEET OF

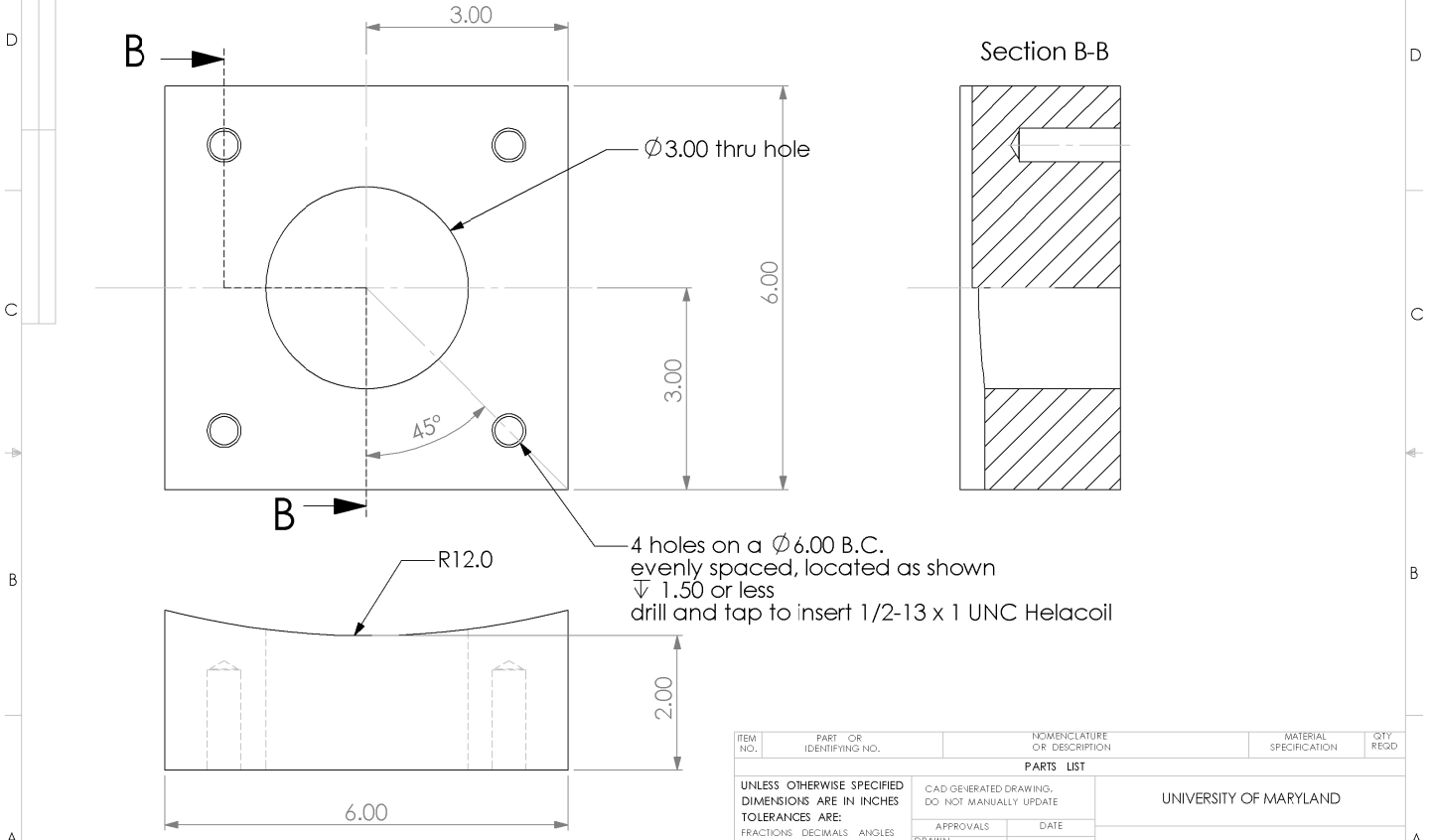

Notes:
1. Part is to be glued to outer barrel
2. Radii Maybe rough cut and sanded/filed to fit

ITEM NO.	PART OR IDENTIFYING NO.	NOMENCLATURE OR DESCRIPTION	MATERIAL SPECIFICATION	QTY REQD

PARTS LIST

UNLESS OTHERWISE SPECIFIED DIMENSIONS ARE IN INCHES
TOLERANCES ARE:
FRACTIONS DECIMALS ANGLES
.XX ± 0.05 .XX ± 0.5°
.XXX ± 0.01 .XXX ± 1/8

MATERIAL: Perspex
FINISH: --

NEXT ASSY | USED ON
APPLICATION
DO NOT SCALE DRAWING

CAD GENERATED DRAWING, DO NOT MANUALLY UPDATE

APPROVALS	DATE
DRAWN	
CHECKED	
RESP ENG	
MFG ENG	
QUAL ENG	

UNIVERSITY OF MARYLAND

B3 - Inlet Flange

SIZE A | DWG. NO. | REV.
SCALE: 1 : 2 | CAD FILE: | SHEET OF

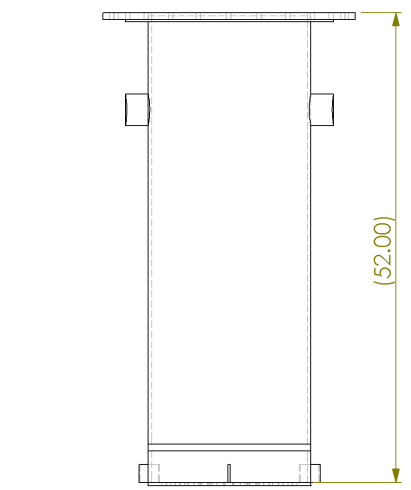

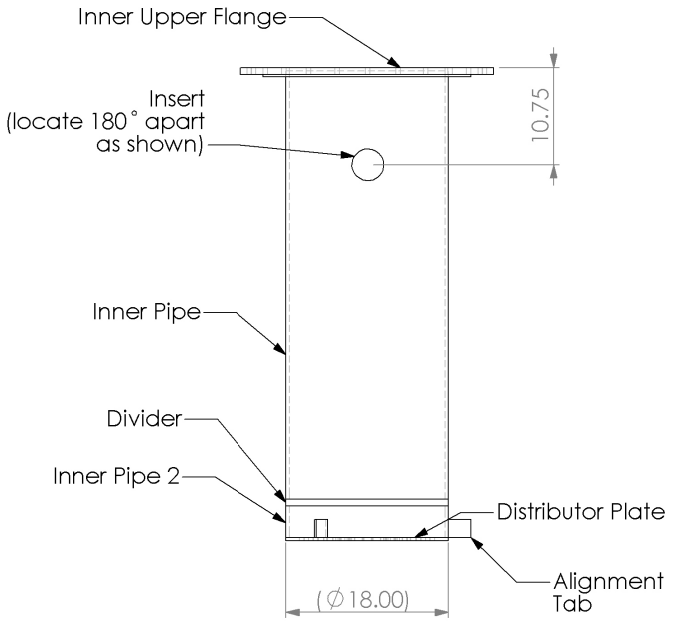

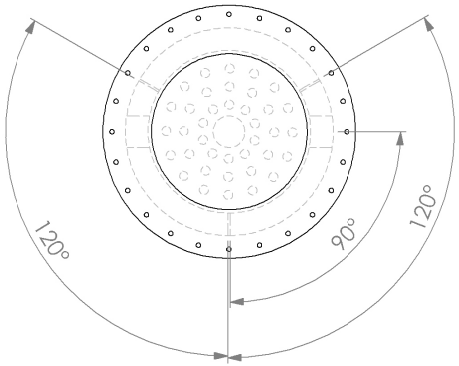

ITEM NO.	PART OR IDENTIFYING NO.	NOMENCLATURE OR DESCRIPTION	MATERIAL SPECIFICATION	QTY REQD

PARTS LIST

UNLESS OTHERWISE SPECIFIED DIMENSIONS ARE IN INCHES
TOLERANCES ARE:
FRACTIONS DECIMALS ANGLES
+ .XX+ .XX + 1
.XXX+.XXX

MATERIAL Perspex

FINISH --

DO NOT SCALE DRAWING

CAD GENERATED DRAWING, DO NOT MANUALLY UPDATE

APPROVALS	DATE
DRAWN	
CHECKED	
RESP ENG	
MFG ENG	
QUAL ENG	

UNIVERSITY OF MARYLAND

C - Inner Barrel and Insert

SIZE A | DWG. NO. | REV.

SCALE: 1:15 | CAD FILE: | SHEET OF

NEXT ASSY	USED ON
APPLICATION	

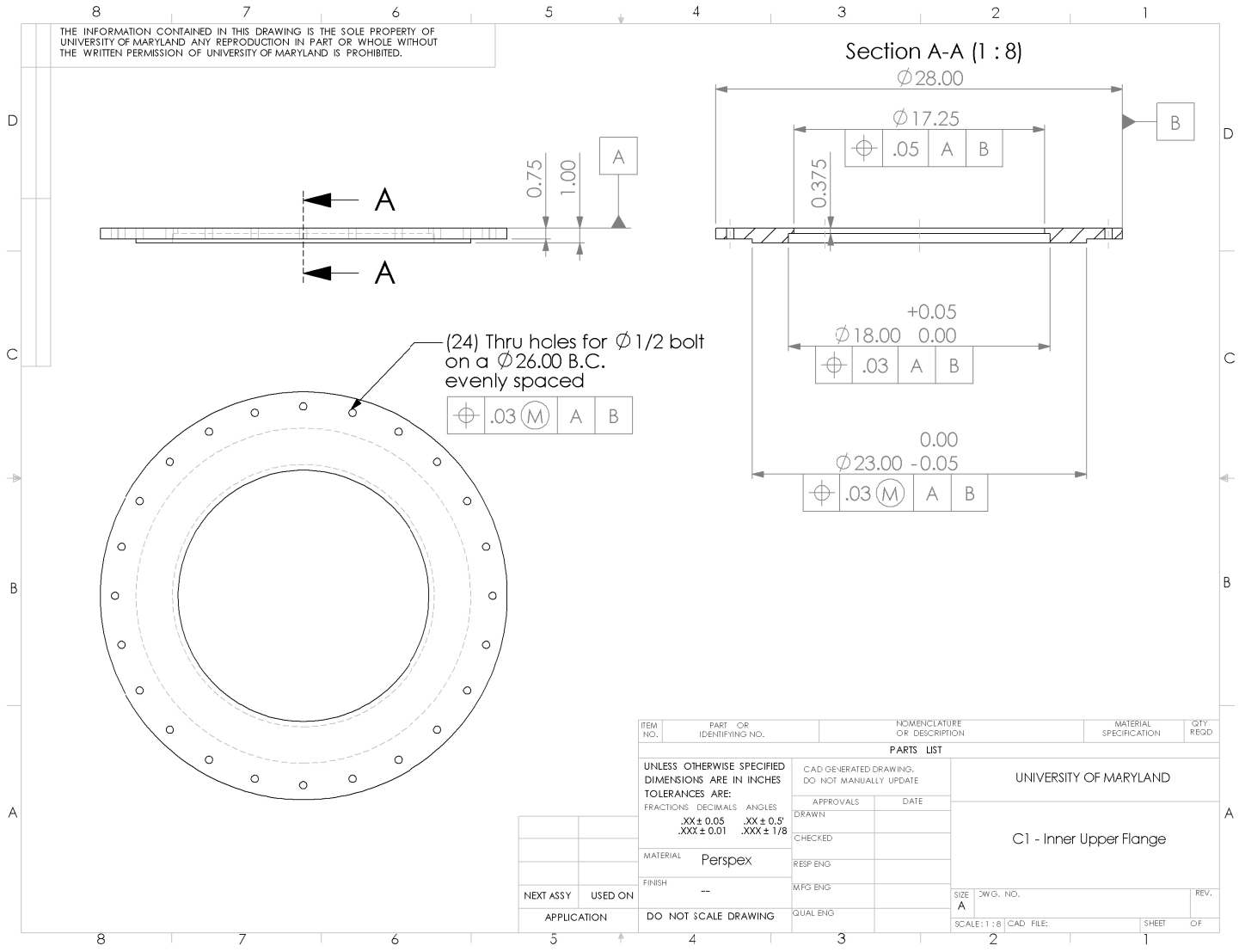
THE INFORMATION CONTAINED IN THIS DRAWING IS THE SOLE PROPERTY OF UNIVERSITY OF MARYLAND ANY REPRODUCTION IN PART OR WHOLE WITHOUT THE WRITTEN PERMISSION OF UNIVERSITY OF MARYLAND IS PROHIBITED.
Section A-A (1 : 8)
∅28.00
∅17.25
.05 A B
0.375
B
0.75
1.00
A
A
A
(24) Thru holes for ∅1/2 bolt on a ∅26.00 B.C. evenly spaced
.03 M A B
+0.05
∅18.00 0.00
.03 A B
0.00
∅23.00 -0.05
.03 M A B
ITEM NO.
PART OR IDENTIFYING NO.
NOMENCLATURE OR DESCRIPTION
MATERIAL SPECIFICATION
QTY REQD
PARTS LIST
UNLESS OTHERWISE SPECIFIED DIMENSIONS ARE IN INCHES
TOLERANCES ARE:
FRACTIONS DECIMALS ANGLES
.XX ± 0.05 .XX ± 0.5°
.XXX ± 0.01 .XXX ± 1/8
CAD GENERATED DRAWING, DO NOT MANUALLY UPDATE
APPROVALS DATE
DRAWN
CHECKED
RESP ENG
MFG ENG
QUAL ENG
UNIVERSITY OF MARYLAND
C1 - Inner Upper Flange
MATERIAL Perspex
FINISH --
NEXT ASSY USED ON
APPLICATION
DO NOT SCALE DRAWING
SIZE A
DWG. NO.
REV.
SCALE: 1 : 8
CAD FILE:
SHEET OF

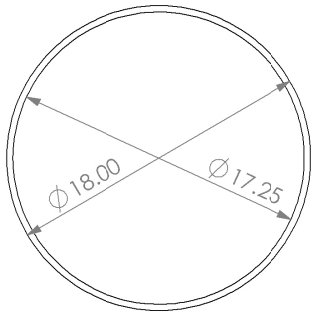

Notes:
1. To be made from standard sized pipe

ITEM NO.	PART OR IDENTIFYING NO.	NOMENCLATURE OR DESCRIPTION	MATERIAL SPECIFICATION	QTY REQD

PARTS LIST

UNLESS OTHERWISE SPECIFIED DIMENSIONS ARE IN INCHES
TOLERANCES ARE:
FRACTIONS DECIMALS ANGLES
+ .XX+ .XX + 1
.XXX+.XXX

MATERIAL Perspex

FINISH --

DO NOT SCALE DRAWING

CAD GENERATED DRAWING, DO NOT MANUALLY UPDATE

APPROVALS	DATE
DRAWN	
CHECKED	
RESP ENG	
MFG ENG	
QUAL ENG	

UNIVERSITY OF MARYLAND

C2 - Inner Pipe

SIZE A | DWG. NO. | REV.

SCALE: 1 : 5 | CAD FILE: | SHEET OF

NEXT ASSY	USED ON
APPLICATION	

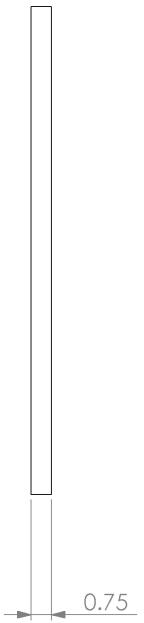

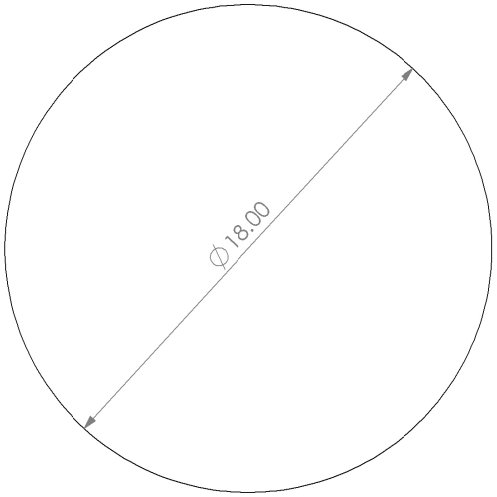

ITEM NO.	PART OR IDENTIFYING NO.	NOMENCLATURE OR DESCRIPTION	MATERIAL SPECIFICATION	QTY REQD

PARTS LIST

UNLESS OTHERWISE SPECIFIED DIMENSIONS ARE IN INCHES
TOLERANCES ARE:
FRACTIONS DECIMALS ANGLES
+ .XX+ .XX + 1
.XXX+.XXX

MATERIAL Perspex

FINISH --

DO NOT SCALE DRAWING

CAD GENERATED DRAWING, DO NOT MANUALLY UPDATE

APPROVALS	DATE
DRAWN	
CHECKED	
RESP ENG	
MFG ENG	
QUAL ENG	

NEXT ASSY | USED ON

APPLICATION

UNIVERSITY OF MARYLAND

C3 - Divider

SIZE A | DWG. NO. | REV.

SCALE: 1 : 5 | CAD FILE: | SHEET OF

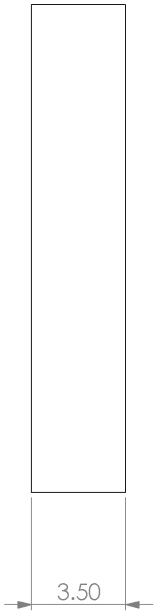

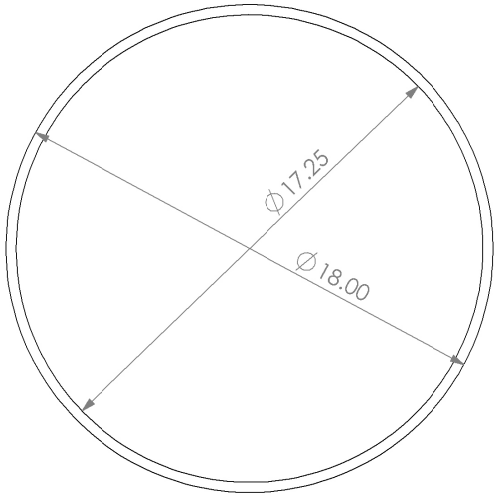

Notes:
1. To be made from standard pipe

ITEM NO.	PART OR IDENTIFYING NO.	NOMENCLATURE OR DESCRIPTION	MATERIAL SPECIFICATION	QTY REQD

PARTS LIST

UNLESS OTHERWISE SPECIFIED DIMENSIONS ARE IN INCHES
TOLERANCES ARE:
FRACTIONS DECIMALS ANGLES
+ .XX+ .XX + 1
.XXX+.XXX

MATERIAL Perspex

FINISH --

DO NOT SCALE DRAWING

CAD GENERATED DRAWING, DO NOT MANUALLY UPDATE

APPROVALS	DATE
DRAWN	
CHECKED	
RESP ENG	
MFG ENG	
QUAL ENG	

UNIVERSITY OF MARYLAND

C4 - Inner Pipe 2

SIZE A | DWG. NO. | REV.

SCALE: 1 : 5 | CAD FILE: | SHEET OF

NEXT ASSY | USED ON

APPLICATION

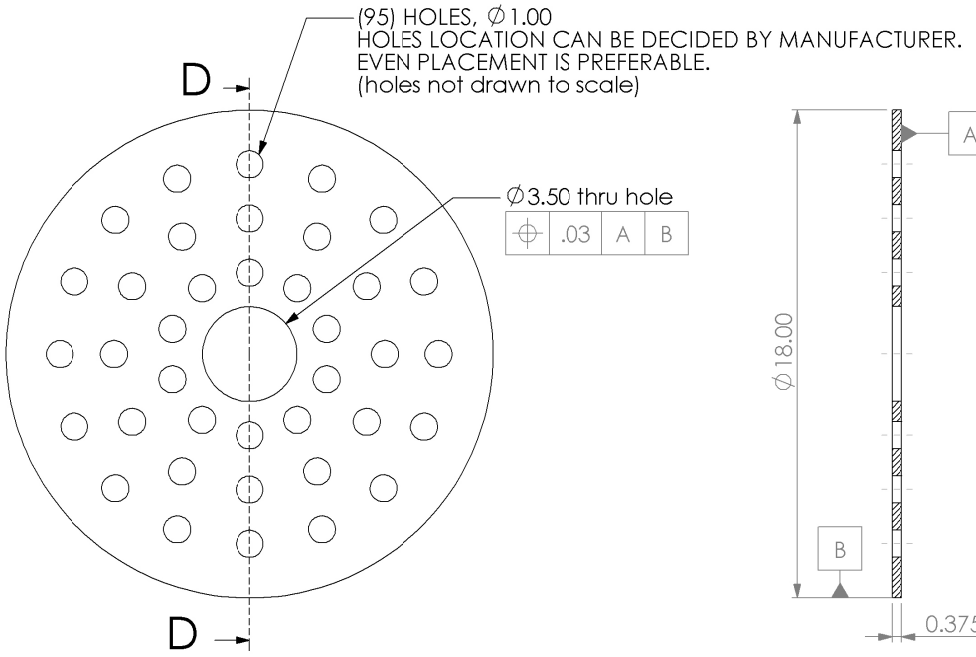

ITEM NO.	PART OR IDENTIFYING NO.	NOMENCLATURE OR DESCRIPTION	MATERIAL SPECIFICATION	QTY REQD

PARTS LIST

UNLESS OTHERWISE SPECIFIED DIMENSIONS ARE IN INCHES
TOLERANCES ARE:
FRACTIONS DECIMALS ANGLES
+ .XX+ .XX + 1
.XXX+.XXX

MATERIAL Perspex

FINISH --

DO NOT SCALE DRAWING

CAD GENERATED DRAWING, DO NOT MANUALLY UPDATE

APPROVALS	DATE
DRAWN	
CHECKED	
RESP ENG	
MFG ENG	
QUAL ENG	

UNIVERSITY OF MARYLAND

C5 - Distributor Plate

SIZE A | DWG. NO. | REV.

SCALE: 1:5 | CAD FILE: | SHEET OF

NEXT ASSY	USED ON
APPLICATION	

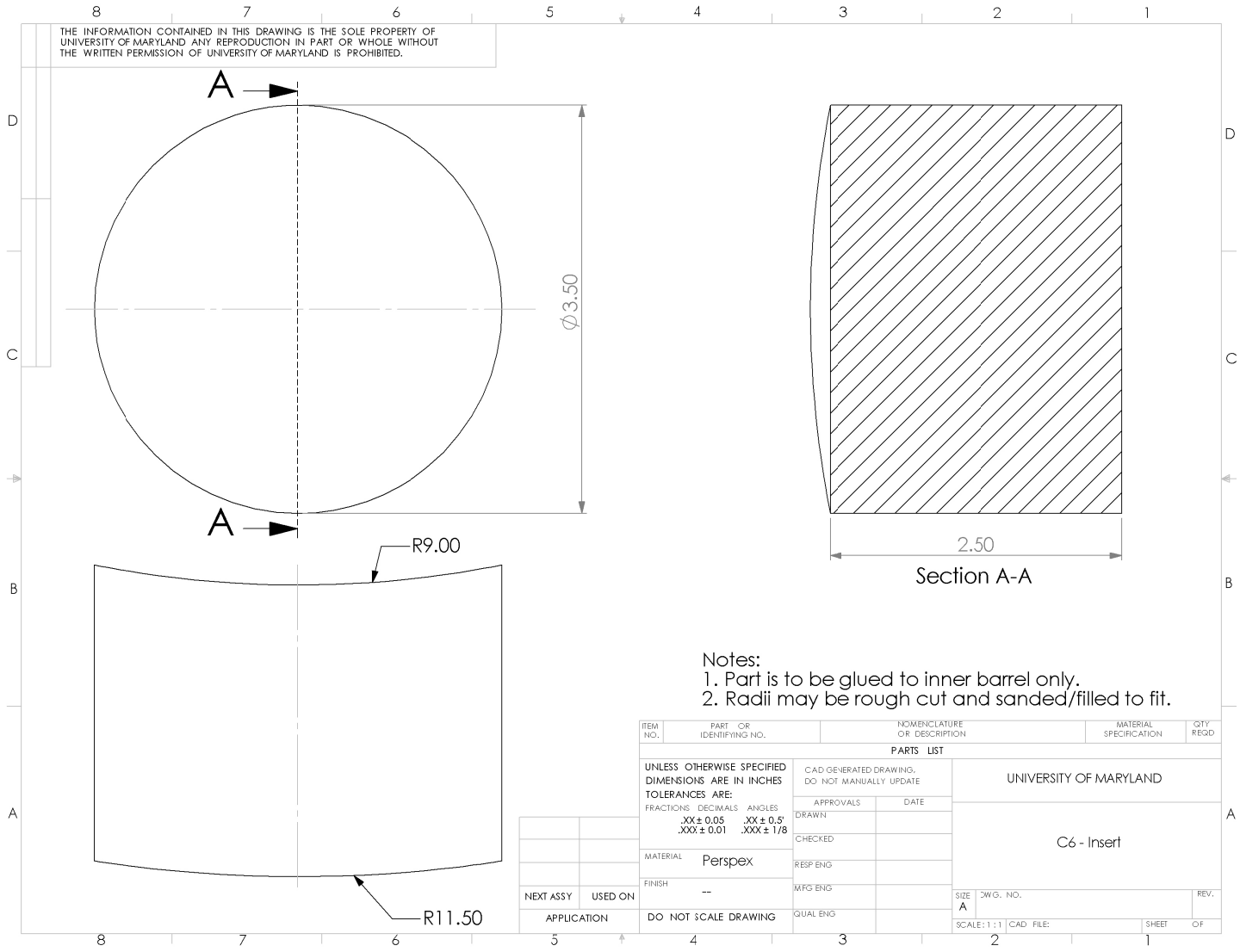
THE INFORMATION CONTAINED IN THIS DRAWING IS THE SOLE PROPERTY OF UNIVERSITY OF MARYLAND ANY REPRODUCTION IN PART OR WHOLE WITHOUT THE WRITTEN PERMISSION OF UNIVERSITY OF MARYLAND IS PROHIBITED.
A
A
Ø3.50
R9.00
R11.50
2.50
Section A-A
Notes:
1. Part is to be glued to inner barrel only.
2. Radii may be rough cut and sanded/filled to fit.
ITEM NO.
PART OR IDENTIFYING NO.
NOMENCLATURE OR DESCRIPTION
MATERIAL SPECIFICATION
QTY REQD
PARTS LIST
UNLESS OTHERWISE SPECIFIED DIMENSIONS ARE IN INCHES
TOLERANCES ARE:
FRACTIONS DECIMALS ANGLES
.XX ± 0.05 .XX ± 0.5'
.XXX ± 0.01 .XXX ± 1/8
MATERIAL Perspex
FINISH --
NEXT ASSY USED ON
APPLICATION
DO NOT SCALE DRAWING
CAD GENERATED DRAWING. DO NOT MANUALLY UPDATE
APPROVALS DATE
DRAWN
CHECKED
RESP ENG
MFG ENG
QUAL ENG
UNIVERSITY OF MARYLAND
C6 - Insert
SIZE A
DWG. NO.
REV.
SCALE: 1 : 1
CAD FILE:
SHEET OF

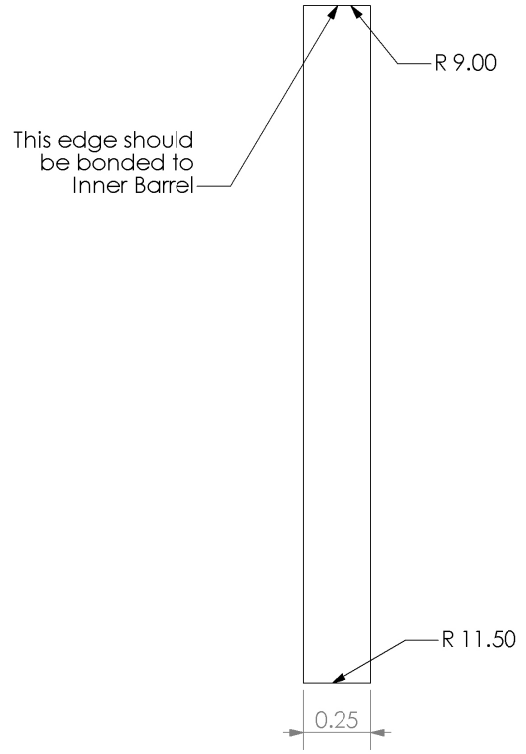

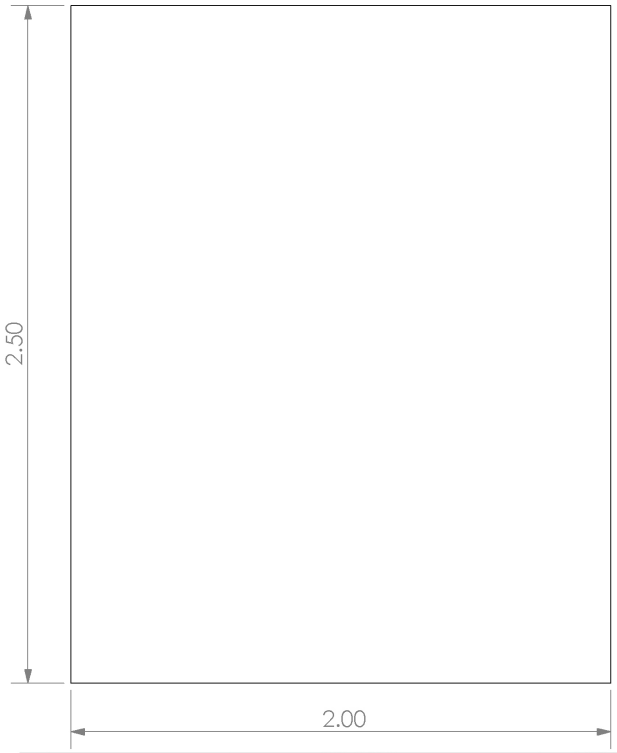

Notes:
1. PART IS TO BE GLUED TO INNER BARREL 3 x 120°
2. Radii may be sanded/filed to fit

ITEM NO.	PART OR IDENTIFYING NO.	NOMENCLATURE OR DESCRIPTION	MATERIAL SPECIFICATION	QTY REQD

PARTS LIST

UNLESS OTHERWISE SPECIFIED DIMENSIONS ARE IN INCHES
TOLERANCES ARE:
FRACTIONS DECIMALS ANGLES
.XX ± 0.05 .XX ± 0.5°
.XXX ± 0.01 .XXX ± 1/8

MATERIAL --

FINISH --

DO NOT SCALE DRAWING

CAD GENERATED DRAWING, DO NOT MANUALLY UPDATE

APPROVALS	DATE
DRAWN	
CHECKED	
RESP ENG	
MFG ENG	
QUAL ENG	

University of Maryland

C7 - Alignment Tab

NEXT ASSY	USED ON
APPLICATION	

SIZE A | DWG. NO. | REV.
SCALE: 2:1 | CAD FILE: | SHEET 1 OF 1

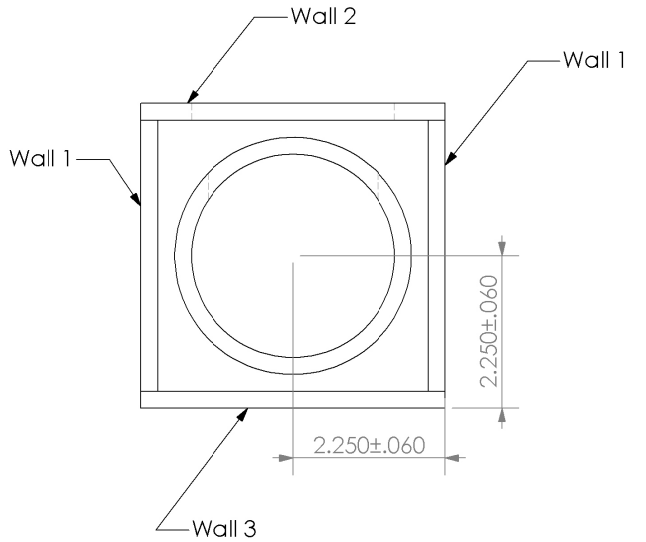

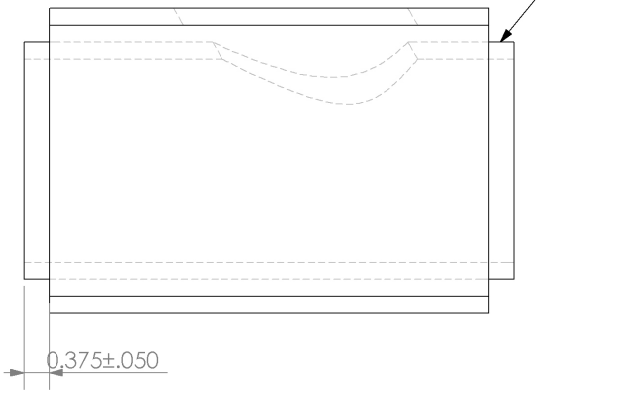

ITEM NO.	PART OR IDENTIFYING NO.	NOMENCLATURE OR DESCRIPTION	MATERIAL SPECIFICATION	QTY REQD

PARTS LIST

UNLESS OTHERWISE SPECIFIED DIMENSIONS ARE IN INCHES
TOLERANCES ARE:
FRACTIONS DECIMALS ANGLES
.XX ± 0.05 .XX ± 0.5°
.XXX ± 0.01 .XXX ± 1/8

MATERIAL Plexiglas
FINISH --

NEXT ASSY | USED ON
APPLICATION | DO NOT SCALE DRAWING

CAD GENERATED DRAWING, DO NOT MANUALLY UPDATE

APPROVALS	DATE
DRAWN	
CHECKED	
RESP ENG	
MFG ENG	
QUAL ENG	

University of Maryland

D - HPI Nozzle

SIZE A | DWG. NO. | REV.
SCALE: 1:2 | CAD FILE: | SHEET 1 OF 2

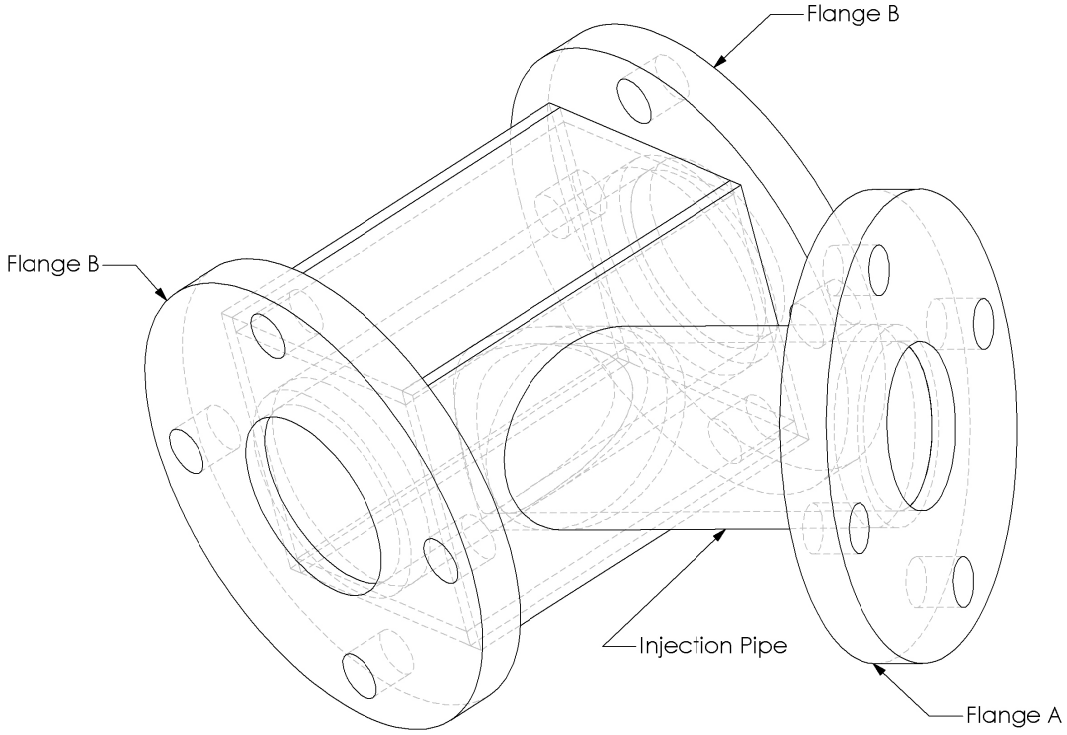

ITEM NO.	PART OR IDENTIFYING NO.	NOMENCLATURE OR DESCRIPTION	MATERIAL SPECIFICATION	QTY REQD

PARTS LIST

UNLESS OTHERWISE SPECIFIED DIMENSIONS ARE IN INCHES
TOLERANCES ARE:
FRACTIONS DECIMALS ANGLES
.XX ± 0.05 .XX ± 0.5°
.XXX ± 0.01 .XXX ± 1/8

MATERIAL --

FINISH --

DO NOT SCALE DRAWING

CAD GENERATED DRAWING.
DO NOT MANUALLY UPDATE

APPROVALS	DATE
DRAWN	
CHECKED	
RESP ENG	
MFG ENG	
QUAL ENG	

NEXT ASSY	USED ON
APPLICATION	

University of Maryland

D - HPI Nozzle

SIZE A | DWG. NO. | REV.

SCALE: 1:2 | CAD FILE: | SHEET 2 OF 2

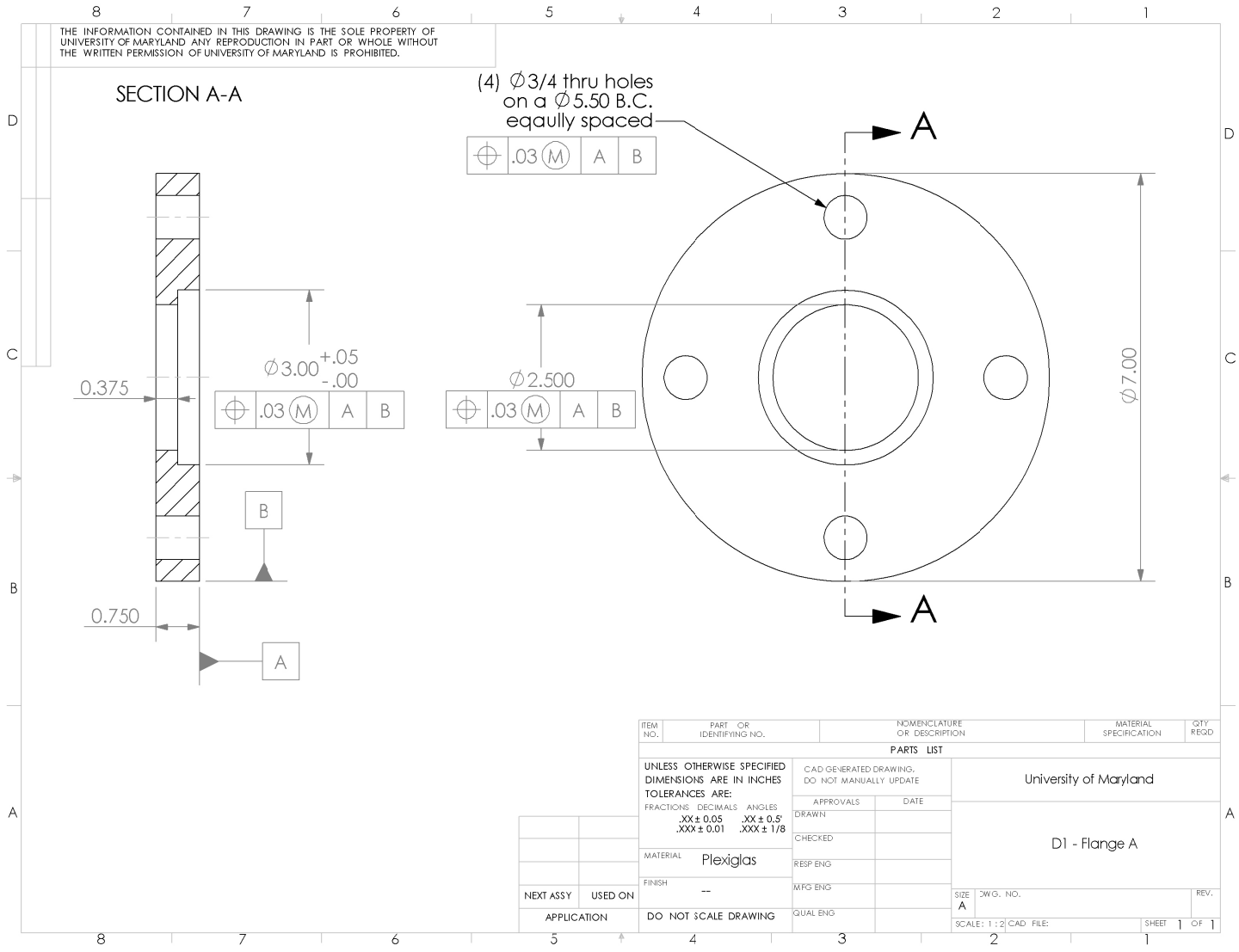
THE INFORMATION CONTAINED IN THIS DRAWING IS THE SOLE PROPERTY OF UNIVERSITY OF MARYLAND ANY REPRODUCTION IN PART OR WHOLE WITHOUT THE WRITTEN PERMISSION OF UNIVERSITY OF MARYLAND IS PROHIBITED.
SECTION A-A
(4) ∅3/4 thru holes on a ∅5.50 B.C. eqaully spaced
.03 M A B
∅3.00 +.05 -.00
0.375
∅2.500
∅7.00
0.750
A
B
ITEM NO.
PART OR IDENTIFYING NO.
NOMENCLATURE OR DESCRIPTION
MATERIAL SPECIFICATION
QTY REQD
PARTS LIST
UNLESS OTHERWISE SPECIFIED DIMENSIONS ARE IN INCHES
TOLERANCES ARE:
FRACTIONS DECIMALS ANGLES
.XX ± 0.05 .XX ± 0.5°
.XXX ± 0.01 .XXX ± 1/8
MATERIAL Plexiglas
FINISH --
NEXT ASSY USED ON
APPLICATION
DO NOT SCALE DRAWING
CAD GENERATED DRAWING, DO NOT MANUALLY UPDATE
APPROVALS DATE
DRAWN
CHECKED
RESP ENG
MFG ENG
QUAL ENG
University of Maryland
D1 - Flange A
SIZE A
DWG. NO.
REV.
SCALE: 1:2
CAD FILE:
SHEET 1 OF 1

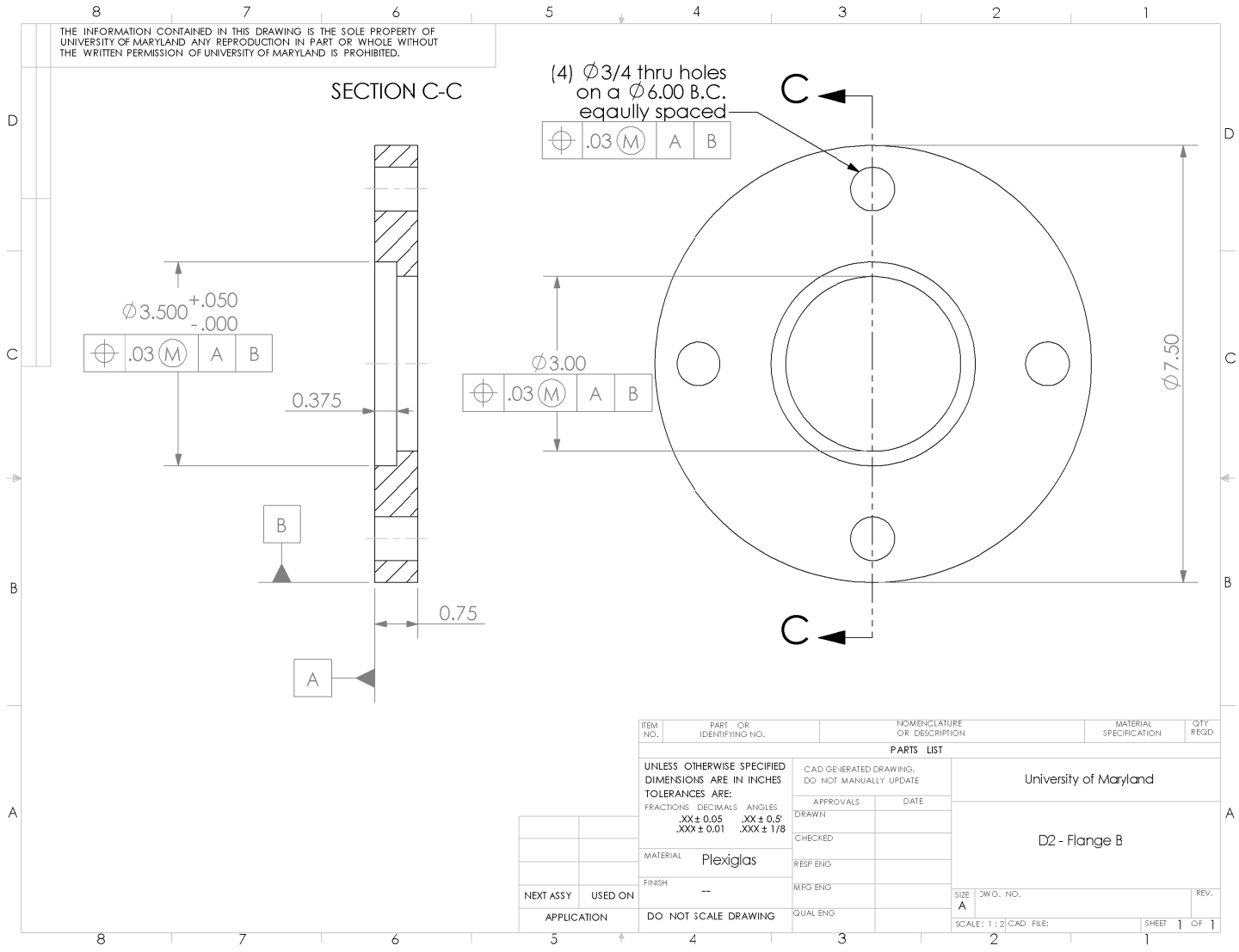
THE INFORMATION CONTAINED IN THIS DRAWING IS THE SOLE PROPERTY OF UNIVERSITY OF MARYLAND ANY REPRODUCTION IN PART OR WHOLE WITHOUT THE WRITTEN PERMISSION OF UNIVERSITY OF MARYLAND IS PROHIBITED.
SECTION C-C
(4) ∅3/4 thru holes on a ∅6.00 B.C. eqaully spaced
.03 M A B
∅3.500 +.050 -.000
.03 M A B
0.375
∅3.00
.03 M A B
∅7.50
B
0.75
A
C
C
ITEM NO.
PART OR IDENTIFYING NO.
NOMENCLATURE OR DESCRIPTION
MATERIAL SPECIFICATION
QTY REQD
PARTS LIST
UNLESS OTHERWISE SPECIFIED DIMENSIONS ARE IN INCHES TOLERANCES ARE:
FRACTIONS DECIMALS ANGLES
.XX ± 0.05 .XX ± 0.5°
.XXX ± 0.01 .XXX ± 1/8
CAD GENERATED DRAWING, DO NOT MANUALLY UPDATE
APPROVALS DATE
DRAWN
CHECKED
RESP ENG
MFG ENG
QUAL ENG
University of Maryland
D2 - Flange B
MATERIAL Plexiglas
FINISH --
NEXT ASSY USED ON
APPLICATION
DO NOT SCALE DRAWING
SIZE A
DWG. NO.
REV.
SCALE: 1:2
CAD FILE:
SHEET 1 OF 1

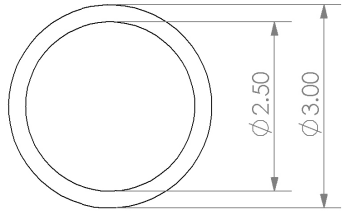

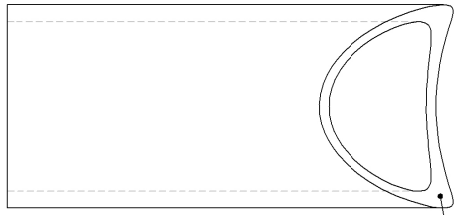

Glue edge to Pipe D4

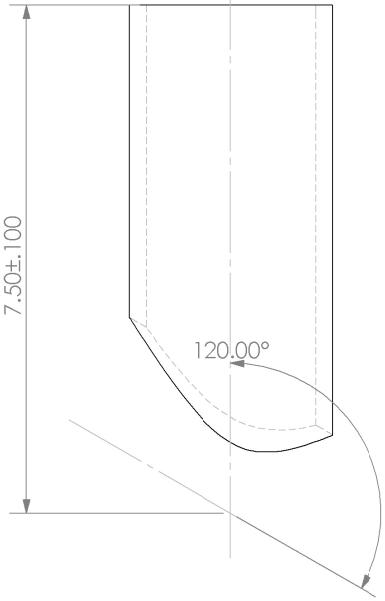

Note:
1. To be drilled with ∅3.0 tool with drilling axis passing thru center axis of part.

ITEM NO.	PART OR IDENTIFYING NO.	NOMENCLATURE OR DESCRIPTION	MATERIAL SPECIFICATION	QTY REQD
		PARTS LIST		

UNLESS OTHERWISE SPECIFIED DIMENSIONS ARE IN INCHES
TOLERANCES ARE:
FRACTIONS DECIMALS ANGLES
.XX ± 0.05 .XX ± 0.5°
.XXX ± 0.01 .XXX ± 1/8

MATERIAL Plexiglas
FINISH --

NEXT ASSY | USED ON
APPLICATION | DO NOT SCALE DRAWING

CAD GENERATED DRAWING, DO NOT MANUALLY UPDATE

APPROVALS	DATE
DRAWN	
CHECKED	
RESP ENG	
MFG ENG	
QUAL ENG	

University of Maryland

D3 - Injection Pipe

SIZE A | DWG. NO. | REV.
SCALE: 1:2 | CAD FILE: | SHEET 1 OF 1

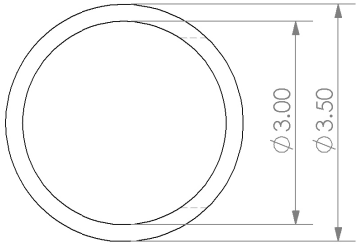

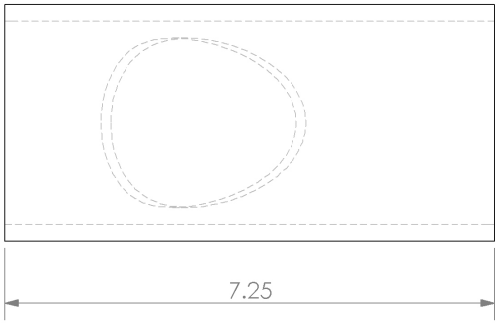

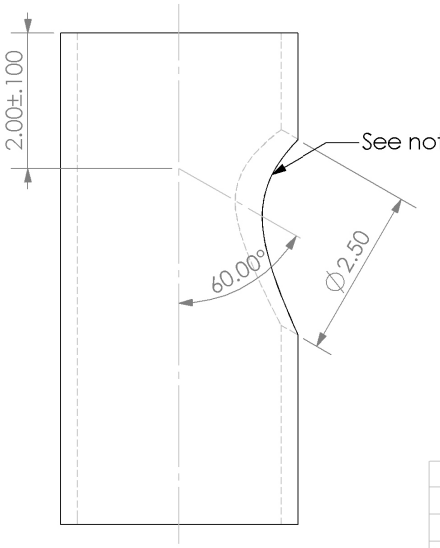

Notes:
1. To be bored with ∅2.50 tool with axis of tool intersecting the centerline of the pipe.

ITEM NO.	PART OR IDENTIFYING NO.	NOMENCLATURE OR DESCRIPTION	MATERIAL SPECIFICATION	QTY REQD
		PARTS LIST		

UNLESS OTHERWISE SPECIFIED DIMENSIONS ARE IN INCHES
TOLERANCES ARE:
FRACTIONS DECIMALS ANGLES
.XX ± 0.05 .XX ± 0.5°
.XXX ± 0.01 .XXX ± 1/8

MATERIAL Plexiglas
FINISH --

NEXT ASSY | USED ON
APPLICATION | DO NOT SCALE DRAWING

CAD GENERATED DRAWING, DO NOT MANUALLY UPDATE

APPROVALS	DATE
DRAWN	
CHECKED	
RESP ENG	
MFG ENG	
QUAL ENG	

University of Maryland

D4 - Pipe

SIZE A | DWG. NO. | REV.
SCALE: 1:2 | CAD FILE: | SHEET 1 OF 1

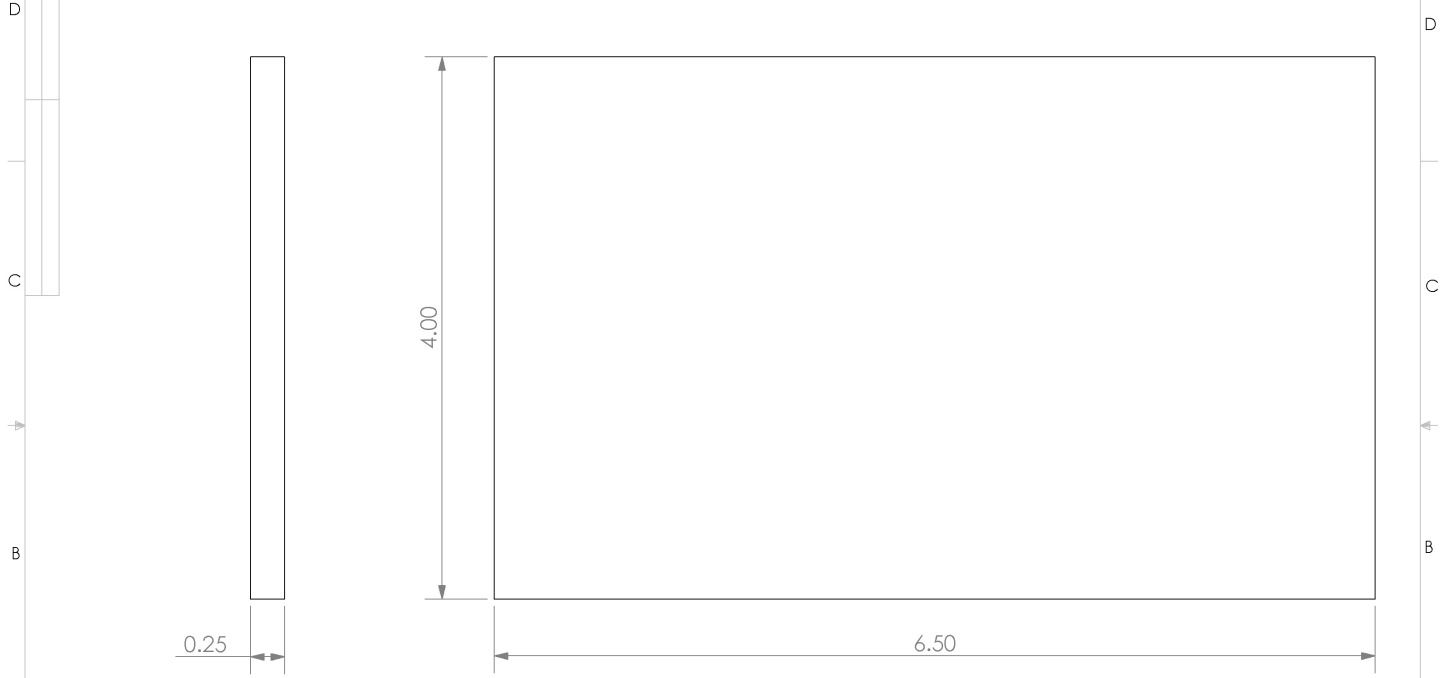

ITEM NO.	PART OR IDENTIFYING NO.	NOMENCLATURE OR DESCRIPTION	MATERIAL SPECIFICATION	QTY REQD

PARTS LIST

UNLESS OTHERWISE SPECIFIED DIMENSIONS ARE IN INCHES
TOLERANCES ARE:
FRACTIONS DECIMALS ANGLES
.XX ± 0.05 .XX ± 0.5°
.XXX ± 0.01 .XXX ± 1/8

MATERIAL Plexiglas
FINISH --

NEXT ASSY | USED ON
APPLICATION
DO NOT SCALE DRAWING

CAD GENERATED DRAWING.
DO NOT MANUALLY UPDATE

APPROVALS	DATE
DRAWN	
CHECKED	
RESP ENG	
MFG ENG	
QUAL ENG	

University of Maryland

D5 - Wall 1

SIZE A | DWG. NO. | REV.
SCALE: 1:1 | CAD FILE: | SHEET 1 OF 1

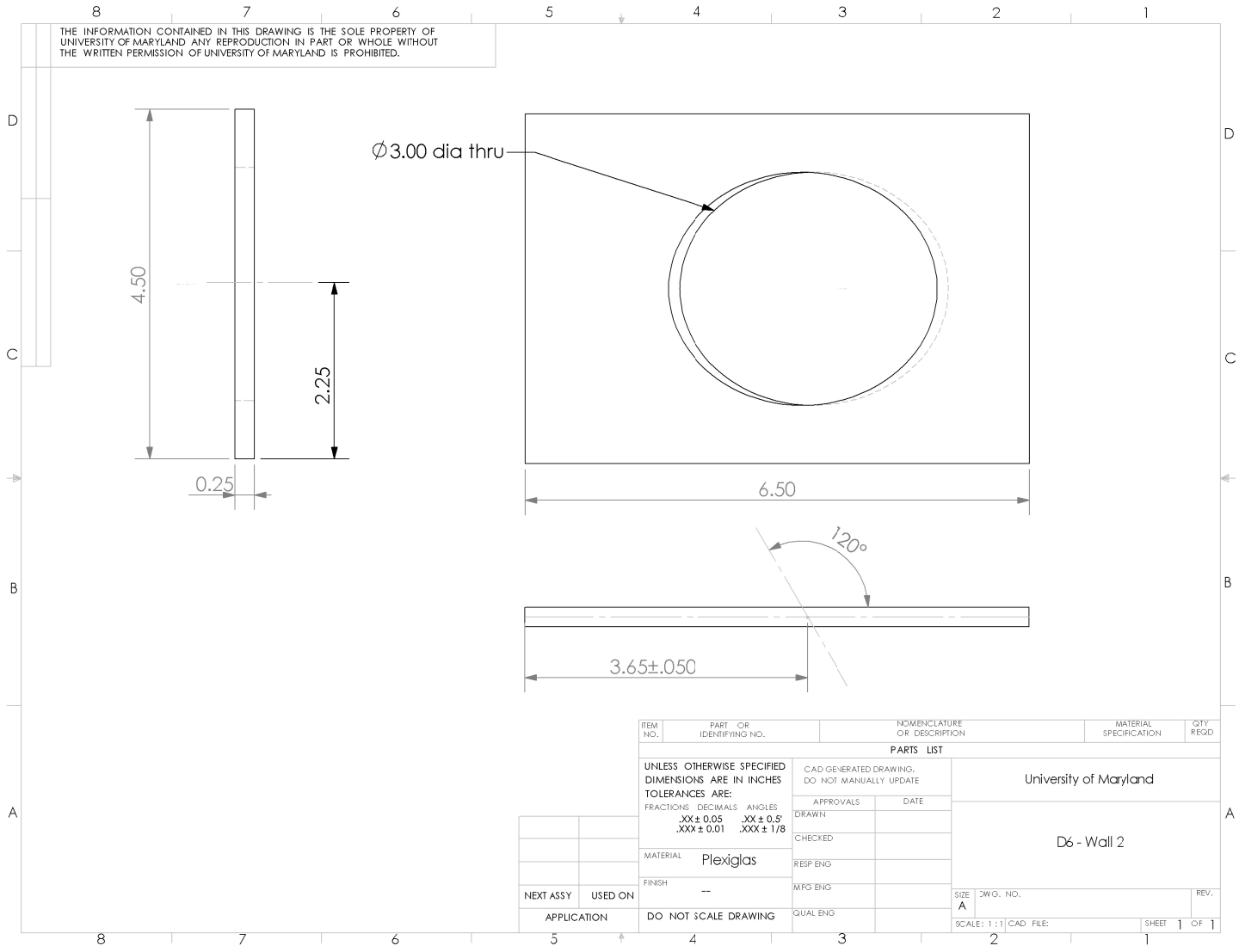
THE INFORMATION CONTAINED IN THIS DRAWING IS THE SOLE PROPERTY OF UNIVERSITY OF MARYLAND ANY REPRODUCTION IN PART OR WHOLE WITHOUT THE WRITTEN PERMISSION OF UNIVERSITY OF MARYLAND IS PROHIBITED.
∅3.00 dia thru
4.50
2.25
0.25
6.50
120°
3.65±.050
ITEM NO.
PART OR IDENTIFYING NO.
NOMENCLATURE OR DESCRIPTION
MATERIAL SPECIFICATION
QTY REQD
PARTS LIST
UNLESS OTHERWISE SPECIFIED DIMENSIONS ARE IN INCHES TOLERANCES ARE:
FRACTIONS DECIMALS ANGLES
.XX ± 0.05 .XX ± 0.5°
.XXX ± 0.01 .XXX ± 1/8
MATERIAL Plexiglas
FINISH --
NEXT ASSY USED ON
APPLICATION
DO NOT SCALE DRAWING
CAD GENERATED DRAWING, DO NOT MANUALLY UPDATE
APPROVALS DATE
DRAWN
CHECKED
RESP ENG
MFG ENG
QUAL ENG
University of Maryland
D6 - Wall 2
SIZE A
DWG. NO.
REV.
SCALE: 1:1
CAD FILE:
SHEET 1 OF 1

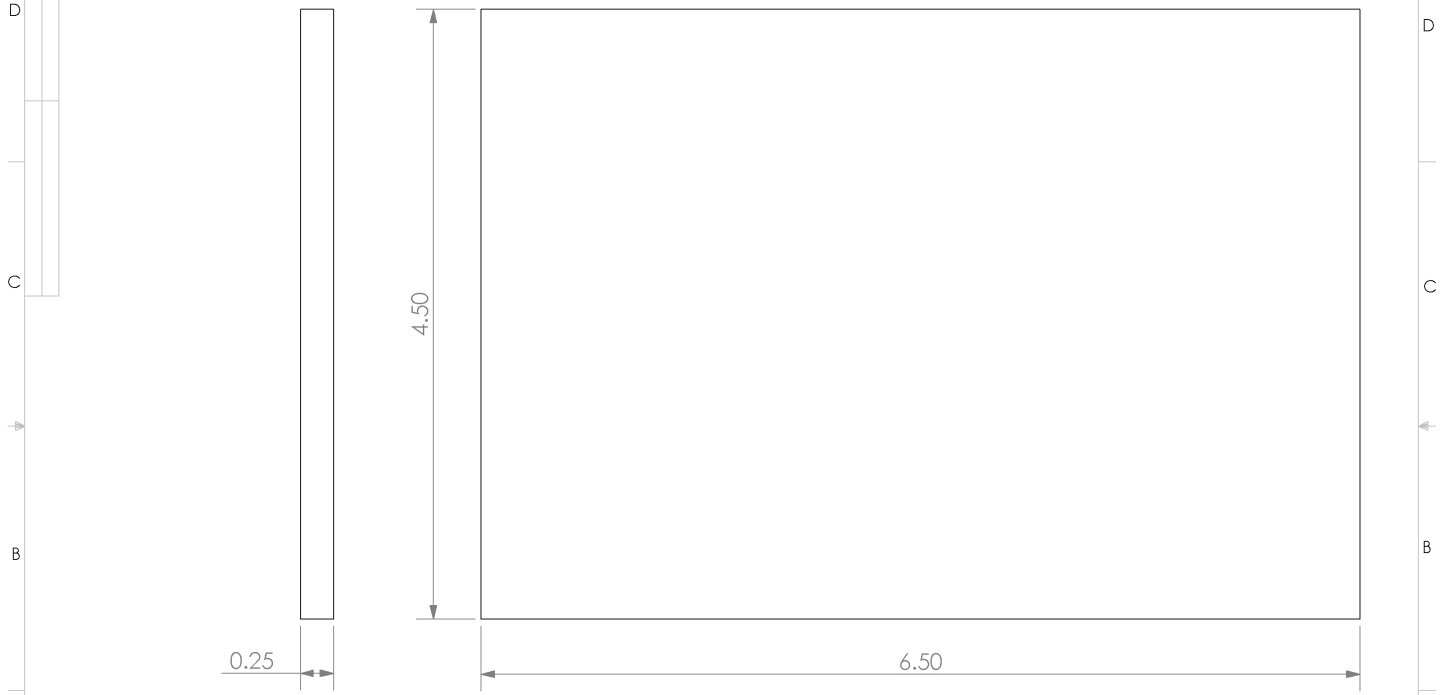

ITEM NO.	PART OR IDENTIFYING NO.	NOMENCLATURE OR DESCRIPTION	MATERIAL SPECIFICATION	QTY REQD

PARTS LIST

UNLESS OTHERWISE SPECIFIED
DIMENSIONS ARE IN INCHES
TOLERANCES ARE:
FRACTIONS DECIMALS ANGLES
.XX ± 0.05 .XX ± 0.5°
.XXX ± 0.01 .XXX ± 1/8

MATERIAL: Plexiglas
FINISH: --

NEXT ASSY | USED ON
APPLICATION
DO NOT SCALE DRAWING

CAD GENERATED DRAWING.
DO NOT MANUALLY UPDATE

APPROVALS	DATE
DRAWN	
CHECKED	
RESP ENG	
MFG ENG	
QUAL ENG	

University of Maryland

D7 - Wall 3

SIZE A | DWG. NO. | REV.
SCALE: 1:1 | CAD FILE: | SHEET 1 OF 1

Appendix B: Addition plume visualizations

SP2

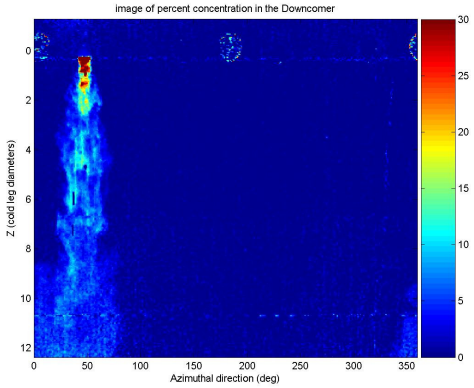

T=10 seconds

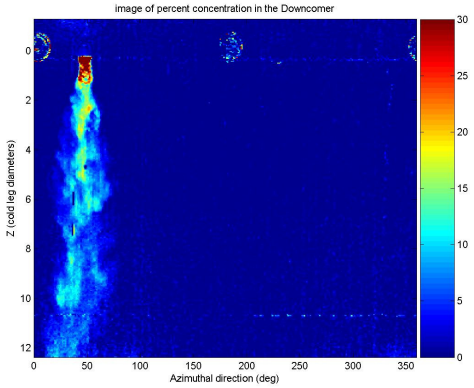

T=15 seconds

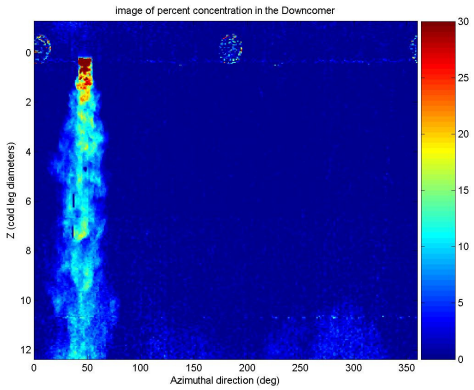

T=20 seconds

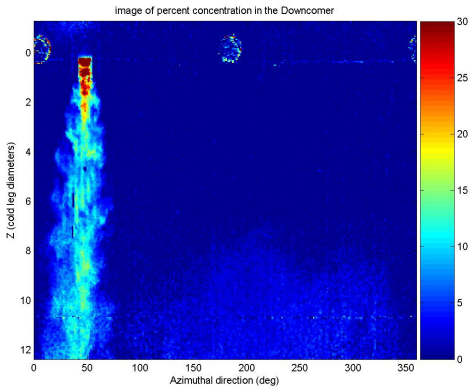

T=25 seconds

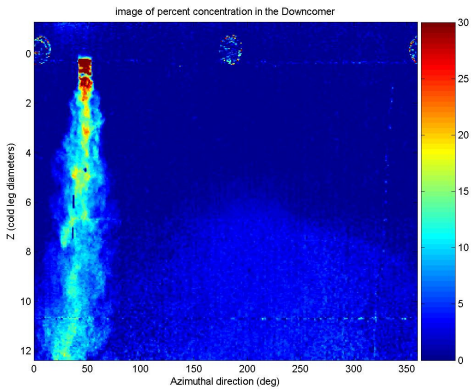

T=30 seconds

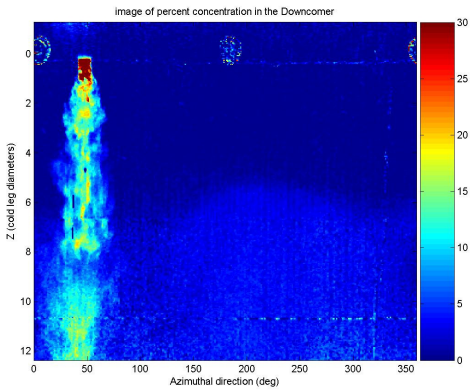

T=35 seconds

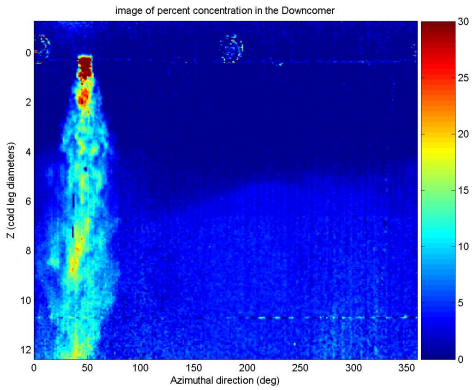

T=40 seconds

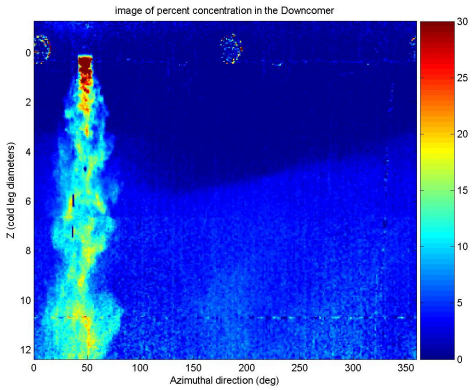

T=45 seconds

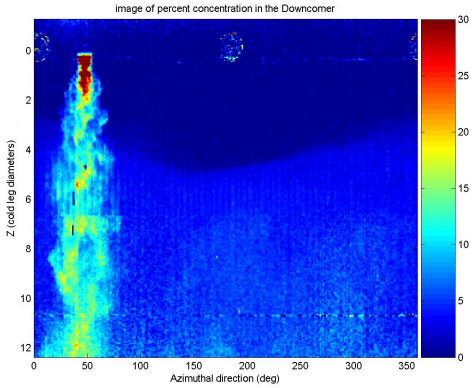

T=50 seconds

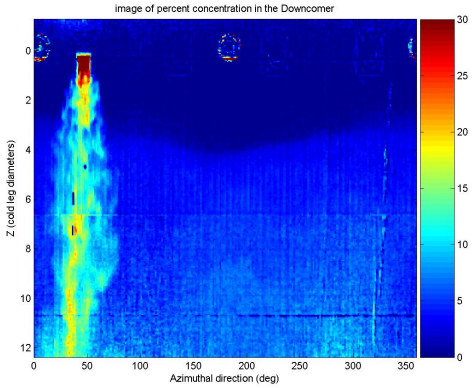

T=55 seconds

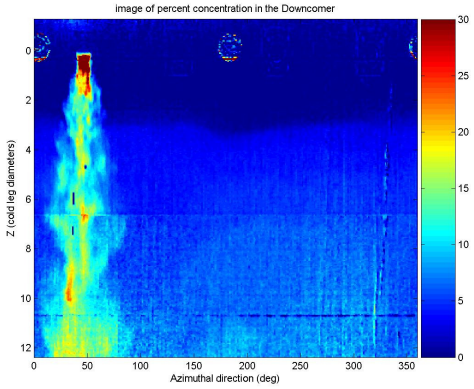

T=60 seconds

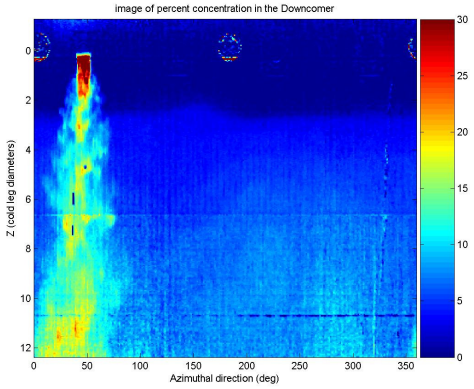

T=65 seconds

SP3

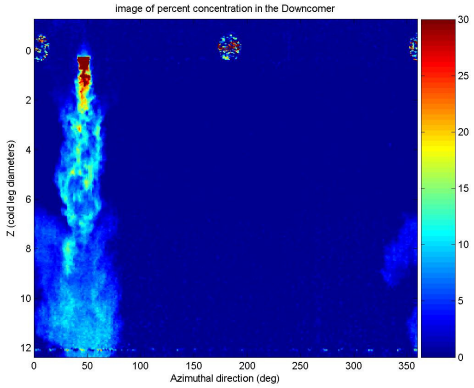

T=10 seconds

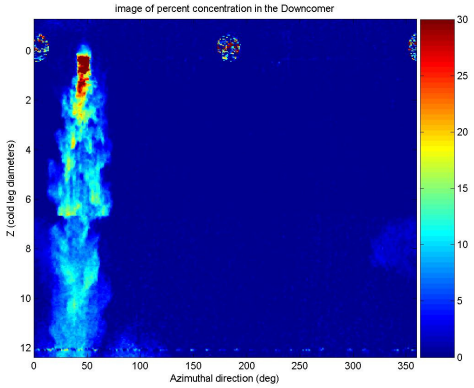

T=15 seconds

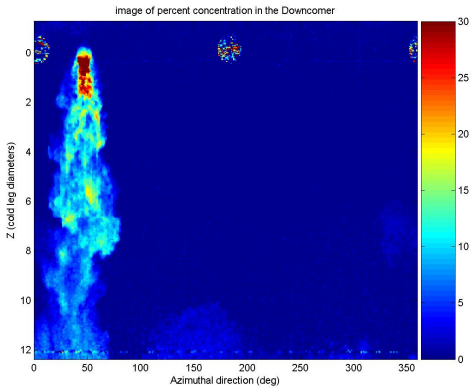

T=20 seconds

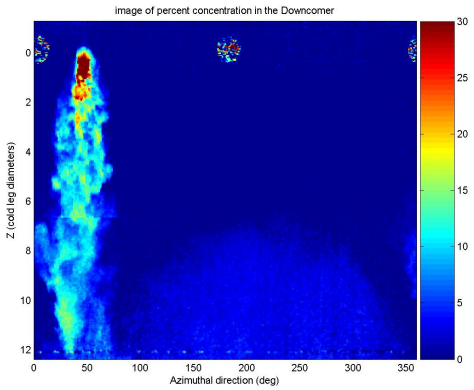

T=25 seconds

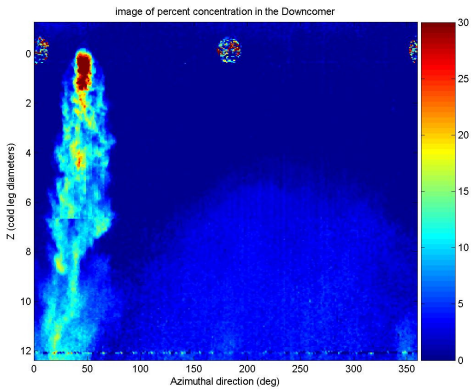

T=30 seconds

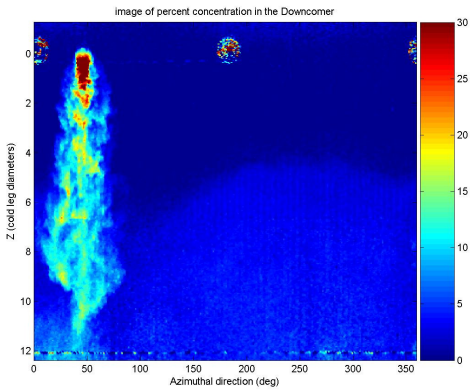

T=35 seconds

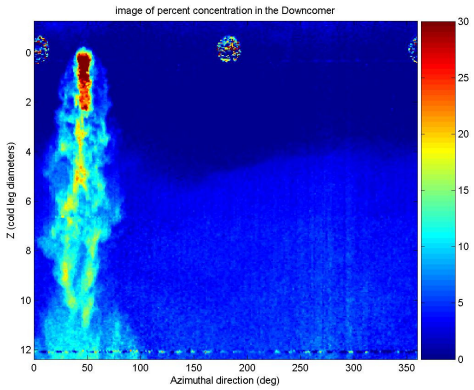

T=40 seconds

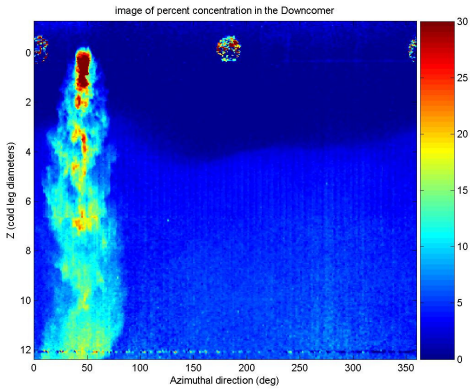

T=45 seconds

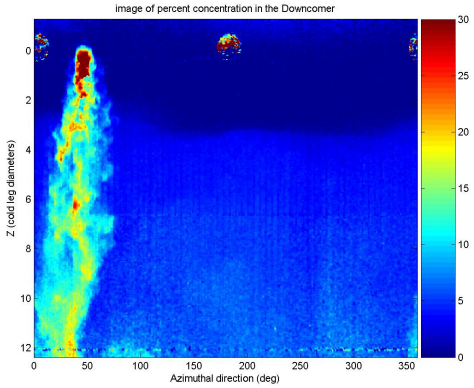

T=50 seconds

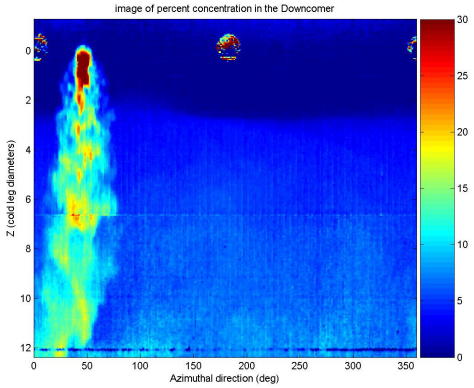

T=55 seconds

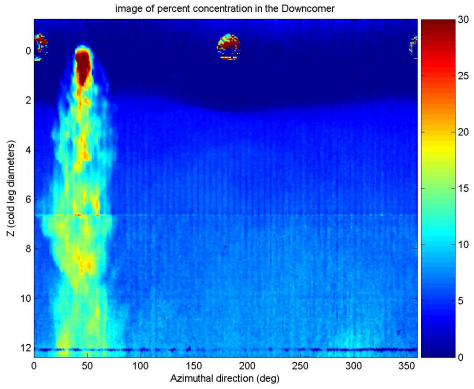

T=60 seconds

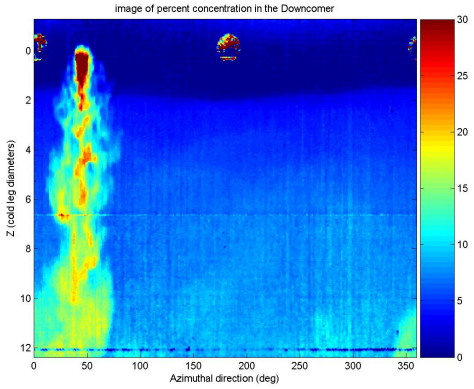

T=65 seconds

SP4

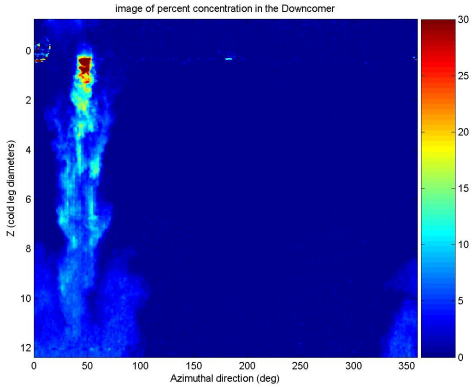

T=10 seconds

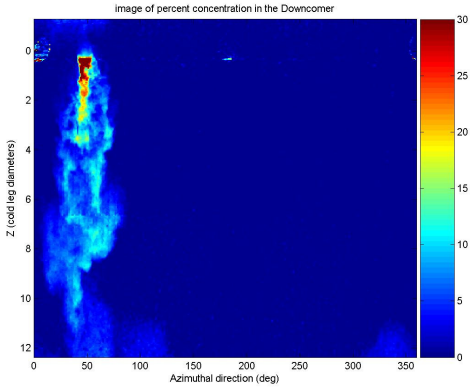

T=15 seconds

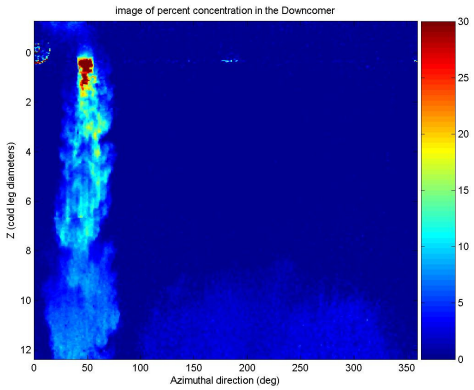

T=20 seconds

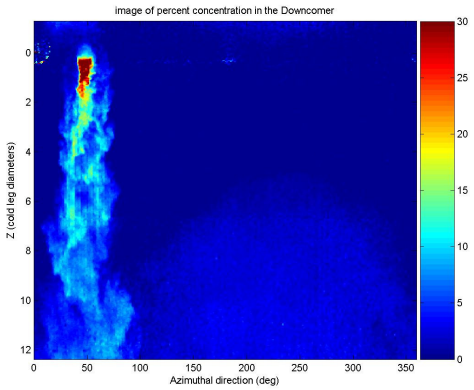

T=25 seconds

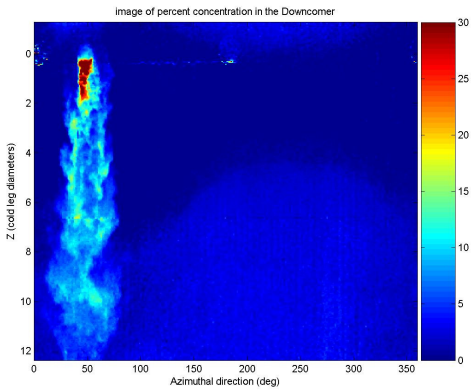

T=30 seconds

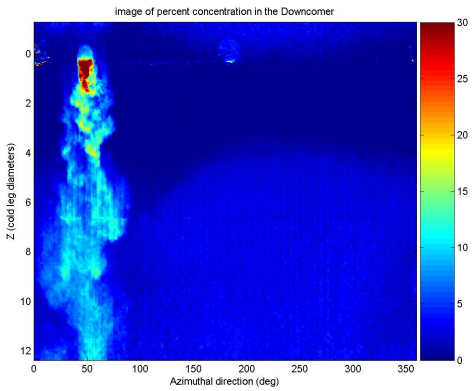

T=35 seconds

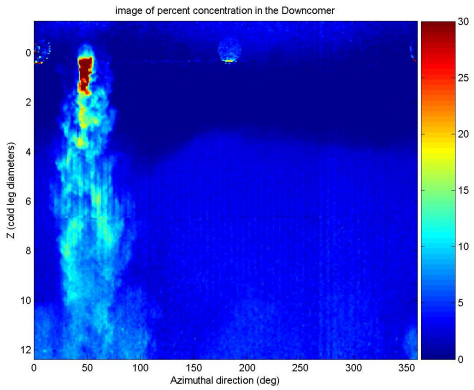

T=40 seconds

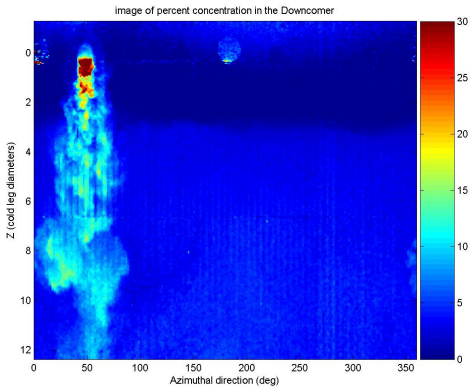

T=45 seconds

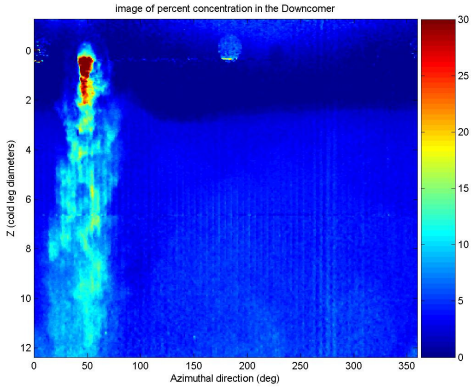

T=50 seconds

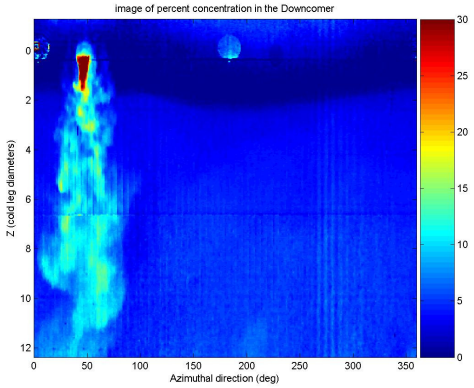

T=55 seconds

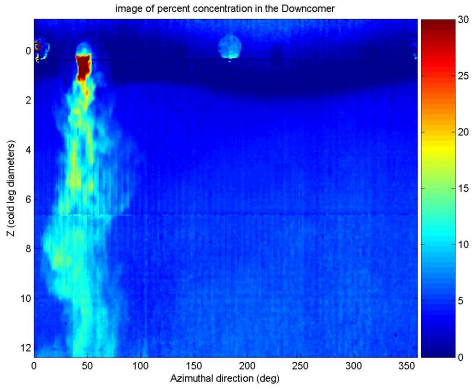

T=60 seconds

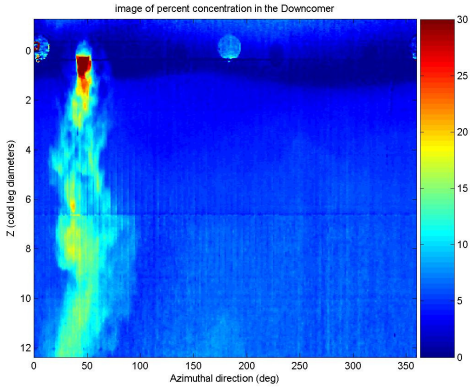

T=65 seconds

SP5

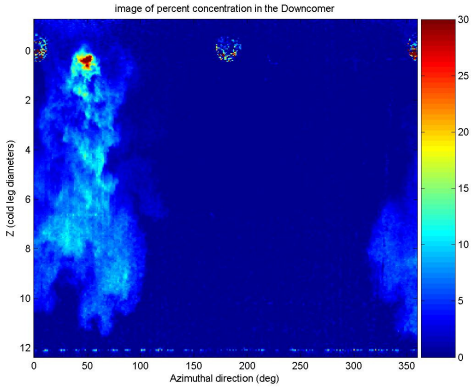

T=10 seconds

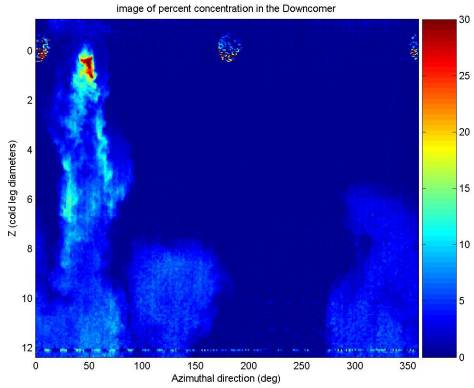

T=15 seconds

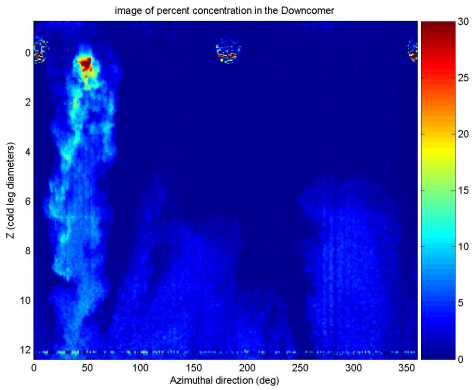

T=20 seconds

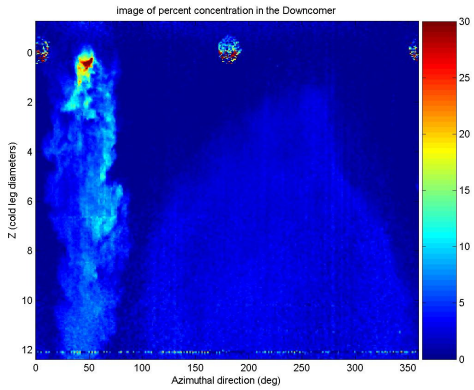

T=25 seconds

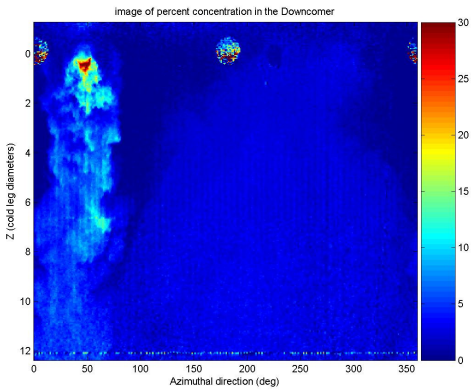

T=30 seconds

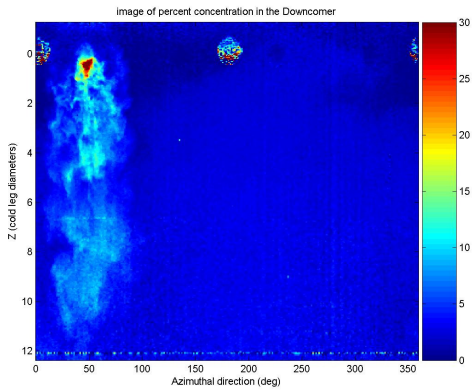

T=35 seconds

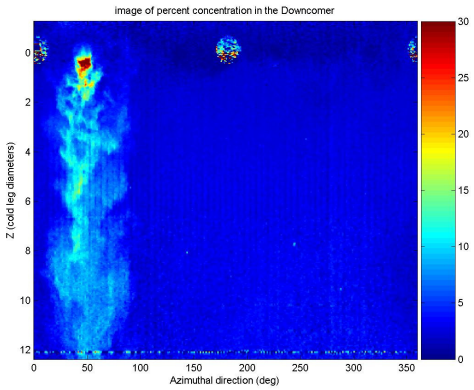

T=40 seconds

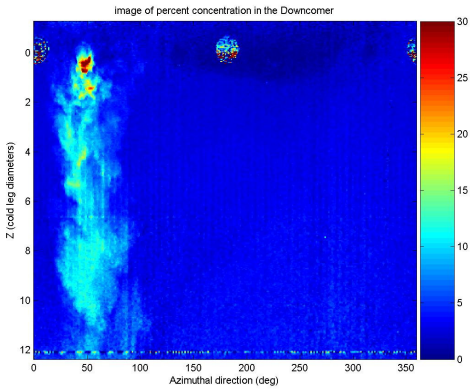

T=45 seconds

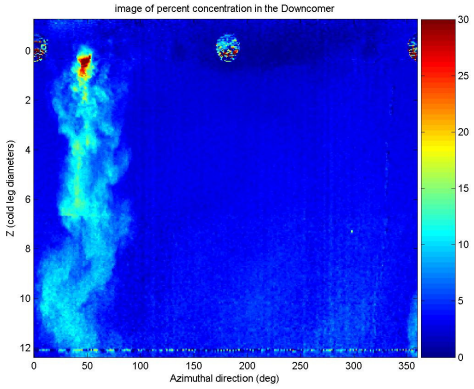

T=50 seconds

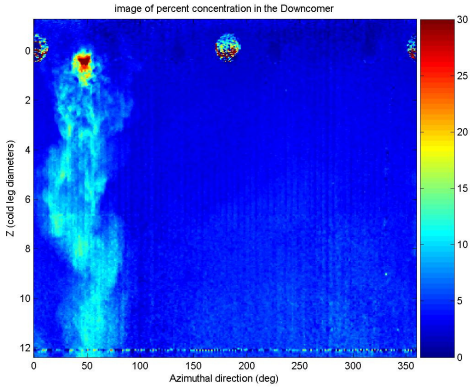

T=55 seconds

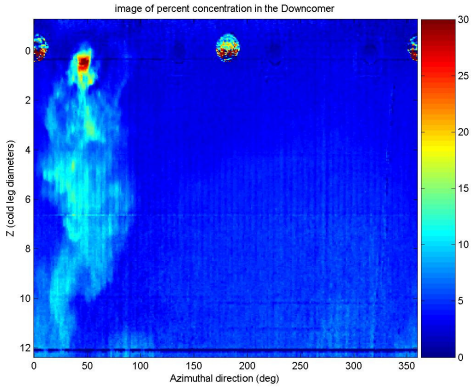

T=60 seconds

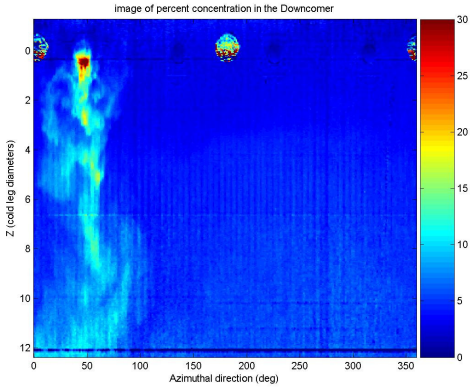

T=65 seconds

SP6

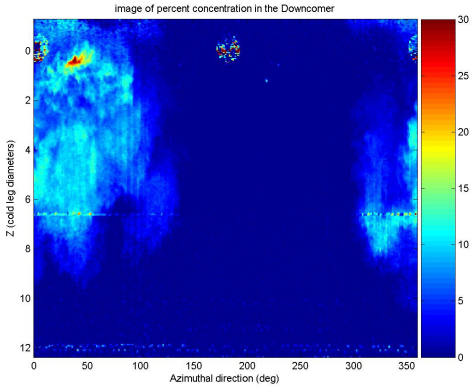

T=10 seconds

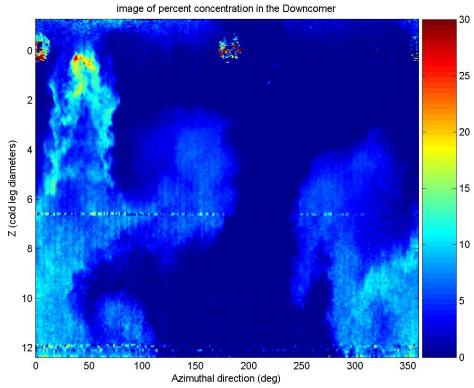

T=15 seconds

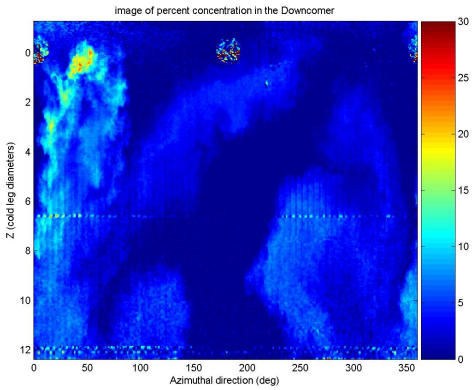

T=20 seconds

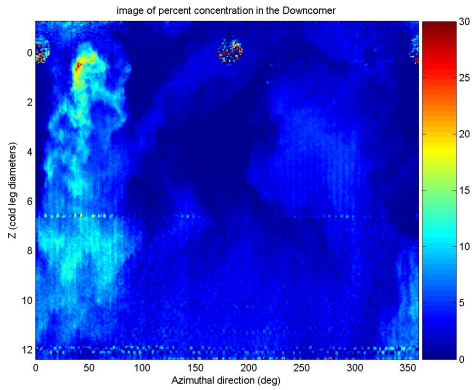

T=25 seconds

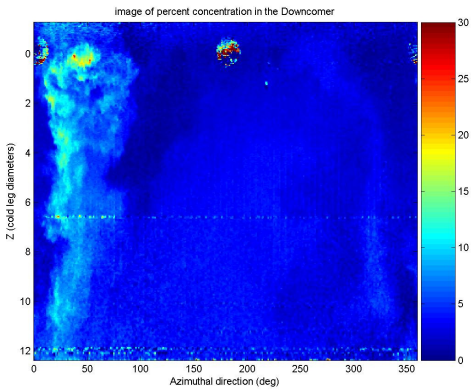

T=30 seconds

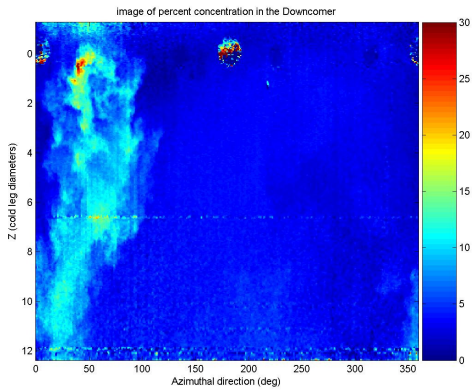

T=35 seconds

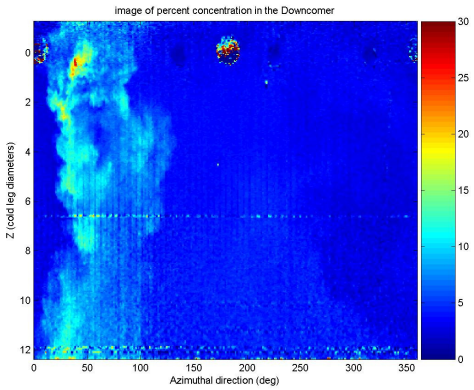

T=40 seconds

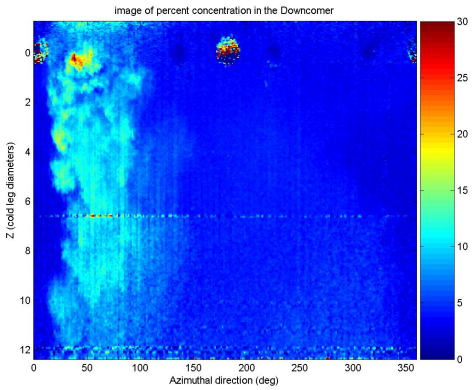

T=45 seconds

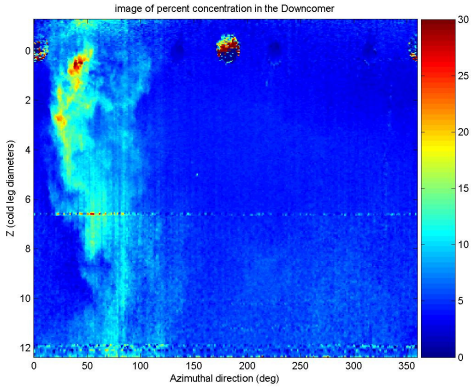

T=50 seconds

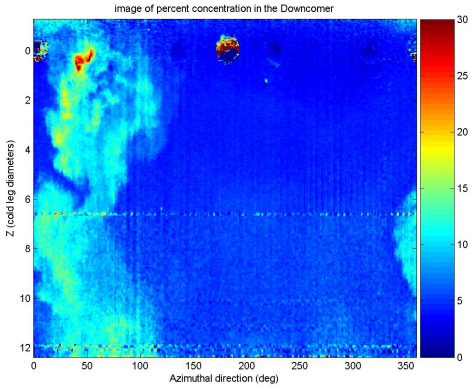

T=55 seconds

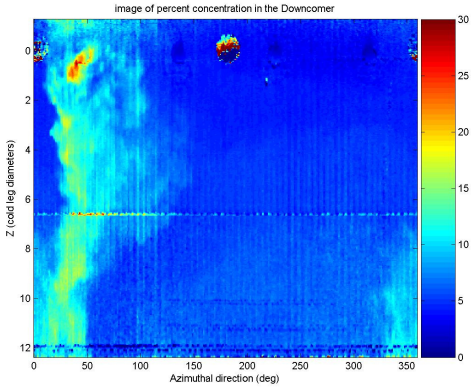

T=60 seconds

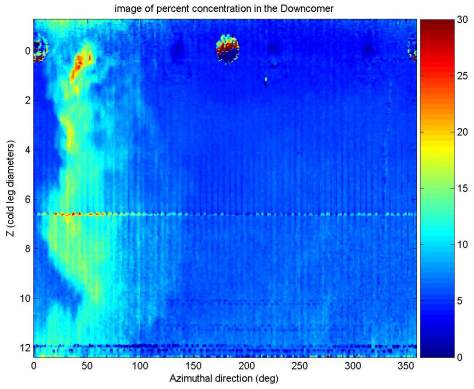

T=65 seconds

MP2

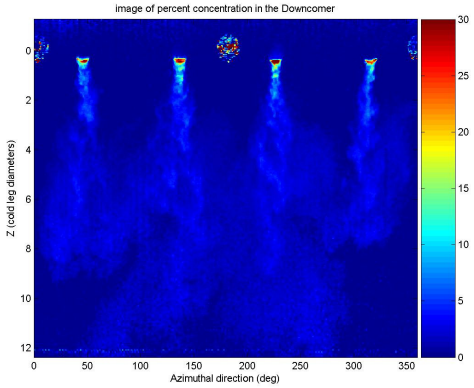

T=10 seconds

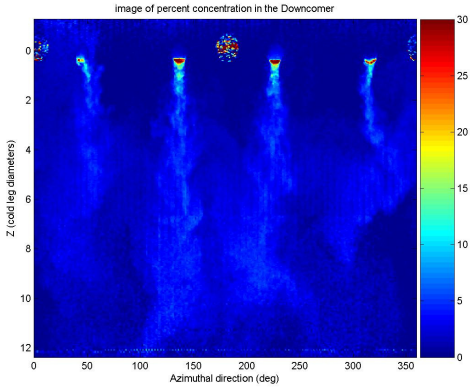

T=15 seconds

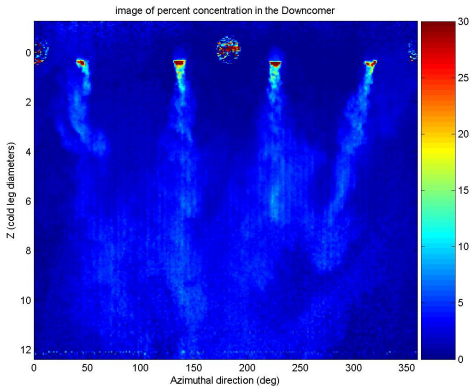

T=20 seconds

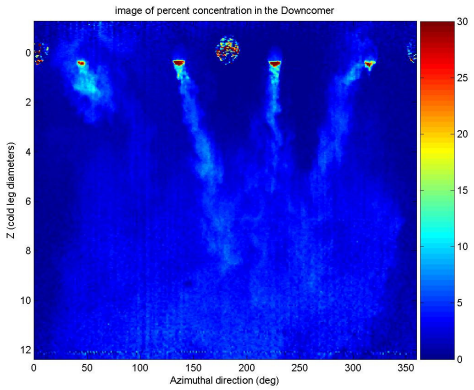

T=25 seconds

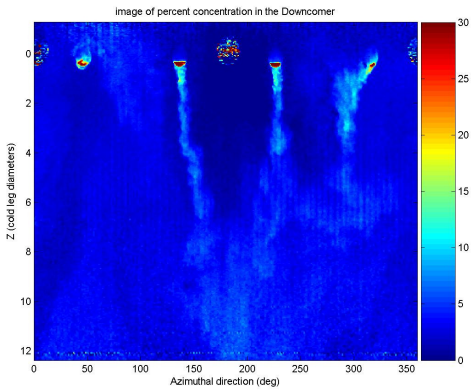

T=30 seconds

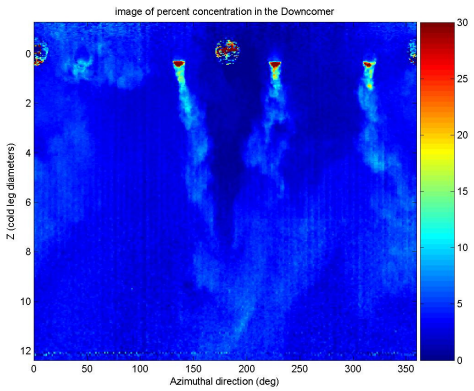

T=35 seconds

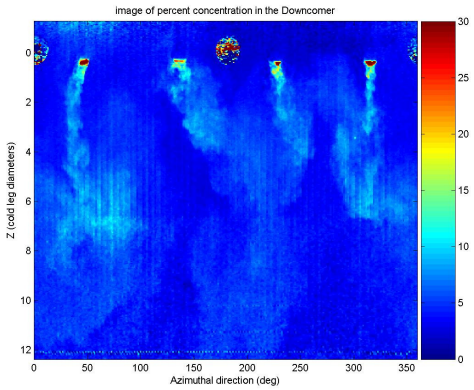

T=40 seconds

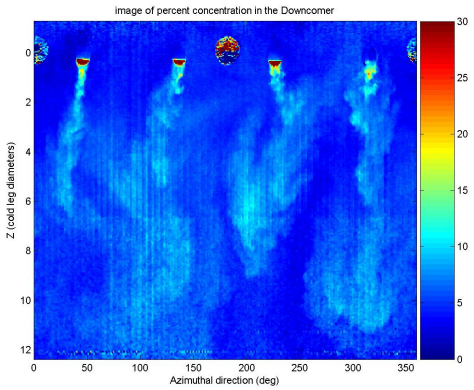

T=45 seconds

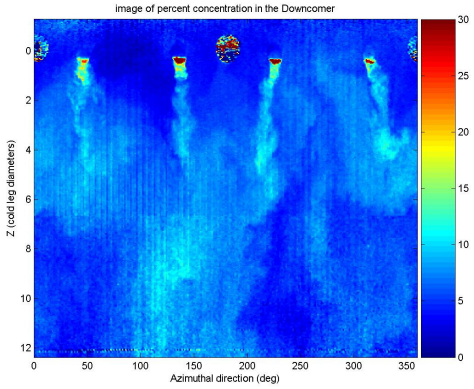

T=50 seconds

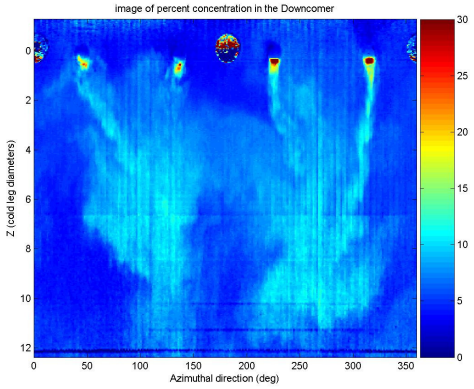

T=55 seconds

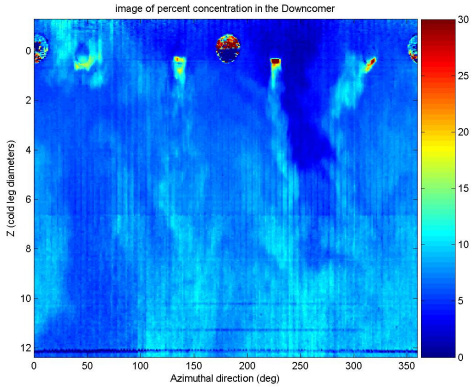

T=60 seconds

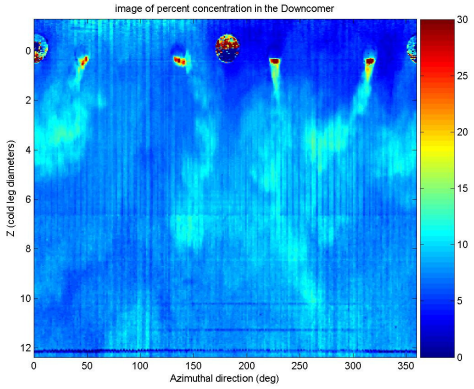

T=65 seconds

MP3

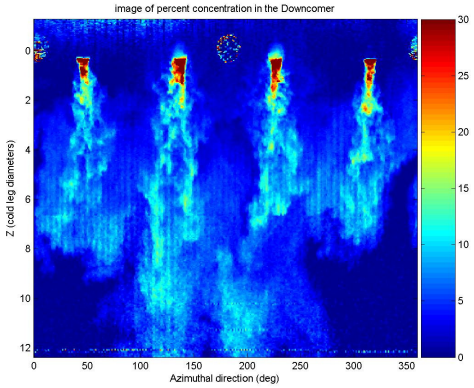

T=10 seconds

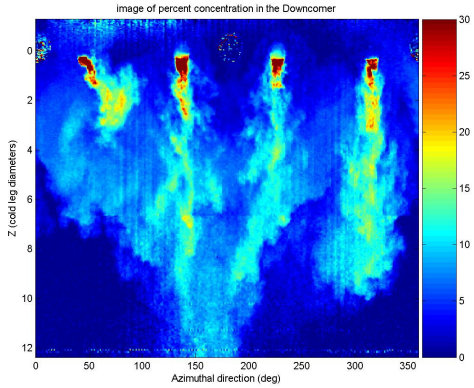

T=15 seconds

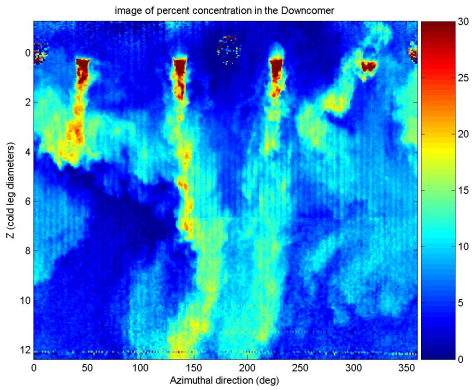

T=20 seconds

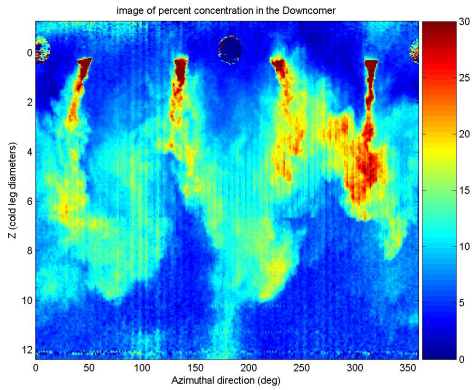

T=25 seconds

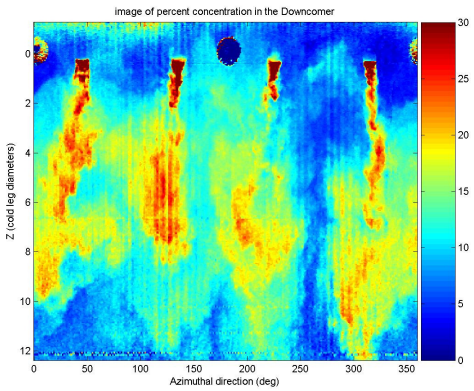

T=30 seconds

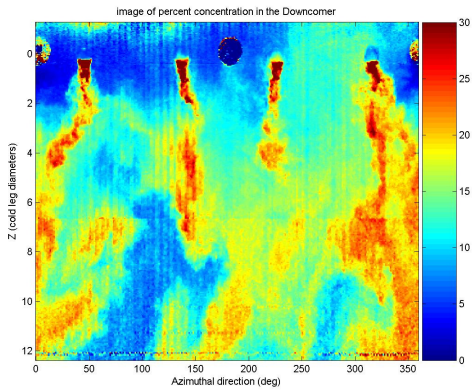

T=35 seconds

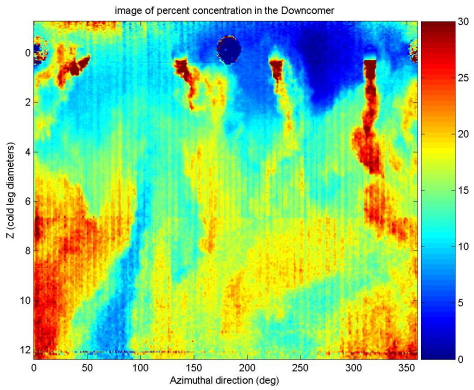

T=40 seconds

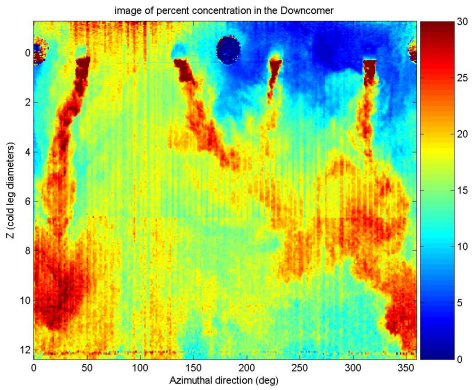

T=45 seconds

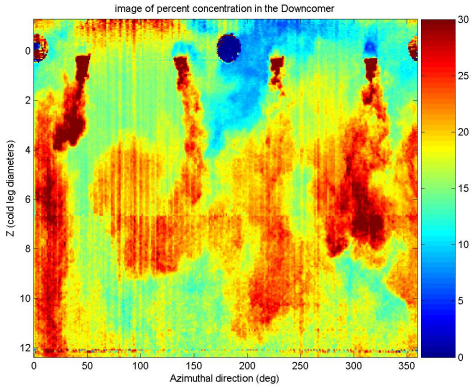

T=50 seconds

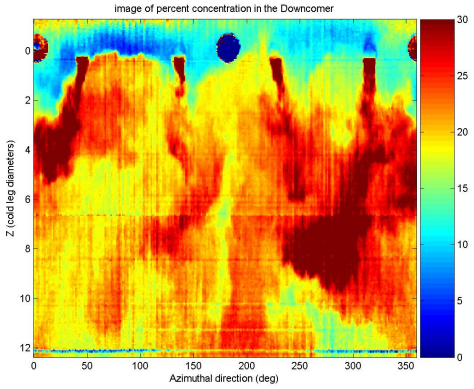

T=55 seconds

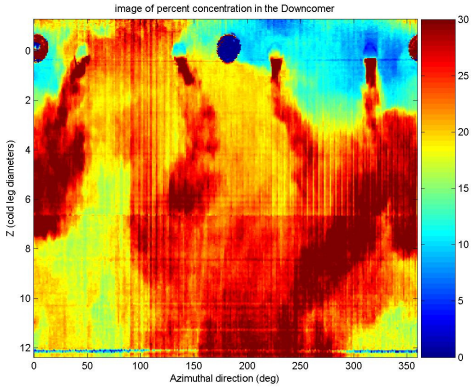

T=60 seconds

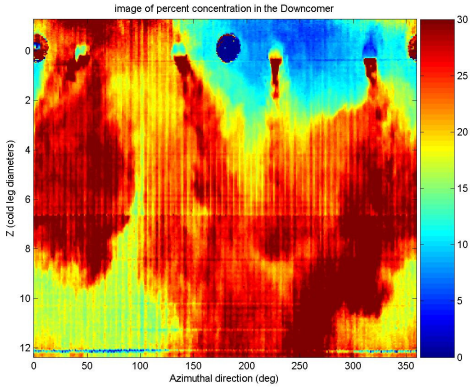

T=65 seconds

MP4

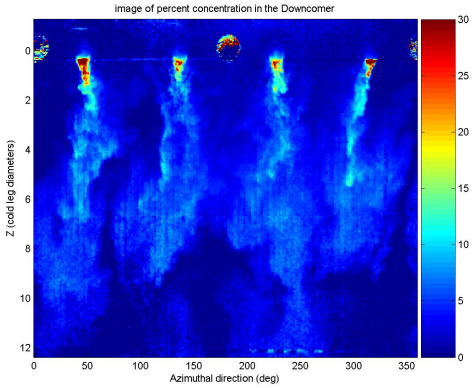

T=10 seconds

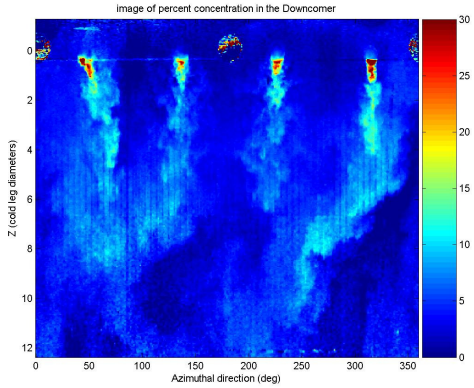

T=15 seconds

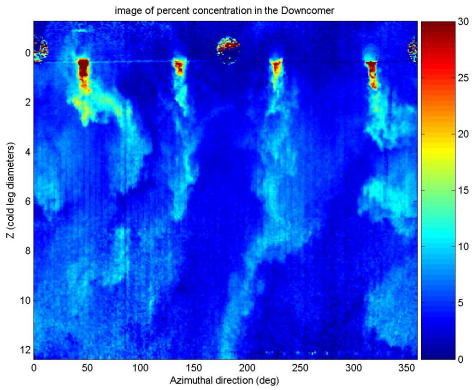

T=20 seconds

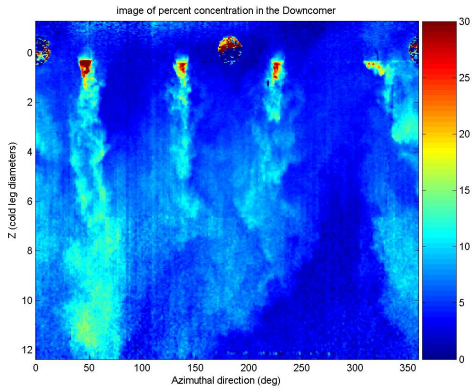

T=25 seconds

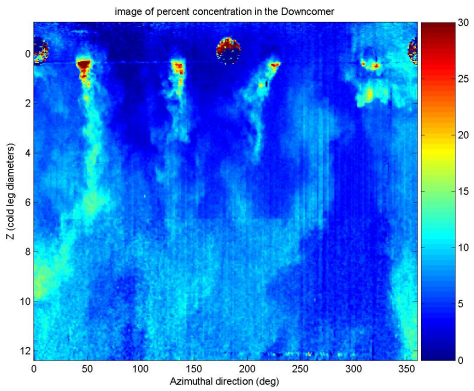

T=30 seconds

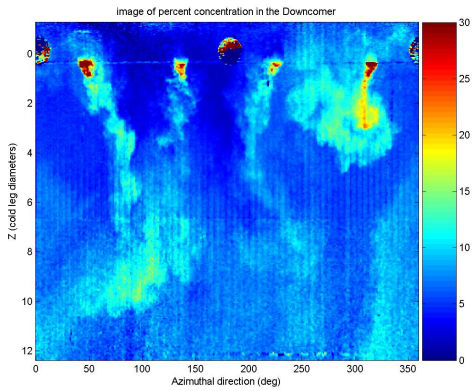

T=35 seconds

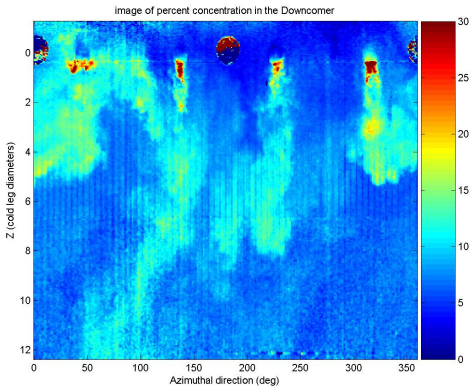

T=40 seconds

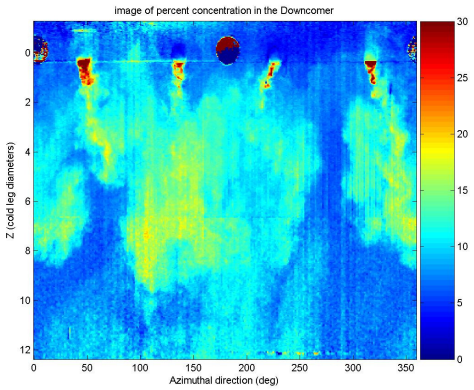

T=45 seconds

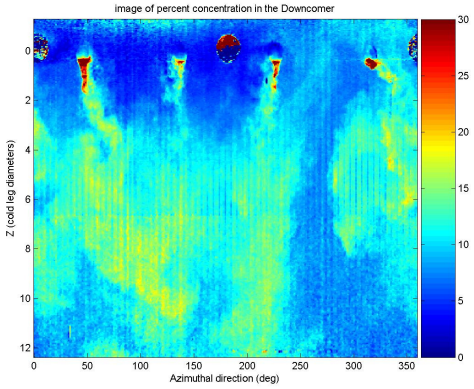

T=50 seconds

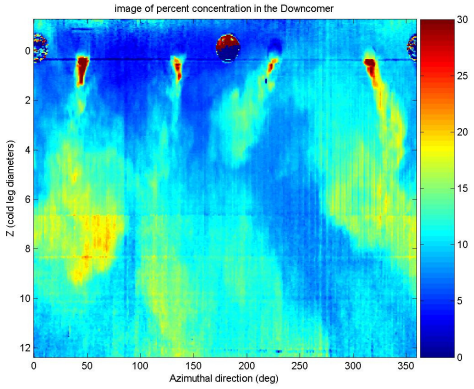

T=55 seconds

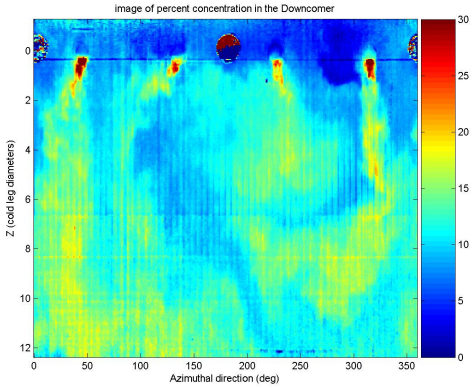

T=60 seconds

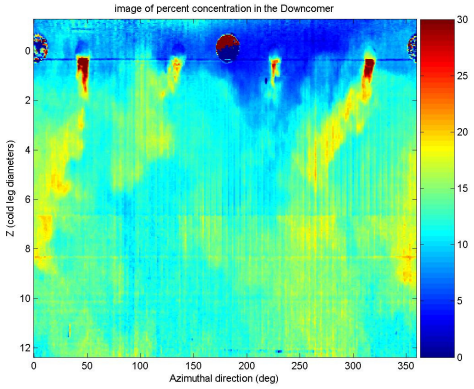

T=65 seconds

MP5

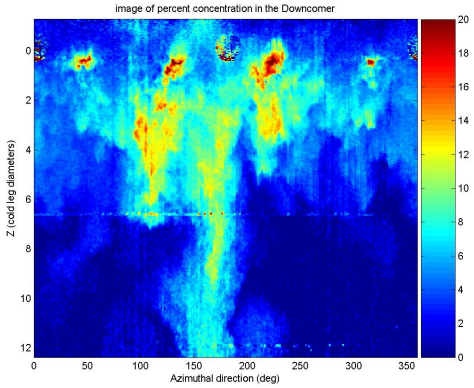

T=10 seconds

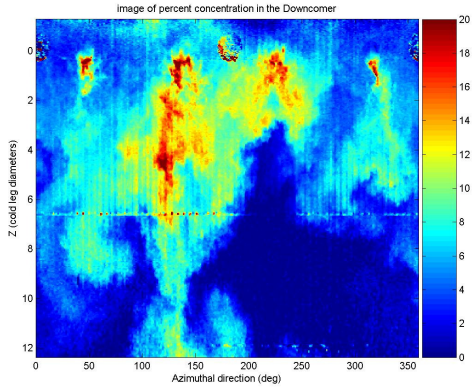

T=15 seconds

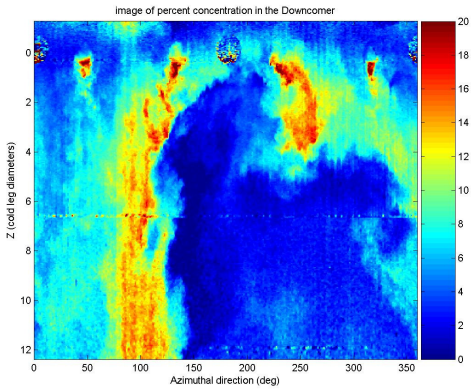

T=20 seconds

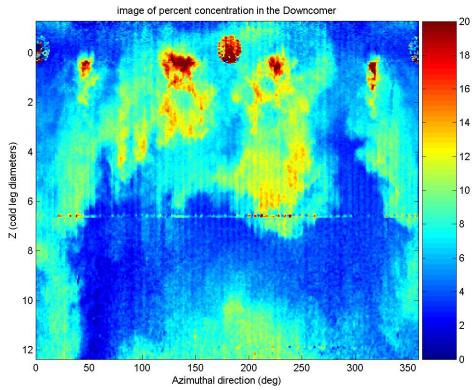

T=25 seconds

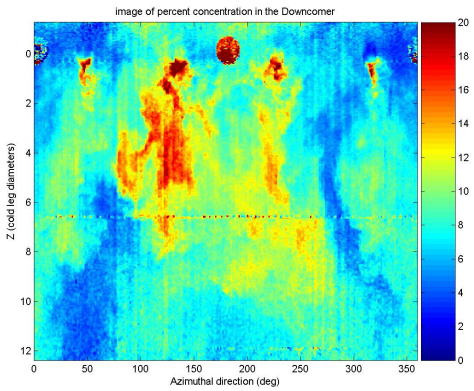

T=30 seconds

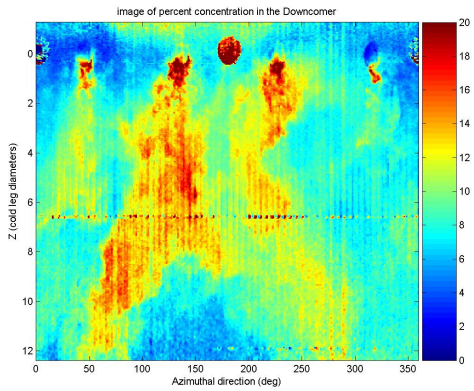

T=35 seconds

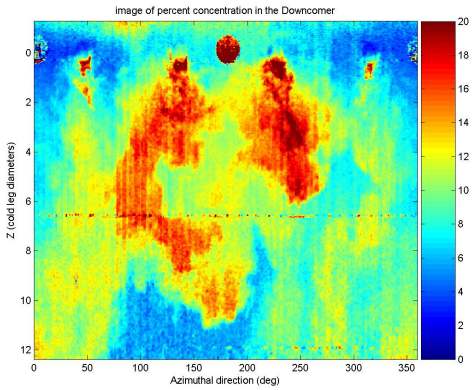

T=40 seconds

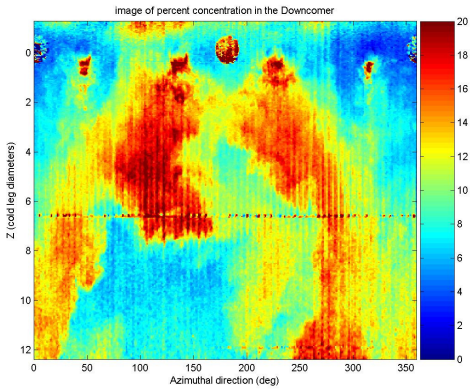

T=45 seconds

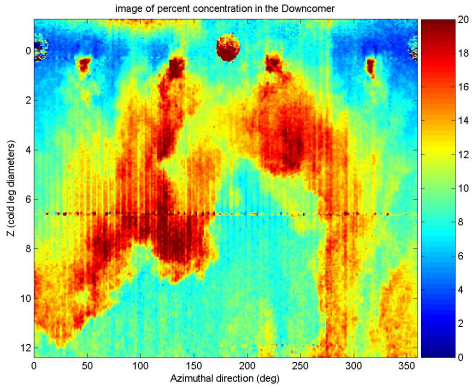

T=50 seconds

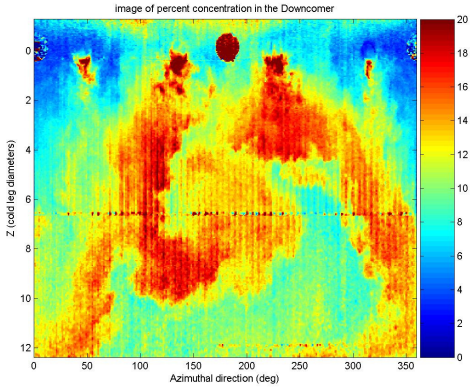

T=55 seconds

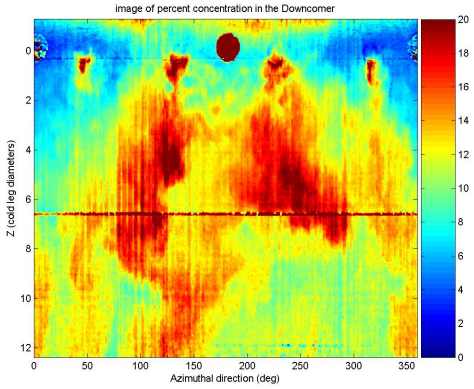

T=60 seconds

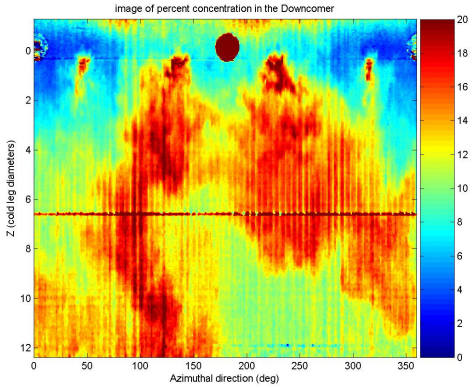

T=65 seconds

References

1. K. Iyer and T.G. Theofanous, "Flooding-Limited Thermal Mixing: The case of High Froude number injection" Nuclear Science and Engineering (1991), V108, pp.198-207

2. T.G. Theofanous, Yan H. "A unified interpretation of One-fifth to full Scale Thermal mixing experiments related to pressurized thermal shock" NUREG/CR-5677, (1991).

3. T.G. Theofanous and H.P. Nourbakhsh, "PWR Downcomer Fluid Temperature Transients Due to High Pressure Injection at Stagnated Loop Flow," *Proc. Joint NRC/ANS Meeting on Basic Thermal Hydraulic Mechanisms in LWR Analysis*, Bethesda, Maryland, Sept. 14-15, 1982, NUREG/CP-0043, 583-613.

4. Iyer K., T.G. Theofanous, "Decay of Buoyancy-Driven Stratified Layers with Applications to Pressurized Thermal Shock: Reactor Predictions", Nuclear Science and Engineering (1991), 108, 184-197

5. Huq, P. and Rex E. Britter, "Turbulence evolution and mixing in a two-layer stably stratified fluid", J. Fluid Mech. (1995), vol. 285, pp. 41-67

6. Reyes, J.N. Jr., Groome, J.T., Lafi, A.Y., Abel, K., Antoine, S., Haugh, B., Tang, H., Wachs, D., Welter, K., You, Y., Young, E., Davis, I., and Linrud, C., "Final Report for the OSU APEX-CE Integral System Test Facility," NUREG/CR-????, (2004).

7. Theofanous, T.G., S. Angelini, and H. Yan, “Universal treatment of plume and stresses for pressurized thermal shock evaluation”, Nuclear Engineering and Design (1994), 146, 1-14

8. Turner, J. S., *Buoyancy Effects in Fluids*, Cambridge University Press, (1973).

9. Wicks, P.J, “Interaction of Buoyant Plumes in Open-Channel Flow” J. Austral. Math. Soc. Ser. B 33(1992), 451-473

10. Soteriou, M.C., Y. Doug, and B.M. Cetegen, “Lagrangian simulation of the unsteady near field dynamics of planar buoyant plumes” Physics of Fluids V 14 #9 (2002), pp. 3118-3140

11. Townsend, A. A., “Entrainment and the structure of turbulent flow” Journal of Fluid Mechanics V41 (1970), pp. 13-46

12. Shusser, M., and M. Gharib, “A model for vortex ring formation in a starting buoyant plume” Journal of Fluid Mechanics V416 (2000), pp. 173-185

13. Defina, A., S. Lanzoni, and F. Susin, “Stability of a stratified shear flow in a tilted tube” Physics of Fluids V11, #2 (1999), pp. 344-355

14. Bernard, P. and J. Wallace, *Turbulent flow: analysis, measurement, and prediction,* John Wiley & Sons, New Jersey, (2002)

15. Panton, R.*, Incompressible flow,* John Wiley & Sons, New York, (1996)

16. Incropera, F. and D. DeWitt, *Fundamentals of Heat and Mass Transfer*, John Wiley & Sons, New York, (1996)

17. Walker, D A, *A fluorescence technique for measurement of concentration in mixing liquids*, J. Phys.E: Sci. Instrum. V20 (1987), pp. 217-224

18. Morton, B. R., Taylor, G. I. & Turner, J. S. *Turbulent gravitational convection for maintained and instantanoes sources.* Proc. R. Soc. Lond. A V234 (1956), pp 1-23

19. Reyes, J.N., Scaling Analysis Report for the OSU APEX-CE Intergral System test Facility, NUREG/CR-6731, U.S. Nuclear Regulatory Commission, June 2002.

20. Valenzuela, J. A., Dolan, F.X., Thermal and fluid mixing in ½-scale facility. Vol. 2 – Data report. EPRI NP-3802, NUREG/CR-3426, September 1985.

21. Dolan, F.X., Valenzuela, J. A., Thermal and fluid mixing in ½-scale facility. Vol. 1 – Facility and test design report. EPRI NP-3802, NUREG/CR-3426, September 1985.

22. Rothe, P. H., Ackerson, M. F., Fluid and thermal mixing in a model cold leg and downcomer with loop flow. EPRI NP-2312, April 1982.

23. Tuomisto, H., P. Mustonen, "Thermal Mixing Tests in a Semiannular Downcomer with Interacting Flows from Cold Legs," U.S. Nuclear Regulatory Commission, NUREG/IA-0004, October 1986.

24. Tuomisto, H., Experiments and analysis of the thermal mixing and stratification during overcooling accidents in a pressurized water reactor. ANS Proceedings 1987 National Heat Transfer Conference, Pittsburg, PA, August 9-12, 1987.

25. Igarashi, K., Maeda, M., Takao, T., Uchiumi, M., Oki, Y., Shimamoto, K., 1995. Operation of Rhodamine 6G dye laser in water solution. Jpn. J. Appl. Phys. 34, 3093-3096.

26. Villermaux, E. & Hopfinger, E. J., Periodically arranged co-flowing jets. *J. Fluid Mech.* Vol 263 pp 63-92, 1994